THE UNIVERSITY
of EDINBURGH

d- and *f*-Metal Alkoxy-Tethered *N*-Heterocyclic Carbene Complexes

Andrew A. Fyfe

A thesis submitted for the degree of Doctor of Philosophy

July 2015

Declaration

The work described in this thesis is entirely my own, except where I have either acknowledged help from a named person or given reference to a published source. Text taken from another source will be enclosed in quotation marks and a reference given. This thesis has not been submitted, in whole or in part, for any other degree.

Signature: Date:

Research is what I'm doing when I don't know what I'm doing.

Wernher von Braun

Acknowledgements

Firstly, I'd like to thank Prof. Polly Arnold for allowing me to do a PhD within her group and for all her ideas during the past three and a half years.

I'd also like to thank all the members of the Love\Arnold group from my time in the group. A special thanks to Dr Thomas Cadenbach for all his help and ideas; Dr's Stephen Mansell and Guy Jones for trying to teach me crystallography; Drs Johann Hlina and Joy Farnaby for their useful advice; Colin Finn for entering all the mad races with me and Jamie McKinven for making sure I knew where the fire extinguishers were in the lab. Thanks also to those who I have collaborated with: Dr Alexander Pöthig, Dr Sax Anton Mason and Alistair MacNair.

Finally, I'd think to thank my family who have supported me throughout my PhD. And pretended to understand what I've been doing for the past three and a half years.

Abstract

Chapter one is an introduction, outlining the structure and bonding of *N*-heterocyclic carbenes (NHCs). It then goes on to give examples of *f*-metal NHC complexes and describes any reactivity or catalytic activity.

Chapter two describes the synthesis of the transition metal NHC complexes [Fe(L^{Mes})$_2$] **3** and [Co(L^{Mes})$_2$] **4** (L^{Mes} = $OCMe_2CH_2$(1-C{NCH_2CH_2NMes})). The heterobimetallic complexes [(L^{Mes})Fe(μ-L^{Mes})U(μ-{$N(SiMe_3)Si(Me)_2CH_2$})(N($SiMe_3$)$_2$)$_2$] **5** and [(L^{Mes})Co(μ-L^{Mes})U(μ-{$N(SiMe_3)Si(Me)_2CH_2$})(N($SiMe_3$)$_2$)$_2$] **6** were prepared from the reaction between [({Me_3Si}$_2$N)$_2$U($NSiMe_3SiMe_2CH_2$)] and **3** or **4**, respectively. Complex **5** was also synthesised by the reaction between **3** and [U(N{$SiMe_3$}$_2$)$_2$]. The diamagnetic analogue [(L^{Mes})Zn(μ-L^{Mes})Th(μ-{$N(SiMe_3)Si(Me)_2CH_2$})(N($SiMe_3$)$_2$)$_2$] **9** was prepared from the reaction between [Zn(L^{Mes})$_2$] and [({$SiMe_3$}$_2$N)$_2$Th($NSiMe_3SiMe_2CH_2$)].

The reactivity of **5** is discussed. When **5** was reacted with 2,6-dimethylphenyl isocyanide, [({$SiMe_3$}$_2$N)$_2$U{$N(SiMe_3)Si(Me_2)C(CH_2)N(2,6-Me-C_6H_3)$}] **8** was isolated. The reaction with CO resulted in the formation of [({Me_3Si}$_2$N)$_2$U{$N(SiMe_3)Si(Me_2)C(CH_2)CO$}]. **5** showed no reactivity with azides, boranes or *m*-chloroperbenzoic acid and decomposed when exposed to H_2, CO_2 or KC_8. The reaction between **6** and 2,6-di-*tert*-butylphenol formed the previously reported monometallic complex [({$SiMe_3$}$_2$N)$_2$U($OC_6H_3tBu_2$)]. The serendipitous synthesis of the iron *ate* complex [Na(Fe{L^{Mes}}$_2$)$_2$]$^+$ [Fe(ArO)$_3$]$^-$ **10** (Ar = 2,6-*t*Bu-C_6H_3) is also described.

Chapter three describes the synthesis of the aryloxide complexes [HC(3-*t*Bu-5-Me-C_6H_2OH)(3-*t*Bu-5-Me-C_6H_2O)μ-(3-*t*Bu-5-Me-C_6H_2O)Co(THF)]$_2$ **11** and [HC(3-*t*Bu-5-Me-C_6H_2OH)(3-*t*Bu-5-Me-C_6H_2O)μ-(3-*t*Bu-5-Me-C_6H_2O)Zn(THF)$_n$] **13**.

Treatment of **11** with pyridine *N*-oxide resulted in the formation of the pyridine-*N*-oxide adduct [HC(3-*t*Bu-5-Me-C_6H_2OH)(3-*t*Bu-5-Me-C_6H_2O)μ-(3-*t*Bu-5-Me-C_6H_2O)Co(C_5H_5NO)]$_2$ **12**. When **11** was treated with [($\{Me_3Si\}_2N)_2U(NSiMe_3SiMe_2CH_2$)], no reaction occured at room temperature but at 80°C decomposition occured. When **11** was treated with [$(NH_4)_2Ce(NO_3)_6$] the protonated proligand HC(3-*t*Bu-5-Me-$C_6H_2OH)_3$ reformed. The reactivity of **11** with [($\{Me_3Si\}_2N$)Ce(L^{iPr})$_2$] is also discussed.

Chapter three also discusses the preparation of the heterobimetallic complex [HC(3-*t*Bu-5-Me-$C_6H_2O)_2$-μ-(3-*t*Bu-5-Me-C_6H_2O)KCo]$_2$ **14** and the salt-elimination chemistry of the complex. The preparation of [HC(3-*t*Bu-5-Me-$C_6H_2O)_2$-μ-(3-*t*Bu-5-Me-C_6H_2O)KZn]$_2$ **15** is also outlined.

Chapter four discusses the reactivity of [Ce(L^{iPr})$_3$] (L^{iPr} = $OCMe_2CH_2$(1-C{NCHCHN*i*Pr})) in C-H and N-H activation and as a catalyst for organic reactions. [Ce(L^{iPr})$_3$] displayed no C-H activation chemistry with RC≡CH (R = $SiMe_3$, Ph, *t*Bu), diphenyl acetone, indene or fluorene. [Ce(L^{iPr})$_3$] also showed no N-H activation chemistry with pyrrole or indole, nor did it react with the lignin model compound $PhOCH_2Ph$.

When treated with an excess of benzyl chloride, [Ce(L^{iPr})$_3$] underwent ligand decomposition to form the acylazolium chloride [($C_6H_5C(O)$)$OCMe_2CH_2$(1-C(C_6H_5C(O)){NCHCHN*i*Pr})]Cl **18** and $CeCl_3$. When [Ce(L^{iPr})$_3$] was added to a mixture of benzaldehyde and benzyl chloride, as a coupling catalyst, the complex decomposed. [Ce(L^{iPr})$_4$] was tested as a catalyst from the benzoin condensation and for the coupling of benzalehyde and benzyl chloride, however, it resulted in the decomposition of [Ce(L^{iPr})$_4$].

Chapter four also outlines the catalytic activity of **3**. The complex showed no reactivity as a hydrogenation catalyst towards alkenes, aldehydes or ketones but

did display reactivity as a hydroboration catalyst for alkenes, aldehydes or ketones.

Chapter five presents the conclusions for chapters two to four.

The final chapter contains the experimental details from the previous chapters.

Lay summary

Complexes containing two different metal centres can react in a manner that is different from the analogous complexes containing a single metal. In order to explore the chemistry of such complexes, a series of complexes containing two different metal centres were prepared and their reactivity investigated. While most of these reactions showed either no reactivity or resulted in decomposition, those from which a product could be isolated showed that there was no cooperative reactivity between the two metals. Instead the reactivity was identical to that of the monometallic complex.

In addition, the reactivity of a monometallic cerium complex towards C-H and N-H bonds was also explored but no reactivity was observed. Also, a series of cerium and iron complexes were investigated for catalytic activity towards organic reactions. While the reactions using the cerium complexes resulted in decomposition the reactions using the iron complex did display catalytic activity.

List of Abbreviations

Å Angstrom(s)

Ad Adamantyl

An actinide

Ar aryl

atm atmosphere

BBN 9-borabicyclo[3.3.1]nonane

br broad

***i*Bu** *iso*-butyl

***t*Bu** *tert*-butyl

Bz benzyol, $C(=O)C_6H_5$

calcd calculated

CAN ceric ammonium nitrate, $(NH_4)_2Ce(NO_3)_6$

$\mathbf{C_{carbene}}$ carbenic carbene

cf. *confer*, compare

coord. coordinated

Cp cyclopentadienyl

Cp* pentamethyl cyclopentadienyl

d doublet

DABCO 1,4-diazabicyclo[2.2.2]octane

DBN 1,5-diazabicyclo[4.3.0]non-5-ene

DBU 1,8-diazabicyclo[4.5.0]undec-7-ene

DFT density functional theory

Dipp 2,6-diisopropylphenyl

DME 1,2-dimethoxyethane

dmpe bis(dimethylphosphino)ethane, $Me_2PCH_2CH_2PMe_2$

DMSO dimethylsulfoxide, MeS(=O)Me

δ chemical shift in parts per million, delta

eq. equivalents

Et ethyl

FTIR Fourier transform infrared (spectroscopy)

gem geminal

h hour(s)

Hz Hertz

IMes 1-C{NMesCHCHNMes}

IBBN 9-iodo-9-borabicyclo[3.3.1]nonane

KC_8 potassium graphite

kJ mol^{-1} kilojoules per mole

L^{Mes} $[OCMe_2CH_2(1\text{-}C\{NCH_2CH_2NMes\})]$

Ln lanthanide

$\mathbf{L_n}$ generic ligand; n = number of ligands

$\mathbf{L^{iPr}}$ [$OCMe_2CH_2$(1-C{NCHCHN*i*Pr})]

M molar

m multiplet

m *meta-*

***m*CPBA** *m*-chloroperbenzoic acid

Me methyl

MeIm [1-C{NCHCHNMe}]

Mes mesityl

mg milligram(s)

MHz megahertz

mL millilitre(s)

mmol millimol(s)

NHC *N*-heterocyclic carbene

NMR nuclear magnetic resonance

o *ortho-*

p *para-*

***t*Pe** *tert*-pentyl, $C(CH_3)_2CH_2CH_3$

Ph phenyl

ppm parts per million

***i*Pr** *iso*-propyl

py pyridine

***d*^{5}-pyridine** deuterated pyridine

py-*N*O pyridine *N*-oxide

R alkyl or aryl

RE rare-earth element

rt room temperature

s singlet

salen *N,N'*-bis(salicylidene)ethylenediamine

sept. septet

t triplet

TEA triethylamine

TfO$^-$ trifluoromethanesulfonate, $CF_3SO_3^-$

THF tetrahydrofuran

***d*^{8}-THF** deuterated tetrahydrofuran

TIMEN^{mes} $N[CH_2CH_2\{CNCHCHN\}Mes]_3$

TM transition metal

TMEDA tetramethylethylenediamine, $Me_2NCH_2CH_2NMe_2$

TMS trimethyl silyl

tol toluene

VSEPR theory Valence shell electron pair repulsion theory

° degree

°C degree Celsius

^{13}C{^{1}H} proton decoupled ^{13}C NMR experiment

Chapter 1

Introduction

Considerable work looking at the reactivity of monometallic *N*-heterocyclic carbene (NHC) complexes has been carried out. However, less widely studied are NHC complexes containing two different metal centres. This thesis looks at the synthesis of *d*/*f*-block heterobimetallic NHC complexes and their reactivity towards the activation of small molecules. In addition, it also further explores the reactivity of monometallic NHC complexes.

1.1 *N*-Heterocyclic Carbenes

N-heterocyclic carbenes (NHCs) are two-electron donors which contain a neutral, sp^2 hybridised carbon atom with a strongly nucleophilic lone pair. Typically, they are five membered rings with either an unsaturated backbone, an imidazolin-2-ylidene, or saturated backbone, an imidazolidin-2-ylidene, **figure 1.1**.

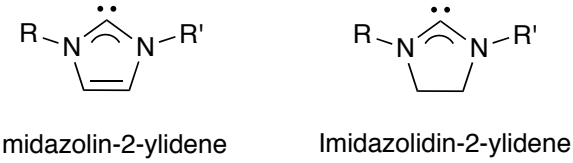

Figure 1.1. Structure of imidazolin-2-ylidene and imidazolidin-2-ylidene.

Carbenes can exist in either a singlet or a triplet state, **figure 1.2**, with the singlet state being strongly favoured in NHCs.

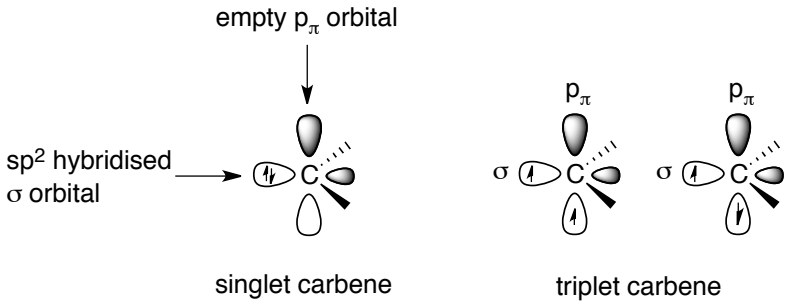

Figure 1.2. Singlet and triplet carbenes.

This is a result of the stabilising effect of the two α-amino groups. Firstly, the lone pair on the carbenic carbon is stabilised through a σ-induction effect by the nitrogen atoms, **figure 1.3**. Secondly, the lone pair on each of the nitrogen atoms donates electron density into the empty p_π orbital on the carbenic carbon; N p_π - C p_π electron donation, **figure 1.3**. Consequently, there is some double bond character to the N-$C_{carbene}$ bond.[1] This combination of σ-withdrawing and π-donation effects increases the HOMO-LUMO gap, stabilising the singlet state.[2][3][4][5][6][7]

Additionally, the cyclic nature of NHCs forces the carbenic carbene to adopt a more bent, sp^2-like geometry further favouring the singlet state.[8]

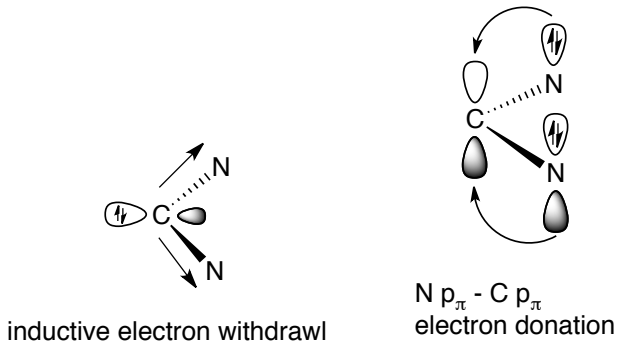

Figure 1.3. Stabilisation effects of the α-amino groups on a singlet NHC.

1.1.1 The first NHCs and their complexes

Wanzlick established the chemistry of NHCs when, in 1960, he demonstrated that heating the imidazolidine **I** results in the formation of the dimeric enetetraamine (Wanzlick dimer) **II** with the α-elimination of chloroform. However, the free carbene **III** could not be isolated, **scheme 1.1**.[9][10][11]

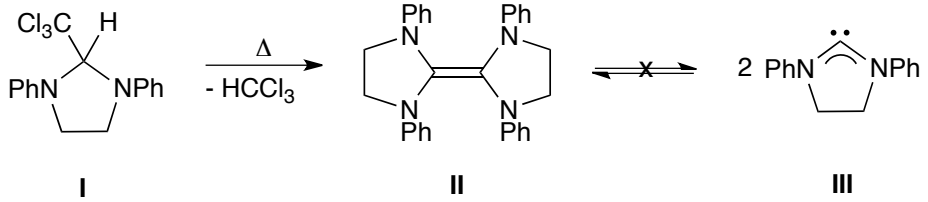

Scheme 1.1. Wanzlick's attempt to form a free NHC.[9][10][11]

Despite being unable to isolate the free carbene, Wanzlick was successful in synthesising metal-NHC complexes. It was demonstrated that treatment of 1,3-diphenylimidazolium perchlorate with mercury(II) acetate in DMSO yields the mercury(II) NHC complex **IV**, **figure 1.2**.[12] Futhermore, Öfele demonstrated that thermolysis of 1,3-dimethylimidazolium-hydridopentacarbonylchromate(II) salt forms the chromium(0)-NHC complex **V**, **figure 1.2**, with the loss of H_2.[13] In 1972, Lappert *et al.* showed that refluxing $[PtCl_2(PEt_3)]_2$ with the enetetraamine

II results in the formation of the platinum(II)-NHC complex **VI**, **figure 1.2**.[14]

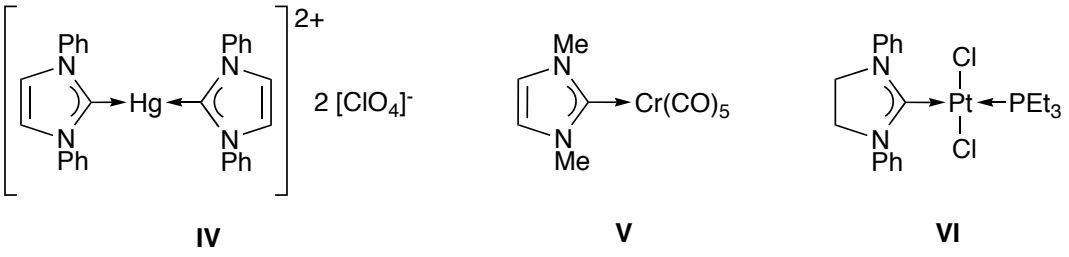

Scheme 1.2. The first metal NHC complexes isolated.[12][13][14]

It was not until 1991 that the first stable, crystalline free NHC **VIII** was isolated by Arduengo and coworkers. This was achieved by the deprotonation of the imidazolium salt **VII** with sodium hydride and a catalytic quantity of DMSO, **scheme 1.3**.[15] Here, the bulky adamantyl *N*-substituents prevent dimerisation.

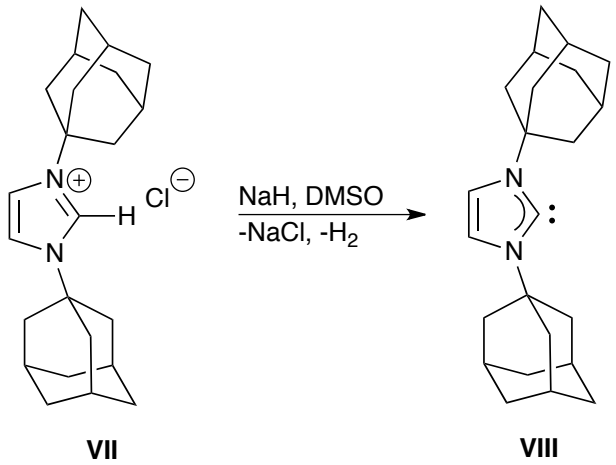

Scheme 1.3. Synthesis of the first stable free NHC **VIII**.[15]

1.1.2 Steric and Electronic Parameters of NHC Complexes

Despite being initially considered to be phosphine mimics due to their strong σ-donating properties, NHCs have become ubiquitous in transition metal chemistry.

[16][17][18][19] NHCs form short, strong bonds to transition metals which are less labile than metal-phosphine bonds rendering the complexes more oxidatively and thermally stable.[20]

NHCs are finding use as replacements for phosphine ligands in transition metal complexes used in homogenous catalysis.[21][22][20] For example, replacement of a phosphine ligand in Grubbs first generation alkene metathesis catalyst **IX**, **figure 1.4**, with an NHC to form the second generation catalyst **X**, **figure 1.4**, results in 10^4 times increase in reaction rate as well as a wider substrate scope.[23][24][25][26][27] The complexes **XI** and **XII**, **figure 1.4**, show high Z-selectivity in alkene metathesis reaction.[28][29]

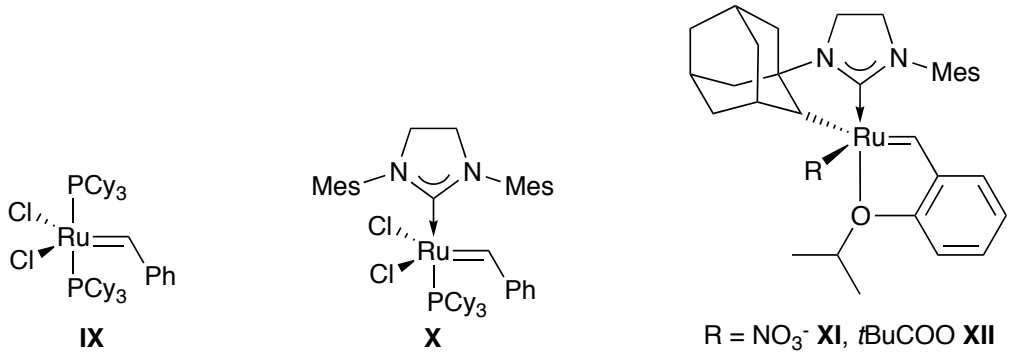

Scheme 1.4. Grubbs first **IX** and second generation **X** - **XII** alkene metathesis catalysts.

Additionally, replacement of a phosphine ligand by an NHC has also improved the activity of many palladium catalysed cross coupling reactions.[30][31][32][33]

Electronic parameters

Much has been written about the electronic nature of NHCs.[34][35] NHCs are strong σ-donating Lewis basic ligands. By synthesising a range of [(NHC)Ir$(CO)_2$Cl] complexes, Nolan *et al.* determined the electron-donating strength for a range

of different NHCs by measuring the carbonyl stretching frequency by FTIR spectroscopy. It was concluded that NHCs are more strongly donating ligands than the most strongly donating tertiary phosphines, whilst there is little variation in the donating strength between NHCs.[36] What differences there are between the NHCs is thought to be a result of the steric bulk of the N-substituents. Comparisons between NHCs with saturated and unsaturated backbones show that there was little difference between the two types, but NHCs with saturated backbones are slightly more electron donating.[36][37][38] Furthermore, replacing the hydrogens on the backbone with chlorines results in significant weakening of the NHC electron-donation strength.[36]

As the carbenic carbon has a vacant p_π orbital, π-backbonding from the metal centre to the NHC ligand is possible. Meyer and coworkers synthesised the group 11 complexes of the tripodal NHC ligand 1,1,1-[tris(3-methylimidazole-2-ylidene)methyl]ethane ([TIME^{Me}]) and determined their electronic structures by DFT. It was found that, in these complexes, π-backdonation accounted for 15-30% of the overall orbital interaction energies.[39] It has also been calculated that NHCs can π-donate electron density into the d-orbitals of coordinated transition metal centres.[40][41] By synthesising a range of model NHC complexes with zero to ten d-electrons, Cavallo and coworkers determined the contributions to bonding due to π-donation and π-backbonding. It was found that complexes with a low number of d-electrons have contributions from both π-donation and π-backbonding while π-backbonding dominates in complexes with a high number of d-electrons.[42]

Bonding in the uranium(III)-NHC complex **XIII** has been studied by Meyer *et al.*, **figure 1.4**. Calculations show that there is π-backbonding from an f-type orbital on the uranium centre into a π-type orbital on the NHC.[43]

On the other hand, DFT calculations suggest that bonding between NHCs and lanthanides is due to σ-donation. Analysis of the bonding between $SmCl_3$ and a

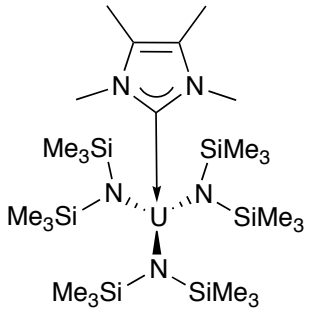

XIII

Figure 1.4. Meyer's uranium(III) NHC complex.[43]

range of model NHCs shows that it is primarily due to σ-donation with negligible π-backdonation.[44] Furthermore, in a competition reaction between $[U(C_5H_4tBu)_3]$ and $[Ce(C_5H_4tBu)_3]$ the NHC ligand, (1-C{NMeCMeCMeNMe}), binds exclusively to the uranium complex, **equation 1.1**.[45]

$$U(C_5H_4tBu)_3 + Ce(C_5H_4tBu)_3 \xrightarrow{NHC} [U(C_5H_4tBu)_3NHC] + Ce(C_5H_4tBu)_3 \quad (1.1)$$

Calculations show that there is π-backdonation in the uranium-NHC complex whilst no interaction exists between the cerium centre and the NHC. However, it was noted that the NHCs preference for uranium is a a subtle combination of a number of factors.[46]

Steric parameters

The sterics of the *N*-substituents can have a significant effect on the structure of NHC complexes.[34][47] Typically, bis(NHC) complexes adopt a *trans*, co-planar geometry but altering the steric bulk of the *N*-substituents can lead to distortions. The *N*-substituents of the nickel NHC complex **XIV**, **figure 1.5**, are small and the two C_3N_2 rings lie on the same plane - the dihedral angle is 0.00° - and perpendicular to the I-Ni-I axis.[48] Increasing the steric bulk by using 2,6-diisopropylphenyl

(Dipp) *N*-substituents, **XV**, **figure 1.5**, causes the linearly arranged NHCs to tilt out of the planar arrangement resulting in a N-$C_{carbene}$-$C_{carbene}$-N dihedral angel of 40.92°.[49]

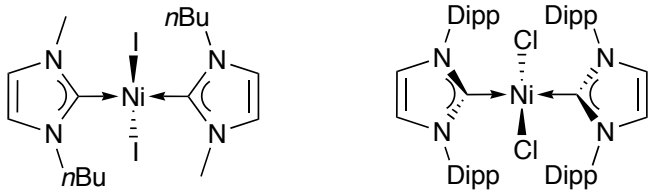

XIV **XV**

Figure 1.5. The effect of increasing the steric bulk of the *N*-substituents.[48][49]

There are examples of NHC complexes adopting a *cis* conformation, though a bidentate bis(NHC) ligand is required, **XVI** and **XVII**, **figure 1.6**.[50][51][52]

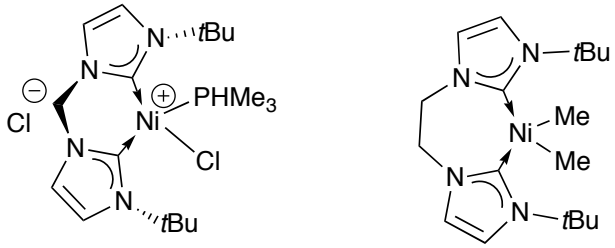

XVI **XVII**

Figure 1.6. *Cis*-ligated bis(NHC) ligands.[50][51][52]

Interestingly, the steric bulk on the *N*-substituent can result in complexes which do not form the structure predicted by VSEPR theory. For example, VSEPR theory predicts that in [Si(I*i*Pr)Cl_4] (I*i*Pr = 1-C{N*i*PrCHCHN*i*Pr}) the NHC should bind axially, **XVIII figure 1.7**.[53] This is due to the electron withdrawing nitrogen atoms of the NHC making the effective electronegativity of the carbeneic carbon greater than that if the chlorine atoms and therefore the NHC should bind axially.[54][47] However, due to clashing between the steric bulk of the *i*Pr groups

and the chlorine atoms, the NHC binds in an equatorial position, **XIX figure 1.7**.[55] A similar situation is observed in the sulfur-NHC complex [S(I*i*Pr)Cl_2].[54]

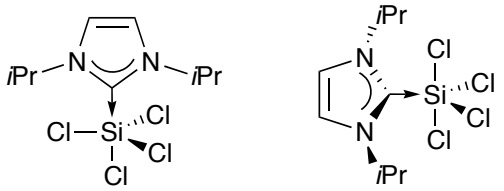

XVIII **XIX**

Figure 1.7. VSEPR predicted structure of [Si(I*i*Pr)Cl_4], **XVIII**, and the actual structure, **XIX**.

1.2 Rare Earth NHC Complexes

The use of neutral NHCs donor-ligands for rare earth and actinide metals is not common as there is a mismatch between the soft carbene and the hard Lewis acidic metal centre often resulting in the lability of the NHC.[56][57][58] In order to retain the NHC within the coordination sphere of the metal, anionic oxygen[59] **XX** or nitrogen[60][61] **XXI** tethers are commonly employed, **figure 1.8**. There are also examples of NHCs with anionic Cp[62] **XXII**, indenyl[63] **XXIII** and fluorenyl[64] **XXIV** tethers, **figure 1.8**, though these are less common.

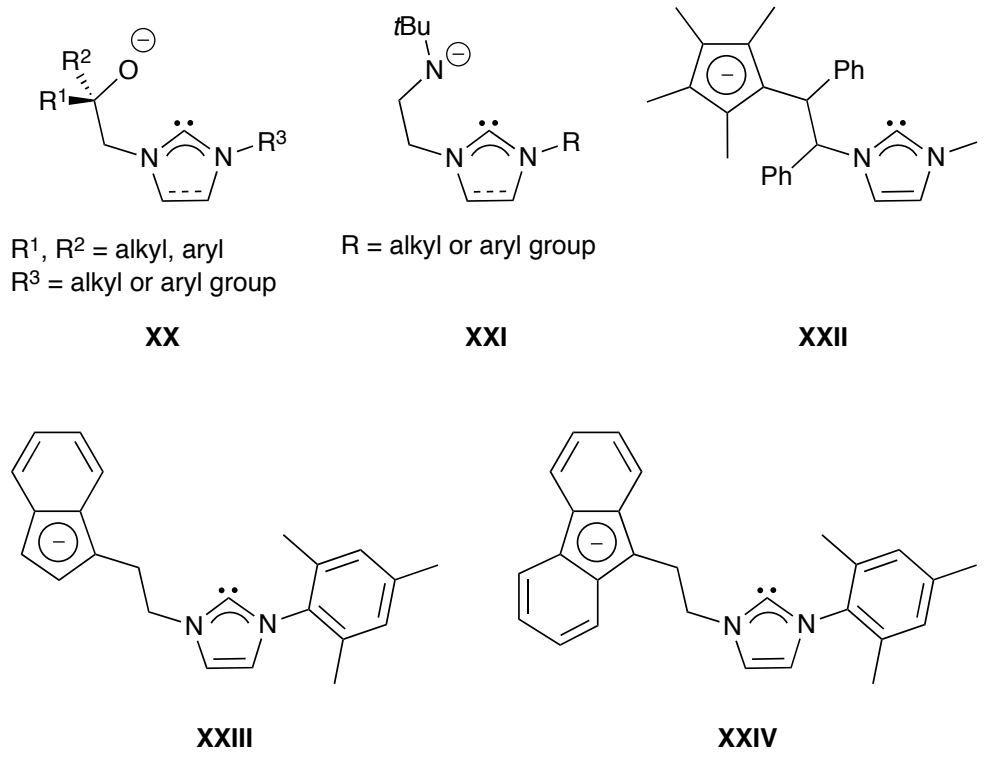

Figure 1.8. NHCs with anionic tethers.

1.2.1 Scandium(III)-NHC complexes

The indenyl[63] and fluorenyl[64] tethered NHC supported scandium(III)-alkyl complexes, **XXV** and **XXVI figure 1.9**, have been reported by Cui and coworkers. Both complexes were synthesised by the deprotonation reaction between HL (**figure 1.9**) (L = $C_9H_7CH_2CH_2$(1-C{NCHCHNMes}) and $C_{13}H_7CH_2CH_2$(1-C{NCHCHNMes})) and the scandium tris-alkyl complex, [Sc(CH_2Si Me_3)$_3$(THF)$_2$]. Both complexes adopt a pseudo-tetrahedral geometry while the ^{13}C NMR spectrum of **XXV** has a resonance due to $C_{carbene}$ at 188.01 ppm, a similar resonance to the $C_{carbene}$ resonance of **XXVI** of 187.64 ppm. The Sc-$C_{carbene}$ bond lengths are also similar at 2.350(3) Å for **XXV** and 2.343(4) Å for **XXVI**. While neither complex displays any reactivity to isoprene polymerisation,[64] **XXVI** does

catalyse the copolymerisation of ethene with 1-hexene or 1-octene to form random copolymers when activated with AliBu$_3$ and [Ph$_3$C][B(C$_6$F$_4$)$_3$].[65]

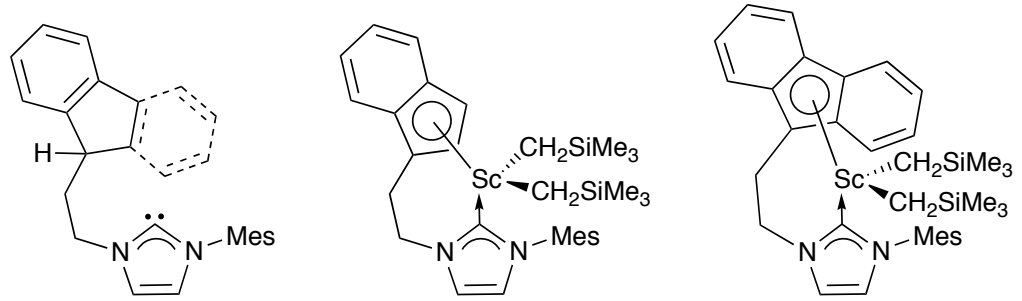

Figure 1.9. Indenyl, **XXV**,[63] and fluorenyl, **XXVI**,[64] tethered scandium NHC complexes

Cui and coworkers have also synthesised the scandium dibromide *bis*(NHC) pincer complex as the THF solvate, **XXVII scheme 1.5**.[66] The complex was generated *in situ* by mixing the pro-ligand H$_2$LBr$_3$, **scheme 1.5**, (H$_2$LBr$_3$ = 2,6-(1-C{NCHCHNMes})$_2$-1-Br-C$_6$H$_3$·2HBr) with ScCl$_3$ and adding three equivalents of nBuLi. The reaction is unusual in that the dibromide rather than the expected dichloride salt was isolated. The scandium centre adopts a square-bipyramidal geometry with the tridentate ligand bound equatorially and the two NHC groups arranged *anti* to one another. The resonance due to the C$_{\text{carbene}}$ occurs at 197.41 ppm on the ^{13}C NMR spectrum. The Sc-C$_{\text{carbene}}$ bond lengths of **XXVII** are longer than those of **XXV** and **XXVI** at 2.397(8) and 2.383(8) Å.

The scandium tris(alkoxy tethered NHC) complex [Sc(L$^{i\text{Pr}}$)$_3$], **XXVIII figure 1.6**, (L$^{i\text{Pr}}$ = OC(Me)$_2$CH$_2$(1-C{NCHCHN}iPr)), was prepared by Arnold and coworkers.[67] **XXVIII** was prepared by the salt elimintion reaction between three equivalents of [K(L$^{i\text{Pr}}$)] and [ScCl$_3$(THF)$_2$], **figure 1.6**. The ^{1}H NMR spectrum shows that, at room temperature, there is a fluxional process between free and

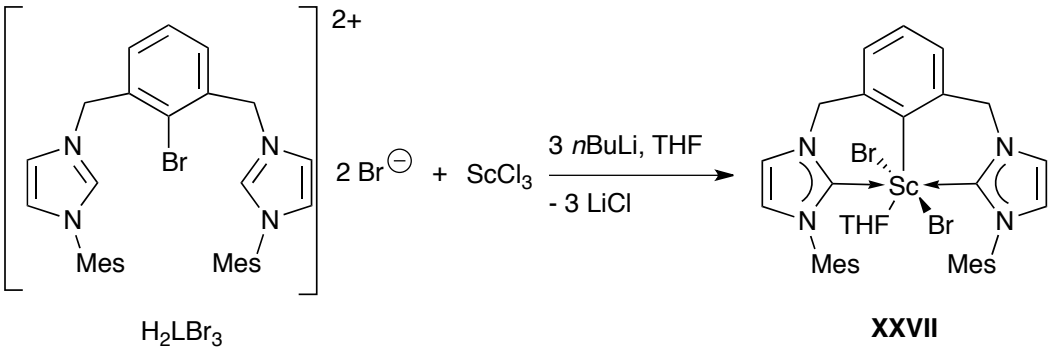

Scheme 1.5. Synthesis of the scandium pincer complex **XXVII**.[66]

bound carbenes while cooling to 233 K two ligand resonances occur in a 2:1 ratio corresponding to two bound carbenes and one free carbene. Further cooling to 203 K shows three inequivalent ligand resonances indicating the ligands are *meridinally* aligned. The ^{13}C NMR spectrum, at 298 K, shows the resonance due to the $C_{carbene}$ at 195.2 ppm. The *mer* orientation for the ligands was confirmed by single crystal x-ray diffraction and the Sc-$C_{carbene}$ bond lengths were determined to be in the range of 2.411(3) to 2.495(3) Å with an average distance of 2.436 Å.

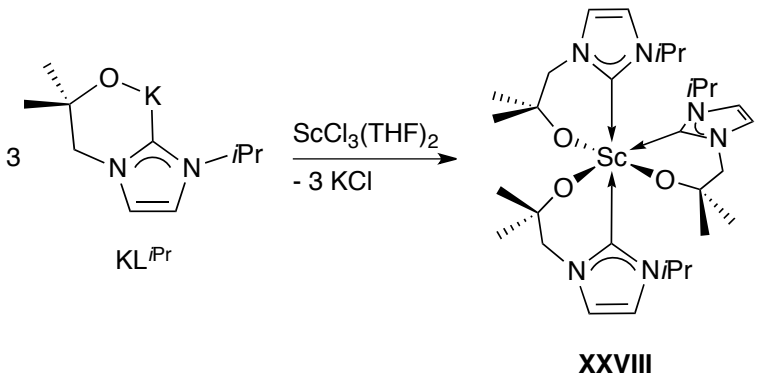

Scheme 1.6. Synthesis of the scandium alkoxy tethered NHC complex **XXVIII**.[67]

Exposure of **XXVIII** to 1 atm of CO_2 leads to the addition of CO_2 across the three Sc-$C_{carbene}$ bonds to form a polymeric product with the formula $[Sc(OCMe_2CH_2(1\text{-}O_2CC\{NCHCHN\textit{i}Pr\}))_3]_n$.[67] Treatment of **XXVIII** with one equivalent of CS_2 lead to the formation of the square pyramidal complex **XXIX**, **figure 1.10**, where CS_2 has added across a single Sc-$C_{carbene}$ bond.[67] Interestingly, the NHC ligated CS_2 molecule does not coordinate to a scandium centre despite being formally anionic. Addition of two or more equivalents of CS_2 to **XXVIII** leads to the formation of **XXX**, **figure 1.10**, where CS_2 adds across two Sc-$C_{carbene}$ bonds. Unusually, even with an excess of CS_2 addition across all three Sc-$C_{carbene}$ bonds was not observed.[67] Furthermore, addition of one equivalent of pyrrole resulted in the formation of the pyrrole adduct $[Sc(L^{iPr})_3{\cdot}HNC_4H_4]$ **XXXI**, **figure 1.10**, where the pyrrole N-H hydrogen bonds to the oxygen of one alkoxy tether.[68]

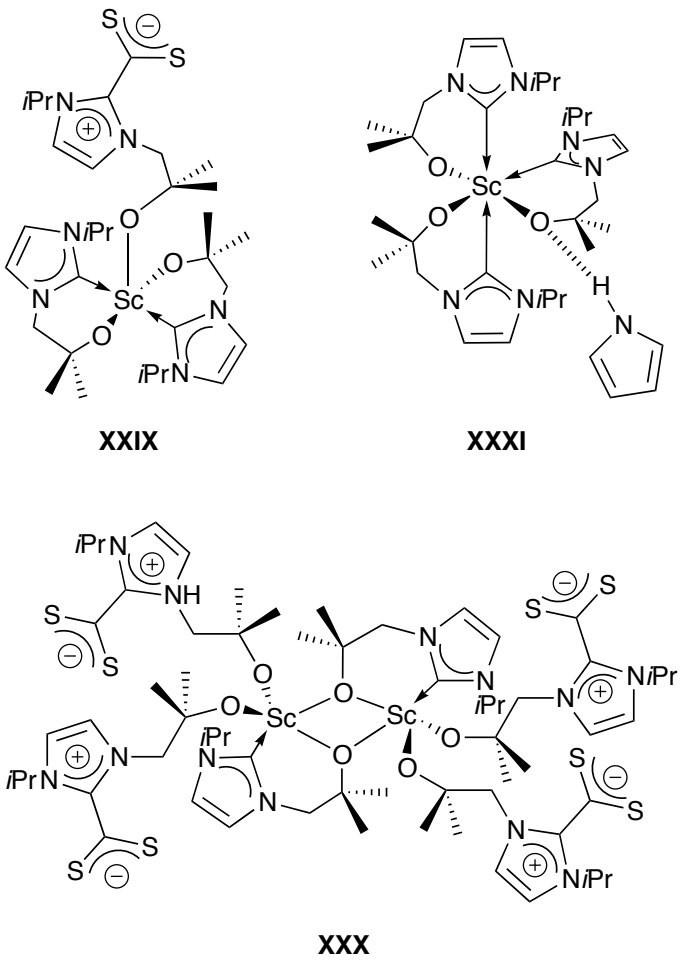

Figure 1.10. Structures of scandium-NHC complexes **XXIX**,[67] **XXX**[67] and **XXXI**.[68]

The scandium alkyl NHC adducts $[(Me_3SiCH_2)_3Sc(1\text{-}C\{N(2,6\text{-}C_6H_3Me_2)CH\}_2)]$ **XXXII** and $[(Me_3SiCH_2)_3Sc(1\text{-}C\{NDippCH\}_2)]$ **XXXIII**, **figure 1.11**, have been reported by Lu and coworkers. Both complexes, when treated with two equivalents of $[Ph_3C][B(C_6F_5)_4]$ display catalytic reactivity for the polymerisation of 1-hexene, 1-octene and 1-decene and **XXXII**, again when treated with two equivalents of $[Ph_3C][B(C_6F_5)_4]$, is also an excellent catalyst for the copolymerisation of 1-hexene with 1,5-hexadiene.[69]

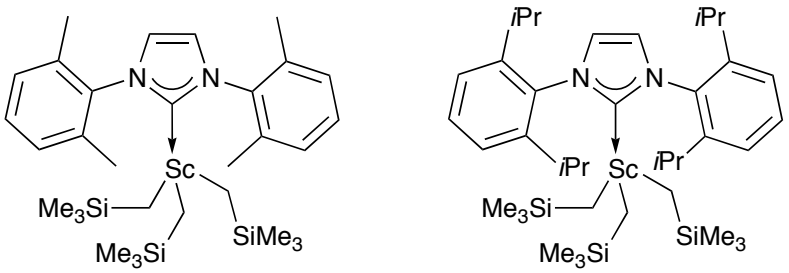

XXXII **XXXIII**

Figure 1.11. NHC adduct of $[Sc(CH_2SiMe_3)_3]$ **XXXII** and **XXXIII**.[69]

1.2.2 Yttrium(III)-NHC complexes

A number of simple yttrium-NHC monoadducts have been reported, the first of which, $[Y(THD)_3(1\text{-}C\{NMeCMe\}_2)]$, **XXXIV figure 1.12**, (THD = tetramethylheptanedioate) was reported by Arduengo and coworkers in 1994.[70] Anwander and coworkers have also reported the monoadduct yttrium-NHC complexes $[Y(N\{SiMe_3\}_2)_3(1\text{-}C\{NMeCH\}_2)]$ **XXXV** and $[Y(N\{SiHMe_2\}_2)_3(1\text{-}C\{NMeCH\}_2)]$ **XXXVI** as well as the bisadduct $[Y(N\{SiHMe_2\}_2)_3(1\text{-}C\{NMeCH\}_2)_2]$ **XXXVII**, **figure 1.12**.[71] The ^{13}C NMR spectra of **XXIV**, **XXVI** and **XXVII** show similar resonances due to the $C_{carbene}$ at 194.26, 190.3 and 194.0 ppm, respectively. No value was reported for **XXXV**.

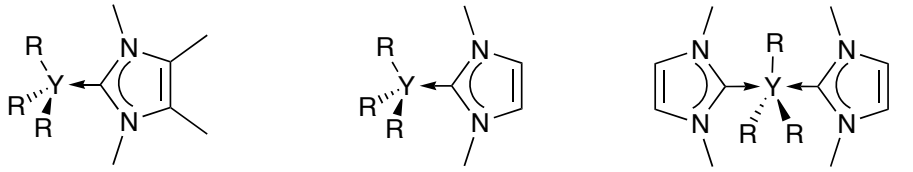

XXXIV
R = *t*BuC(O)CHC(O)*t*Bu

R = $N(SiMe_3)_2$ **XXXV**
R = $N(SiHMe_2)_2$ **XXXVI**

R = $N(SiHMe_2)_2$ **XXXVII**

Figure 1.12. The structures of the yttrium NHC adducts **XXXIV** - **XXXVII**.[70][71]

XXXVI and **XXXVII** were characterised by x-ray diffraction. In the solid

state **XXXVI** adopts a pentagonal bipyramidal geometry with a Y-$C_{carbene}$ bond length of 2.55(1) Å. **XXXVII** adopts a distorted trigonal bipyramidal geometry with an axial N-Y-N angle of 115.5(2)°. The two NHC ligands reside in the axial position with Y-$C_{carbene}$ bond lengths of 2.671(9) and 2.648(8) Å, longer than the Y-$C_{carbene}$ bond length of **XXXVII**.

The first amido-tethered yttrium NHC complex, **XXXVIII scheme 1.7** was prepared by our group by aminolysis reaction between $[Y(N\{SiMe_3\}_2)_3]$ and the lithium bromide adduct of the pro-ligand $[(HL)\cdot LiBr]_2$, **scheme 1.7**, accompanied by the loss of LiBr and $HN(SiMe_3)_2$.[60]

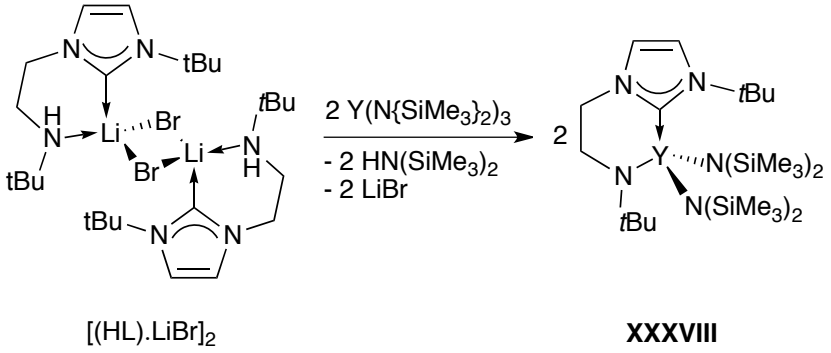

Scheme 1.7. Synthesis of the first yttrium complex supported by an amido-tethered NHC, **XXXVIII**.[60]

XXXVIII is monomeric, with the yttrium(III) centre adopting a distorted tetrahedral geometry. The $C_{carbene}$ resonance occurs as a doublet at 186.28 ppm on the ^{13}C NMR spectrum while the Y-$C_{carbene}$ bond length is 2.501(5) Å. **XXXVIII** shows catalytic reactivity in the polymerisation of lactide.[72] Acting as bifunctional catalyst, the labile carbene attacks the metal coordinated monomer followed by coordination insertion polymerisation of the rest of the lactide monomer, **scheme 1.8**.

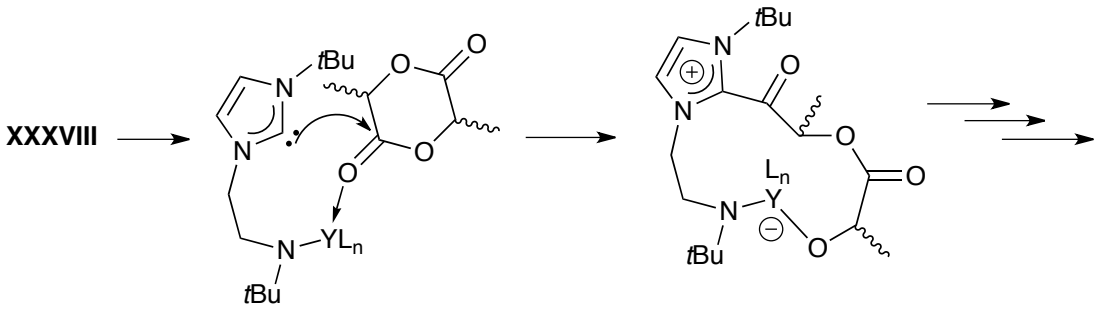

Scheme 1.8. Reaction mechanism for the polymerisation of lactide by **XXXVIII**.[72]

Treatment of **XXXVIII** with potassium naphthalenide, $KC_{10}H_8$, in ethereal solvent yields the heterobimetallic yttrium\potassium complex **XXXIX**, **scheme 1.9**.[73] In **XXXIX**, a backbone carbon has been deprotonated to form an abnormal NHC (aNHC) which is bound to the yttrium centre whilst the normal NHC binds to the potassium ion. Overall the structure is dinuclear through an interaction between the aNHC and the potassium cation of a second molecule. The ^{13}C NMR spectrum shows the resonance due to the $C_{carbene}$ at 199.22 ppm a significant shift from the chemical shift of **XXXVIII** of 186.28 ppm. The resonance due to the C_{aNHC} occurs at 167.52, significantly lower than typical yttrium bound $C_{carbene}$ resonances. The tetrahedral yttrium centre has a Y-C_{aNHC} bond length of 2.447(2) Å, significantly shorter than the Y-$C_{carbene}$ bond lengths previously discussed.

Subsequent addition of trimethylsilyl chloride, Me_3SiCl, to **XXXIX** forms the monomeric ytrrium-NHC complex **XL**, **scheme 1.9**, with the formation of a new backbone C-$SiMe_3$ bond accompanied by the elimination of KCl. The carbenic carbon of **XL** resonates at a significantly lower chemical shift compared to that of **XXXVIII**: 172.73 ppm *c.f.* 186.28 ppm.[73]

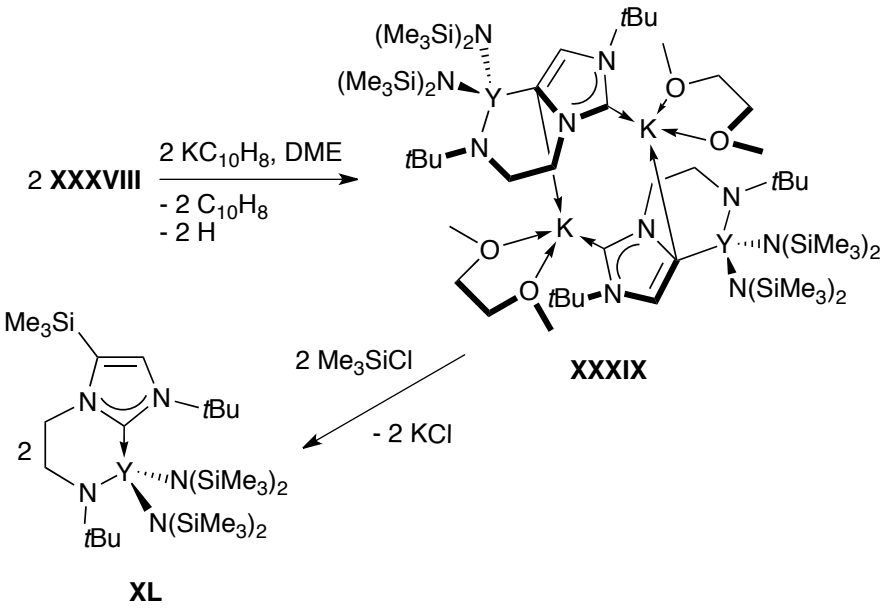

Scheme 1.9. Synthesis of **XXXIX** and **XL**.[73]

The homoleptic yttrium tris(alkoxy-tethered NHC) complex $[Y(L^{iPr})_3]$ **XLI**, **scheme 1.10**, was prepared by the salt elimination reaction between $[K(L^{iPr})]$ and $YCl_3(THF)_3$.[74]

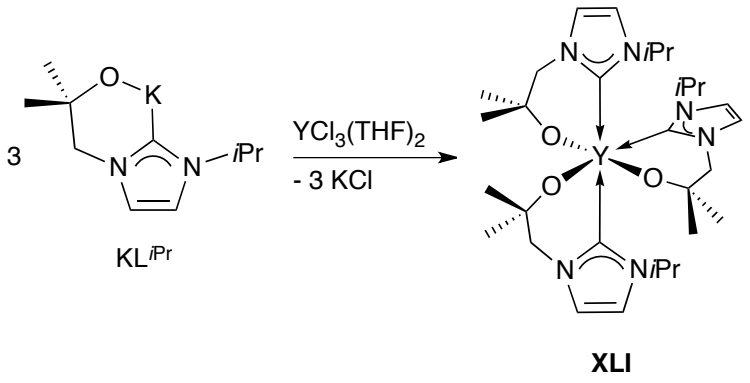

Scheme 1.10. Synthesis of the yttrium alkoxy-tethered NHC complex **XXVIII**.[74]

The $C_{carbene}$ resonance occurs at 197.3 ppm on the ^{13}C NMR spectrum, at the high end of the range of Y-$C_{carbene}$ chemical shifts of 186-194 ppm.[72][61][71][75] Like

the scandium analogue **XXVIII**, **scheme 1.6**, **XLI** adopts a *pseudo*-octahedral geometry about the metal centre with the bidentate ligands arranged in a *mer* geometry about the yttrium centre. The average Y-$C_{carbene}$ bond length is 2.588(12) Å, with a range of 2.561(4) to 2.644(4) Å.

The yttrium tris(aryloxy-tethered NHC) complex **XLII**, **scheme 1.11**, was prepared by Shen and coworkers.[76] By treating the proligand hydrochloride salt [HL·HCl] (**scheme 1.11**) with [LiY(N*i*Pr$_2$)$_4$] and two equivalents of *n*BuLi at −78°C, **XLII** was synthesised. However, if the same reaction was carried room temperature the yttrium-alkoxy NHC complex, **XLIII** was formed.

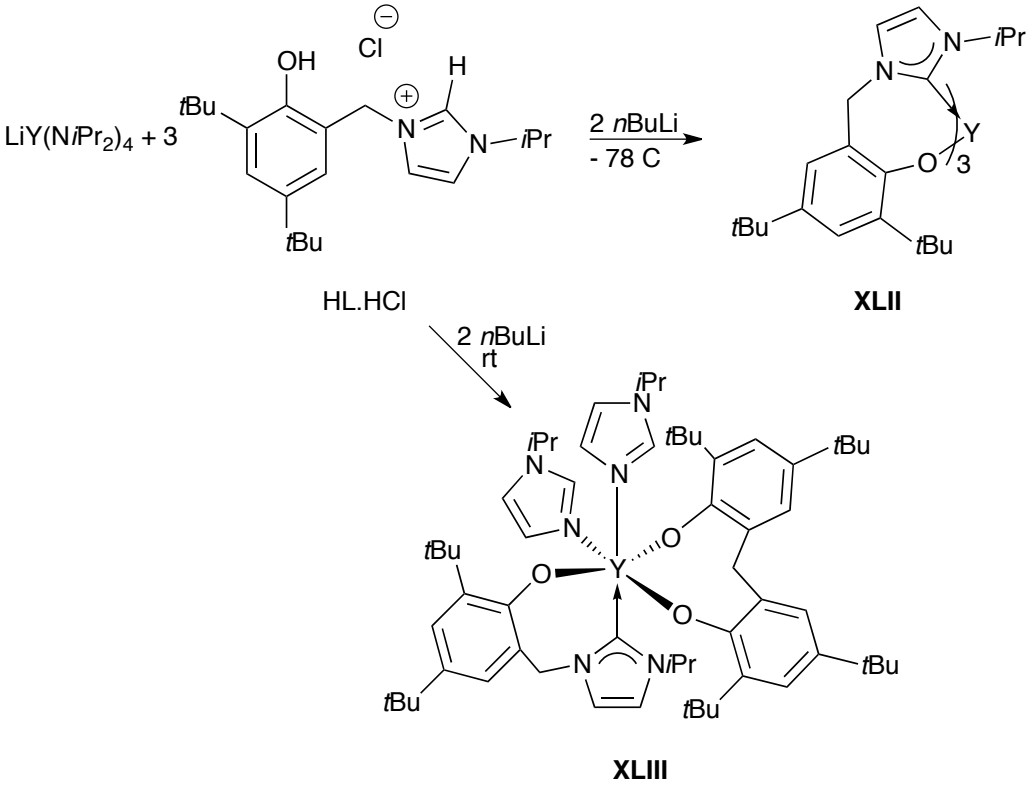

Scheme 1.11. Reactivity of HL.HCl with [LiY(N*i*Pr$_2$)$_4$] and *n*BuLi at −78°C to form **XLII** and at rt to form **XLIII**.[76]

The ^{13}C NMR spectrum of **XLII** shows the $C_{carbene}$ resonance at 199.9 ppm

on the ^{13}C NMR spectrum, a high chemical shift comparable with that of **XLI** of 197.3 ppm. X-ray diffraction studies revealed that **XLII** adopts a distorted octahedral geometry with the ligands in a *mer*-arrangement with Y-$C_{carbene}$ bond lengths in the range of 2.606(3) Å to 2.641(3) Å with an average length of 2.621 Å. **XLIII** results from the cleavage of imidazolium group of [HL·HCl] and subsequent formation of a diphenoxyl methane ligand with the complex adopting an octahedral geometry with the oxygen donor atoms adopting a *mer* arrangement. The $C_{carbene}$ resonates at 198.4 ppm on the ^{13}C NMR spectrum, a similar chemical shift to that of **XLII**, while the Y-$C_{carbene}$ bond distance is 2.576(5) Å, considerably shorter than those for **XLII**.

The interesting enol-functionalised NHC ligand supported yttrium complex **XLIV**, **scheme 1.12**, was prepared by Shen and coworkers.[77] In the first step [Y{N(SiMe$_3$)$_2$}$_3$] was prepared *in situ* between YCl_3 and four equivalents of [NaN(SiMe$_3$)$_2$] while addition of H_2LBr in the second step yielded **XLIV**.

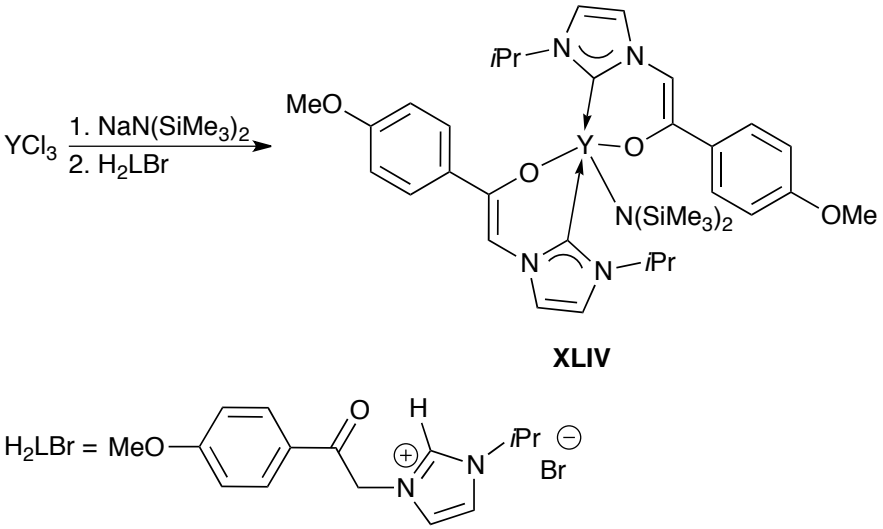

Scheme 1.12. Synthesis of the enol-tethered NHC yttrium comples **XLIV**.[77]

The ^{13}C NMR spectrum shows two $C_{carbene}$ resonances at 188.37 and 187.94 ppm. The five coordinate yttrium centre adopts a distorted trigonal bipyramidal

geometry with Y-$C_{carbene}$ bond lengths of 2.512(5) and 2.513(4) Å. **XLIV** proved to be a good catalyst for the addition of aniline to diisopropylcarbodiimide to form the guanidine **A**, **equation 1.2**, reaching > 99% yield in 3 h with 0.5 mol% catalyst loading.[77]

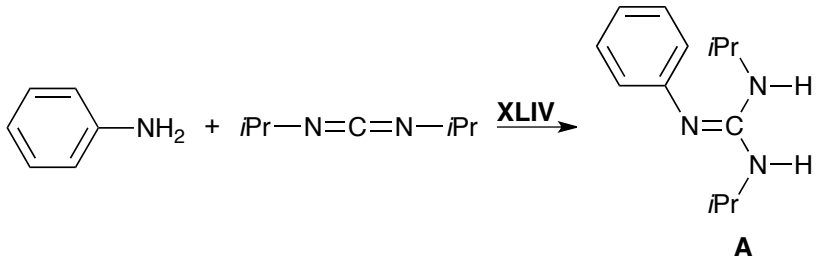

(1.2)

1.2.3 Cerium(III)-NHC complexes

Ephritikhine and coworkers have prepared the cerium(III)-NHC adducts [$(Cp^*)_2$CeI (1-C{NMeCMeCMeNMe})] **XLV** and [$(C_5H_4tBu)_3$Ce(1-C{NMeCMe})$_2$] **XLVI** by the addition of the free carbene (1-C{NMeCMe}$_2$) to [$(Cp^*)_2$CeI] and [$(C_5H_4tBu)_3$Ce], respectively, **figure 1.13**.[45]

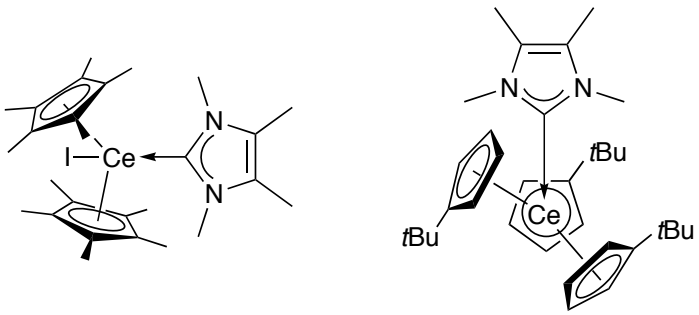

Figure 1.13. The cerium(III)-NHC adducts **XLV** and **XLVI** as prepared by Ephritikhine and coworkers.[45]

Both **XLV** and **XLVI** adopt a tetrahedral geometry with Ce-$C_{carbene}$ bond lengths of 2.72(4) Å and 2.797(4) Å, respectively.

The first cerium(III) complex supported by an amido-tethered NHC ligand was prepared in 2005.[78] [({Me_3Si}$_2$N)$_2$Ce(tBuN(CH$_2$)$_2$(1-C{NCHCHNtBu}))] **XLVII**, **scheme 1.13**, was prepared by the transamination reaction between [(tBuHN(CH$_2$)$_2$(1-C{NCHCHNtBu}))·LiBr] and [Ce(N{$SiMe_3$}$_2$)$_3$] with the loss of LiBr and HN($SiMe_3$)$_2$. Treatment of **XLVII** with LiI formed the iodide-bridged dimer [({Me_3Si}$_2$N)Ce(nBuN(CH$_2$)$_2$(1-C{NCHCHNtBu}))(μ-I)]$_2$ **XLVIII** with the loss of [LiN($SiMe_3$)$_2$].

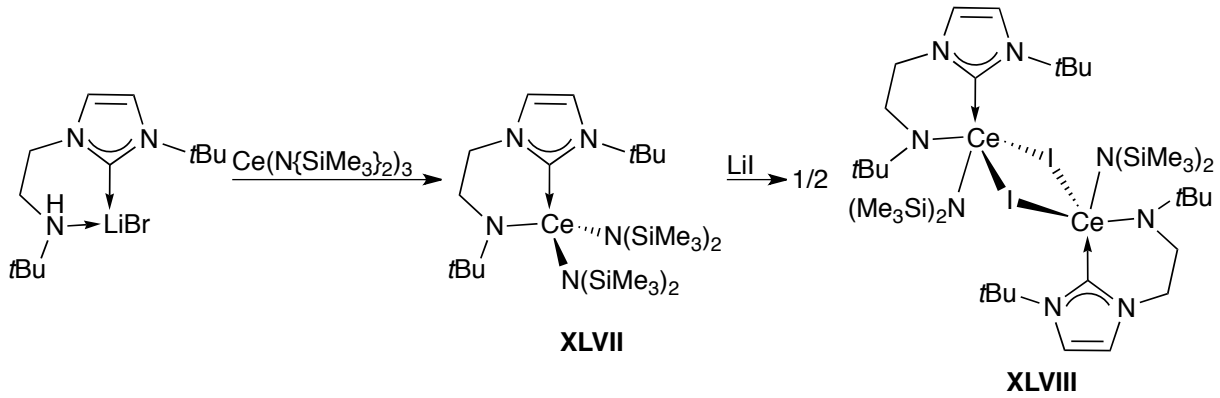

Scheme 1.13. Synthesis of the cerium(III) complex supported by an amido-tethered NHC ligand **XLVII** and its reactivity with LiI to form **XLVIII**.[78]

Complex **XLVII** adopts a tetrahedral geometry in the solid state with a Ce-$C_{carbene}$ bond length of 2.670(2) Å. Each cerium centre of **XLVIII** adopts a trigonal bipyramidal geometry constructed around the planar, transoid Ce_2I_2 four membered ring. The Ce-$C_{carbene}$ bond length is 2.700(3) Å, an elongation of the Ce-$C_{carbene}$ bond length of **XLVII** of 2.670(2) Å.

Cerium(III) complexes supported by alkoxy-tethered NHC ligands have been prepared by the Arnold group.[79] Treatment of [Ce(N{$SiMe_3$}$_2$)$_3$] with one equivalent of HL^{Dipp} (HL^{Dipp} = OCMe$_2$CH$_2$(1-CH{NCH$_2$CH$_2$NDipp})) yielded the tetra-

hedral complex [({Me_3Si}$_2$N)$_2$Ce(L^{Dipp})] **XLIX** (L^{Dipp} = $OCMe_2CH_2$(1-C{NCH_2CH_2NDipp})), **scheme 1.14**. The Ce-$C_{carbene}$ bond proved labile and able to heterolytically cleave E-X bonds (E = $SiMe_3$, PPh_2, Sn*n*Bu_3, BBN; X = Cl, I, N_3) to form the zwitterionic complexes **L**, **scheme 1.14**.

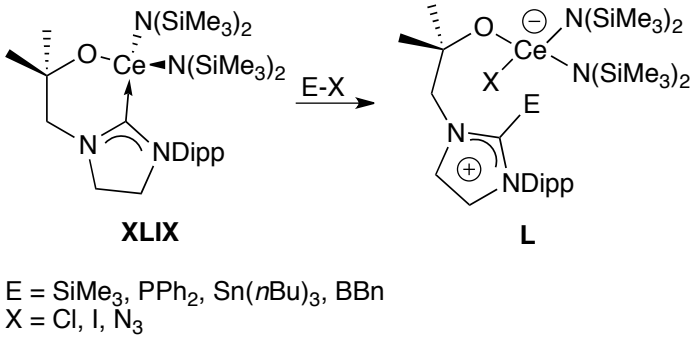

Scheme 1.14. Heterolytic cleavage of E-X by **XLIX**.[79]

Heating complex $\mathbf{L^{SiMe3}}$, **scheme 1.15**, results in the loss of $Me_3SiSiN(SiMe_3)_2$ and formation of [({Me_3Si}$_2$N)Ce(X)(L^{Dipp})] **LI** (X = Cl, I, N_3), which underwent ligand redistribution to form [({Me_3Si}$_2$N)$_2$Ce(L^{Dipp})] and [(X)$_2$Ce(L^{Dipp})]. Finally, **XLIX** could be reformed by the addition of [$KN(SiMe_3)_2$], resulting in the subsequent loss of KX.[79]

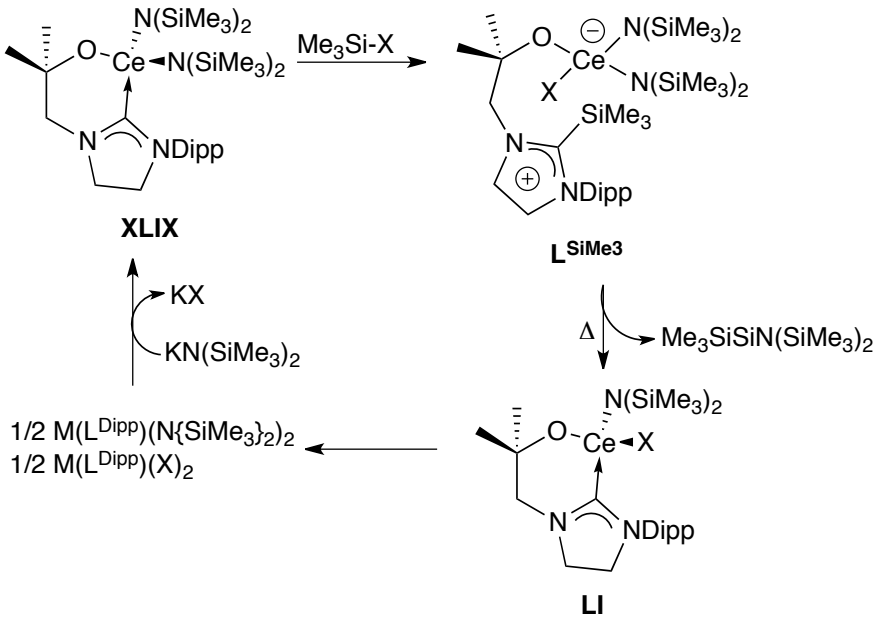

Scheme 1.15. The catalytic reactivity of **XLIX** in the formation of $Me_3SiSiN(SiMe_3)_2$.[79]

Additionally, the bis(NHC) cerium(III) complexes $[(\{Me_3Si\}_2N)Ce(OCMe_2CH_2(1\text{-}C\{NCH_2CH_2NR\}))_2]$ (R = Mes **LII**, Dipp **LIII**) have been prepared by the Arnold group from the protonolysis reaction between two equivalents of HL^R (R = Mes, Dipp) and $[Ce(N\{SiMe_3\}_2)]_3$, **scheme 1.16**.[80]

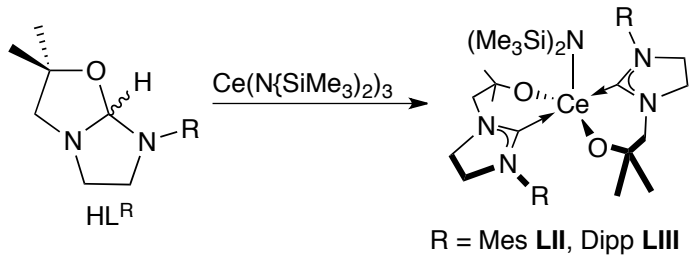

Scheme 1.16. Synthesis of the cerium(III) alkoxy-tethered NHC complexes **LII** and **LIII**.[80]

Both **LII** and **LIII** adopt a distorted trigonal bipyramidal geometry with the

carbene donor in the axial positions and a $C_{carbene}$-Ce-$C_{carbene}$ angle of 168.55(10)° for **LII** and a smaller $C_{carbene}$-Ce-$C_{carbene}$ angle of 128.19(9)° for **LIII** due to the steric bulk of the Dipp substituents. Also as a result of the steric bulk of the Dipp substituents the Ce-$C_{carbene}$ bond lengths of **LIII** are longer at 2.855(3) and 2.813(3) Å compared with those of **LII** of 2.786(4) and 2.798(4) Å.

1.2.4 Cerium(IV)-NHC complexes

Arnold and coworkers prepared the cerium(IV)-NHC complex [({Me_3Si}$_2$N)CeCl (L^{Dipp})] **LIV** from the oxidation of **XLIX** with Ph_3CCl with Gomberg's dimer ($Ph_3C(C_6H_5)CPh_2$) produced as a side product, **scheme 1.17**. Alternatively, **LIV** could also be synthesised from the reaction of the cerium(IV) starting material [Ce(N{$SiMe_3$}$_2$)$_3$Cl] and HL^{Dipp}, **scheme 1.17**.[81] This method proved higher yielding with a 67 % yield compared to a 34 % yield for the oxidation route.

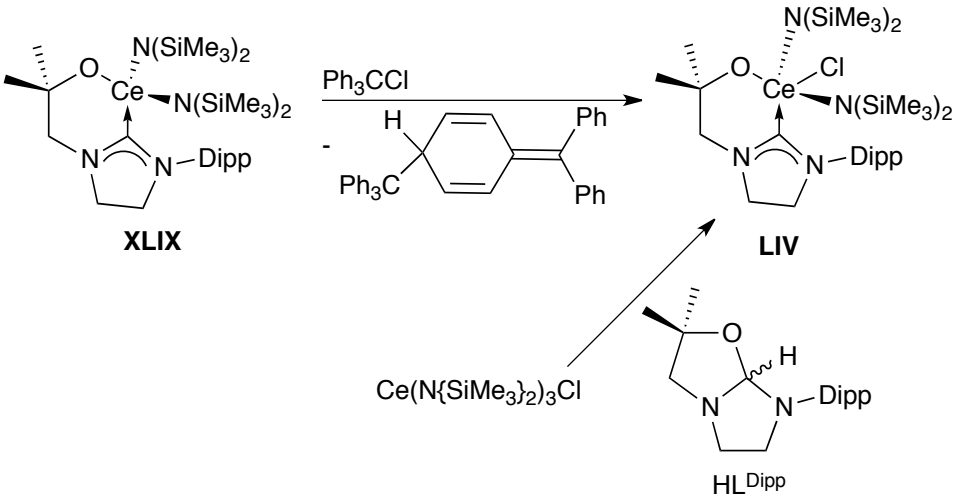

Scheme 1.17. The two possible methods for the synthesis of **LIV**.[81]

The ^{13}C NMR spectrum of **LIV** shows the resonance due to the carbenic carbon at 237.4 ppm, a high chemical shift for a carbene resonance.[81] In the solid

state the complex adopts a trigonal bipyramidal geometry with a Ce-$C_{carbene}$ bond length of 2.692(3) Å.

1.2.5 Neodymium(III)-NHC complexes

The neodymium complexes supported by alkoxy tethered NHC ligands **LV**[82] and **LVI**[77] have been reported by Shen and coworkers. **LV** was prepared from the reaction between two equivalents of H_2LBr and the neodymium amide *ate* complex [LiNd(N*i*Pr$_2$)$_4$], **scheme 1.18**. **LV** has an Nd-$C_{carbene}$ bond length of 2.717(3) Å. Attempts to prepare the mono(L) complex were unsuccessful, yielding only **LV**.[82]

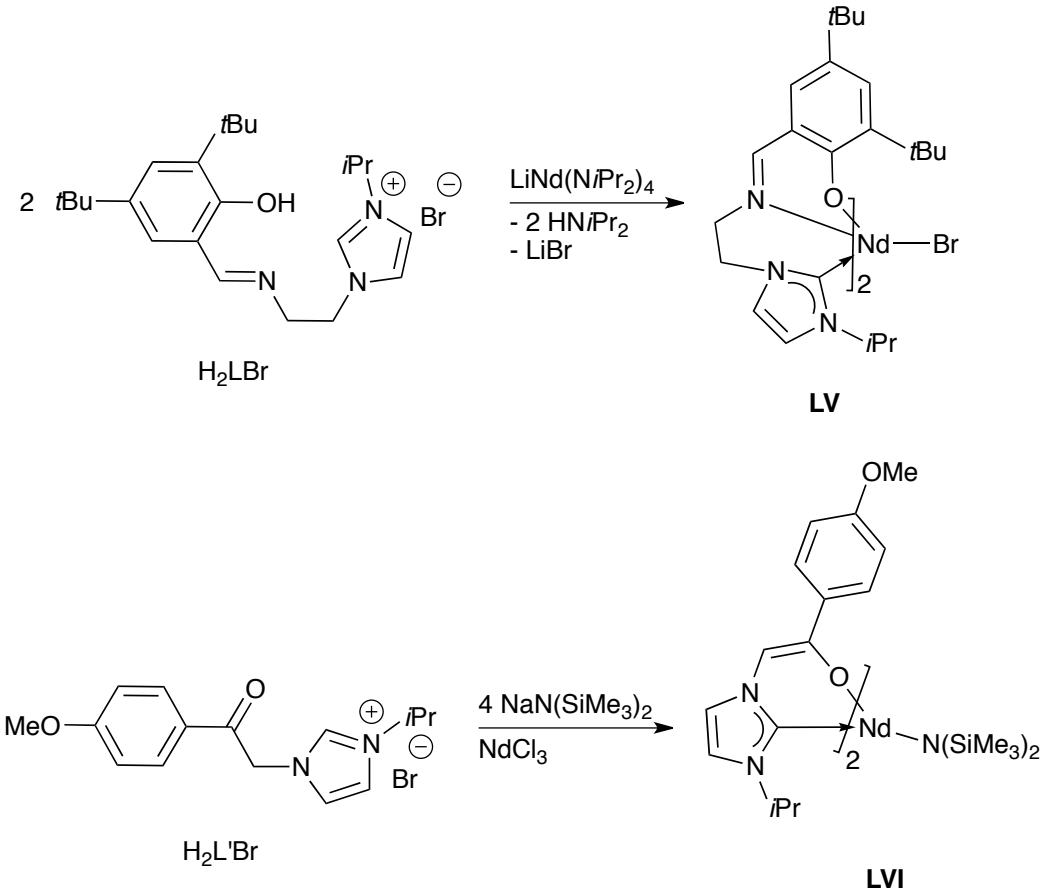

Scheme 1.18. Synthesis of the neodymium NHC complexes **LV**[82] and **LVI**.[77]

The enolate tethered neodymium NHC complex **LVI** was prepared from the reaction of $[Nd(N\{SiMe_3\}_2)_3]$, prepared *in situ*, and $H_2L'Br$, **scheme 1.18**. The Nd-$C_{carbene}$ bond lengths are shorter than those of **LV** at 2.619(4) and 2.624(4) Å.[77]

The Arnold group has prepared the amido tethered NHC supported neodymium complex **LVII**, **scheme 1.19**, from the transamination reaction[83] analogous to the synthesis of **XLVII** (**scheme 1.13**). **LVII** adopts a distorted tetrahedral geometry with a Nd-$C_{carbene}$ bond length of 2.609(3) Å. Treatment of **LVII** with Me_3SiI affords the dimeric product **LVIII**, where the C4 atom has been functionalised with a hydrogen atom being replaced by an Me_3Si group and two iodides bridge between the two neodymium centres.[83] There is also an elongation of the Nd-$C_{carbene}$ bond length from 2.609(3) Å in **LVII** to 2.656(5) Å in **LVIII**. Each Nd centre adopts a distorted trigonal bipyramidal geometry with the amido donors in the axial position and a Nd$\cdots$Nd separation of 5.010 Å. Addition of KC_8 reforms the monomeric neodymium bis(silylamide) NHC complex but now with a Me_3Si functionalised C4 atom on the NHC ring, **LIX**.[83] The Nd-$C_{carbene}$ bond length of **LIX** of 2.648(3) Å is of a similar length to **LVIII** and longer than that of **LVII**.

LVIII proved to be a very useful staring material for the exploration of the the chemistry of neodymium NHC complexes. Treatment of **LVIII** with [Ga(NDippCH)$_2$][K(TMEDA)] results in the formation of **LX**, the first *f*-element-gallium bond, **scheme 1.19**. The Nd-Ga bond is extremely long at 3.2199(3) Å while the Nd-$C_{carbene}$ bond length is 2.669(2) Å, similar to that of **LVIII** (2.656(5) Å). DFT calculations show that the Ga-Nd bond has a Wiberg bond order of 0.827 while a natural bond order analysis shows the bond is 87% Ga and 13% Nd in character and involves Nd $6s6p^{0.01}5d^{0.36}$ and Ga $4s4p^{1.67}$ hybrid orbitals, the latter corresponding to the sp^2 hybridisation of the Ga(I) center.[84]

Furthermore, the bridging iodides proved reactive toward salt elimination re-

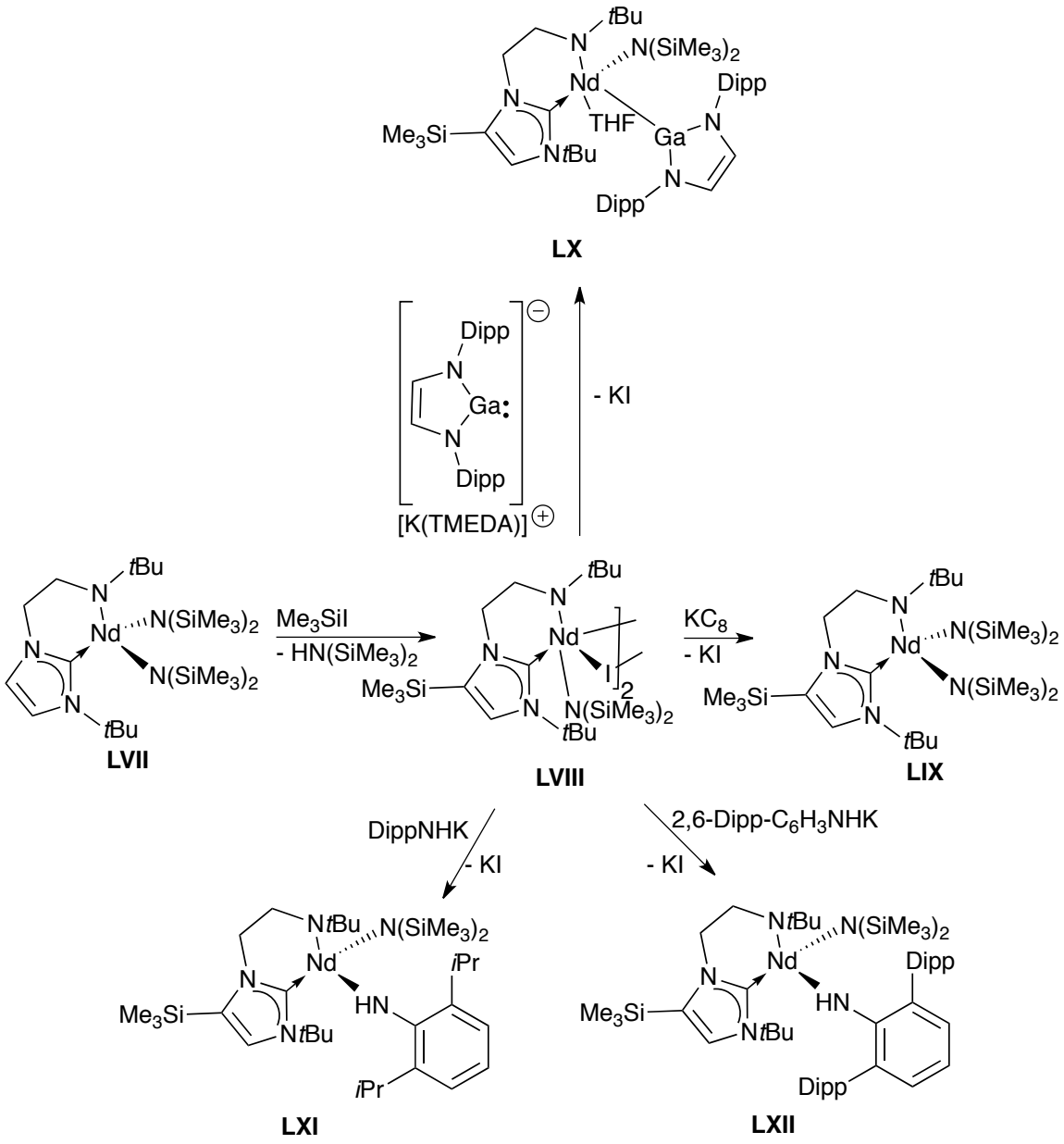

Scheme 1.19. Synthesis and reactivity of **LVIII**.[83][84][85]

actions. Treatment of **LVIII** with DippNHK results in the formation of **LXI**, a monomeric complex with three amido and one NHC donors, with the loss of one equivalent of KI, **scheme 1.19**. The similar complex **LXII** was prepared from

the salt-elimination reaction between **LVIII** and 2,6-Dipp-C_6H_3NHK, **scheme 1.19**.[85]

1.2.6 Samarium(II)-NHC complexes

The samarium(II)-NHC complexes reported in the literature are limited to the NHC adducts of $[Sm(Cp^*)_2]$ **LXIII**,[70] **LXIV**[70] and **LXV**,[86] **figure 1.14**, and $[Sm(C_5Me_4Et)_2]$ **LXVI**,[87] **figure 1.14**.

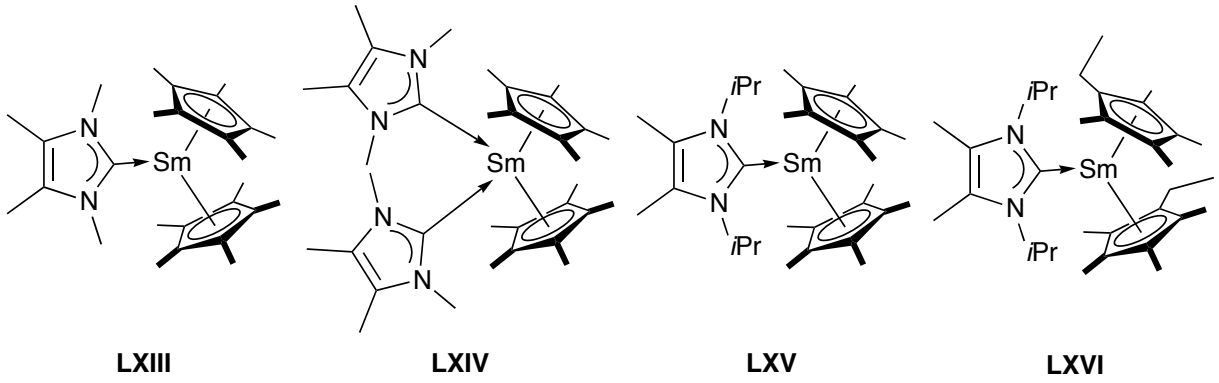

Figure 1.14. The samarium(II)-NHC adducts **LXIII** - **LXVI**.[70][86][87]

The Sm-$C_{carbene}$ bond lengths are 2.837(7) and 2.845(7) Å for **LXIV** and 2.5823(16) Å for **LXV**. **LXV** shows activity for the polymerisation of a range of methacrylate-type unsaturated monomers.[86]

1.2.7 Samarium(III)-NHC complexes

The Arnold group has prepared the samarium(III) amido tethered NHC complex $[NtBu(CH_2)_2$-(1-C{NCHCHN*t*Bu})Sm(N{$SiMe_3$}$_2)_2$] **LXVII** from the transamination reaction between $[HNtBu(CH_2)_2$(1-C{NCHCHN*t*Bu})·LiBr$]_2$ and Sm(N{Si Me_3}$_2)_3$, **scheme 1.20**.[60] **LXVII** adopts a distorted tetrahedral geometry with a Sm-$C_{carbene}$ bond length of 2.588(2) Å.

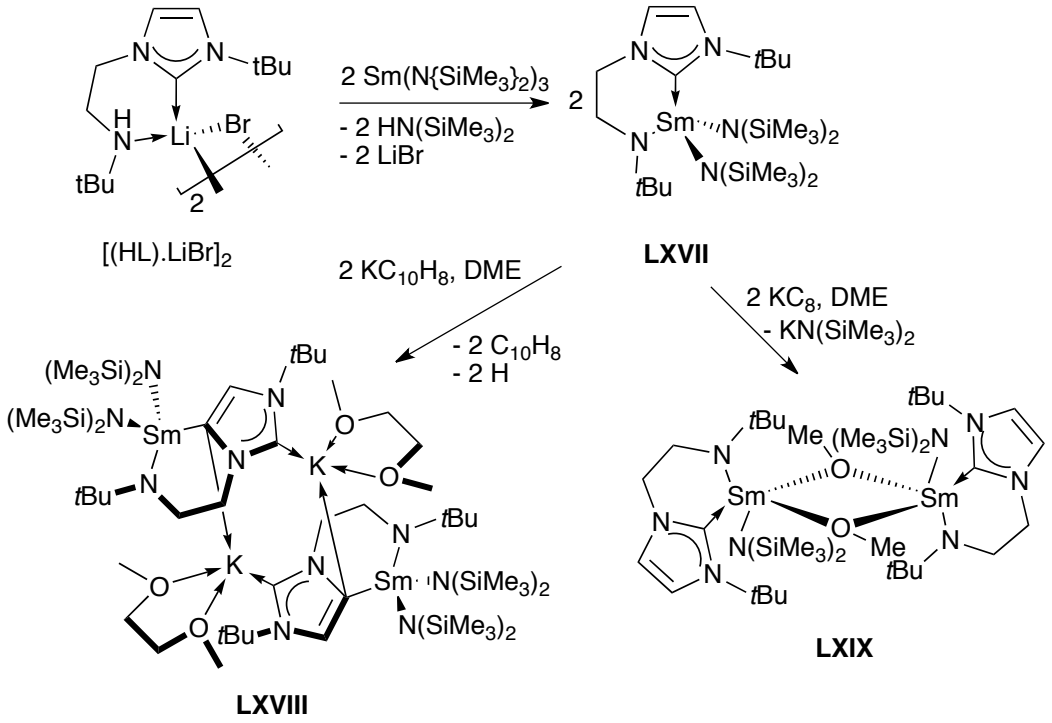

Scheme 1.20. Synthesis and reactivity of **LXVII**.[60][73]

Attempted reduction of **LXVII** with $KC_{10}H_8$ in DME did not afford a samarium(II) product. Instead the dimeric complex **LXVIII**, **scheme 1.20**, where the potassium cation was bound to the NHC and the samarium(III) centre was bound an aNHC, was isolated.[73] The samarium centre adopts a distorted tetrahedral geometry with a Sm-C_{aNHC} bond length of 2.509(3) Å and K-$C_{carbene}$ bond length of 2.954(4) Å. Similarly, the reaction of **LXVII** with KC_8 in DME did not afford a samarium(II) product, instead the dimeric samarium(III) complex **LXIX**, **scheme 1.20**, was isolated.[73] Here, the cleavage of a molecule of DME results in the formation of two methoxy groups which bridge between two samarium(III) centres with Sm-O bond lengths of 2.349(2) and 2.353(2) Å. The Sm-$C_{carbene}$ bond length was 2.682(3) Å.

Shen and coworkers have prepared the bis(phenoxy) tethered NHC samar-

ium(III) *ate* complexes **LXX** from the reaction between H_3LCl, $[Li(THF)Sm(N\mathit{i}Pr_2)_4]$ and 2 *n*BuLi and **LXXI** from H_3LCl, $[Sm\{N(SiMe_3)_2\}_3]$ and 3 $[Na\{N(SiMe_3)_2\}_3]$, **figure 1.15**.[88]

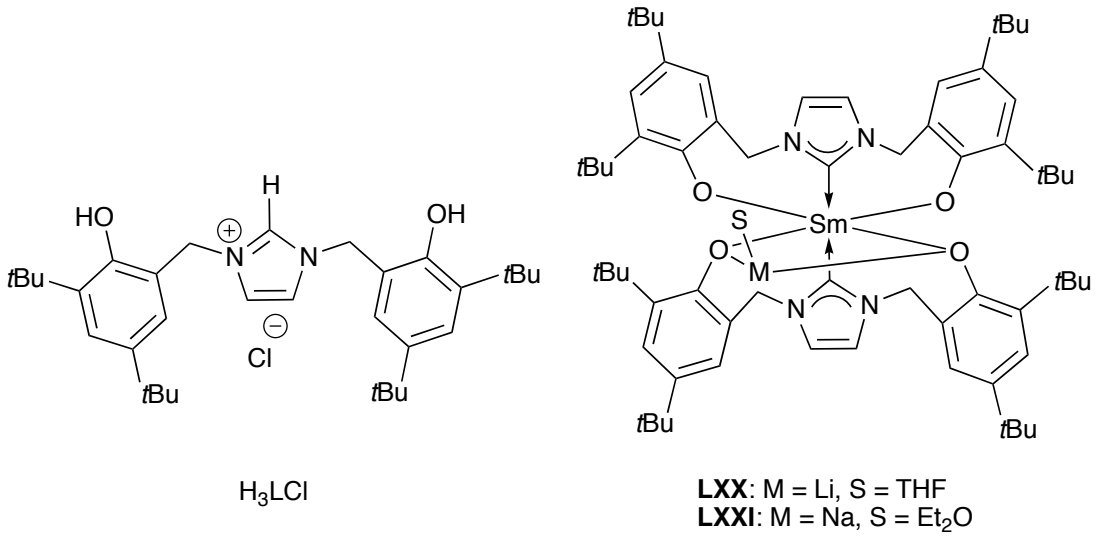

Figure 1.15. Structures of the aryloxide tethered NHC samarium(III) complexes **LXX** and **LXXI**.[88]

The samarium centre adopts a distorted octahedral geometry in both **LXX** and **LXXI** with the alkali metal counterion coordinated to two oxygen donors of a ligand. **LXX** has a Sm-$C_{carbene}$ bond length of 2.584(4) Å, while **LXXI** has a Sm-$C_{carbene}$ bond length of 2.601(3) Å.

1.2.8 Europium(III)-NHC complexes

Only two europium(III)-NHC complexes have been published in the literature. The first, $[(THD)_3Eu(1\text{-}C\{NMeCMe\}_2)]$ **LXXII scheme 1.21**, was prepared by Arduengo and coworkers from the addition of the free carbene $(1\text{-}C\{NMeCMe\}_2)$ to $[(THD)_3Eu]$.[70] **LXXII** adopts a pentagonal-bipyramidal geometry with the NHC ligand in an axial position and an Eu-$C_{carbene}$ bond length of 2.663(4) Å.

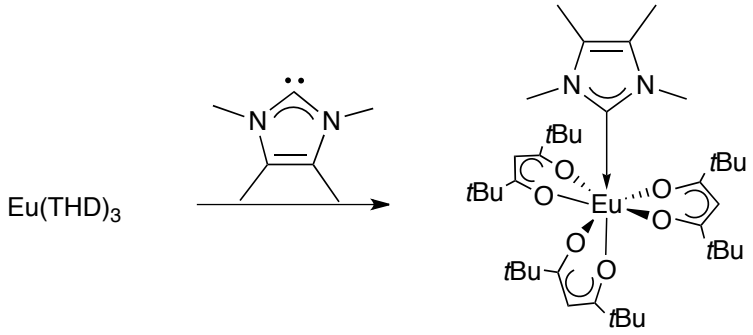

Scheme 1.21. Synthesis of the europium(III)-NHC complex **LXXII**.[70]

The second europium(III)-NHC complex reported was the CNC pincer complex $[C_6H_3Me\text{-}(1\text{-}C\{NCHCHNBn\})_2Eu(N\{SiMe_3\}_2)_2]$ **LXXIII** prepared by Zhu and coworkers in 2014.[89] **LXXIII** adopts a trigonal-bipyramidal geometry with the ligand in a *mer* arrangement and Eu-$C_{carbene}$ bond lengths of 2.552(9) and 2.575(8) Å. **LXXIII** proved to be a good catalyst for the addition of terminal alkynes to carbodiimides to form propiolamidines and tolerated a range of functional groups with yields of 70 to 95 %, **scheme 1.22**.[89]

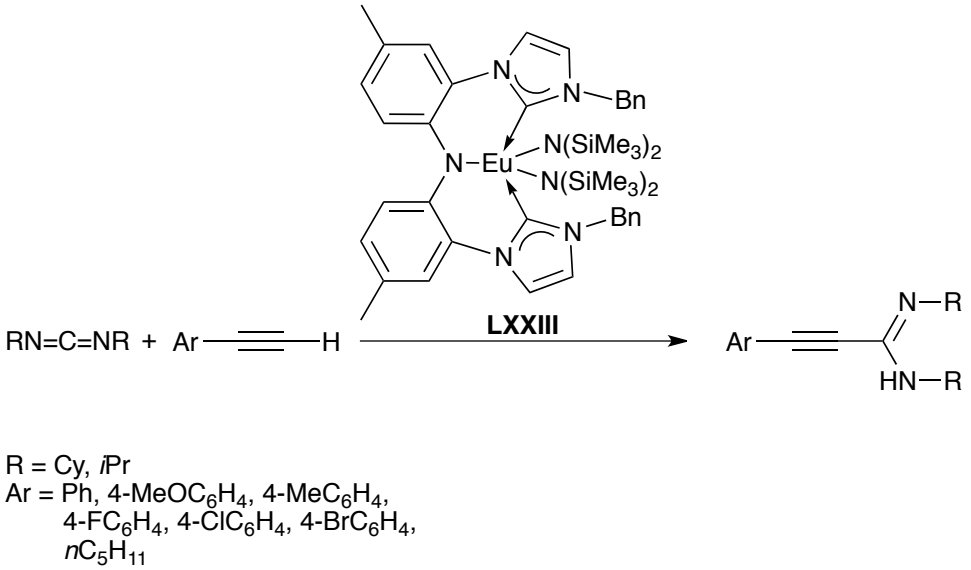

Scheme 1.22. The structure of **LXXIII** and its reactivity as a catalyst for the synthesis of propiolamidines from alkynes and carbodiimides.[89]

1.2.9 Gadolinium(III)-NHC complexes

The only gadolinium(III)-NHC complex reported is the bis(NHC) pincer complex [(2,6-(1-C{NCHCHNMes})$_2$-C$_6$H$_3$)GdBr$_2$(THF)] **LXXIV**, **scheme 1.23**, reported by Lv and Cui in 2010.[90] **LXXIV** was prepared by mixing the proligand [2,6-(1-C{NCHCHNMes})$_2$-1-Br-C$_6$H$_3$)·2HBr], L·2HBr **scheme 1.23** and GdCl$_3$ and adding three equivalents of *n*BuLi.

The gadolinium centre adopts a distorted octahedral geometry with the ligand bound in a *mer*-arrangement and the two NHC groups in an *anti* arrangement with Gd-C$_{\text{carbene}}$ bond lengths of 2.569(10) and 2.579(10) Å. **LXXIV** shows high activity and *cis*-1,4 selectivity (> 97%) for the polymerisation of isoprene when activated with AlR$_3$ (R = Me, Et, *i*Bu) and [Ph$_3$C][B(C$_6$F$_5$)$_4$].

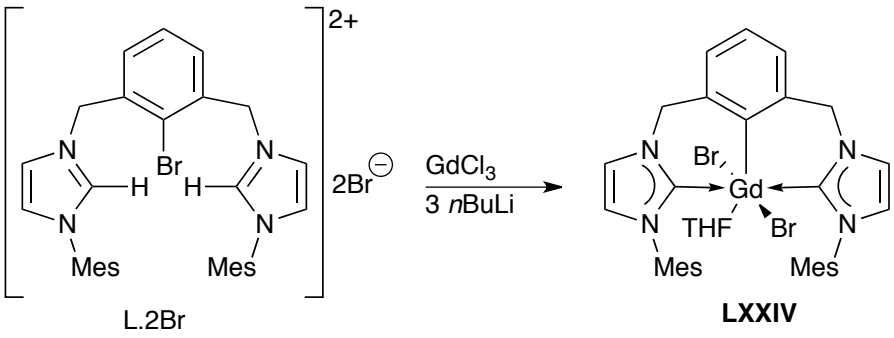

Scheme 1.23. Synthesis of the gadolinium NHC pincer complex **LXXIV**.[90]

1.2.10 Terbium(III)-NHC complexes

There is only a single example of a terbium(III)-NHC complex reported - the tris(dihydrobis(methylimidazolyl)borate) complex [$(BH_2$-($\{$1-C$\{$NCH CHNMe$\}$)$_2$)$_3$ Tb] **LXXV**, **figure 1.16**, as prepared by Long and coworkers.[91]

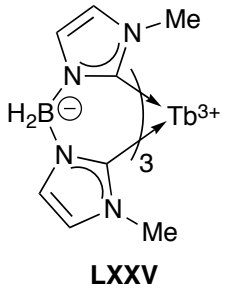

Figure 1.16. Structure of **LXXV**.[91]

The terbium centre adopts a nine coordinate tricapped trigonal prismatic coordination geometry due to the presence of a Tb$\cdots$H$-$BH electrostatic interaction with a separation of 2.74(2) Å.[91] The Tb-$C_{carbene}$ bonds have an average length of 2.578(3) Å. Long and coworkers showed that the strongly donating NHC ligands cause slow magnetic relaxation in **LXXV**.[91]

1.2.11 Dysprosium(III)-NHC complexes

The fluorenyl tethered NHC dysprosium complex [$C_{13}H_8(CH_2)_2$(1-C{HCHCHN Mes})Dy(CH_2SiMe_3)$_2$] **LXXVI**, **figure 1.17**, was prepared by Cui and coworkers.[65] The dysprosium centre adopts a distorted tetrahedral geometry with a Dy-$C_{carbene}$ bond length of 2.502(3) Å and unlike the scandium analogue **XXV** shows no reactivity as a polymerisation catalyst.

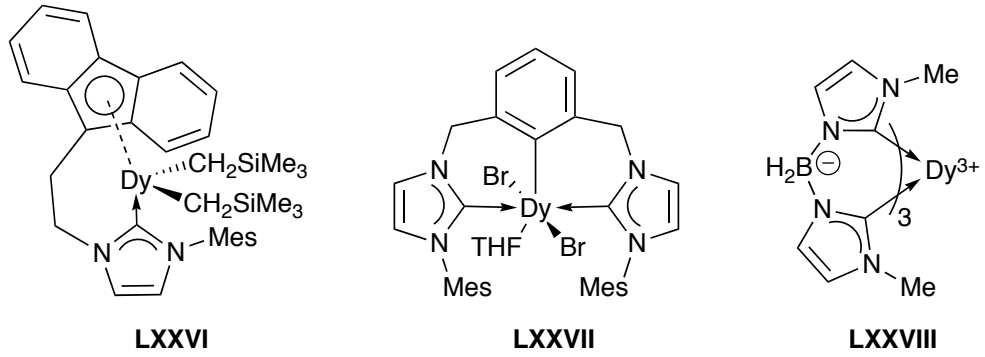

LXXVI **LXXVII** **LXXVIII**

Figure 1.17. Dysprosium NHC complexes **LXXVI**,[65] **LXXVII**[90] and **LXXVIII**.[91]

Lv and Cui also prepared the dysprosium bis(NHC) pincer complex [(2,6-(1-C{NCHCHNMes})$_2$-C_6H_3)$DyBr_2$(THF)] **LXXVII**, **figure 1.17** in a manner analogous to that of **LXXIV**.[90] **LXXVII** adopts a distorted octahedral geometry around the dysprosium centre with the pincer ligand adopting a *mer* geometry with the NHC donors in an *trans* arrangement with Dy-$C_{carbene}$ bond lengths of 2.520(9) and 2.536(9) Å. When activated with AlR_3 (R = Me, Et, *i*Bu) and [Ph_3C][$B(C_6F_5)_4$], **LXXVII** displays high activity for the polymerisation of isoprene with a $> 97\%$ *cis*-1,4 selectivity.

Long and coworkers prepared the dysprosium-NHC complex [(BH_2-(1-C{NCH CHNMe})$_2$)$_3$Dy] **LXXVIII**, **figure 1.17**, which is isostructural to **LXXV**, **figure 1.16**. The average Dy-$C_{carbene}$ bond length is 2.577(4) Å and the Dy$\cdots$H$-$BH electrostatic interaction 2.75(3) Å. Studies of the magnetic susceptibility show

that the strongly donating NHC ligands resulted in slow magnetic relaxation.[91]

1.2.12 Holmium(III)-NHC complexes

The indenyl and fluorenyl tethered NHC holmium complexes $[C_9H_6(CH_2)_2$(1-C{HCHCHNMes})$Ho(CH_2SiMe_3)_2]$ **LXXIX**, **figure 1.18**, and $[C_{13}H_8(CH_2)_2$(1-C{HCH CHNMes})$Ho(CH_2SiMe_3)_2]$ **LXXX**, **figure 1.18**, were reported by Cui and coworkers.[64] Both complexes adopt distorted tetrahedral geometries around the holmium centres with Ho-$C_{carbene}$ bond lengths of 2.490(2) and 2.484(3) Å for **LXXIX** and **LXXX**, respectively. **LXXX** shows high activity for the polymerisation of isoprene when activated by Al*i*Bu_3 and $[Ph_3C][B(C_6F_5)_4]$, displaying a $>$ 98% 3,4-selectivity. **LXXIX** showss lower reactivity and only a 76% 3,4 selectivity.[64]

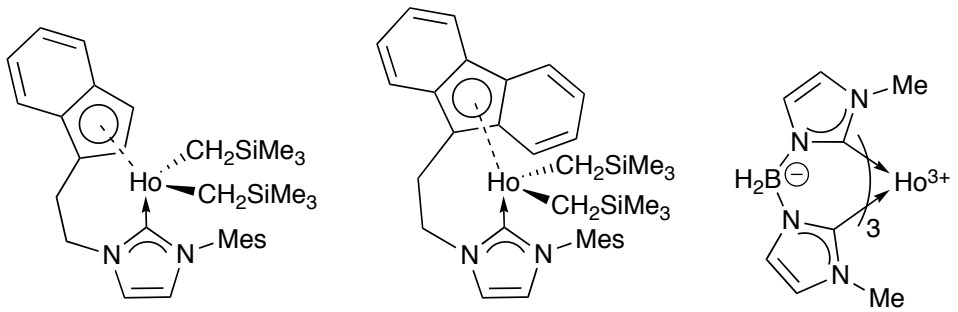

Figure 1.18. Holmium NHC complexes **LXXIX**, **LXXX** and **LXXXI**.[64][91]

Long and coworkers reported the holomium NHC complex $[(BH_2$-({1-C{NCHC HNMe})$_2)_3$Ho] **LXXXI**, **figure 1.18**, which is isostructural to both the dysprosium analogue - **LXXVIII figure 1.17** - and the terbium analogue - **LXXV figure 1.16**.[91] The average Ho-$C_{carbene}$ bond length is 2.556(3) Å while the Ho$\cdots$H$-$BH electrostatic interaction has a separation of 2.71(2) Å.

1.2.13 Erbium(III)-NHC complexes

The first erbium(III)-NHC complex reported was the tris(NHC) adduct [$ErCl_3$(1-C{NMeCHCHNMe})$_3$] **LXXXII**, **figure 1.19**, prepared by Anwander and coworkers, though no crystal structure was obtained.[71]

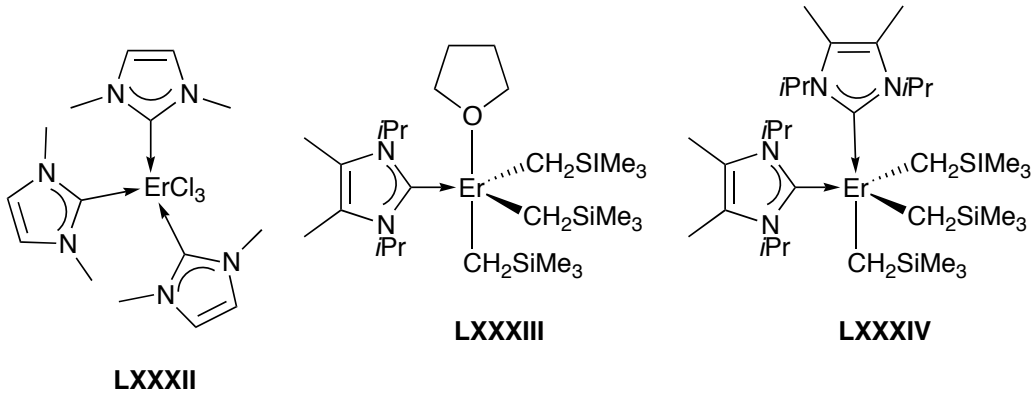

Figure 1.19. Erbium(III) NHC addicts **LXXXII** - **LXXXIV**.[71][92]

The first structurally characterised erbium(III)-NHC complexes were the adducts [$(Me_3SiCH_2)_3$Er(1-C{N*i*PrCMeCMeN*i*Pr})(THF)] **LXXXIII** and [$(Me_3SiCH_2)_3$Er(1-C{N*i*PrCMeCMeN*i*Pr})$_2$] **LXXXIV**, **figure 1.19**.[92] X-ray diffraction studies showed that **LXXXIII** adopts a trigonal bipyramidal geometry with the carbene bound in an axial position with a Er-$C_{carbene}$ bond length of 1.520(6) Å and the alkyl ligands adopting a *fac* arrangement. Only poor quality crystals of **LXXXIV** were obtained and no structure was reported.

Shen and coworkers prepared the erbium complexes supported by aryloxy tethered NHC ligands, **LXXXV**,[82] and **LXXXVI**, **scheme 1.24**.[93] Both complexes were obtained from the same proligand H_2LBr with **LXXXV** prepared from the reaction of the proligand with [LiEr(N*i*Pr$_2$)$_4$] and **LXXXVI** from the reaction of H_2LBr with four equivalents of *n*BuLi and $ErCl_3$.

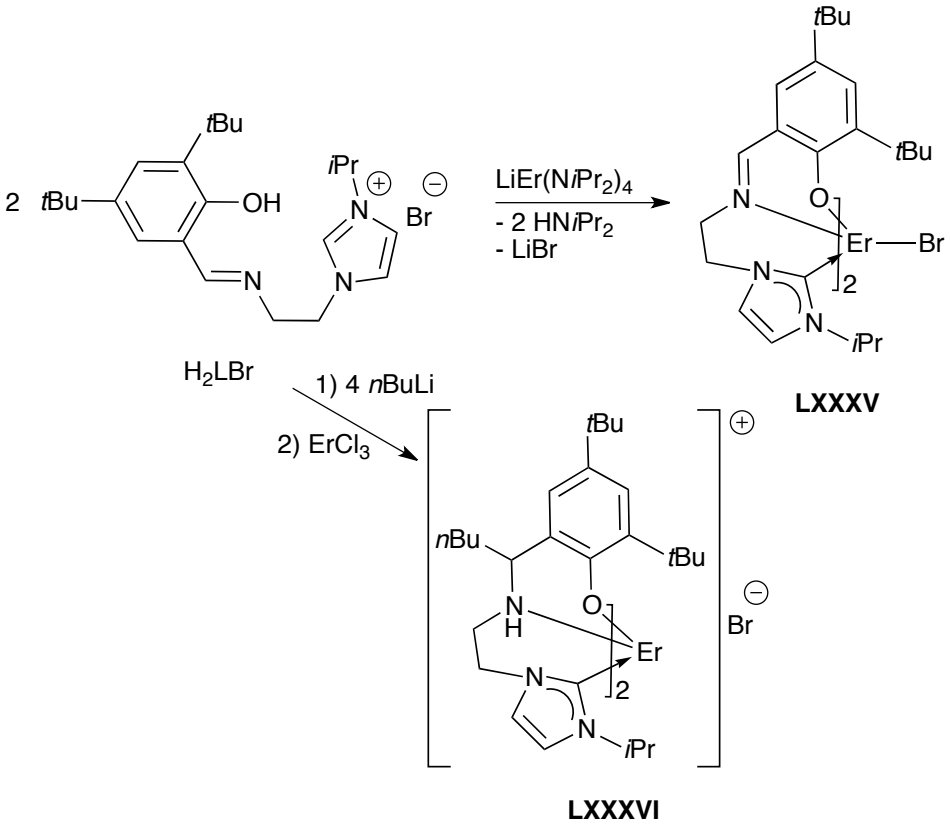

Scheme 1.24. Synthesis of **LXXXV**[82] and **LXXXVI**.[93]

LXXXV adopts a capped-octahedral geometry with each ligand bound through the arlyoxide, imine and carbene donors with a Er-$C_{carbene}$ bond length of 2.568(7) Å. Additionally, the bromide is bound directly to the erbium centre in the capping position.[82] On the other hand, **LXXXVI** exists as an ion pair due to the steric bulk of the ligand forcing the dissociation of the bromide from the erbium centre.[93] Four equivalents of *n*BuLi were required in order to reduce the imine to an amine. The cationic erbium centre adopts an octahedral geometry and is bound to each ligand through the alkoxide, amine and carbene donors with a Er-$C_{carbene}$ bond length of 2.572(7) Å.[93]

1.2.14 Ytterbium(II)-NHC complexes

The first ytterbium(II)-NHC complexes prepared were the NHC adducts [Yb(Cp*)$_2$(1-C{NRCMeCMeNR})] (R = Me **LXXXVII**, *i*Pr **LXXXVIII**), [Yb($C_6H_3tBu_2$)$_2$(1-C{NMe CMeCMeNMe})] **LXXIX** and [Yb(C_6Me_4Et)$_2$(1-C{NRCMeCMeNR})] (R = Me, **XC**, *i*Pr **XCI**), **figure 1.20**.[87][94] The ^{13}C NMR spectrum shows resonances due to the carbenic carbon at 205.0, 200.7 and 201.8 ppm for **LXXXVII**, **LXXXVIII** and **LXXXIX**, respectively.[87] The carbenic carbons of **XC** and **XCI** resonate at 205.0 and 198.1 ppm, respectively.[94] The Yb-$C_{carbene}$ bond length in **LXXIX** is 2.598(3) Å[87] and in **XC** 2.552(4) Å.[94]

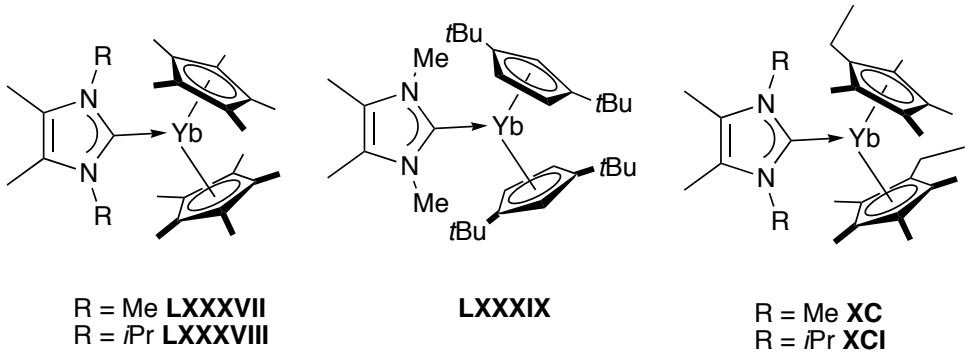

Figure 1.20. Structures of the ytterbium(II)-NHC adducts **LXXXVII** - **XCI**.[87][94]

Cui and coworkers prepared the three coordinate yttrium(II) alkyl NHC-adduct complexes [({Me_3 Si}$_2$N)$_2$Yb(1-C{NMesCHCHNMes)] **XCII** and [({Me_3Si}$_2$N)$_2$Yb (1-C{N*i*PrCMeCMeN*i*Pr)] **XCIII**, **figure 1.21**.[95]

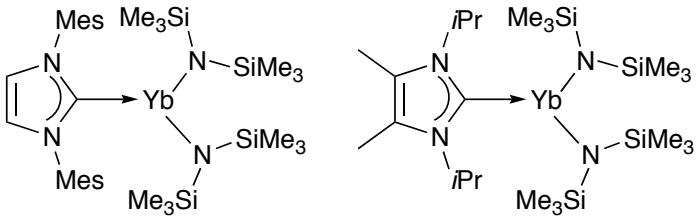

XCII **XCIII**

Figure 1.21. Structures of the ytterbium(II)-NHC adducts **XCII** - **XCIII** as reported by Chen and coworkers.[95]

The $C_{carbene}$ resonance occurs at 197.9 and 205.4 ppm for **XCII** and **XCIII**, respectively, on the ^{13}C NMR spectrum and the Yb-$C_{carbene}$ bond length of **XCII** is 2.600(3) Å, slightly longer than the Yb-$C_{carbene}$ bond length for **XCIII** and **XCI**. Both complexes catalyse the cross-dehydrogenative-coupling of amines and silanes, **equation 1.3**.

$$PhSiH_3 + HNR_2 \xrightarrow[R = SiMe_3,\ iPr,\ Et,\ tBu,\ Dipp]{\textbf{XCII or XCIII}} PhSiH_2NR_2 + PhSiH(NR_2)_2 \quad (1.3)$$

1.2.15 Ytterbium(III)-NHC complexes

The ytterbium(III)-NHC ion pair complex [HN-(C_6H_3Me-(1-C{NCHCHNBn}))$_2$Yb] [({Me_3Si}$_2$NNa)$_5$Cl] **XCIV** was prepared from the reaction between H_3LCl_2, six equivalents of $NaN(SiMe_3)_2$ and half an equivalent of $YbCl_3$, **scheme 1.25**.[89] The ytterbium cation adopts an octahedral geometry with the ligands adopting a *mer* arrangement and Yb-$C_{carbene}$ bond lengths between 2.447(4) - 2.463(4) Å while the chloride counterion adopts a pentagonal geometry within an inverse crown.

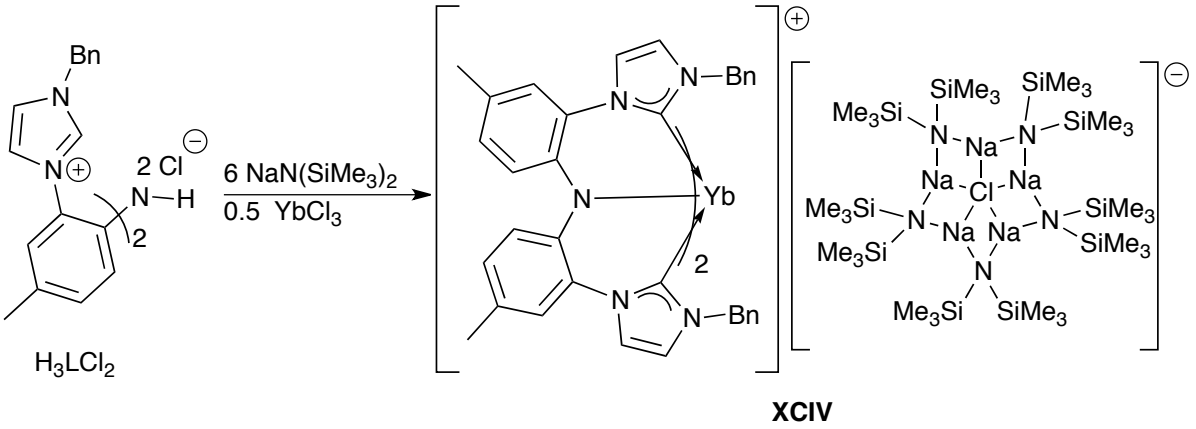

H_3LCl_2

XCIV

Scheme 1.25. Synthesis of **XCIV**.[89]

However, treatment of H_3LCl_2 with 2 equivalents of nBuLi or $LiCH_2SiMe_3$ followed by $[(\{Me_3Si_2\}N)_3Yb(\mu\text{-}Cl)Li(THF)_3]$ yields the ytterbium(III)-NHC ion pair complex $[HN\text{-}(C_6H_3Me\text{-}(1\text{-}C\{NCHCHNBn\}))_2Yb]$ $[Yb(N\{SiMe_3\}_2)_3Cl]$ **XCV** with the organic molecule L′ also produced, **scheme 1.26**.[89]

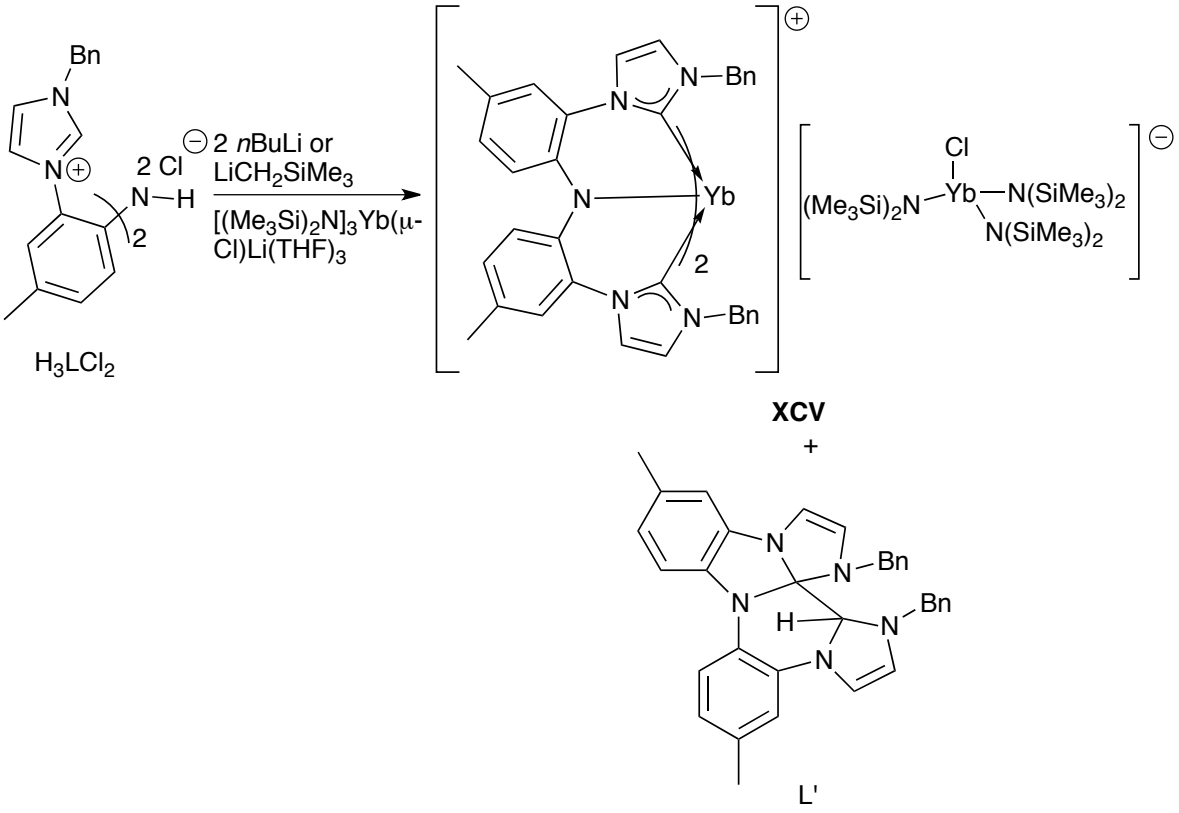

Scheme 1.26. Synthesis of **XCV**.[89]

The cationic ytterbium centre of **XCV** adopts an octahedral geometry with the ligands arranged in a *mer* geometry and Yb-$C_{carbene}$ bond lengths in the range of 2.457(5) to 2.463(6) Å, similar to the analogous bond lengths of **XCIV**. The anionic ytterbium(III) counterion adopts a tetrahedral geometry being bound to three $(Me_3Si_2)N$ ligands and a chloride ion.

Shen and coworkers prepared the aryloxy-tethered NHC ytterbium(III) complexes $[(i Pr_2N)Yb(O\text{-}4,6\text{-}t Bu\text{-}C_6H_2\text{-}2\text{-}CH_2(1\text{-}C\{NCHCHNR\}))_2]$, R = *i*Pr **XCVI**, Me **XCVII**, **scheme 1.27**.[96] Treatment of the hydrochloride salt of the proligand H_2LCl with half an equivalent of $LiYb(N i Pr_2)_4$ and *n*BuLi yielded **XCVI** and **XCVII**. However, attempts to make the mono-ligand complex, $[(i Pr_2N)_2Yb(O\text{-}4,6\text{-}t Bu\text{-}C_6H_2\text{-}2\text{-}CH_2(1\text{-}C\{NCHCHNR\}))]$ yielded only **XCVI** or **XCVII**. These

complexes were the first bis-aryloxy tethered NHC complexes of ytterbium.[96] In the solid state both **XCVI** and **XCVII** adopt a distorted trigonal-bipyramidal geometry with the carbene donors in the axial position and the O and N donors in the equatorial positions. The Yb-$C_{carbene}$ bond lengths of 2.483(4) and 2.491(4) Å for **XCVI** and are shorter than the Yb-$C_{carbene}$ bond lengths for **XCVII** of 2.526(7) and 2.543(7) Å.

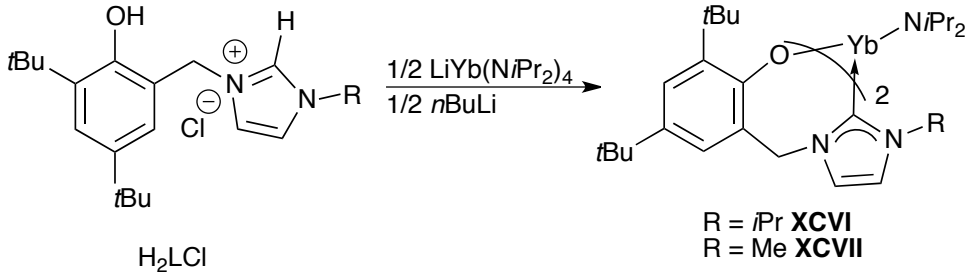

Scheme 1.27. Synthesis of **XCVI** and **XCVII**.[96]

1.2.16 Lutetium(III)-NHC complexes

Okuda and coworkers prepared the lutetium(III)-NHC adduct $[(Me_3CH_2)_3Lu(IMes)]$ **XCVIII** from the solvent displacement reaction between $[(Me_3CH_2)_3Lu(THF)_2]$ and IMes (IMes = (1-C{NMesCHCHNMes})), **scheme 1.28**.[97] The $C_{carbene}$ resonance occurs at 202.76 ppm on the ^{13}C NMR spectrum.[97] In the solid state **XCVIII** adopts a tetrahedral geometry with a Lu-$C_{carbene}$ bond length of 2.488(3) Å. When **XCVIII** was stirred in solution at −30°C the complex underwent C-H activation of an *ortho* methyl group, to form **XCIX** with the loss of $SiMe_4$.[98] **XCIX** adopts a distorted trigonal bipyramidal geometry and shows no difference in the Lu-$C_{carbene}$ bond length with a distance of 2.491(2) Å. Similarly, there is no significant shift of the $C_{carbene}$ resonance on the ^{13}C NMR spectrum, occurring at 201.26 ppm. ^1H and ^{13}C NMR studies show that the bis C-H activated ligand

C could be prepared from the reaction of $[(Me_3CH_2)_3Lu(THF)_2]$ and an excess of IMes. The tris C-H activated ligand **CI** was not formed due to steric congestion.[98]

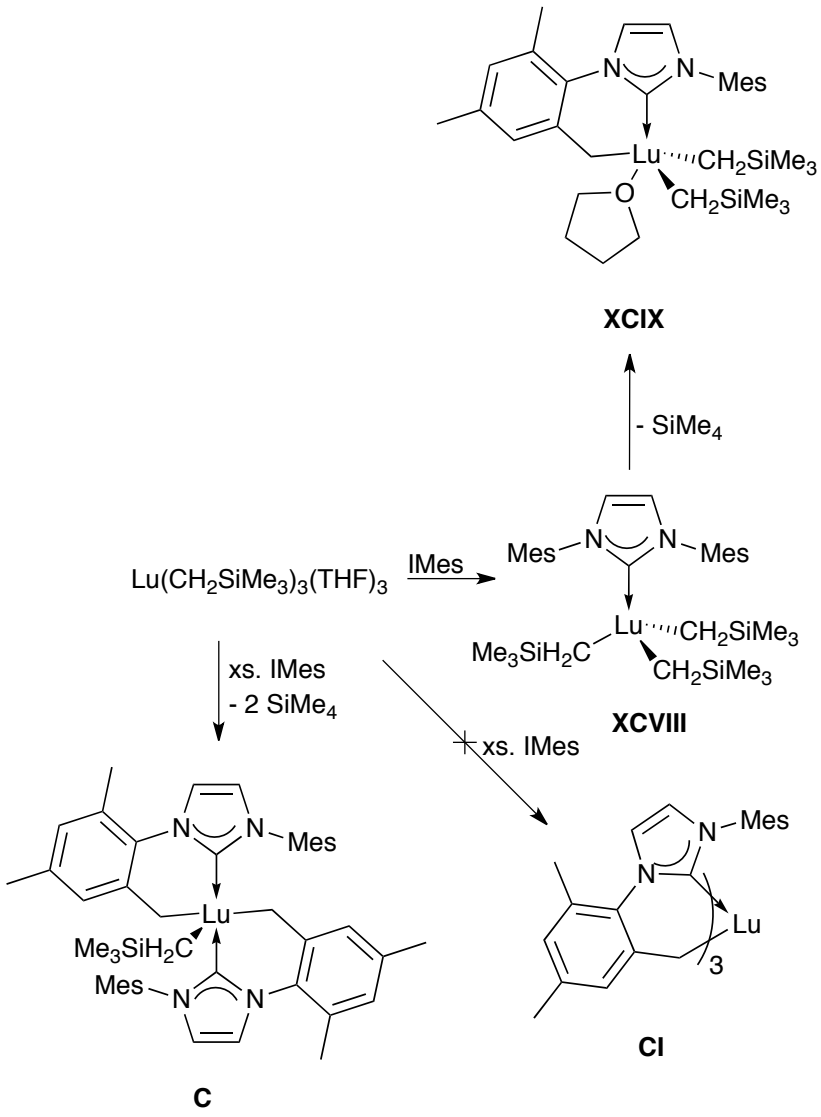

Scheme 1.28. Synthesis and C-H activation chemistry of **XCVIII**.[97][98]

A number of lutetium(III)-NHC complexes have proven to be highly effective polymerisation catalysts. Cui and coworkers prepared the amidino tethered NHC lutetium alkyl complex [2,6-iPrC$_6$H$_3$N=C(C$_6$H$_5$)NH(CH$_2$)$_2$-(1-C{NCHCHNMes}) Lu(CH$_2$SiMe$_3$)$_2$], **CII**, **scheme 1.29**.[99] **CII** adopts a twisted tetragonal geometry with the carbenic carbon occurring at 176.7 ppm on the ^{13}C NMR spectrum and a Lu-C$_{carbene}$ bond length of 1.516(4) Å. When activated with [Ph$_3$C][B(C$_6$F$_5$)$_4$] **CII** is a highly active and highly (> 98% at 25 °C) 3,4-selective isoprene polymerisation catalyst. **CII** also copolymerises isoprene and ϵ-caprolactone when activated with [Ph$_3$C][B(C$_6$F$_5$)$_4$] to form a syndiotactic diblock copolymer.[99]

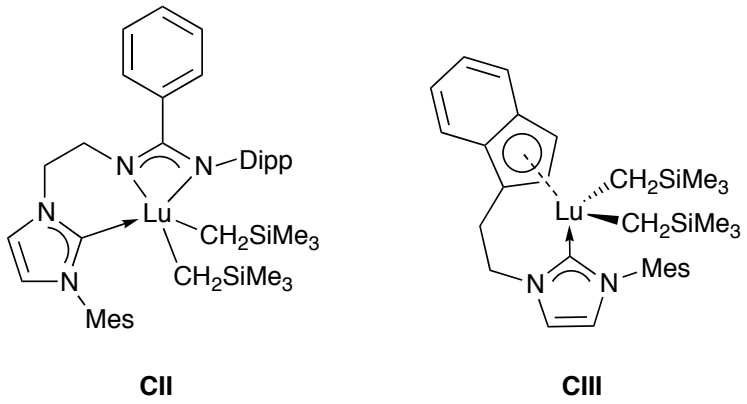

Scheme 1.29. Structures of lutetium NHC complexes **CII**[99] and **CIII**.[63][64]

Additionally, Cui and coworkers have prepared the indenyl tethered NHC lutetium alkyl complex [(C$_9$H$_6$)CH$_2$CH$_2$(1-C{NCHCHNMes})Lu(CH$_2$SiMe$_3$)$_2$], **CI II**, **scheme 1.29**, which adopts a tetrahedral geometry with a Lu-C$_{carbene}$ bond length of 2.431(3) Å and a C$_{carbene}$ resonanace at 199.18 ppm in the ^{13}C NMR spectrum.[63][64] **CIII**, like **CII**, proved a good catalyst for the polymerisation of isporene with a > 97% 3,4-selectivity at 25°C when activated with [Ph$_3$C][B(C$_6$F$_5$)$_4$].[64]

1.3 Actinide NHC complexes

While NHC complexes have been characterised for most of the lanthanides, far fewer actinide NHC complexes have been characterised. One thorium and several uranium NHC complexes, the first of which was reported in 2001,[100] have been reported.

1.3.1 Thorium(IV)-NHC complexes

The only thorium-NHC complex reported, $[Th(OCMe_2CH_2(1\text{-}C\{NCHCHN\textit{i}Pr\}))_4]$ **CIV**, was prepared from the salt elimination reaction between $[ThCl_4(DME)_2]$ (DME = $MeOCH_2CH_2OMe$) and four equivalents of KL^{iPr}, **scheme 1.30**.[68]

Scheme 1.30. Synthesis of **CIV**.[68]

The low temperature ^1H NMR spectrum of **CIV** shows two magnetically inequivalent ligand environments in an 1:1 ratio which result from a twist in the backbone of the NHC. The solid state structure shows that all four ligands are bound bidentate with the thorium centre adopting a square-antiprismatic geometry. This is different from $[Ce(L^{iPr})_4]$ and $[U(L^{iPr})_4]$ which have coordination numbers of 6 and 7, respectively, due to the small ionic radii of 111 pm for Ce(IV) and 114 pm for U(IV) compared with 119 pm for Th(IV).[101][59] The Th-$C_{carbene}$ bond lengths are long at 2.852(6) to 2.884(5) Å, resulting from the weakness of the interaction between the carbene and actinide centre.[68]

1.3.2 Uranium(III)-NHC complexes

Most of the uranium(III)-NHC complexes reported have been adducts of (1-C{NMe CMe}$_2$) and were prepared by mixing the free NHC with the appropriate uranium(III) starting material.

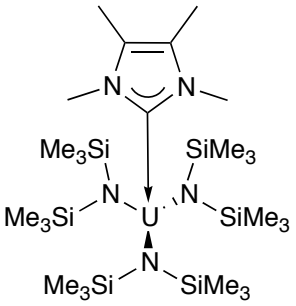

XIII

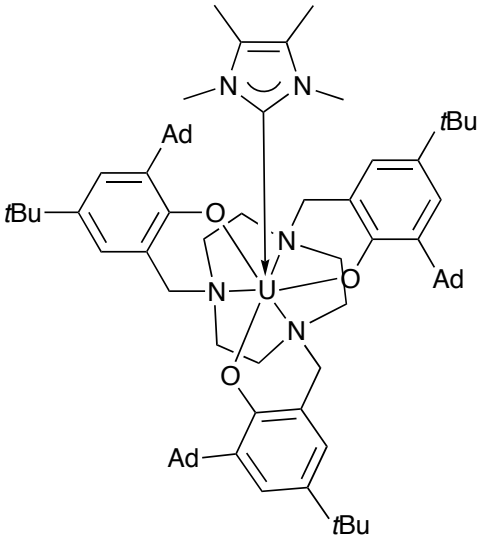

CV

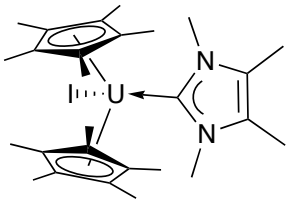

CVI

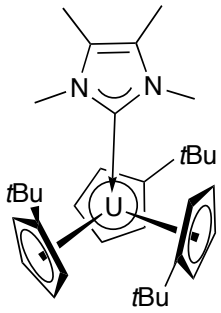

CVII

Figure 1.22. Uranium(III)-NHC complexes.[43][45]

Meyer and coworkers have prepared the uranium(III)-NHC adduct [({Me_3Si}$_2$ N)$_3$U(1-C{NMeCMe}$_2$)] **XIII**, **figure 1.22**, from the addition of (1-C{NMeCMe}$_2$) to the uranium(III) silylamide [U{N(SiMe)$_2$}$_3$] and the tris(aryloxide)tri- azacyclononane uranium-NHC complex **CV**, **figure 1.22**.[43] **XIII** and **CV** have U-$C_{carbene}$ bond lengths of 2.672(5) Å and 2.789(14) Å, respectively. The short U-$C_{carbene}$ bond of **XIII** can be seen in the UV-vis-NIR spectra where the charge transfer band showed a large shift from 478 nm in [U{N(SiMe)$_2$}$_3$] to the lower wavelength 594 nm upon carbene binding. Computational studies show π-backbonding from the f-type orbitals of the uranium to the π-type orbitals of the carbene.

Similarly, Ephritikhine and coworkers have prepared the uranium(III)-NHC adducts [U(Cp*)$_2$I (1-C{NMeCMe}$_2$)], **CVI** and [U(C_5H_4tBu)(1-C{NMeCMe}$_2$)], **CVII figure 1.22**.[45] Both complexes adopt a distorted tetrahedral geometry with U-$C_{carbene}$ bond lengths of 2.687(5) Å and 2.768(5) Å for **CVI** and **CVII**, respectively, similar to the U-$C_{carbene}$ bond lengths of **XIII** and **CV**.

The Arnold group has prepared the alkoxy tethered NHC uranium(III) complex [({Me_3Si}$_2$N)$_2$U(OCMe$_2$CH$_2$(1-C{NCH$_2$CH$_2$NDipp}))] **CVIII**, **scheme 1.23**.[79] The uranium centre adopts a distorted tetrahedral geometry with a U-$C_{carbene}$ bond length of 2.693(4) Å. **CVIII** shows interesting reactivity with CO_2, CO and Ph_2CN_2, **figure 1.23**.[102]

Treatment of **CVII** with CO_2 results in the formation of [U(OCMe$_2$CH$_2$(1-C {NCH$_2$CH$_2$NDipp}))(N{$SiMe_3$}$_2$)(OSiMe$_3$)(OCNSiMe$_3$)]$_n$ **CIX**. The solid state strucuture was not obtained though elemental analysis suggested that single CO_2 insertion had occurred. Furthermore, its was only soluble in THF or pyridine suggesting a oligomeric or polymeric structure. **CIX** was characterised by FTIR spectroscopy and had an absorbance at 2285 cm^{-1} due to the isocyanate O=C=NSiMe$_3$ ligand.[102]

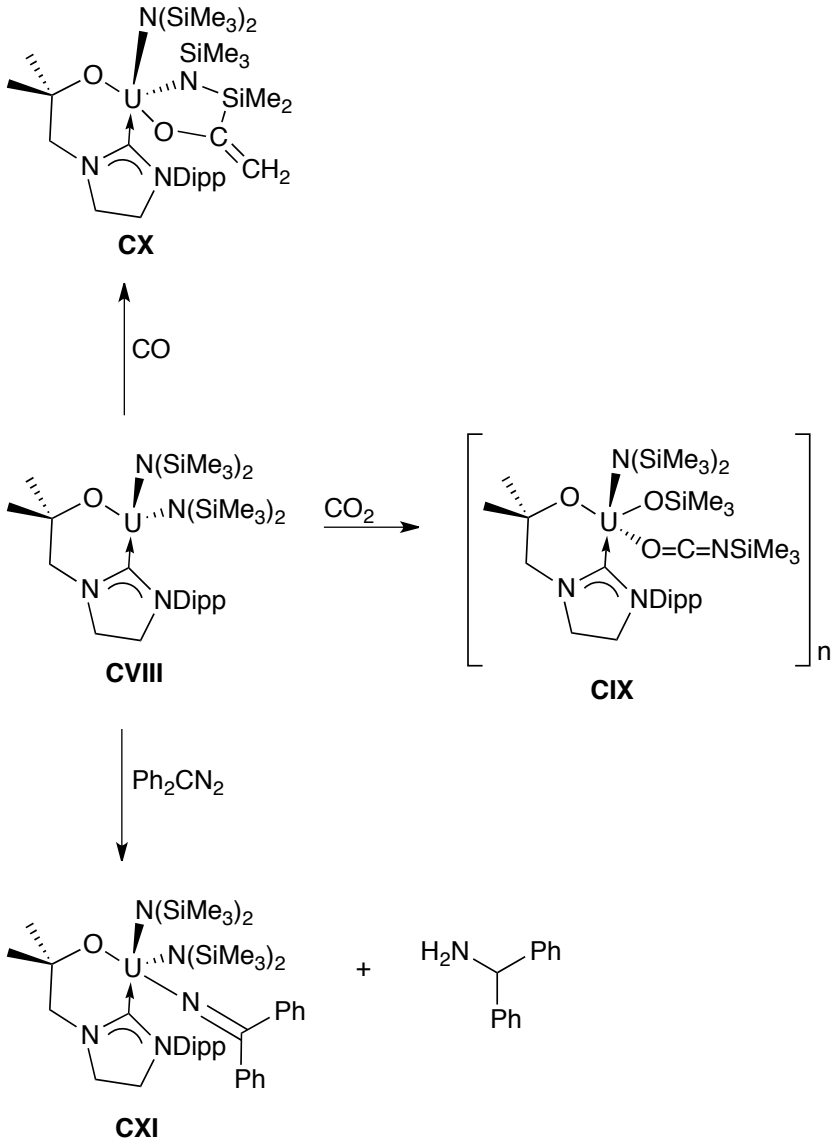

Figure 1.23. Reactivity of **CVIII** with CO_2, CO and Ph_2CN_2.[79][102]

CVIII reacts with CO to give the metallacyclic product [U(OCMe$_2$CH$_2$(1-C{NC H$_2$CH$_2$NDipp}))(N{SiMe$_3$}$_2$)(OC{CH$_2$}SiMe$_2$N{SiMe$_3$})] **CX**. The uranium centre has been oxidised from the + 3 oxidation state in **CVIII** to the + 4 state in **CX**. X-ray diffraction studies revealed that the uranium centre adopts a distorted trigonal bipyramidal geometry with the amide and carbene ligand in the

equatorial sites and the oxygen ligands in the axial positions. There is a contraction of the U-$C_{carbene}$ bond from 2.693(4) Å in **CVIII** to 2.630(6) Å in **CX**.[102]

CVIII reacts with Ph_2CN_2 to form the uranium ketimido complex [U($OCMe_2CH_2$(1-C{NCH_2CH_2NDipp}))(N{$SiMe_3$}$_2$)$_2$(N=C(Ph_2))] **CXI**, with $H_2NCH(Ph)_2$ formed as a by product. Again, the uranium centre is oxidised from + 3 in **CVII** to + 4 in **CXI**, though the reaction mechanism is not yet clear.[102] The uranium centre adopts a distorted trigonal bipyramidal geometry with the amide and carbene donor in the equatorial positions and a U-$C_{carbene}$ bond length of 2.719(5) Å, significantly longer than the U-$C_{carbene}$ bond lengths of **CVIII** and **CX**.[102]

1.3.3 Uranium(IV)-NHC complexes

The first uranium(IV)-NHC complex [(Cp*)$_2$U(O){1-C$(NMeCMe)_2$}] **CXII**, **figure 1.24**, was reported by Evans and coworkers in 2004.[103]

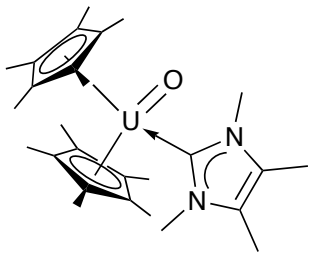

CXII

Figure 1.24. Structure of **CXII**.[103]

As well as being the first reported uranium(IV)-NHC complex, **CXII** is also a rare example of a uranium mono-oxo complex and has a U-$C_{carbene}$ bond length of 2.636(9) Å.

Danopoulos and coworkers have prepared the uranium(IV) bis(NHC) pincer complex [C_5H_3N-2,5-(1-C{$NCHCHNPh$})$_2UCl_4$], **CXIII figure 1.25**, by the addition of UCl_4 to the free carbene, **figure 1.25**. In the solid state the uranium

centre adopts a distorted pentagonal bipyramidal geometry with an approximate C_2 axis passing through the pyridine N atom and uranium and U-$C_{carbene}$ bond lengths of 2.573(5) and 2.587(5) Å.[104]

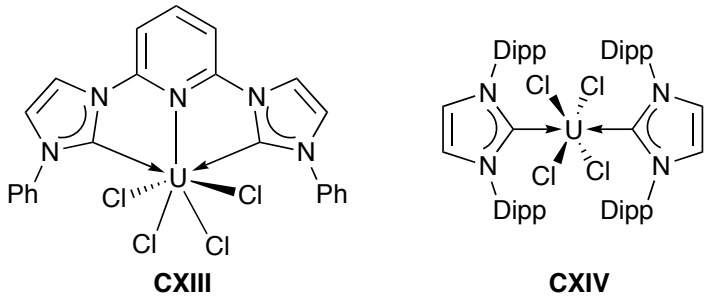

CXIII **CXIV**

Figure 1.25. NHC adducts of UCl_4 **CXIII**[104] and **CXIV**.[105]

The uranium(IV) bis(NHC) complex $[UCl_4(1\text{-}C\{NDippCH_2\}_2)_2]$ **CXIV figure 1.25** was synthesised in a similar manner by adding the free carbene to UCl_4. **CXIV** has U-$C_{carbene}$ bond lengths of 2.675(7) and 2.687(7) Å and short Cl· · ·$C_{carbene}$ contacts as a result of the steric repulsion between the aryl and chloride groups.[105]

Arnold and coworkers have prepared the uranium(IV) complexes supported by alkoxy-tethered NHC complexes $[U(L^{iPr})_4]$ **CXV** and $[UI(L^{iPr})_4]$ **CXVI**, **scheme 1.31**.[59]

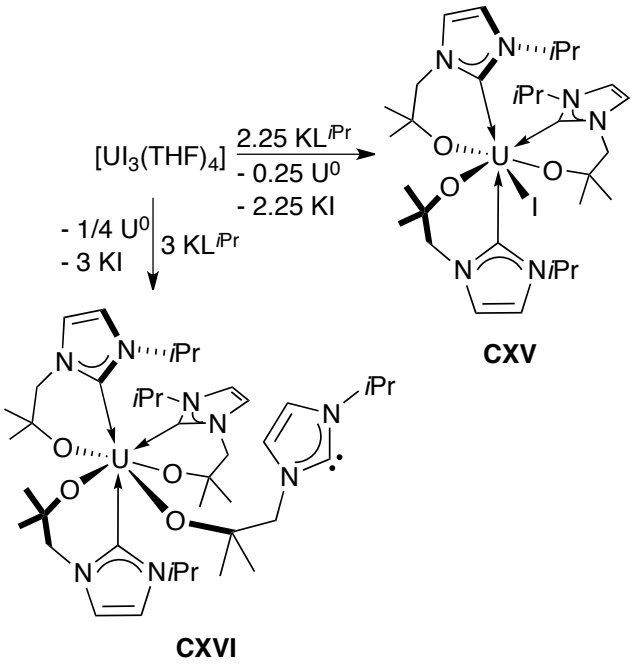

Scheme 1.31. Synthesis of the uranium(IV) alkoxy tethered carbene complexes **CXV** and **CXVI**.[59]

The reaction of $[UI_3(THF)_4]$ with KL^{iPr} afforded two disproportionation products: a uranium(IV) alkoxy tethered NHC complex and a quarter equivalent of uranium metal. Thus **CXV** was prepared with 2.25 equivalents of KL^{iPr} and had three ligands bound bidentate and an iodide. Using three equivalents of KL^{iPr} yields **CXVI** where three of the ligands are bound bidentate with U-$C_{carbene}$bond lengths of of 2.748(3), 2.799(3) and 2.696(3) Å and one ligand bound monodentate through the anionic oxygen tether. In both cases the complexes are pentagonal bipyramidal with the axial positions being occupied by three oxygen, an iodide and a carbene donors in **CXV** and one carbene and three oxygen donors in **CXVI**. The axial positions are occupied with two carbene donors in both complexes.[59]

1.3.4 Uranium(VI)-NHC complexes

The first examples of uranium(VI)-NHC complexes were the bis(NHC) adducts of the uranyl dication UO_2^{2+}, $[UO_2Cl_2(1\text{-}C\{NMesCXCXNMes\})_2]$ (X = H **CXVII**, X = Cl **CXVIII**), **equation 1.4**.[100] Both **CXVII** and **CXVIII** are octahedral with the NHC ligands in a *trans* arrangement. The U=O bond lengths for **CXVII** and **CXVIII** are 1.761(4) and 1.739(3) Å, respectively while the U-$C_{carbene}$ bond lengths are 2.626(7) and 2.609(4) Å for **CXVII** and **CXVIII**, respectively. The longer U=O bond length for **CXVIII** is the result of the weaker σ-donor activity of (1-C{NMesCClCClNMes}) compared with (1-C{NMesCHCHNMes}).

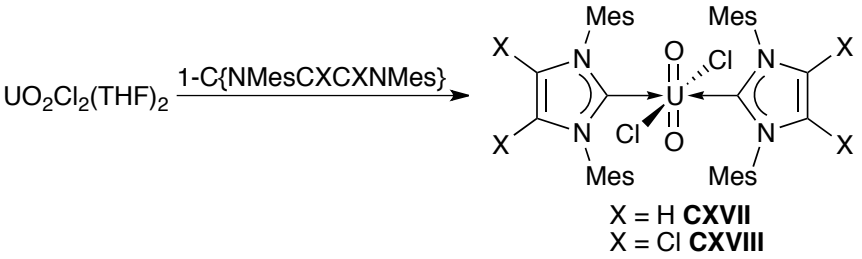

(1.4)

The Arnold group has prepared the amido-tethered NHC uranyl complexes $[(NtBuCH_2CH_2(1\text{-}C\{NCHCHNR\}))_2UO_2]$ (R = *t*Bu **CXIX**, Mes **CXX**) from the aminolysis reaction between $HNtBuCH_2CH_2(1\text{-}C\{NCHCHNR\})$ and $[UO_2(N\{SiMe_3\}_2)_2]$, **scheme 1.32**.[106] Both complexes adopt an octahedral geometry and **CXIX** formed the *trans* isomer in a 90% yield with the remaining 10% being the *cis* isomer, though this was not isolated, while **CXX** formed the *trans* isomer exclusively. The U-$C_{carbene}$ bond lengths are 2.640(5) Å and 2.633(7) Å for **CXIX** and **CXX**, respectively. On the ^{13}C NMR spectrum of **CXIX**, the $C_{carbene}$ resonate at 262.80 for the *trans* isomer.

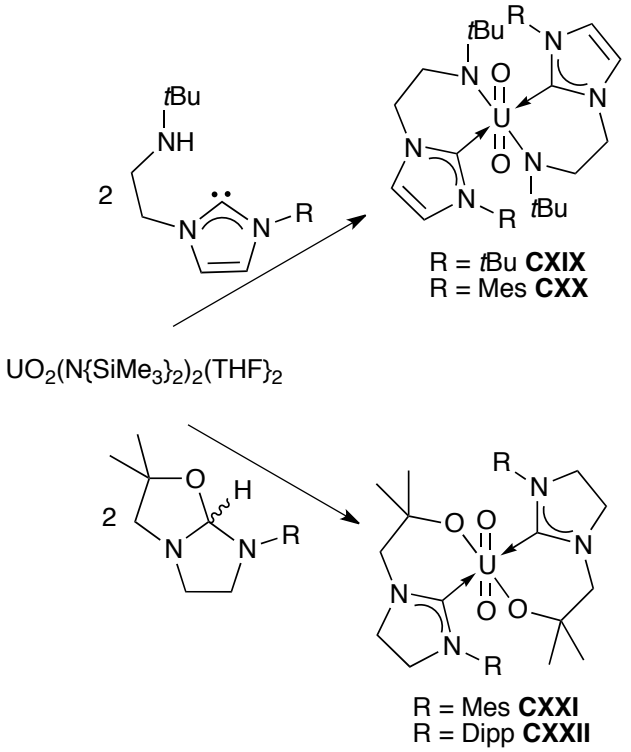

Scheme 1.32. Synthesis of U-NHC complexes **CXIX** - **CXXII**.[106][107]

The Arnold group also prepared the alkoxy tethered NHC uranyl complexes $[UO_2(OCMe_2CH_2(1\text{-}C\{NCH_2CH_2NR\}))_2]$ (R = Mes **CXXI**, Dipp **CXXII**), **scheme 1.32**.[107] The ^{13}C NMR spectrum for **CXXI** and **CXXII** displayed $C_{carbene}$ resonances at 281.6 and 283.6 ppm, respectively, the highest frequency carbene resonances for a metal-NHC complex. In the solid state both structures adopt an octahedral geometry with the NHC donors in a *trans* configuration and a linear O=U=O unit. For **CXXI** the U-$C_{carbene}$ bond length is 2.580(4) Å and for **CXXII** the U-$C_{carbene}$ bond length is 2.612(2) Å.[107]

1.4 Aims

The Arnold group has designed a series of alkoxy-tethered NHC ligands which, with a hard anionic oxygen donor and soft carbene donor, are ideally set up to bridge between a hard f-metal centre and soft transition metal. The second chapter of this thesis describes the synthesis of the iron and cobalt complexes bearing the alkoxy-tethered NHC ligand L^{Mes}, $[Fe(L^{Mes})_2]$ and $[Co(L^{Mes})_2]$, respectively, and their subsequent reaction with $[(\{Me_3Si\}_2N)_2U\{N(SiMe_3)Si(Me_2)CH_2\}]$ to form heterobimetallic complexes. The reactivity of these complexes towards a range of small molecules has been investigated with the aim exploiting the cooperative reactivity between the two metals.

Chapter three describes the reactivity of the tris(3,5-dialkyl-2-hydroxyp- henyl)-methane molecule $HC(3\text{-}t\text{Bu-}5\text{-Me-}C_6H_2OH)_3$ with $[Co(N\{SiMe_3\}_2)_2(THF)]$ and $[Zn(N\{SiMe_3\}_2)_2]$ to form cobalt-aryloxide and zinc-aryloxide complexes which are used to prepare a series of s/d-block and d/f-block heterobimetallic complexes.

The fourth chapter describes the reactivity of the monometallic cerium NHC complex $[Ce(L^{iPr})_3]$ towards C-H and N-H acidic substrates and the reactivity of $[Ce(L^{iPr})_3]$, $[Ce(L^{iPr})_4]$ and $[Fe(L^{Mes})_2]$ as catalysts for a series of organic reactions.

References

1. S. Diez-Gonzalez, editor, *N-Heterocyclic Carbenes: From Laboratory Curiosities to Efficient Synthetic Tools*, The Royal Society of Chemistry, 2011.

2. A. J. Arduengo, H. V. R. Dias, R. L. Harlow and M. Kline, *J. Am. Chem. Soc.*, 1992, **114**, 5530.

3. A. J. Arduengo, H. V. R. Dias, D. A. Dixon, R. L. Harlow, W. T. Klooster and T. F. Koetzle, *J. Am. Chem. Soc.*, 1994, **116**, 6812.

4. C. Heinemann and W. Thiel, *Chem. Phys. Lett.*, 1994, **217**, 11.

5. C. Heinemann, T. Müller, Y. Apeloig and H. Schwarz, *J. Am. Chem. Soc.*, 1996, **118**, 2023.

6. M. Tafipolsky, W. Scherer, K. Öfele, G. Artus, B. Pedersen, W. A. Hermann and G. S. McGrady, *J. Am. Chem. Soc.*, 2002, **124**, 5865.

7. D. Nemcsok, K. Wichmann and G. Frenking, *Organometallics*, 2004, **23**, 3640.

8. M. N. Hopkinson, C. Richter, M. Schedler and F. Glorius, *Nature*, 2014, **510**, 485.

9. H. W. Wanzlick, *Angew. Chem.*, 1962, **74**, 129.

10. H. W. Wanzlick and H. J. Kleiner, *Angew. Chem.*, 1961, **73**, 493.

11. H. W. Wanzlick and E. Schikora, *Angew. Chem.*, 1960, **72**, 494.

12. H. W. Wanzlick and H. J. Schönherr, *Angew. Chem. Int. Ed.*, 1968, **7**, 141.

13. K. Öfele, *J. Organomet. Chem.*, 1968, **12**, P42.

14. D. J. Cardin, B. Cetinkaya, M. F. Lappert, L. Manojlović-Muir and K. W. Muir, *J. Chem. Soc. D, Chem. Commun.*, 1971, 400.

15. A. J. Arduengo, R. L. Harlow and M. Kline, *J. Am. Chem. Soc.*, 1991, **113**, 361.

16. R. H. Crabtree, *J. Organomet. Chem.*, 2005, **690**, 5451.

17. F. E. Hahn and M. C. Jahnke, *Angew. Chem. Int. Ed.*, 2008, **47**, 3122.

18. F. Glorius, *N-Heterocyclic Carbenes in Transition Metal Catalysis*, Springer, Berlin, 2007.

19. S. Gaillard, C. S. J. Cazin and S. P. Nolan, *Acc. Chem. Res.*, 2012, **45**, 778.

20. C. M. Crudden and D. P. Allen, *Coord. Chem. Rev.*, 2004, **248**, 2247.

21. W. A. Herrmann, K. Öfele, D. V. Preysing and S. K. Schneider, *J. Organomet. Chem.*, 2003, **687**, 229.

22. K. J. Cavell and D. S. McGuinness, *Coord. Chem. Rev.*, 2004, **248**, 671.

23. P. Schwab, R. H. Grubbs and J. W. Ziller, *J. Am. Chem. Soc.*, 1996, **118**, 100.

24. T. Weskamp, W. C. Schattenmann, M. Spiegler and W. A. Hermann, *Angew. Chem. Int. Ed.*, 1988, **37**, 2490.

25. M. Scholl, S. Ding, C. W. Lee and R. H. Grubbs, *Org. Lett.*, 1999, **1**, 953.

26. T. M. Trnka, J. P. Morgan, M. S. Sanford, T. E. Wilhelm, M. Scholl, T.-L. Choi, S. Ding, M. W. Day and R. H. Grubbs, *J. Am. Chem. Soc.*, 2003, **125**, 2546.

27. J. A. Love, M. S. Sanford, M. W. Day and R. H. Grubbs, *J. Am. Chem. Soc.*, 2003, **125**, 10103.

28. K. Endo and R. H. Grubbs, *J. Am. Chem. Soc.*, 2011, **133**, 8525.

29. B. K. Keitz, K. Endo, P. R. Patel, M. B. Herbert and R. H. Grubbs, *J. Am. Chem. Soc.*, 2012, **134**, 693.

30. G. Altenhoff, R. Goddard, C. W. Lehmann and F. Glorius, *Angew. Chem. Int. Ed.*, 2003, **42**, 3690.

31. W. A. Hermann, *Angew. Chem. Int. Ed.*, 2002, **41**, 1290.

32. C. Zhang, J. Huang, M. L. Trudell and S. P. Nolan, *J. Org. Chem.*, 1999, **64**, 3804.

33. W. A. Hermann, C.-P. Reisinger and M. Spiegler, *J. Organomet. Chem.*, 1998, **557**, 93.

34. S. Díez-González and S. P. Nolan, *Coord. Chem. Rev.*, 2007, **251**, 874.

35. D. J. Nelson and S. P. Nolan, *Chem. Soc. Rev.*, 2013, **42**, 6723.

36. R. A. Kelly, H. Clavier, S. Giudice, N. M. Scott, E. D. Stevens, J. Bordner, I. Samardjiev, C. D. Hoff, L. Cavallo and S. P. Nolan, *Organometallics*, 2008, **27**, 202.

37. A. C. Hillier, W. J. Sommer, B. S. Yong, J. L. Petersen, L. Cavallo and S. P. Nolan, *Organometallics*, 2003, **22**, 4322.

38. S. Fantasia, J. L. Petersen, H. Jacobsen, L. Cavallo and S. P. Nolan, *Organometallics*, 2007, **26**, 5880.

39. X. Hu, I. Castro-Rodriguez, K. Olsen and K. Meyer, *Organometallics*, 2004, **23**, 755.

40. X. Hu, Y. Tang, P. Gantzel and K. Meyer, *Organometallics*, 2003, **22**, 612.

41. N. M. Scott, R. Dorta, E. D. Stevens, A. Correa, L. Cavallo and S. P. Nolan, *J. Am. Chem. Soc.*, 2005, **127**, 3516.

42. H. Jacobsen, A. Correa, C. Constabile and L. Cavallo, *J. Organomet. Chem.*, 2006, **691**, 4350.

43. H. Nakai, X. Hu, L. N. Zakharov, A. L. Rheingold and K. Meyer, *Inorg. Chem.*, 2004, **43**, 855.

44. L. Maron and D. Bourissou, *Organometallics*, 2007, **26**, 1100.

45. T. Mehdoui, J.-C. Berthet, P. Thuéry and M. Ephritikhine, *Chem. Commun.*, 2005, 2860.

46. L. Gagliardi and C. J. Cramer, *Inorg. Chem.*, 2006, **45**, 9442.

47. O. Kühl, *Coord. Chem. Rev.*, 2009, **253**, 2481.

48. D. S. McGuinness, W. Mueller, P. Wasserscheid, K. J. Cavell, B. W. Skelton, A. H. White and W. Englert, *Organometallics*, 2002, **21**, 175.

49. A. L. MacKinnon and M. C. Baird, *J. Organomet. Chem.*, 2003, **683**, 114.

50. R. E. Douthwaite, D. Haüssinger, M. L. H. Green and P. J. Silcock, *Organometallics*, 1999, **18**, 4584.

51. R. E. Douthwaite, M. L. H. Green, P. J. Silcock and P. T. Gomes, *Organometallics*, 2001, **20**, 2611.

52. R. Fränkel, J. Kniczek, W. Ponikwar, H. Nöth, K. Polborn and W. P. Fehlhammer, *Inorg. Chim. Acta*, 2001, **312**, 23.

53. R. J. Gillespie, *Chem. Soc. Rev.*, 1992, **21**, 59.

54. N. Kuhn, H. Bohnen, J. Fahl, D. Bläser and R. Boese, *Chem. Ber.*, 1996, **129**, 1579.

55. N. Kuhn, T. Kratz, D. Bläser and R. Boese, *Chem. Ber.*, 1995, **128**, 245.

56. P. L. Arnold and S. T. Liddle, *Chem. Commun.*, 2006, 3959.

57. P. L. Arnold and I. J. Casely, *Chem. Rev.*, 2009, **109**, 3599.

58. S. T. Liddle, I. S. Edworthy and P. L. Arnold, *Chem. Soc. Rev.*, 2007, **36**, 1732.

59. P. L. Arnold, A. J. Blake and C. Wilson, *Chem. Eur. J*, 2005, **11**, 6095.

60. P. L. Arnold, S. A. Mungur, A. J. Blake and C. Wilson, *Angew. Chem. Int. Ed.*, 2003, **42**, 5981.

61. I. S. Edworthy, A. J. Blake, C. Wilson and P. L. Arnold, *Organometallics*, 2007, **26**, 3684.

62. A. P. da Costa, J. A. Mata, B. Royo and E. Peris, *Organometallics*, 2010, **29**, 1832.

63. B. Wang, D. Wang, D. Cui, W. Gao, T. Tang, X. Chen and X. Jing, *Organometallics*, 2007, **26**, 3167.

64. B. Wang, D. Cui and K. Lv, *Macromolecules*, 2008, **41**, 1983.

65. C. Yao, C. Wu, B. Wang and D. Cui, *Organometallics*, 2013, **32**, 2204.

66. K. Lv and D. Cui, *Organometallics*, 2008, **27**, 5438.

67. P. L. Arnold, I. A. Marr, S. Zlatogorsky, R. Bellabarba and R. P. Tooze, *Dalton Trans.*, 2014, **43**, 34.

68. P. L. Arnold, T. Cadenbach, I. H. Marr, A. A. Fyfe, N. L. Bell, R. Bellabarba, R. P. Tooze and J. B. Love, *Dalton Trans.*, 2014, **43**, 14346.

69. Y. Pan, T. Xu, Y.-S. Ge and X.-B. Lu, *Organometallics*, 2011, **30**, 5687.

70. A. J. Arduengo, M. Tamm, S. J. McLain, J. C. Calabrese, F. Davidson and W. J. Marshall, *J. Am. Chem. Soc.*, 1994, **116**, 7927.

71. W. A. Herrmann, F. C. Munck, G. R. J. Artus, O. Runte and R. Anwander, *Organometallics*, 1997, **16**, 682.

72. D. Patel, S. T. Liddle, S. A. Mungur, M. Rodden, A. J. Blake and P. L. Arnold, *Chem. Commun.*, 2006, 1124.

73. P. L. Arnold and S. T. Liddle, *Organometallics*, 2006, **25**, 1485.

74. P. L. Arnold, S. Zlatogorsky, N. A. Jones, C. D. Carmichael, S. T. Liddle, A. J. Blake and C. Wilson, *Inorg. Chem.*, 2008, **47**, 9042.

75. S. P. Downing, S. C. Guadano, D. Pugh, A. A. Danopoulos, R. M. Bellabarba, M. Hanton, D. Smith and R. P. Tooze, *Organometallics*, 2007, **26**, 3762.

76. Z.-G. Wang, H.-M. Sun, H.-S. Yao, Q. Shen and Y. Zhang, *Organometallics*, 2006, **25**, 4436.

77. Z. Li, M. Xue, H. Yao, H. Sun, Y. Zhang and Q. Shen, *J. Organomet. Chem.*, 2012, **713**, 27.

78. S. T. Liddle and P. L. Arnold, *Organometallics*, 2005, **24**, 2597.

79. Z. R. Turner, R. Bellabarba, R. P. Tooze and P. L. Arnold, *J. Am. Chem. Soc.*, 2010, **132**, 4050.

80. P. L. Arnold, Z. R. Turner, A. I. Germeroth, I. J. Casely, R. Bellabarba and R. P. Tooze, *Dalton Trans.*, 2010, **39**, 6808.

81. P. L. Arnold, Z. R. Turner, N. Kaltsoyannis, P. Pelekanaki, R. Bellabarba and R. P. Tooze, *Chem. Eur. J*, 2010, **16**, 9623.

82. J. Zhang, H. Yao, Y. Zhang, H. Sun and Q. Shen, *Organometallics*, 2008, **27**, 2672.

83. P. L. Arnold and S. T. Liddle, *Chem. Commun.*, 2005, 5638.

84. P. L. Arnold, S. T. Liddle, J. McMaster, C. Jones and D. P. Mills, *J. Am. Chem. Soc.*, 2007, **129**, 5360.

85. P. L. Arnold and S. T. Liddle, *C. R. Chim.*, 2008, **11**, 603.

86. M. Glanz, S. Dechert, H. Schumann, D. Wolff and J. Springer, *Z. Anorg. Allg. Chem.*, 2000, **626**, 2467.

87. H. Schumann, M. Glanz, J. Winterfeld, H. Hemling, N. Kuhn and T. Kratz, *Chem. Ber.*, 1994, **127**, 2369.

88. H. Yao, Y. Zhang, H. Sun and Q. Shen, *Eur. J. Inorg. Chem.*, 2009, 1920.

89. X. Gu, X. Zhu, Y. Wei, S. Wang, S. Zhou, G. Zhang and X. Mu, *Organometallics*, 2014, **33**, 2372.

90. K. Lv and D. Cui, *Organometallics*, 2010, **29**, 2987.

91. K. R. Meihaus, S. G. Minasian, W. W. Lukens, S. A. Kozimor, D. K. Shuh, T. Tyliszczak and J. R. Long, *J. Am. Chem. Soc.*, 2014, **136**, 6056.

92. H. Schumann, D. M. M. Freckmann, S. Schutte, S. Dechert and M. Hummert, *Z. Anorg. Allg. Chem.*, 2007, **633**, 888.

93. H. Yao, J. Zhang, Y. Zhang, H. Sun and Q. Shen, *Organometallics*, 2010, **29**, 5841.

94. H. Schumann, M. Glanz, J. Winterfeld, H. Hemling, N. Kuhn and T. Kratz, *Angew. Chem. Int. Ed.*, 1994, **33**, 1733.

95. W. Xie, H. Hu and C. Cui, *Angew. Chem. Int. Ed.*, 2012, **51**, 11141.

96. Z.-G. Wang, H.-M. Sun, H.-S. Yao, Y.-M. Yao, Q. Shen and Y. Zhang, *J. Organomet. Chem.*, 2006, **691**, 3383.

97. W. Fegler, T. P. Spaniol and J. Okuda, *Dalton Trans.*, 2010, **39**, 6774.

98. W. Fegler, T. Saito, K. Mashima, T. P. Spaniol and J. Okuda, *J. Organomet. Chem.*, 2010, **695**, 2794.

99. C. Yao, D. Liu, P. Li, C. Wu, S. Li, B. Liu and D. Cui, *Organometallics*, 2014, **33**, 684.

100. W. J. Oldham, S. M. Oldham, B. L. Scott, K. D. Abney, W. H. Smith and D. A. Costa, *Chem. Commun.*, 2001, 1348.

101. I. J. Casely, S. T. Liddle, A. J. Blake, C. Wilson and P. L. Arnold, *Chem. Commun.*, 2007, 5037.

102. P. L. Arnold, Z. R. Turner, A. I. Germeroth, I. J. Casely, G. S. Nichol, R. Bellabarba and R. P. Tooze, *Dalton Trans.*, 2013, **42**, 1333.

103. W. J. Evans, S. A. Kozimor and J. W. Ziller, *Polyhedron*, 2004, **23**, 2689.

104. D. Pugh, J. A. Wright, S. Freeman and A. A. Danopoulos, *Dalton Trans.*, 2006, 775.

105. B. M. Gardner, J. McMaster and S. T. Liddle, *Dalton Trans.*, 2009, 6924.

106. S. A. Mungur, S. T. Liddle, C. Wilson, M. J. Sarsfield and P. L. Arnold, *Chem. Commun.*, 2004, 2738.

107. P. L. Arnold, I. J. Casely, Z. R. Turner and C. D. Carmichael, *Chem. Eur. J*, 2008, **14**, 10415.

Chapter 2

d-/*f*-Block Heterobimetallic NHC Complexes

2.1 Introduction

Heterobimetallic complexes containing *d*-block and *f*-block metals are interesting as the synergic effect of the two metals often leads to interesting structural properties and reactivity. For example, Thomas and coworkers have shown that the uranium-cobalt phosphinoamide complex [ICo(PhNPiPr$_2$)U(η^2-PhNPiPr$_2$)$_3$] **CX XIII**, **figure 2.1**, forms a Co→U dative bond.[1] The heterobimetallic complexes [{N[*o*-(NCH$_2$PiPr$_2$)C$_6$H$_4$]$_3$}AnCo(CO)$_3$] (An = Th, U) **CXXIV** contain a Co-An bond, has been prepared by J. Arnold and coworkers.[2] The *d*-/*f*-block heterobimetallic NHC complex [Nd(L′)(N(SiMe$_3$)$_2$){FeCp(CO)$_2$}] **CXXV** (L′ = tBuNC H$_2$CH$_2${C(NCSiMe$_3$CHNtBu)}) has been previously reported by our group.[3] Interestingly, this compound has an unsupported Nd−Fe bond with the tethered NHC ligand remaining bound to the neodymium centre through both the carbene and alkoxy donors. A search of the literature shows there is only one example of a *d*-/*f*-block heterobimetallic NHC complex where the NHC bridges between the

two metal centres, [MCl(MeIm)][UO_2(Ar$_2$nacnac)(μ-*N*,*C*-$C_4H_5N_2$)$_2$] (M =Fe, Co) **CXXVI**, **figure 2.1**.[4] Here, the NHC ligand coordinates to iron(II) or cobalt(II) centre through the soft carbene donor and to uranyl through the anionic nitrogen donor.

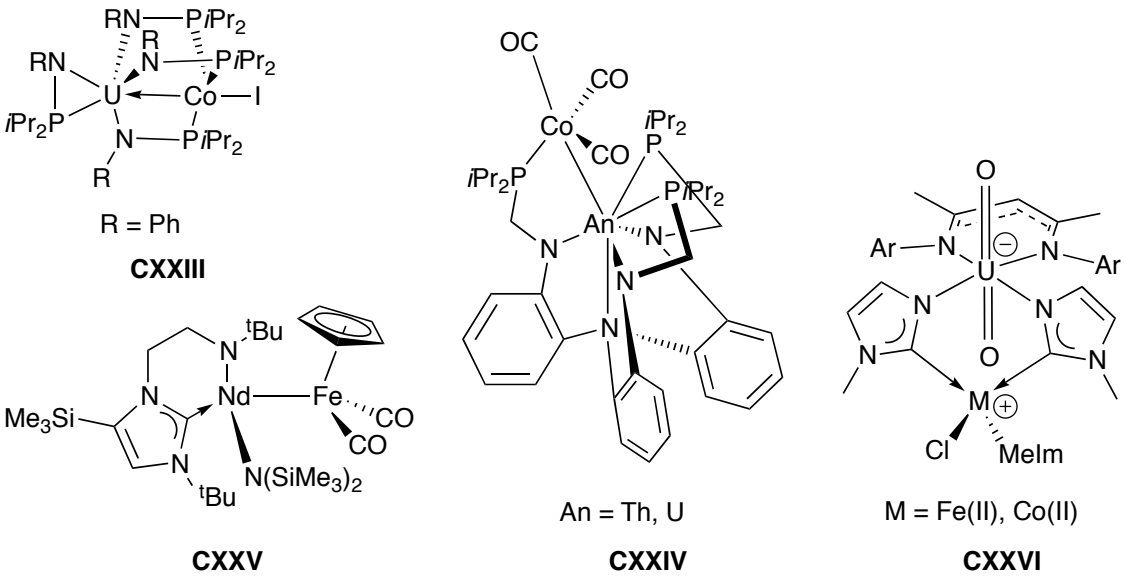

Figure 2.1. Example heterobimetallic complexes.

The unusual 'tuck-over' heterobimetallic complex [$Cp_2Ln(\mu$-H)(μ-η^1:η^5-C_5H_4)Ru(dmpe)] (Ln = Y, Lu) **CXXVII**, **scheme 2.1**, was prepared from the reaction between [$Cp_2Ln(CH_2SiMe_3)(THF)$] and [HRu(dmpe)Cp] (dmpe = bis(dimethylphosphino)ethane; Ln = Y, Lu) with the loss of tetramethylsilane. The Y-Cp σ-bond proved highly reactive and readily underwent insertion with alkynes to form [$Cp_2Y(\mu$-H){μ-(Ph)CC(Ph)(C_5H_4)}Ru(dmpe)] **CXXVIII**.[5]

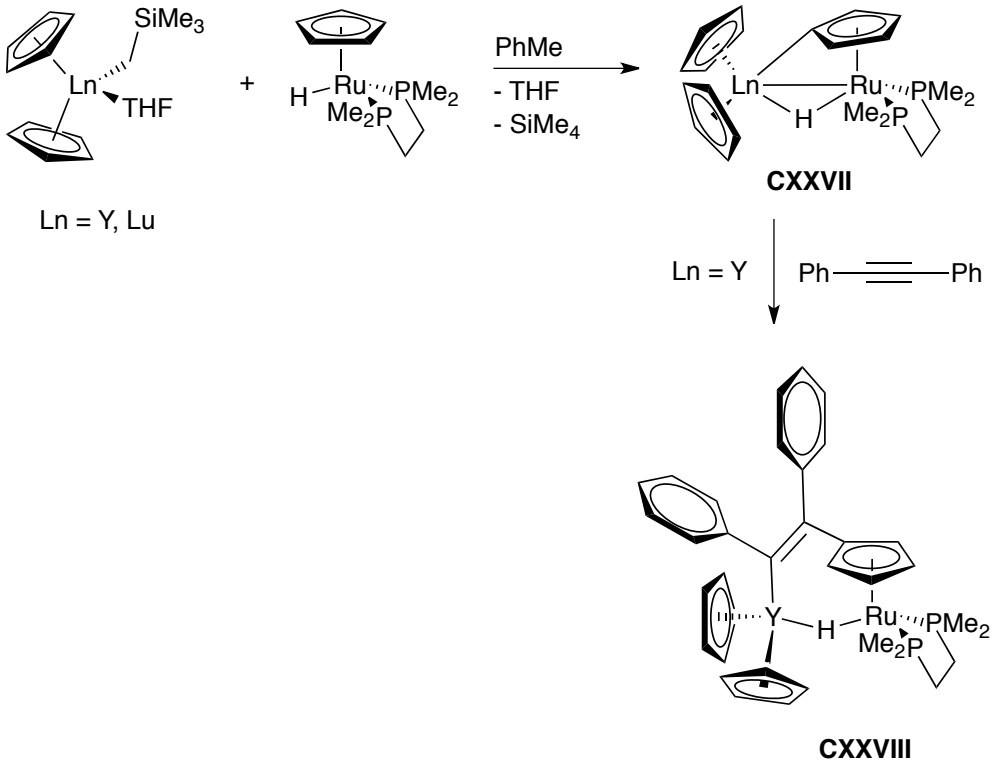

Scheme 2.1. Synthesis and reactivity of Ln-Ru heterobimetallic complex.[5]

Similarly, Hou and coworkers synthesised the Ln-Ru heterobimetallic complexes **CXXIX** and **CXXX** (Ln = Y, Ho and Dy), **figure 2.2**.[6] It was found that the $\mathbf{CXXIX}^{Y}$ reacts with carbon monoxide while $\mathbf{CXXX}^{Y}$ displays reactivity with organic nitriles, isonitriles, the imine PhCHNMe and group IX transition-metal carbonyls inserted into the $Y-CH_2$ bond.

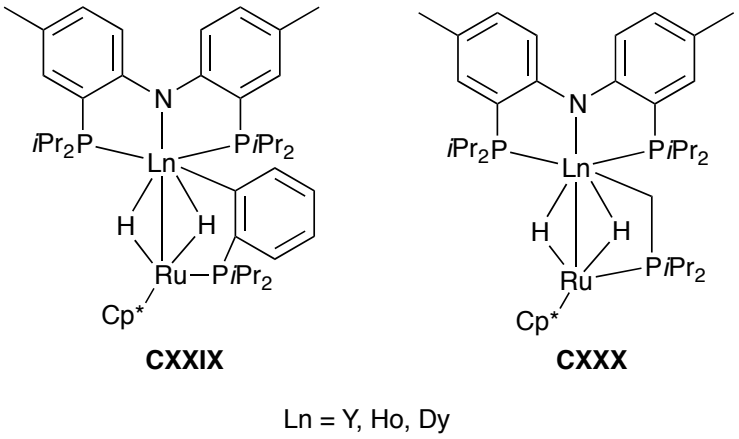

Figure 2.2. Structure of heterobimetallic complexes **CXXIX** and **CXXX**.[6]

2.2 General Approach

Initial attempts to make *d*-/*f*-block heterobimetallic complexes involved the addition of simple transition metal complexes to previously synthesised *f*-block tethered NHC complexes. It was thought the soft carbene ligand would bind preferentially to a transition metal centre while the anionic tether would remain bound to the *f*-block centre, **scheme 2.2**. However, when CoI_2 or $[Fe(N\{SiMe_3\})_2]$ were added to the previously synthesised cerium(III) and yttrium(III) complexes, $[(L^{Mes})_2Ce(N\{SiMe_3\}_2)]$[7] and $[(L^{iPr})_2Y(Cp)]$[8] (L^{Mes} = $OCMe_2CH_2$(1-C{NCH_2CH_2N}Mes)), no reaction was observed, **scheme 2.3**.

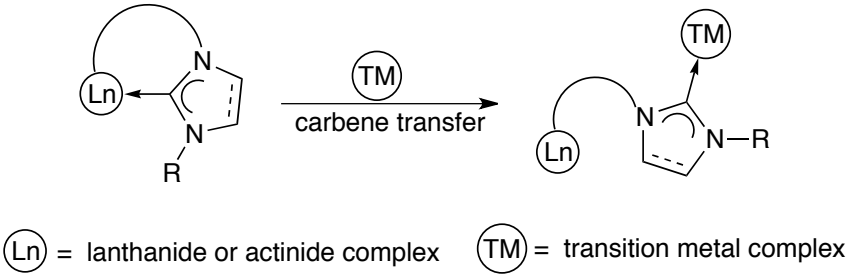

Scheme 2.2. Carbene transfer for bimetallic complex formation.

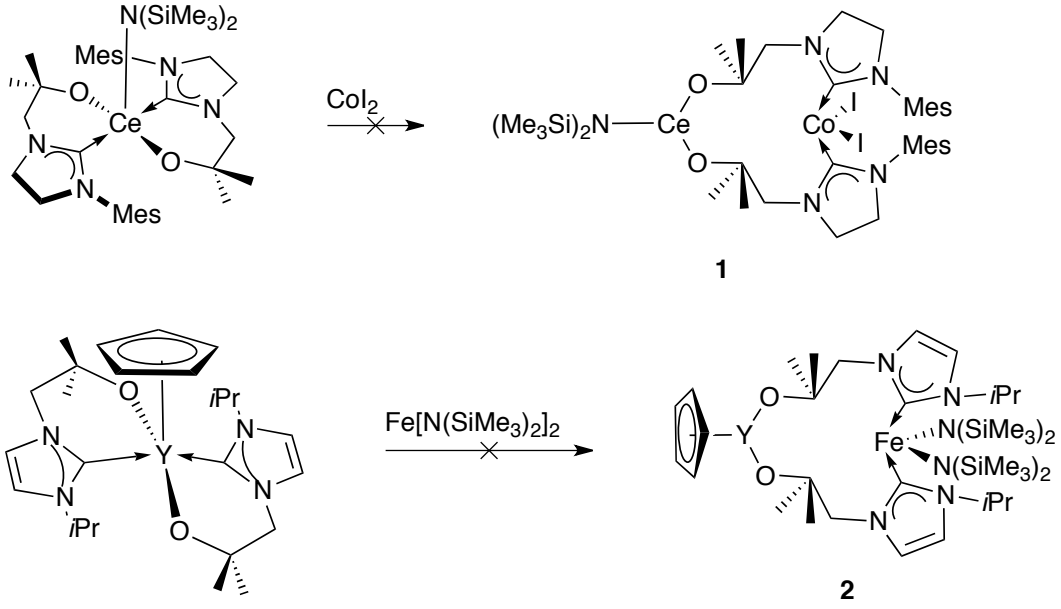

Scheme 2.3. Two example reactions which failed to produce heterobimetallic complexes using the carbene transfer method.

However, the addition of a transition metal alkoxy tethered NHC complex to an f-metal complex did result in d-/f-block heterobimetallic complex formation, **scheme 2.4**.

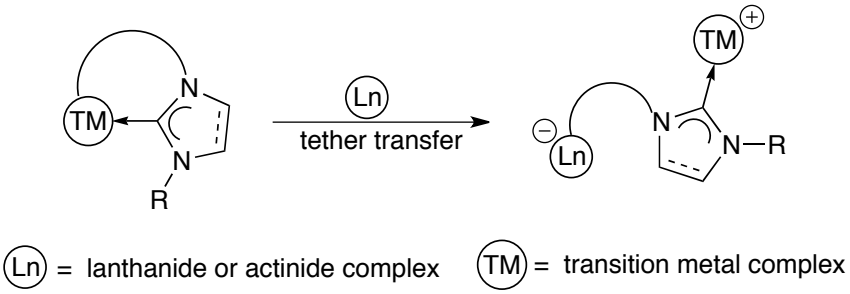

Scheme 2.4. Mechanism for bimetallic complex formation.

Here, the carbene remains bound to the transition metal centre while the alkoxy tether binds to the lanthanide or actinide complex.

2.3 Synthesis of $[M(L^{Mes})_2]$, M = Fe, Co

2.3.1 Synthesis of $[Fe(L^{Mes})_2]$, 3

The iron(II)-NHC complex $[Fe(L^{Mes})_2]$ **3** was synthesised by the protonolysis reaction of $[Fe(N\{SiMe_3\}_2)_2]$ with two equivalents of HL^{Mes}, **equation 2.1**. The organic molecule HL^{Mes} has been shown previously to be a carbene precursor, easily deprotonatable to form a bidentate alkoxy tethered NHC.[9] The ^{1}H NMR spectrum of **3** shows one set of paramagnetically shifted ligand resonances ranging from 26.80 ppm to −75.13 ppm. The *gem*-dimethyl groups occur as a single resonance at 26.80 ppm while the *o*-Me and *p*-Me groups occur as a single resonance at 3.63 ppm. Three resonances at −24.08, −52.65, −65.55 and the resonance at −75.13 ppm, integrating to two protons each, correspond to the three CH_2 groups and the two equivalent mesityl *m*-CH's. This is in contrast to the ^{1}H NMR spectrum of the previously reported, diamagnetic but isostructural, zinc analogue $[Zn(L^{Mes})_2]$ where the *gem*-dimethyl groups resonate as two singlets and all three mesityl methyl groups are inequivalent.[10]

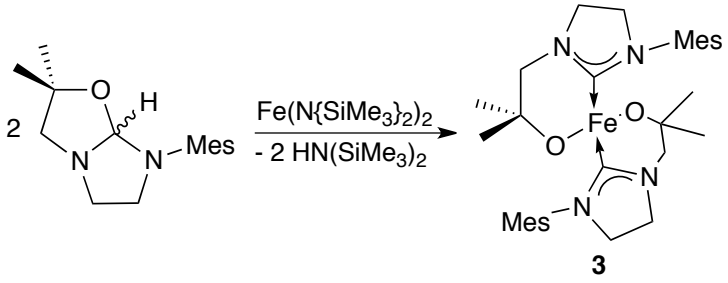

(2.1)

Crystals suitable for single crystal X-ray diffraction were obtained form a concentrated benzene solution at room temperature. The asymmetric unit contains two molecules **3** both of which are discussed here as the bond lengths and angles are different for the two units. **Figure 2.3** shows the solid state structure and

table 2.1 gives selected bond lengths and angles.[‡] The NHC ligands are bound to the iron centres through both the carbene donor and the alkoxy tether. Both Fe1 and Fe2 adopt a distorted tetrahedral geometry. For Fe1, the O1-Fe1-O2 angle is 121.13(16)° and the C1-Fe1-C17 angle is 115.77(16)°. For Fe2, the O3-Fe2-O4 angle is 119.3(2)° while the C49-Fe2-C33 angle is 116.1(3)°. The Fe-$C_{carbene}$ bond distances are 2.079(4) Å and 2.068(4) Å for Fe1-C1 and Fe1-C17, respectively, while the Fe2-C33 bond length is 2.058(4) Å and Fe2-C49 bond length is 2.057(6) Å. These are within the range for typical $Fe^{II}-C_{carbene}$ bond lengths of 1.95-2.17 Å.[11][12][13] The Fe-O bond lengths are 1.900(4) Å and 1.1914(4) Å for Fe1-O1 and Fe1-O2, respectively; and 1.874(5) Å and 1.889(5) Å for Fe2-O4 and Fe2-O3, respectively.

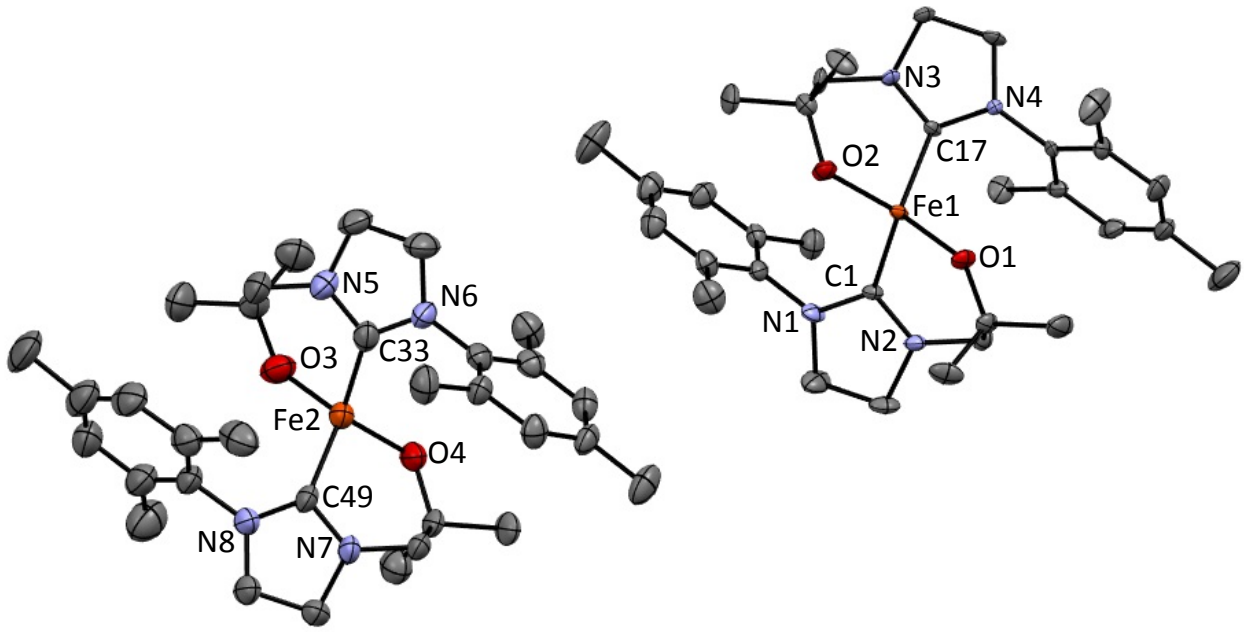

Figure 2.3. Solid state structure of **3**. Displacement elipsoids are shown at 50% probability level.

[‡]The CIF data for all structures presented in this thesis are provided on the accompanying CD.

Table 2.1: Selected bond lengths (Å) and angles (°) for **3**.

Bond		Bond\Angle	
Fe1-C1	2.079(4)	Fe2-O3	1.889(5)
Fe1-C17	2.068(4)	Fe2-O4	1.874(5)
Fe1-O1	1.900(4)	O1-Fe1-O2	121.13(16)
Fe1-O2	1.1914(4)	C1-Fe1-C17	115.90(17)
Fe2-C33	2.058(4)	O3-Fe2-O4	119.3(2)
Fe2-C49	2.057(6)	C33 -Fe2-C49	116.1(3)

Whilst not being as well developed as other late transition metal complexes,[14][15] iron-NHC complexes have received increasing attention in recent years. A search of the Cambridge Crystallographic Database (CCD) yields 257 structurally characterised iron-NHC complexes while there are nearly 900 results for ruthenium-NHC complexes but only 44 Zn-NHC complexes. **Table 2.2** gives the number of results for different metal-NHC complexes.[16]

Table 2.2: Number of structurally characterised metal-NHC complexes reported in the CCD.

M-NHC	no. results	M-NHC	no. results
Fe	257	Co	105
Ru	899	Ni	552
Os	50	Zn	44

To the best of our knowledge, **3** is the first iron complex supported by alkoxy-tethered NHC ligands. There are, however, some examples of bidentate bis(NHC) iron(II) complexes **CXXXI - CXXXIII**,[17][15][18] **figure 2.4**, which, as with **3**, adopt a distorted tetrahedral geometry.

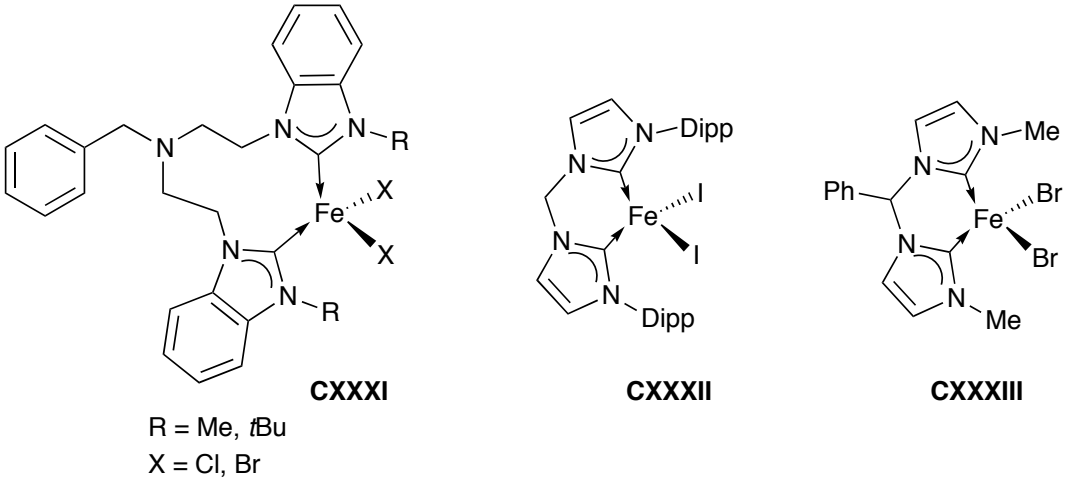

Figure 2.4. Examples of tetrahedral bidentate bis(NHC) iron(II) complexes.[17][15][18]

CXXXI was shown to be an effective catalyst for the homocoupling of Grignard reagents[15] while **CXXXIII** was shown to be an effective catalyst for the Grignard-alkyl halide cross coupling reaction.[18]

2.3.2 Synthesis of $[Co(L^{Mes})_2]$, 4

$[Co(L^{Mes})_2]$ **4** was synthesised in a similar way to **3**. Addition of two equivalents of HL^{Mes} to $[Co(N\{SiMe_3\}_2)_2(THF)]$ in hexane affords $[Co(L^{Mes})_2]$ as yellow solid in an 85% yield, **equation 2.2**.

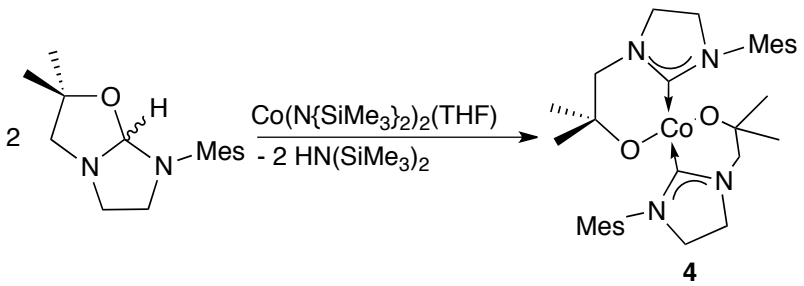

(2.2)

4 displays no observable ^1H NMR spectrum as the resonances were paramagnetically broadened into the base line. **4** is highly soluble in arene solvents and

attempts to crystallise the complex from benzene, toluene or hexane yielded thin needle shaped crystals that were unsuitable for x-ray analysis. Addition of a donor such as triphenyl phosphine or 4,4-bipyridine did not coordinate to the cobalt centre, instead the donor crystallised out of solution. However, elemental analysis is consistent with the assignment of **4**; calculated results, C 66.53, H 8.03 and N 9.70, and found results C 66.36, H 8.16 and N 9.62.

To the best of our knowledge there are no other examples of cobalt complexes supported by alkoxy-tethered NHC ligands reported in the literature. However, cobalt(II) benzyl-tethered NHC complexes have been previously reported, **CXXXIV - CXXXVII**[19][20] **figure 2.5**. They adopt a distorted square planar geometry and show insertion reactivity into the Co-C_{benzyl} bond. **Table 2.2** shows the paucity of Co-NHC complexes, with only 105 structurally characterised examples reported in the literature, compared to 257 examples for iron-NHC complexes.

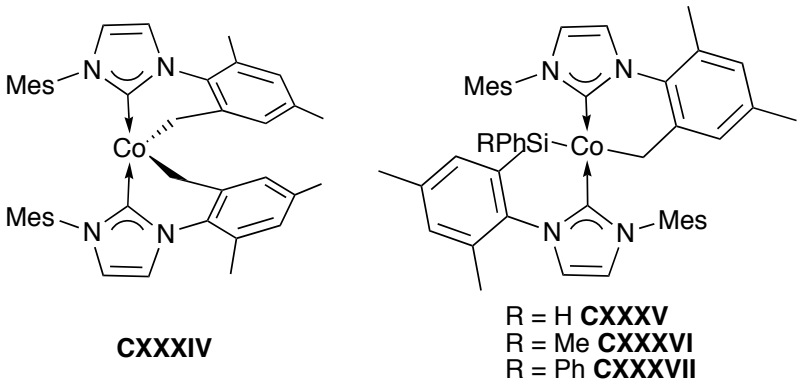

Figure 2.5. Example distorted square planar benzyl-tethered NHC cobalt(II) complexes.[19][20]

2.4 Synthesis of [(L^{Mes})TM(μ-L^{Mes})U-(μ-{$N(SiMe_3)Si(Me)_2CH_2$})($N\{SiMe_3\}_2$)$_2$], (TM = Fe, Co)

As previously noted, there is only one example of a *d*-/*f*-block heterobimetallic NHC complex reported in the literature, **CXXVI scheme 2.1**,[4] and the bidentate alkoxy-tethered NHC ligands developed by the Arnold group are ideally set up to bridge between two metal centres as it has both a soft carbene donor and a hard anionic oxygen donor. Iron complexes and iron-NHC complexes have been shown to have very interesting reactivity.[21][22][23][24][25][26] Furthermore, the synergic effect between a Lewis acidic *f*-element and a Lewis acidic transition metal could lead to reactivity that is enhanced or completely different when compared to monometallic *f*-element or transition metal complexes. Thus, the transition metal complexes **3** and **4** are ideally set up to react with a suitable lanthanide or actinide complex.

Treatment of [M(L^{Mes})$_2$] (M = Fe **3**, Co **4**) with the uranium(IV) metallacycle [($\{Me_3Si\}_2N)_2U\{N(SiMe_3)Si(Me_2)CH_2\}$] affords the *d*-/*f*-block heterobimetallic complexes, [(L^{Mes})Fe(μ-L^{Mes})U(μ-{$N(SiMe_3)Si(Me)_2CH_2$})($N\{SiMe_3\}_2$)$_2$] **5** and [(L^{Mes})Co(μ-L^{Mes})U(μ-{$N(SiMe_3)Si(Me)_2CH_2$})($N\{SiMe_3\}_2$)$_2$] **6** in 76 % yield and 81 % yield, respectively, after work up, **equation 2.3**.

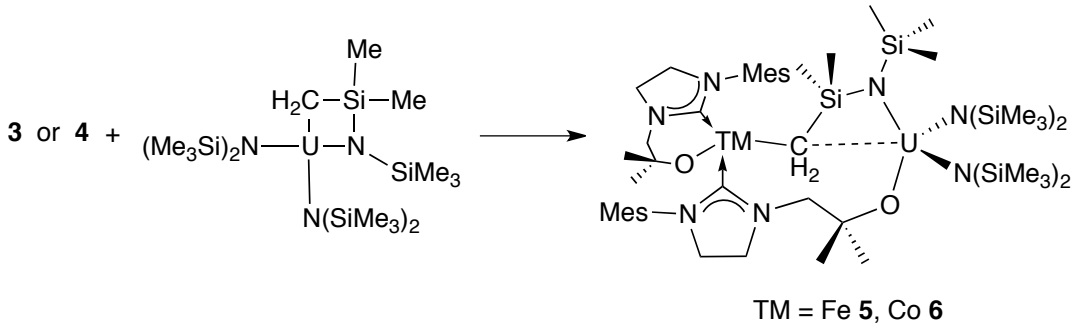

(2.3)

In both **5** and **6** one of the alkoxy tethers binds to the uranium metallacycle while the carbene remains bound to the transition metal. The $\{CH_2Si(Me_2)N(SiMe_3)\}$ ligand of the metallacycle acts as a second bridging ligand with the amide remaining bound to the uranium while the CH_2 binds to the transition metal. There is no change in the oxidation states of the metals, with the transition metal centre remaining in the $+2$ oxidation state and the uranium remaining the $+4$ oxidation state.

2.4.1 $[(\mathbf{L^{Mes}})\mathbf{Fe}(\mu\text{-}\mathbf{L^{Mes}})\mathbf{U}(\mu\text{-}\{\mathbf{N(SiMe_3)Si(Me)_2CH_2}\})(\mathbf{N\{SiMe_3\}_2})_2]$, 5

The ^{1}H NMR spectrum of **5** shows paramagnetically shifted and broadened ligand resonances from 91.17 ppm to -87.39 ppm. The two terminal $[N(SiMe_3)_2]$ groups are inequivalent, displaying resonances at -18.25 and -26.43 ppm. On the bridging silylamide ligand, the protons of the $SiMe_3$ group resonate at 51.97 ppm while the protons of the $SiMe_2$ group resonate at 29.36 ppm. Due to its position between two paramagnetic centres, the protons of the bridging CH_2 could not be located. These chemical shifts have changed significantly from those of the uranium metallcycle, **table 2.3**, where the two $[N(SiMe_3)_2]$ groups are equivalent and occur at

−13.03 ppm, while the protons of th $NSi(CH_3)_3$ and $NSi(CH_3)_2$ groups resonate at 9.62 and 11.23 ppm, respectively.[27]

Table 2.3: Comparison of ^{1}H NMR spectrum chemical shifts of **5** and $[(\{Me_3Si\}_2N)_2U\{N(SiMe_3)Si(Me_2)CH_2\}]$. Chemical shifts given in ppm

Protons	**5**	$[(\{Me_3Si\}_2N)_2U\{N(SiMe_3)Si(Me_2)CH_2\}]$
$N(Si\mathit{Me}_3)_2$	−18.25, −26.43	−13.03
$NSi\mathit{Me}_3$	51.97	9.62
$NSi\mathit{Me}_2$	29.63	11.23
$C\mathit{H}_2$	not observed	−118.4

Only one set of alkoxy tethered carbene ligands is observed in the ^{1}H NMR spectrum. This is presumably the ligand bound bidentate to the iron centre, as the other ligand is bound to two paramagnetic metals and is probably the one not observed. The two *gem*-methyl groups occur at 91.17 and 79.00 ppm while the three CH_2 groups occur at −61.81, −75.01 and 87.39 ppm. The *p*-methyl protons resonate at −45.53 and the *o*-methyl groups resonate at 0.12 ppm. The *o*- and *p*-methyl groups are display considerably different chemical shifts when compared to $[Fe(L^{Mes})_2]$, where they occur as a single resonance at 3.63 ppm. The CH_2 groups, on the other hand, occur in the region of −50 to −90 ppm in both complexes. Also the *gem*-dimethyl protons resonate at 26.80 ppm in **3**, whereas they occur as two singlets in **5**.

The ^{29}Si NMR spectrum displays three resonances at −21.84 −74.60 and −81.91 ppm. This is consistent with the silicon atoms of the two terminal $[N(SiMe_3)_2]$ groups being equivalent with the other resonances due to the $NSiMe_3$ and $NSiMe_2$ groups on the bridging silylamide. These chemical shifts are similar to those of $[(\{Me_3Si\}_2N)_2U\{N(SiMe_3)Si(Me_2)CH_2\}]$, which has three resonances in the ^{29}Si NMR spectrum at −74, −83 and −152 ppm due to the two terminal $[N(SiMe_3)_2]$

and the $NSiMe_3$ and $NSiMe_2$ groups.[28].

In the solid state **5**, **figure 2.6**, the U-N bond lengths, **table 2.4**, for the terminal silylamide ligands are 2.292(4) Å for U1-N6 and 2.329(4) Å for U1-N7; the U-N bond length for the bridging silylamide ligand, U1-N5, is shorter at 2.274(3) Å. These bonds are within the range of typical U^{IV}-$N_{silylamide}$ bond lengths of 2.246 Å[29] to 2.379 Å.[30] The U1-N5-Si1 angle of 105.20(15)° is significantly smaller than the U-N-Si bond angles for the terminal silylamides which are in the range 110.71(17)° to 131.42(19)°, **table 2.5** gives the U-N-Si angles. This small angle is a result of C33 being bound the the iron centre and having an interaction with the uranium centre. There is little distortion in the tetrahedral geometry of Si1 which bond angles of 107.8(2)° for C33-Si1-C35 and 106.12(16)° for C33-Si1-N5.

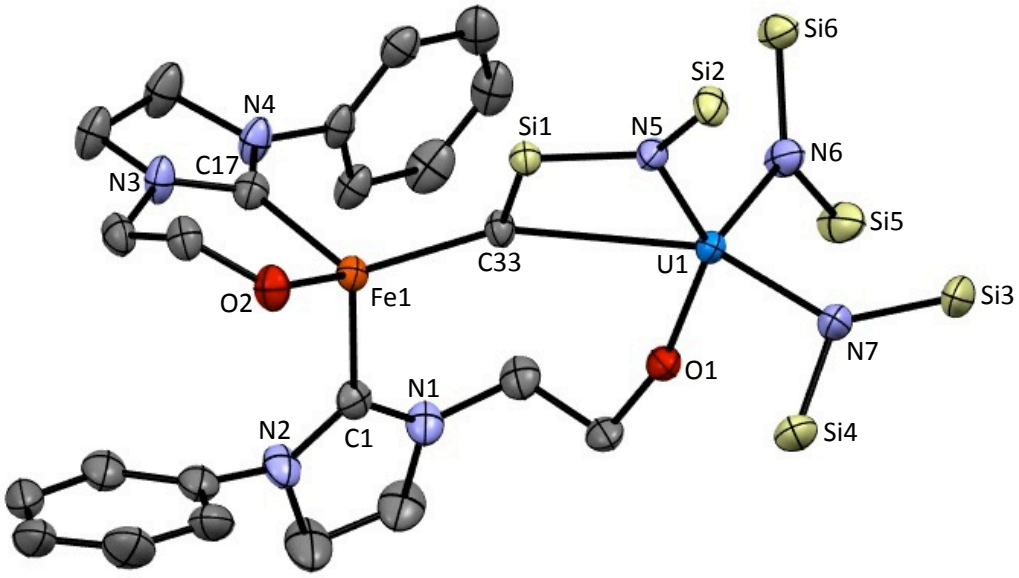

Figure 2.6. Solid state structure of **5**. For clarity, H atoms and methyl groups are omitted. Displacement elippsoids drawn at 50% probability.

Table 2.4: Selected bond lengths (Å) for **5**.

Bond		Bond	
Fe1-C1	2.144(4)	U1-N6	2.292(4)
Fe1-C17	2.086(4)	U1-N7	2.329(4)
Fe1-C33	2.152(3)	U1$\cdots$C33	2.891(3)
Fe1-O2	1.878(3)	Si1-C33	1.856(4)
U1-O1	2.111(3)	U1-N5	2.274(3)
Fe$\cdots$U	4.934		

The uranium centre adopts a highly distorted trigonal bipyramidal geometry, with a N6-U1-N7 angle of 106.91(12)°and an O1-U1-N5 angle of 138.79(11)°. This large O1-U1-N5 accommodates an electrostatic interaction with the δ −ve C33, with a U1$\cdots$C33 separation of 2.891(3) and is outside the range of previously published U−CH_2 bonds of 2.368(7) Å[31] to 2.752(11) Å.[32] However, it is shorter than the C-H→U agostic interactions reported by Scott and co-workers of 3.056(14) Å and 3.218(10) Å.[32] The N5-U1-C33 angle is 66.52°and O1-U1-C33 angle is 76.21°.

Table 2.5: U-N-Si angles (°) for **5**.

Angle		Angle	
U1-N5-Si1	105.20(15)	U1-N6-Si6	125.32(18)
U1-N5-Si2	130.71(17)	U1-N7-Si3	131.42(19)
U1-N6-Si5	117.36(18)	U1-N7-Si4	110.71(17)

The iron centre is also four coordinate with one ligand being bound bidentate and to the bridging NHC ligand through the carbene donor and to the bridging silylamide through the CH_2 group. The Fe−$C_{carbene}$ bond lengths are 2.144(4) Å

for Fe1-C1 and 2.086(4) Å Fe1-C17. Comparison of the Fe1-C17 bond length with the Fe−$C_{carbene}$ bond lengths of **3** shows no significant change. Fe1-C1 is longer than the Fe-$C_{carbene}$ bond lengths in **3** and of a similar length to the Fe-$C_{carbene}$ bond length of **CXXVI**, **scheme 2.1**, of 2.095(5) Å.[4] The Fe1-O2 bond length of 1.878(3) Å in **5** is shorter than those in **3**, 1.900(4) Å and 1.914(4) Å. The Fe1-C33 bond length is 2.152(3) Å, within the range of previously published Fe−CH_2 bonds (1.876(8) - 2.336(2) Å[33][34]). Fe1 has a distorted tetrahedral geometry with a C1-Fe1-C17 angle of 98.2(9)°and an O2-Fe1-C33 angle of 115.6(6)°, **table 2.6**. The $C_{carbene}$-Fe-$C_{carbene}$ angle is much more acute in **5** than those in the crystallographically independent molecules in **3**; 98.29(15)°compared with 115.9(2)° and 116.1(2)°.

Table 2.6: Fe-ligand angles (°) for **5**.

Angle		Angle	
O2-Fe1-C17	94.62(14)	C1-Fe1-C33	109.06(15)
C1-Fe1-C17	98.29(15)	O2-Fe1-C1	113.60(15)
O2-Fe1-C33	115.66(13)	C17-Fe1-C33	124.18(16)

The complex decomposed when heated above 30°C, regardless of solvent, and did not produce a ^{1}H NMR spectrum which could be interpreted, though $HN(SiMe_3)_2$ was identified. This is possibly a result of thermally activated cyclometallation at the U···CH_2 interaction, as has been observed in early transition metal chemistry[35] and in the synthesis of $[(\{Me_3Si\}_2N)_2An\{N(SiMe_3)Si(Me_2)CH_2\}]$ (An = U, Th),[27] followed by loss of $HN(SiMe_3)_2$ and decomposition.

Alternative synthesis of 5

The reaction between **3** and $[U\{N(SiMe_3)_2\}_3]$ yields **5**, as evidenced by ^{1}H NMR spectrum and x-ray crystallographic data that were identical the the data pro-

duced from the reaction between **3** and $[(\{Me_3Si\}_2N)_2U\{N(SiMe_3)Si(Me_2)CH_2\}]$. A speculative mechanism is outlined in **scheme 2.5**.

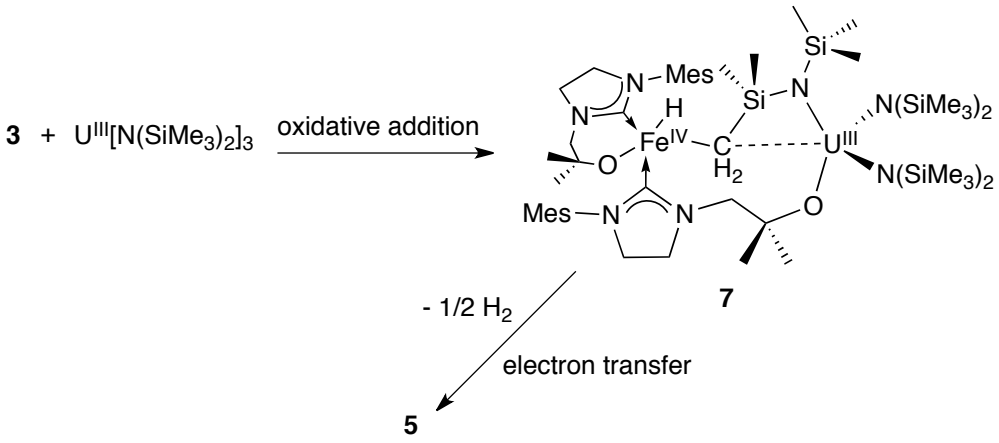

Scheme 2.5. Alternative synthesis of **5**.

Here, the alkoxy tether transferes to the uranium centre while a CH bond from one of the $[N(SiMe_3)_2]$ groups oxidatively adds to the iron centre to form an iron(IV) hydride. The uranium centre remains in the + 3 oxidation state. In the second step the uranium iron hydride complex **7** loses $\frac{1}{2}H_2$ and undergoes electron transfer to form **5**, with the iron centre in the + 2 oxidation state and the uranium centre in the + 4 oxidation state

2.4.2 Reactivity of 5 with 2,6-dimethylphenyl isocyanide

The reaction between **5** and 2,6-dimethylphenyl isocyanide proved complicated with partial decomposition occurring, however the U^{IV} metallacycle, $[(\{SiMe_3\}_2N)_2U\{N(SiMe_3)Si(Me_2)C(CH_2)N(2,6-Me-C_6H_3)\}]$ **8** was isolated in 26% yield, **equation 2.4**.

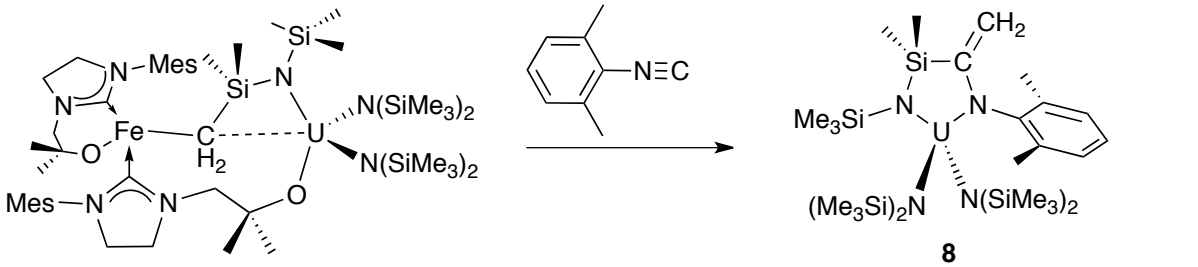

5 **8**

\+ decomposition products

(2.4)

The ^{1}H NMR spectrum of the reaction mixture showed multiple products. The resonances due to the two [$N(SiMe_3)_2$] groups of **8** occurred as a broad singlet at −61.63 ppm while resonances at −0.16, −0.23 and −24.44 ppm are due to the protons of the methyl groups of $SiMe_3$, $NSiMe_3$ and *o*-Me. The two CH_2 groups resonate at 55.47 and −14.72 and the *p*-CH resonates at −0.32 ppm. Furthermore, there are three very broad resonances at 17.22, 1.10 and −2.70 ppm which could not be assigned as a ligand containing complex and could be due to the decomposition of the iron containing moiety of **5**. Further complicating the spectrum were a number of diamagnetic resonances which did not correspond to HL^{Mes}. The reaction between **5** and two equivalents of 2,6-dimethylphenyl isocyanide produced analogous products with sets of resonances due to an equivalent of unreacted isocyanide. As further comparison, one equivalent of 2,6-dimethyl isocyanide was added to **3** and no reaction occurred even when the reaction was heated to 70°C for 16 h.

As stated, **8** was isolated from the reaction mixture as a crystalline solid, **figure 2.7**, and to the best of our knowledge this analogue has not been reported in the literature. Here, the isocyanide inserts into the U$\cdots$$CH_2$ interaction, to form new N−U and C−Si bonds while cleaving the CH_2−Fe and CH_2−Si bonds to form a terminal alkene. The structure consists of a 5-membered {−U^{IV}−N−Si−C−N−}

metallacycle with a 2,6-dimethylphenyl group and and $SiMe_3$ group on each of the nitrogen atoms, a $=CH_2$ on the carbon atom and two methyl groups on the silicon atom. The uranium centre has two terminal $[N(SiMe_3)_2]$ groups.

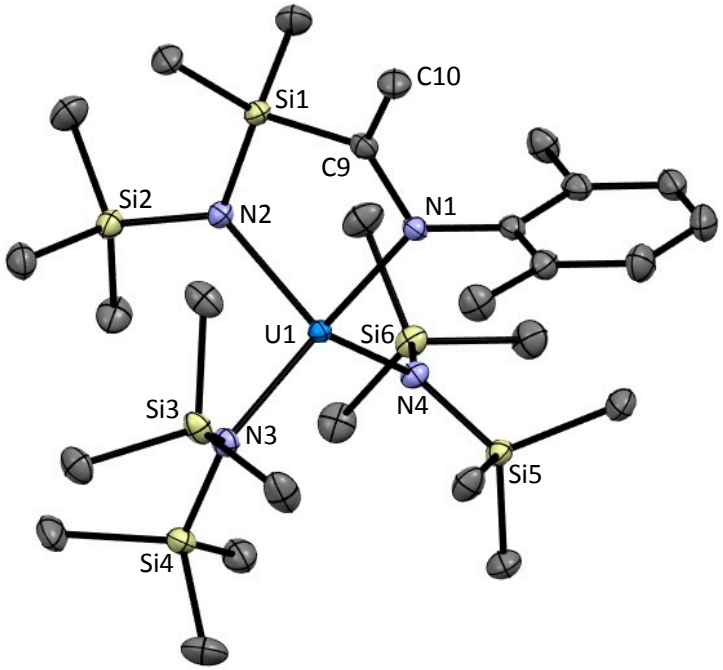

Figure 2.7. Solid state structure of **8**. For clarity, hydrogen atoms and crystallised solvent are not shown. Displacement elipsoids are shown at 50% probability.

Table 2.7: Bond lengths (Å) and angles (°) for **8**.

Bond		Bond		Angle	
U1-N1	2.2554(17)	N2-Si1	1.7378(18)	U1-N2-Si1	109.84(9)
U1-N2	2.2336(17)	N1-C9	1.426(3)	N2-Si1-C9	106.49(9)
U1-N3	2.2701(18)	C9-Si1	1.899(2)	Si1-C9-N1	119.20(15)
U1-N4	2.2679(17)			C9-N1-U1	109.88(13)
C9-C10	1.346(3)			N1-U1-N2	89.45(6)
				N3-U1-N4	117.50(6)

The uranium centre remains in the +4 oxidation state and adopts a distorted tetrahedral geometry with an N1-U1-N2 angle, **table 2.7**, of 89.45(6)° while N3-U1-N4 has a larger angle of 117.50(6)° due to the steric bulk of the [$N(SiMe_3)_2$] groups. The two terminal U-N bonds are 2.2701(18) Å and 2.2679(17) Å for U1-N3 and U1-N4, respectively and within the range of typical U^{IV}-$N_{silylamide}$ bond lengths of 2.246 Å[29] to 2.379 Å.[30] The U1-N1 and U2-N2 bond lengths are shorter at 2.2554(17) Å and 2.2336(17) Å, respectively. The C9-C10 bond length of 1.346(3) Å is typical of C=C double bond.

This reactivity has been previously noted by Simpson and Andersen between [($\{Me_3Si\}_2N)_2M\{N(SiMe_3)Si(Me_2)CH_2\}$] (M = U, Th) and isocyanides, **CXXXIX**, or CO, **CXXXVIII**, **scheme 2.6**.[36]

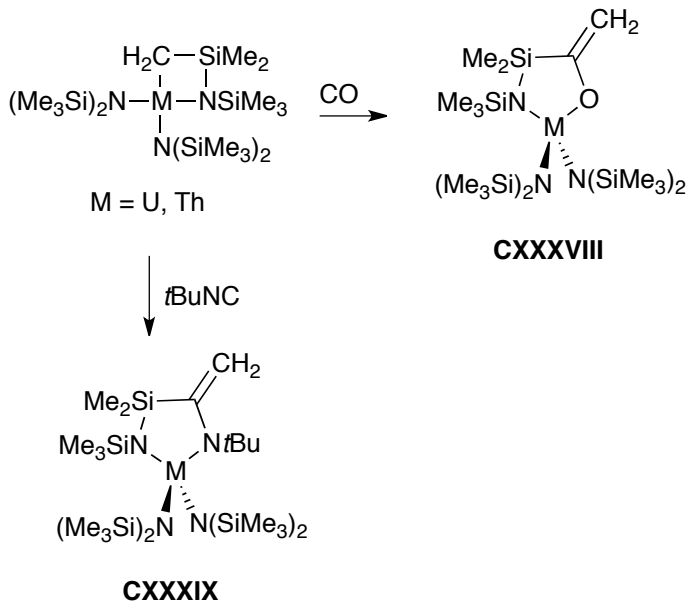

Scheme 2.6. Reactivity of [($\{Me_3Si\}_2N)_2M\{N(SiMe_3)Si(Me_2)C(CH_2)N(2,6-Me-C_6H_3)\}$] (M = U, Th) with CO and *t*BuNC.[36]

2.4.3 Reactivity of 5 with CO

The CO chemistry of uranium(III) has been extensively studied. [U(η−C_8H_6 {Si(iPr)$_3$−1, 4 }$_2$)(η^5−Cp^R)] (Cp^R = C_5Me_5 or C_5Me_4H) reductively homologates CO to form the deltate dianion **CXL**,[37] squarate dianion **CXLI**[38] or the ynediolate **CXLII** if one equivalent of CO is used,[39] **figure 2.8**. The reaction between CO and [U(N{$SiMe_3$}$_2$)$_3$] gives exclusively the ynediolate and forms ene-diolate [U(N{$SiMe_3$}$_2$)$_3$]$_2$[(μ−η^1:η^1OCCO)] when heated.[40] The CO chemistry of iron is a fundamental area of organometallic chemistry and has been studied for over one hundred years.[41]

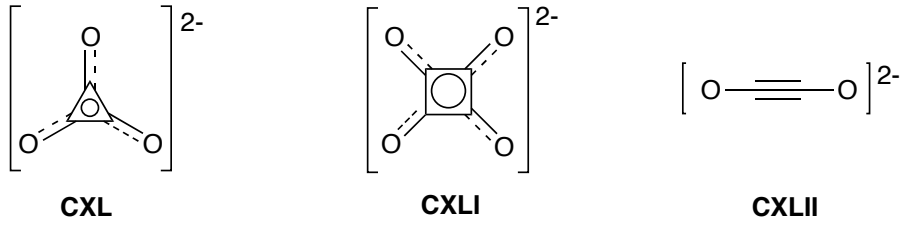

Figure 2.8. Structure of the deltate **CXL**, squarate **CXLI** and ynediolate **CXLII** dianions.

To this end the reactivity of **5** with CO was investigated. A degassed solution of **5** in C_6D_6 in a Young's tap NMR tube was pressurised with 1 atm of CO, resulting in the formation of a precipitate. Analysis of the ^{1}H NMR spectrum showed the formation of [({$SiMe_3$}$_2$N)$_2$U{N($SiMe_3$)Si(Me_2)C(CH_2)CO}], **equation 2.5**, previously described by Simpson and Andersen.[36] The precipitate was isolated but could not be analysed by ^{1}H NMR spectroscopy as it proved insoluble even in hot d^5-pyridine. It is proposed that the precipitate results from the iron-containing decomposition products.

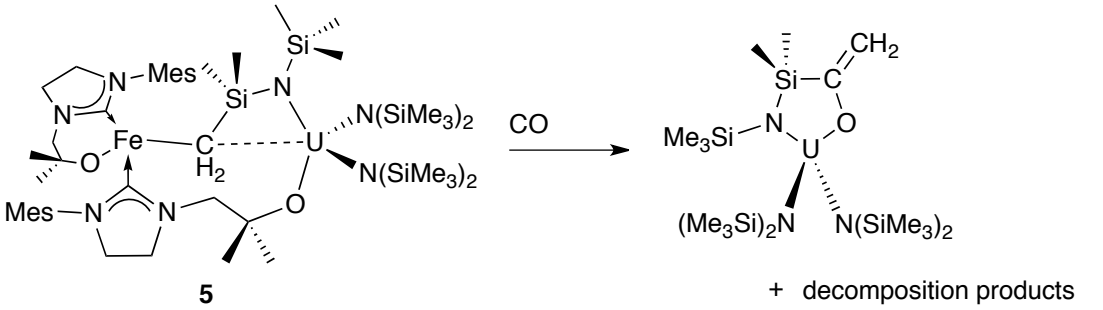

(2.5)

2.4.4 Rectivity of 5 with azides

Previous work in our group has shown that organic azides can add across metal-carbene bond of **CXLIII**, breaking the nitrogen-R bond when R = $SiMe_3$, PPh_2, $Sn(n\text{Bu})_3$ (**CXLIV**) or form the insertion product when R = Ad (**CXLV**), and forming a zwitterionic complex,[42] **scheme 2.7**.

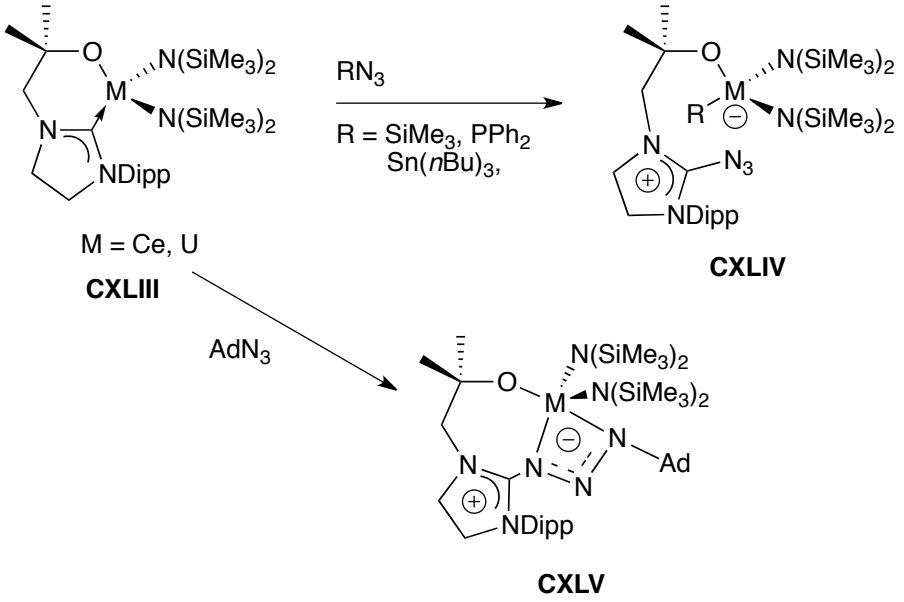

Scheme 2.7. Previously published reactivity of organic azides across the M-carbene bond.[42]

To this end, one equivalent of **5** was added to RN_3 (R = Ph_3Si, Ad, TMS) in toluene solution, **scheme 2.8**. However, analysis of the ^1H NMR spectrum showed no reaction had occurred.

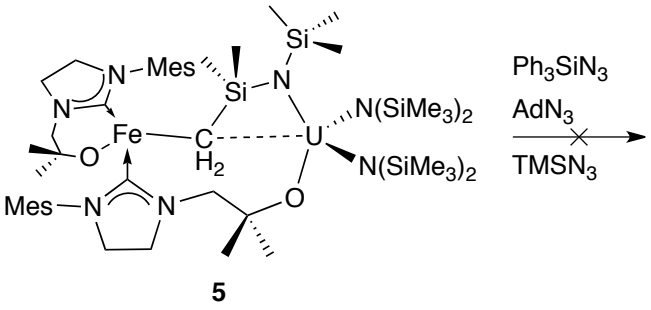

Scheme 2.8. Reactivity between **5** and azides.

It has been shown that photolysis of a of an iron(II) azide can form, with the loss of dinitrogen gas, a terminal iron(IV) nitride,[43] **equation 2.6**.

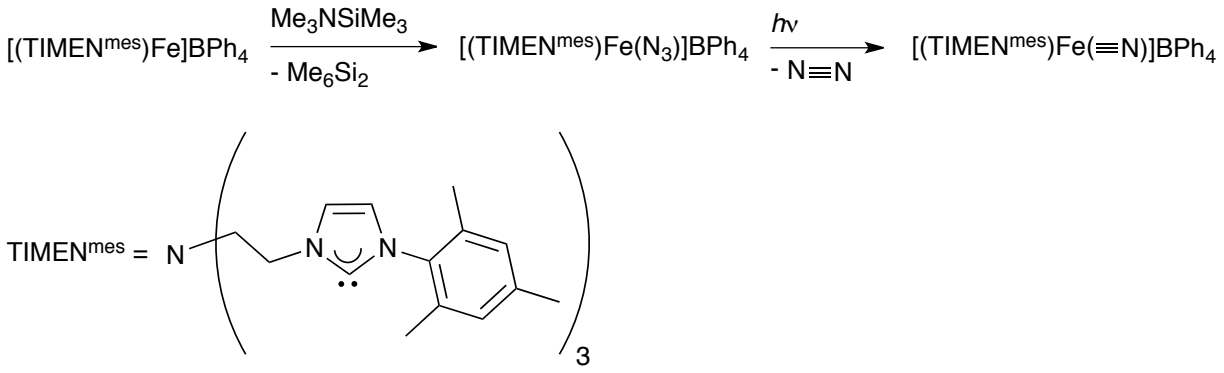

(2.6)

Thus, the mixture of **5** and $TMSN_3$ was irradiated under UV light in an attempt to form a terminal azide. However, analysis of the ^1H NMR spectrum revealed that no reaction had occurred. Similarly, no reaction was observed between **5** and NaN_3, which has been shown to generate terminal azides,[44] whether or not it was irradiated with UV light. No reaction occurred upon addition of 18-crown-6 in attempt to abstract the sodium cation.

2.4.5 Reaction of 5 with boranes

Boranes have been shown to add across metal-carbene bonds in an manner analogous to azides,[42] and to coordinate to NHCs.[45][46] Therefore, reactions between **5** and several boranes were carried out. However, none were successful, the ^1H NMR spectrum showing only starting materials, **scheme 2.9**.

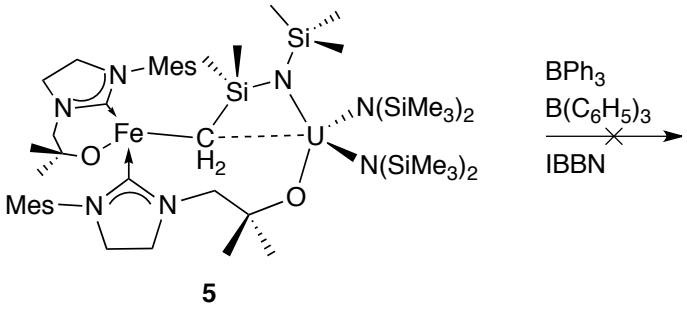

5

Scheme 2.9. Reactivity of **5** with boranes.

2.4.6 Redox reactions of 5

Addition of one equivalent of *m*-chloroperbenzoic acid (*m*CPBA) to **5** in THF with the aim of oxidising **5** did not result in a reaction according to the ^{1}H NMR spectrum, **scheme 2.10**. Both **5** and *m*CPBA could be identified in the ^{1}H NMR spectrum. Heating the reaction resulted in the decomposition of **5**.

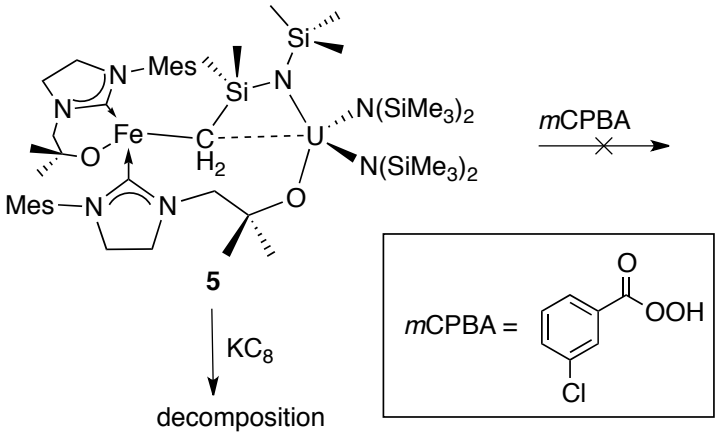

Scheme 2.10. Oxidation and reduction agents with **5**.

Previous work published by our group has shown that potassium graphite (KC_8) is capable of reducing U^V to U^{IV}.[47] In an attempt to reduce **5**, one equivalent of KC_8 was added and the reaction carried out in THF. The reaction was allowed to stir for 16 h during which time graphite formed as a black precipitate and was removed by filtration. ^{1}H NMR spectroscopy of the supernatant showed decomposition of **5**.

2.4.7 Reactivity of 5 with CO_2 and H_2

Our group has previously used uranium(III)- and scandium(III)-NHC complexes to activate CO_2.[48][49][50] CO_2 also reacts with $[U(N\{SiMe_3\}_2)_3]$ to give $[U(OSi(Me_3)_4)]$ and $O{=}C{=}NSiMe_3$ as an elimination product.[51] A degassed benzene solution of **5** in a Young's tab NMR tube was pressurised with 1 bar of either dried CO_2 or H_2. The ^{1}H NMR spectrum revealed decomposition of **5** when exposed to either CO_2 or H_2, **scheme 2.11**.

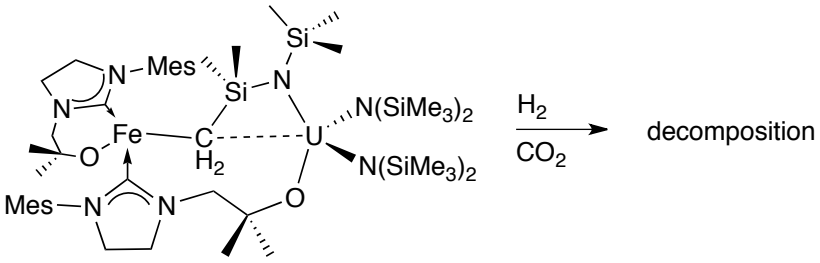

Scheme 2.11. Decomposition of **5** by CO_2 or H_2.

2.4.8 $[(L^{Mes})Co(\mu\text{-}L^{Mes})U(\mu\text{-}\{N(SiMe_3)Si(Me)_2CH_2\})(N\{SiMe_3\}_2)_2]$, 6

The ^{1}H NMR spectrum of **6** shows paramagnetically shifted ligand resonances over a broad range. The resonances due to the two $[N(SiMe_3)_2]$ groups come at

−39.70 and −0.27 ppm while the protons of the $SiMe_3$ group resonate at 50.58 ppm. There is a large difference in the chemical shifts of the two $[N(SiMe_3)_2]$ groups of **6**, those of **5** which resonate at −18.25 and −26.43 ppm and those of the uranium metallacycle in which both groups are equivalent and resonate at −13.03 ppm. The $SiMe_3$ group has a similar chemical shift in both **6** and **5** of 50.58 and 51.97 ppm, respectively, both of which are greatly shifted from $SiMe_3$ chemical shift in the metallacycle of 9.62 ppm. Three CH_3 groups are observed at 54.67, −4.39 and −20.82 ppm.

The ^{29}Si NMR spectrum of **6** shows a single resonance at −21.86 ppm. A similar chemical shift has been seen for the U^{IV} complex, $[(PH_2)U(TREN^{TIPS})]$ −21ppm.[52] This single resonance is at odds with the ^{1}H NMR spectrum in which the two $[N(SiMe_3)_2]$ groups are inequivalent and the protons of the $SiMe_2$ and $SiMe_3$ protons show distinct resonances. Furthermore, it is also different to the ^{29}Si NMR of **5** which displays three separate resonances at −21.84 −74.60 and −81.91 ppm.

The structure of **6**, **figure 2.9**, is isostructural with **5** in the solid state. The cobalt centre adopts a distorted square planar geometry with *cis* ligand angles from 91.29(14)°- 94.83(12)° and highly distorted *trans* ligand angles of 146.23(15)° and 159.03(15)° for O2-Co1-C1 and C17-Co1-C33 respectively, **table 2.9**.

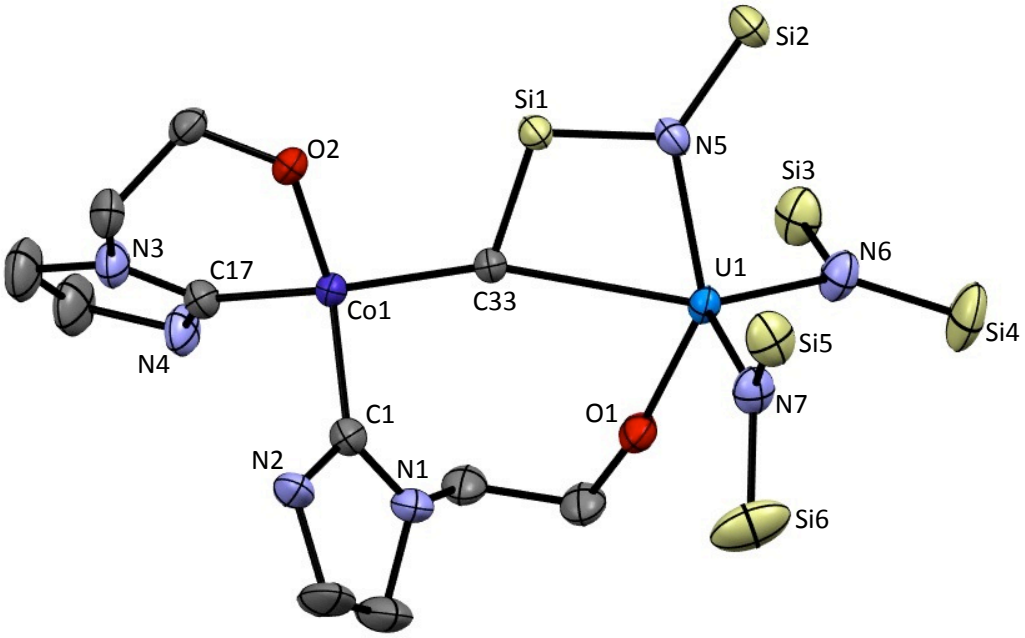

Figure 2.9. Solid state structure of **6**. For clarity, H atoms, methyl and mesityl groups are omitted. Displacement elipsoids drawn at 50% probability.

Table 2.8: Selected bond lengths (Å) for **6**.

Bond		Bond	
Co1-C1	1.904(4)	U1-N6	2.333(3)
Co1-C17	1.908(4)	U1-N7	2.338(3)
Co1-C33	2.084(3)	U1-N5	2.267(3)
Co1-O2	1.863(2)	U1···C33	2.798(3)
U1-O1	2.101(3)	Si1-C33	1.860(3)
Co···U	4.780		

Interestingly, both Co-$C_{carbene}$ bond lengths are the same within standard uncertainty, at 1.904(4) Å for Co-C1 and 1.908(4) Å for Co1-C17, **table 2.8**. These are toward the short end of the Co-$C_{carbene}$ bond length range; 1.91 Å - 2.13 Å[53][54] and shorter than the Co-$C_{carbene}$ bonds of **CXXVI**, **figure 2.1**, (2.047(6)

Table 2.9: Cobalt-ligand angles (°) for **6**.

Angle		Angle	
O2-Co1-C17	91.29(14)	C1-Co1-C33	91.31(15)
C1-Co1-C17	94.70(16)	O2-Co1-C1	146.23(15)
O2-Co1-C33	94.83(12)	C17-Co1-C33	159.03(15)

Å).[4] The Co1-O2 bond is 1.863(2) Å and the Co1-C33 bond length is 2.084(3) Å which is within the range of previously published Co−CH_2 bonds of 1.913 Å[55] to 2.191(12) Å.[56] The uranium centre adopts a distorted tetrahedral geometry with an O1-U1-N5 angle of 142.19(10)° and an N7-U1-N6 bond angle of 115.37(12)°. The wide O1-U1-N5 angle allows an interaction between C33 and U1; this has a separation of 2.798(3) Å and O1-U1-C33 and N5-U1-C33 angles of 77.72(10)° and 68.13(10)°, respectively. While all the U-N bond lengths are within the range of typical U^{IV}-$N_{silylamide}$ bond lengths of 2.246 Å[29] to 2.379 Å,[30] the U1-N5 distance of the bridging silylamide ligand is shorter than the terminal silylamide U-N bonds: 2.267(3) Å for U1-N5 compared with 2.333(3) Å and 2.338(3) Å for U1-N6 and U1-N7, respectively. Also, the U1-N5-Si1 angle is considerably smaller, due to the ligand bridging to the cobalt centre, than the terminal U-N-Si angles, **table 2.10**. The C33-Si1-N5 angle is consistent with a tetrahedral geometry, with an angle of 104.86(15)°. The U1$\cdots$C33 separation of 2.789(3) Å is outside the range of previously published U−CH_2 bonds of 2.368(7) Å[31] to 2.752(11) Å.[32] However, it is shorter than the C-H→U agostic interactions reported by Scott and co-workers of 3.056(14) Å and 3.218(10) Å.[32]

Table 2.10: U-N-Si angles (°) for **6**.

Angle		Angle	
U1-N5-Si1	103.49(14)	U1-N7-Si6	115.94(17)
U1-N5-Si2	133.44(17)	U1-N4-Si4	126.94(18)
U1-N7-Si5	128.67(18)	U1-N6-S3	113.79(16)

2.4.9 Reactivity of 6 with 2,6-*tert*-butylphenol

In attempt to replace the two $N(SiMe_3)_2$ ligands of **6**, two equivalents of 2,6-di-*tert*-butylphenol were added. The solution was heated to 85°C to force the reaction to completion. Cooling the solution to −30°C resulted in a crop of pale yellow crystals, **scheme 2.12**. However, x-ray analysis determined the structure to be $[(\{SiMe_3\}_2N)_3U(O\text{-}2,6\text{-}t\text{Bu-}C_6H_3)]$ **CXLVI**.

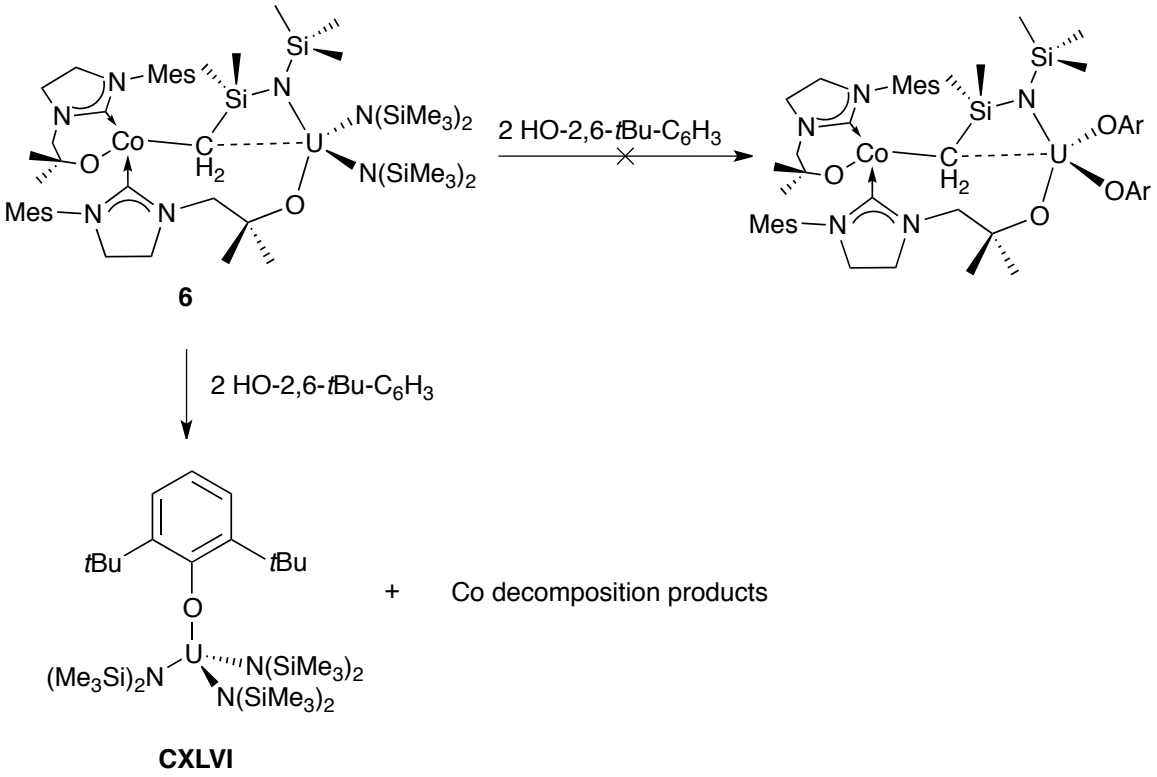

Scheme 2.12. Reactivity of **6** with 2,6-di-*tert*-butylphenol.

Instead of reacting with the two terminal silylamide groups, one equivalent of 2,6-di-*tert*-butylphenol has reacted with the bridging CH_2 and the aryloxide binds to the uranium in preference to the alkoxy tether. **CXLVI**, **scheme 2.12**, is formed and the cobalt-containing moiety of **6** reacts with the second equivalent of 2,6-di-*tert*-butylphenol and decomposes. **CXLVI** has been previously reported by by Watkin and co-workers as the product of the reaction between $[(\{Me_3Si\}_2N)_2U\{N(SiMe_3)Si(Me_2)CH_2\}]$ and 2,6-di-*tert*-butylphenol, **equation 2.7**.[57]

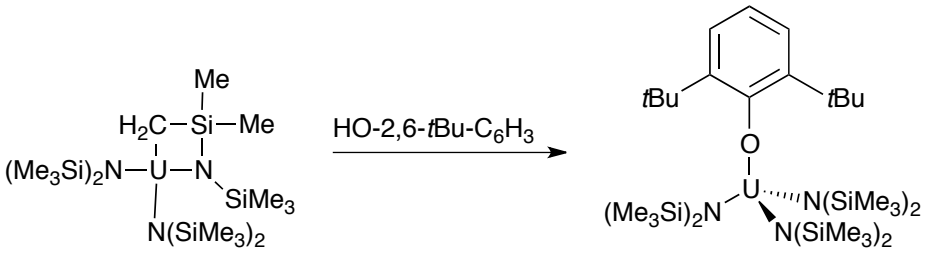

CXLVI (2.7)

The ^{29}Si NMR spectrum of **CXLVI** shows two resonances at 20.23 ppm and −132.16 ppm. This is due to the steric bulk of the (N$\{SiMe_3\}_2$) and *t*Bu groups restricting the rotation about the U-N bonds of the silylamide ligands, resulting in two sets of magnetically inequivalent Si atoms. The ^{1}H NMR spectrum reported in the literature shows this restricted rotation results in three inequivalent silylamide resonances in a 1:1:1 ratio.[57] The ^{1}H NMR spectrum collected was consistent with that previously published.[57] The ^{1}H NMR spectrum does not show an unreacted equivalent of 2,6-di-*tert*-butylphenol. There are, however, a large number of paramagnetically shifted resonances from 90 to −60 ppm, each integrating to one or two protons. It is possible they result from cobalt containing decomposition products.

This reactivity is consistent with that of **5**. Both **5** and **6** display the same reactivity as the free uranium metallacycle while the transition metal fragment then undergoes decomposition.

2.4.10 Comparison of 5 and 6

In both **5** and **6** the uranium centre adopts a distorted tetrahedral geometry while the transition metals adopt different geometries. The iron has a distorted tetrahedral geometry while the cobalt centre has a distorted square planar geometry in

6, **figure 2.10**. As the distorted tetrahedral geometry of **3** is conserved in **5**, this would suggest that **4** adopts a distorted square planar geometry.

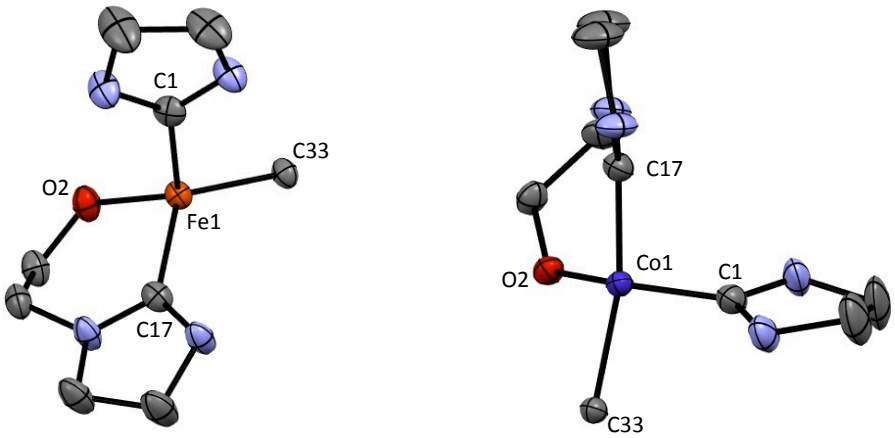

Figure 2.10. Comparison of Fe and Co fragments of **5** and **6**, respectively.

The bond lengths around the iron centre in **5** range from 94.62(14)°- 124.18(16)°, bracketing the value for an ideal tetrahedral geometry of 109.5°, while the angle between ligands in **6** are approximately 90°for *cis* ligands (91.29(14)°- 94.83(12)°) and 146.23(15)° and 159.03(15)° for the *trans* ligands, **table 2.11**. Furthermore, both Fe−$C_{carbene}$ bond lengths are the same (1.904(4) Å and 1.908(4) Å) in **6** while in **5** the Co−$C_{carbene}$ of the bridging ligand is longer than that of the ligand bound bidentate to the iron centre (2.144(4) Å *cf.* 2.086(4) Å).

This has a consequence on the geometry of the rest of the structure. **5** adopts an open structure, as can be seen from the M···M separation of 4.934 Å, whereas **6** adopts a more compact structure with a M···M separation of 4.780 Å. The U-C33 and TM-C33 bond lengths are both elongated in **5** compared with **6**. This can also be seen the the bridging NHC ligand, which has a twist in **6** in order to bridge the shorter gap and is more linear in **5**. This can be seen in the N1-C4-C5-O1 dihedral angles: -137.5(3)° for **6** and -65.5(5)° for **5**, **figure 2.11**. In **6**, O2 and Si1 adopt an almost eclipsed conformation with an O2-Co1-C33-Si1 dihedral angle

Table 2.11: Comparison of the bond angles (°) around the transition metal in **5** and **6**.

Angle	**5**	**6**
C1-M1-C17	98.29(15)	94.70(16)
C17-M1-O2	94.62(14)	91.29(14)
O2-M1-C33	115.66(13)	94.83(12)
C1-M1-C33	109.06(15)	91.31(15
O2-M1-C1	113.60(15	146.23(15)
C17-M1-C33	124.18(16)	159.03(15)

of −15.42° whereas the O2-Fe1-C33-Si1 dihedral is −25.69°.

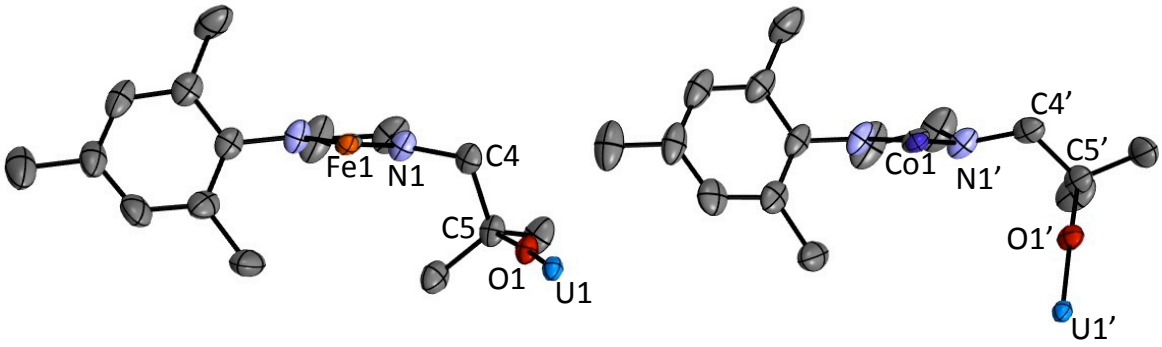

Figure 2.11. Bridging NHC ligand viewed down the TM-$C_{carbene}$ bond. Left, TM = Fe **5**; right TM = Co **6**.

2.5 $[(L^{Mes})Zn(\mu\text{-}L^{Mes})Th\text{-}(\mu\text{-}\{N(SiMe_3)Si(Me)_2CH_2\})(N\{SiMe_3\}_2)_2]$, 9

The heterobimetallic complex $[(L^{Mes})Zn(\mu\text{-}L^{Mes})Th(\mu\text{-}\{N(SiMe_3)Si(Me)_2CH_2\})(N\{SiMe_3\}_2)_2]$ **9**, the diamagnetic analogue of **5** and **6**, was prepared on an NMR scale in C_6D_6 from the reaction between the previously published $[Zn(L^{Mes})_2]$[10] and the thorium(IV) metallacycle, $[(\{Me_3Si\}_2N)_2Th\{N(SiMe_3)Si(Me_2)CH_2\}]$. The ^1H NMR spectrum of **9** shows the diastereotopic $Zn-CH_2$ protons resonate as two triplets at 4.31 and 3.37 ppm and each has a coupling constant of 5.1 Hz. Unlike **5** and **6** where the the two $[N(SiMe_3)_2]$ units are inequivalent, they are equivalent in **9**, resonating as a singlet at 0.39 ppm. These protons are also equivalent in the thorium metallacycle, with a chemical shift of 0.35 ppm.[27] The $SiMe_3$ group on the bridging silylamide resonates at 0.59 ppm while the $SiMe_2$ group resonates at 0.54 ppm. Both these resonances are shifted from those of the metallacycle of 0.33 and 0.63 ppm for the $SiMe_3$ and the $SiMe_2$ protons, respectively.[27]

The NHC backbone CH_2 resonances occur as a multiplet at 2.84 ppm, a similar chemical shift of 2.80-2.89 ppm is observed for $[Zn(L^{Mes})_2]$.[10] The aromatic CH's occur as two singlets at 6.82 and 6.94 ppm. The CH_2 protons of the alkoxy tethers are equivalent and resonate as two doublets, integrating to two protons each, at 2.03 and 2.13 ppm. However, in $[Zn(L^{Mes})_2]$ they are inequivalent and occur as two doublets at 2.78 and 2.33 ppm. The protons of the *o*-Me groups resonate at 0.34 and 0.80 ppm whilst the protons of the *p*-Me groups resonated 0.45 and 0.92 ppm. Whilst the mesitly CH_3 groups resonate in a 2:1 ratio in **9**, with the *o*-Me groups being equivalent, in $[Zn(L^{Mes})_2]$ the three mesityl methyl groups are inequivalent, resonating at 2.61, 2.19 and 2.03 ppm. The *gem*-dimethyl protons are inequivalent on each ligand with the protons of the bridging ligand occurring at 3.12 and 2.59 ppm and those of the other ligand resonating at 2.35 and 1.15 ppm. This is similar

to $[Zn(L^{Mes})_2]$ where the *gem*-dimethyl protons are inequivalent and resonate at 1.37 and 1.17 ppm

2.6 Reactivity of 3 with a 'prefunctionalised' metallacycle

Previous work within the Arnold group has shown that $[(\{Me_3Si\}_2N)_2U\{N(SiMe_3)Si(Me_2)CH_2\}]$ reacts with half an equivalent of the borane dimer $(HBBN)_2$ (BBN = 9-borabicyclo[3.3.1]nonane) to form $[(\{SiMe_3\}_2N)_2U\{N(SiMe_3)SiMe_2CH_2BBN\text{-}H\}]$ **CXLVII**, **equation 2.8**.[58]

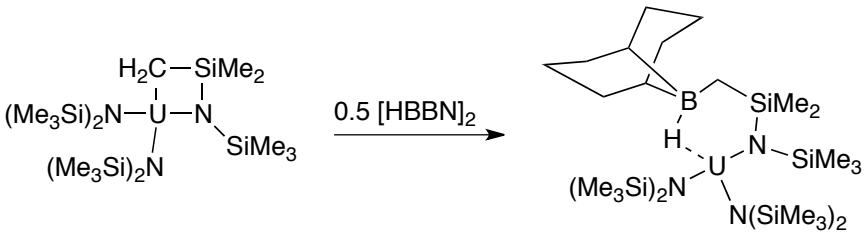

CXLVII (2.8)

As **5** displayed no reactivity with boranes, one equivalent of **3** was added to the prefunctionalised metallacycle **CXLVII** in an attempt to circumvent this lack of reactivity, **equation 2.9**.

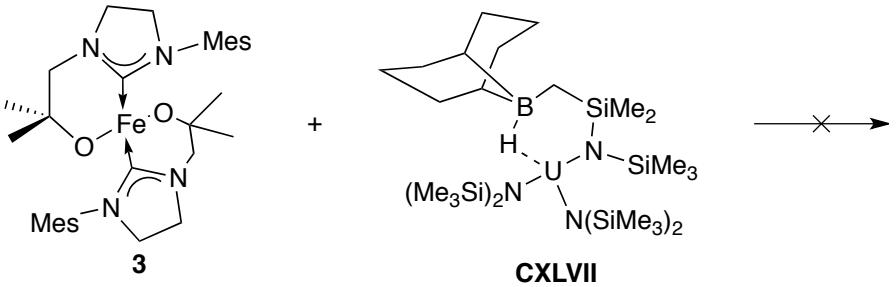

(2.9)

The reaction was carried out at both room temperature and reflux (in benzene) however, analysis of the resulting ^{1}H NMR spectrum showed that no reaction occurred under either set of conditions.

2.7 Synthesis of $[Na(Fe\{L^{Mes}\}_2)_2]^+$ $[Fe(ArO)_3]^-$

The unusual iron *ate* complex $[Na(Fe\{L^{Mes}\}_2)_2]^+$ $[Fe(ArO)_3]^-$ **10** (Ar = 2,6-*t*Bu-C_6H_3) was isolated from a reaction between **5** and three equivalents of 2,6-tert-butylphenol containing a Na^+ impurity, **equation 2.10** gives a possible equation for the reaction. The likely source of sodium impurity is from the the uranium metallacycle which is synthesised in a reaction between $[UI_4(Et_2O)_2]$ and $[NaN(SiMe_3)_2]$.[27]

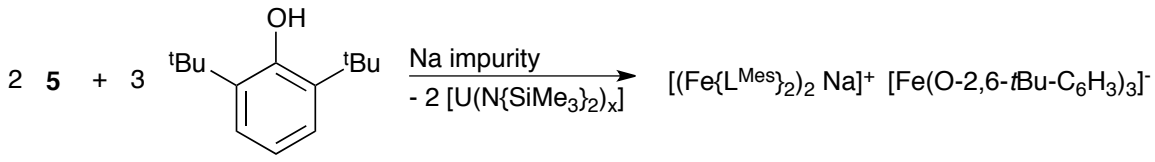

(2.10)

The solid state structure of **10**, **figure 2.12**, shows that Fe3 is formally anionic as the iron(II) centre is surrounded by three aryloxide ligands. Fe3 lies in a trigonal planar geometry with each of the three O-Fe3-O angles approximately 120.00°, **table 2.12**, while the three Fe3-O bonds are very similar at 1.842(2), 1.859(2) and 1.856(2) Å for Fe3-O5, Fe3-O6 and Fe3-O7, respectively. The Fe3-O-C bonds are approximately linear with an Fe3-O5-C65 angle of 168.3(2)°, an Fe3-O6-C71 angle of 171.4(2)° and an Fe3-O7-C77 angle of 179.6(2)°.

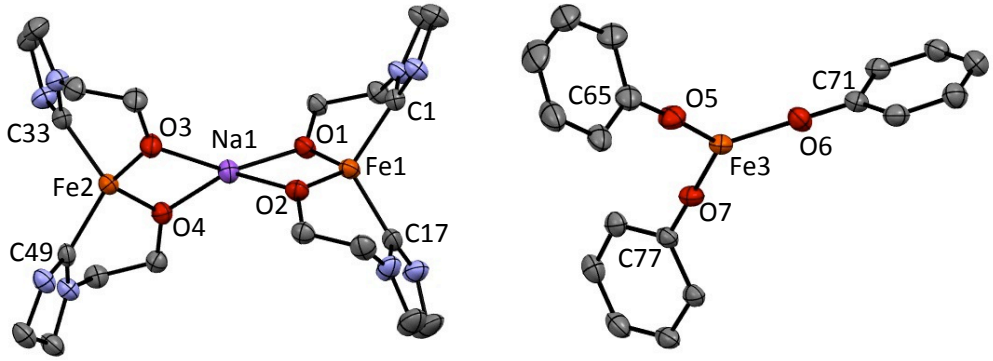

Figure 2.12. Solid state structure of **10**. For clarity, H atoms, methyl, *t*Bu and mesityl groups are omitted. Displacement elipsoids drawn at 50% probability.

Table 2.12: Selected bond lengths (Å) and angles (°) of **10**.

Bond		Bond		Angle	
Na1-O1	2.348(2)	Fe1-O1	1.907(2)	O1-Na1-O2	79.09(8)
Na1-O2	2.317(2)	Fe1-O2	1.914(2)	O3-Na1-O4	79.08(8)
Na1-O3	2.314(2)	Fe2-O3	1.903(2)	O5-Fe3-O6	120.49(10)
Na1-O4	2.337(3)	Fe2-O4	1.899(2)	O6-Fe3-O7	120.22(10)
Fe1-C1	2.051(3)	Fe3-O5	1.842(2)	O7-Fe3-O5	119.28(10)
Fe1-C17	2.051(3)	Fe3-O6	1.859(2)	Fe3-O5-C65	168.3(2)
Fe2-C33	2.058(3)	Fe3-O7	1.856(2)	Fe1-O6-C71	171.4(2)
Fe2-C49	2.044(3)			Fe1-O7-C77	179.6(2)

Na1 adopts a very distorted tetrahedral geometry being coordinated to the four oxygen atoms of two molecules of **3** with an O1-Na1-O2 angle of 79.09(8)°and an O3-Na1-O4 angle of 79.08(8)°. The Na1-O1 and Na1-O2 bond lengths are 2.348(2) Å and 2.317(2) Å, respectively, while the Na1-O3 and Na1-O4 are 2.314(2) Å and 2.337(3) Å, respectively. The Fe-$C_{carbene}$ bond lengths are 2.051(3) Å for Fe1-C1 and Fe1-C17 and 2.058(3) Å and 2.044(3) Å for Fe2-C33 and Fe2-C49, respectively.

Comparison of the Fe-$C_{carbene}$ of **3** shows no significant lengthening or shortening of the bond lengths of **10** with bond lengths of approximately 2.0 Å, **table 2.13**.

Table 2.13: Comparison of the Fe-$C_{carbene}$ bond lengths (Å) of **3** and **10**.

Bond	**3**	**10**
Fe1-C1	2.079(4)	2.051(3)
Fe1-C17	2.068(4)	2.051(3)
Fe2-C33	2.058(4)	2.058(3)
Fe2-C49	2.057(6)	2.044(3)

Similarly, there is no significant change in the lengths of the Fe-O bonds of **10** compared to **3**. The approximate bond lengths for both complexes are 1.9 Å, **table 2.14**

Table 2.14: Comparison of the Fe-O bond lengths (Å) of **3** and **10**.

Bond	**3**	**10**
Fe1-O1	1.900(4)	1.907(2)
Fe1-O2	1.914(4)	1.914(2)
Fe2-O3	1.889(5)	1.903(2)
Fe2-O4	1.874(5)	1.899(2)

Boyle and coworkers have published the similar complex $[Li(THF)_4][Fe(O{-}2,6{-}t Bu{-}C_6H_3]$ **CXLVIII**, **figure 2.13**.[59] As with **10**, the lithium cation adopts a highly distorted tetrahedral geometry while the iron centre is bound to three aryloxide ligands in a trigonal planar geometry.

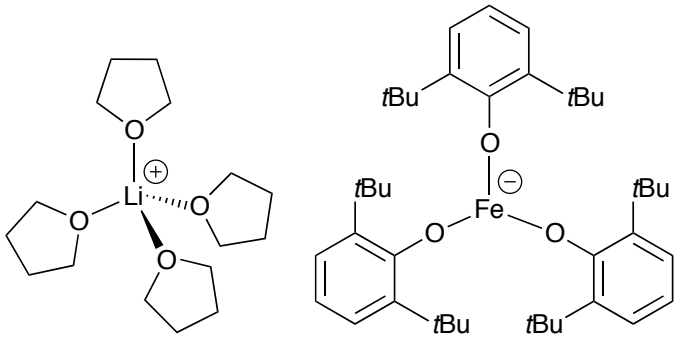

CXLVIII

Figure 2.13. Structure of $[Li(THF)_4][Fe(O{-}2,6{-}t Bu{-}C_6H_3)]$ **CXLVIII**, previously synthesised by Boyle and co-workers.[59]

CXLVIII has an average Fe-OAr bond length of 1.86Å, similar to the Fe-OAr bond lengths of 1.842(2) - 1.859(2) Å in **10**. The Fe-O-C bond angles are similar in both complexes, **table 2.15**.

Table 2.15: Comparison of the Fe-O-C bond angles (°) of **10** and **CXLVIII**.

10	**CXLVIII**
168.3(2)	164.60
171.4(2)	173.32
179.6(2)	176.67

Additionally, the O-Fe-O bond angles for both complexes are similar at 116 - 120°, **table 2.16**

Table 2.16: Comparison of the O-Fe-O bond angles (°) of **10** and **CXLVIII**.

10	**CXLVIII**
120.49(10)	116.39
120.22(10)	122.02
119.28(10)	121.58

2.8 Summary

In conclusion, the transition metal NHC complexes **3** and **4** have been prepared and reacted with $[(\{SiMe_3\}_2N)_2U(NSiMe_3SiMe_2CH_2)]$ to form the *d*-/*f*-block heterobimetallic complexes **5** and **6**, respectively. No reaction occurred between **3** and the uranium-boron metallacycle **CXLVII** ocurred. Additionally, the diamagnetic analogue **9** was also prepared from the known starting materials $[Zn(L^{Mes})_2]$ and $[(\{SiMe_3\}_2N)_2Th(NSiMe_3SiMe_2CH_2)]$.

5 displayed reactivity analogous to that of $[(\{SiMe_3\}_2N)_2U(NSiMe_3SiMe_2CH_2)]$ when reacted with 2,6-dimethyl isocyanide or CO to form metallacylces **8** and **CXXXIX**, respectively. Similarly, **6** reacted with 2,6-ditertbutyl phenol to form **CXLVI**. **3** and **4** do not appear in the reaction mixture and do not react with 2,6-dimethyl isocycanide or CO, respectively, on their own. This suggests a complicated reaction mechanism. **5** showed no reactivity with boranes or azides while reaction with CO_2 or H_2 led to decomposition of the complex. **5** was also inert to oxidation with *m*CPBA and underwent decomposition when KC_8 was added in an attempt to reduce the complex.

Additionally, the iron *ate* complex **10** was isolated and resulted from the presence of a sodium impurity in the reaction reaction between **5** and 2,6-ditertbutyl phenol.

References

1. J. W. Napoline, S. J. Kraft, E. M. Matson, P. E. Fanwick, S. C. Bart and C. M. Thomas, *Inorg. Chem.*, 2013, **52**, 12170.

2. A. L. Ward, W. W. Lukens, C. C. Lu and J. Arnold, *J. Am. Chem. Soc.*, 2014, **136**, 3647.

3. P. L. Arnold, J. McMaster and S. T. Liddle, *Chem. Comm.*, 2009, 818.

4. M. F. Schettini, G. Wu and T. W. Hayton, *Chem. Comm.*, 2012, **48**, 1484.

5. A. P. Sobaczynski, T. Bauer and R. Kempe, *Organometallics*, 2013, **32**, 1363,

6. W. W. N. O, X. Kang, Y. Luo and Z. Hou, *Organometallics*, 2014, **33**, 1030.

7. P. L. Arnold, Z. R. Turner, A. I. Germeroth, I. J. Casely, R. Bellabarba and R. P. Tooze, *Dalton Trans.*, 2010, **39**, 6808.

8. P. L. Arnold, T. Cadenbach, I. H. Marr, A. A. Fyfe, N. L. Bell, R. Bellabarba, R. P. Tooze and J. B. Love, *Dalton Trans.*, 2014, **43**, 14346.

9. P. L. Arnold, I. J. Casely, Z. R. Turner and C. D. Carmichael, *Chem. Eur. J*, 2008, **14**, 10415.

10. P. L. Arnold, I. J. Casely, Z. R. Turner, R. Bellabarba and R. P. Tooze, *Dalton Trans.*, 2009, 7236.

11. D. S. McGuinness, V. C. Gibson and J. S. Steed, *Organometallics*, 2004, **23**, 6288.

12. O. Kaufhold, F. E. Hahn, T. Pape and A. Hepp, *J. Organomet. Chem.*, 2008, **693**, 3435.

13. A. A. Danopoulos, N. Tsoureas, J. A. Wright and M. E. Light, *Organometallics*, 2004, **23**, 166.

14. M. I. Ingleson and R. A. Layfield, *Chem. Comm.*, 2012, **48**, 3579.

15. J. Wu, W. Dai, J. H. Farnaby, N. Hazari, J. J. L. Roy, V. Mereacre, M. Murugesu, A. K. Powell and M. K. Takase, *Dalton Trans.*, 2013, **42**, 7404.

16. F. H. Allen, *Acta. Crystallogr., Sect. B*, 2002, **58**, 380.

17. S. Zlatogorsky, C. A. Muryn, F. Tuna, D. J. Evans and M. J. Ingleson, *Organometallics*, 2011, **30**, 4974.

18. S. Meyer, C. M. Orben, S. Demeshko, S. Dechert and F. Meyer, *Organometallics*, 2011, **30**, 6692.

19. Z. Mo, D. Chen, X. Leng and L. Deng, *Organometallics*, 2012, **31**, 7040.

20. Z. Mo, Y. Liu and L. Deng, *Angew. Chem. Int. Ed.*, 2013, **52**, 10845.

21. M. M. Rodriguez, E. Bill, W. W. Brennessel and P. L. Holland, *Science*, 2011, **334**, 780.

22. D. Bézier, J.-B. Sortais and C. Darcel, *Adv. Synth. Catal.*, 2013, **355**, 19.

23. T. M. Figg, P. L. Holland and T. R. Cundari, *Inorg. Chem.*, 2012, **51**, 7546

24. W. M. Czaplik, M. Mayer, J. Cvengroš and A. J. von Wangelin, *ChemSusChem.*, 2009, **2**, 396.

25. V. Lavallo and R. H. Grubbs, *Science*, 2009, **326**, 559.

26. K. Riener, S. Hanslinger, A. Raba, M. P. Högrel, M. Cokoja, W. A. Herrmann and F. E. Kühn, *Chem. Rev.*, 2014, **114**, 5215.

27. A. Dormund, A. E. Bouadili, A. Aaliti and C. Moise, *J. Organomet. Chem.*, 1985, **288**, C1

28. C. J. Windorff and W. J. Evans, *Organometallics*, 2014, **33**, 3786.

29. J. L. Brown, G. Wu and T. W. Hayton, *Organometallics*, 2013, **32**, 1193.

30. S. Fortier, J. R. Walensky, G. Wu and T. W. Hayton, *J. Am. Chem. Soc.*, 2011, **133**, 6894.

31. N. R. Andreychuk, S. Ilango, B. Vidjayacoumar, D. J. Emslie and H. A. Jenkins, *Organometallics*, 2013, **32**, 1466.

32. R. Boaretto, P. Roussel, A. J. Kingsley, I. J. Munslow, C. J. Sanders, N. W. Alcock and P. Scott, *Chem. Comm.*, 1999, 1701.

33. R. H. Fong and W. H. Hersh, *J. Am. Chem. Soc.*, 1987, **9**, 2843.

34. B. A. Frazier, V. A. Williams, P. T. Wolczanski, S. C. Bart, K. Meyer, T. R. Cundari and E. B. Lobkovsky, *Inorg. Chem.*, 2013, **52**, 3295.

35. I. P. Rothwell, *Polyhedron*, 1985, **4**, 177.

36. S. J. Simpson and R. A. Andersen, *J. Am. Chem. Soc.*, 1981, **103**, 4063.

37. O. T. Summerscales, F. G. N. Cloke, P. B. Hitchcock, J. C. Green and N. Hazari, *Science*, 2006, **311**, 829.

38. O. T. Summerscales, F. G. N. Cloke, P. B. Hitchcock, J. C. Green and N. Hazari, *J. Am. Chem. Soc.*, 2006, **128**, 9602.

39. A. S. Frey, F. G. N. Cloke, P. B. Hitchcock, I. J. Day, J. C. Green and G. Aitken, *J. Am. Chem. Soc.*, 2008, **130**, 13816.

40. P. L. Arnold, Z. R. Turner, R. Bellabarba and R. P. Tooze, *Chem. Sci.*, 2011, **2**, 77.

41. L. Mond and C. Langer, *J. Chem. Soc., Trans.*, 1891, **59**, 1090.

42. Z. R. Turner, R. Bellabarba, R. P. Tooze and P. L. Arnold, *J. Am. Chem. Soc.*, 2010, **132**, 4050.

43. C. Vogel, F. W. Heineman, J. Sutter, C. Anthon and K. Meyer, *Angew. Chem. Int. Ed.*, 2008, **47**, 2681.

44. D. M. King, F. Tuna, E. J. McInnes, J. McMaster, W. Lewis, A. J. Blake and S. T. Liddle, *Nat. Chem.*, 2013, **5**, 482.

45. H. Braunschweig, C.-W. Chiu, K. Radachi and T. Kupfer, *Angew. Chem. Int. Ed.*, 2010, **49**, 2041.

46. J. Monot, A. Solovyev, H. Bonin-Dubarle, E. Derat, D. P. Curran, M. Roberts, L. Fensterbank, M. Malacria and E. Lacôte, *Angew. Chem. Int. Ed.*, 2010, **49**, 9166.

47. G. M. Jones, P. L. Arnold and J. B. Love, *Angew. Chem. Int. Ed.*, 2012, **51**, 12584.

48. P. L. Arnold, Z. R. Turner, A. I. Germeroth, I. J. Casely, G. S. Nichol, R. Bellabarba and R. P. Tooze, *Dalton Trans.*, 2013, **42**, 1333.

49. W. Ding and D. Wang, *Organometallics*, 2014, **33**, 7007.

50. P. L. Arnold, I. H. Marr, S. Zlatogorsky, R. Bellabarba and R. P. Tooze, *Dalton Trans.*, 2014, **43**, 34.

51. S. M. Mansell, N. Kaltsoyannis and P. L. Arnold, *J. Am. Chem. Soc.*, 2011, **133**, 9036.

52. B. M. Gardner, G. Balázs, M. Scheer, F. Tuna, E. J. L. McInnes, J. McMaster, W. Lewis, A. J. Blake and S. T. Liddle, *Angew. Chem. Int. Ed.*, 2014, **53**, 4484.

53. R. E. Cowley, R. P. Bontchev, J. Sorrell, O. Sarracino, Y. Feng, H. Wang and J. M. Smth, *J. Am. Chem. Soc.*, 2007, **129**, 2424.

54. Z. Xi, B. Liu, C. Lu and W. Chen, *Dalton Trans.*, 2009, 7008.

55. L. G. Marzilli, S. M. Polson, L. Hansen, S. J. Moore and P. A. Marzilli, *Inorg. Chem.*, 1997, **36**, 3854.

56. C. Creutz, M. H. Chou, E. Fujita and D. J. Szalda, *Coord. Chem. Rev.*, 2005, **249**, 375.

57. J. M. Berg, D. L. Clark, J. C. Huffman, D. E. Morris, A. P. Sattelberger, W. E. Streib, W. G. V. D. Sluys and J. G. Watkin, *J. Am. Chem. Soc.*, 1992, **114**, 10811.

58. S. M. Mansell, F. Bonnet, M. Visseaux and P. L. Arnold, *Dalton Trans.*, 2013, **42**, 9033.

59. T. J. Boyle, M. L. Neville, C. A. Apblett, S. M. Hoppe and M. Gembicky, *Polyhedron*, 2013, **65**, 89.

Chapter 3

Synthesis of Heterobimetallic Complexes Using C_3-Symmetric Triphenoxymethane Ligands

3.1 Introduction

Dinger and Scott have synthesised a number of C_3-symmetric triphenoxymethane molecules,[1] **figure 3.1 CL**, which act as mimics for calix[3]arenes, **figure 3.1 CXLIX**,[2] which are difficult to synthesise due to their strained cyclic structure.[3]

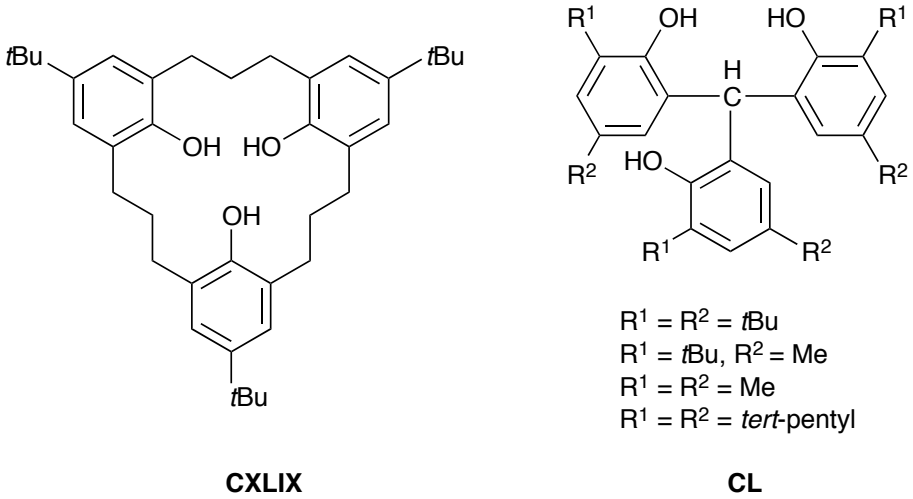

CXLIX **CL**

Figure 3.1. CXLIX, a calix[3]arene prepared by Yamato and co-workers[3] and **CL**, the model molecules prepared by Dinger and Scott.[1]

Dinger and Scott have synthesised the tri-lithium, sodium and potassium salts of a number of tris(3,5-dialkyl-2-hydroxyphenyl)methanes.[4] These complexes adopt a dimeric, hexanuclear structure, **CLI** and **CLII figure 3.2**. It was also noted that the complexes decomposed or gave multiple products when reacted with transition metal salts.

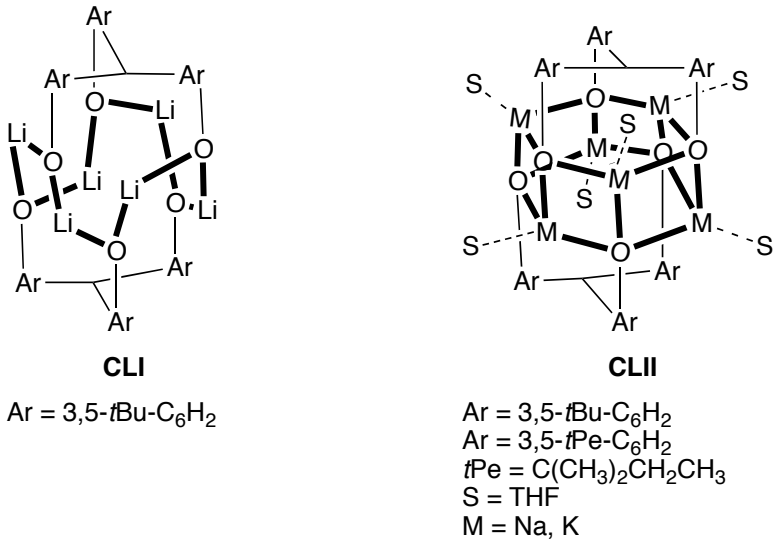

Figure 3.2. Alkali metal complexes of tris(3,5-dialkyl-phenol)methanes.[4]

Additionally, a series of zinc(II) triphenoxymethane complexes were prepared which form clusters in the solid state and in solution, **CLIII** and **CLIV figure 3.3**. The complexes were tested for cyclohexene oxide/CO_2 copolymerisation, however, most complexes showed little catalytic activity due to instability at the reactive zinc centres.[5]

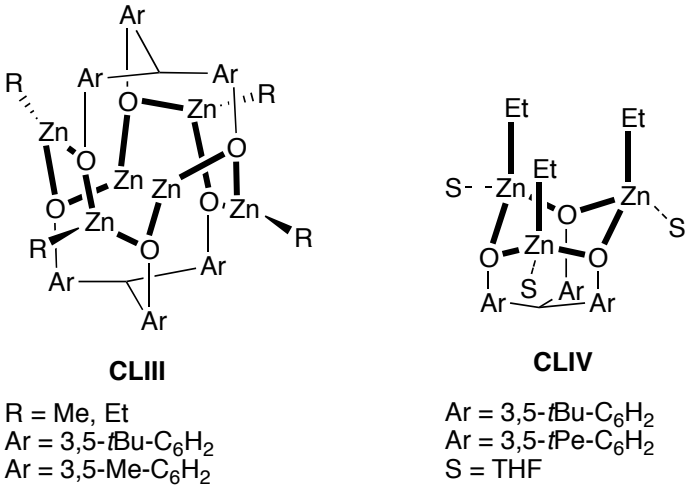

Figure 3.3. Zinc(II) triphenoxymethane complexes synthesised by Dinger and Scott.[5]

Further functionalisation of triphenoxymethane molecules has led to their use as ligands in the solvent extraction of f-element cations.[6][7] The tripodal ligand **CLV**, **figure 3.4**, shows a high affinity for Th(IV) cations in a 1 M nitric acid solution containing Th(IV), La(III), Ce(III), Nd(III), Eu(III) and Yb(III) cations. **CLV** was also found to have a high affinity for Pu(IV) over U(IV), Am(III) and Eu(III)[7] while **CLVI** has been shown to be a useful ligand in the extraction of heavier trivalent lanthanides.[6]

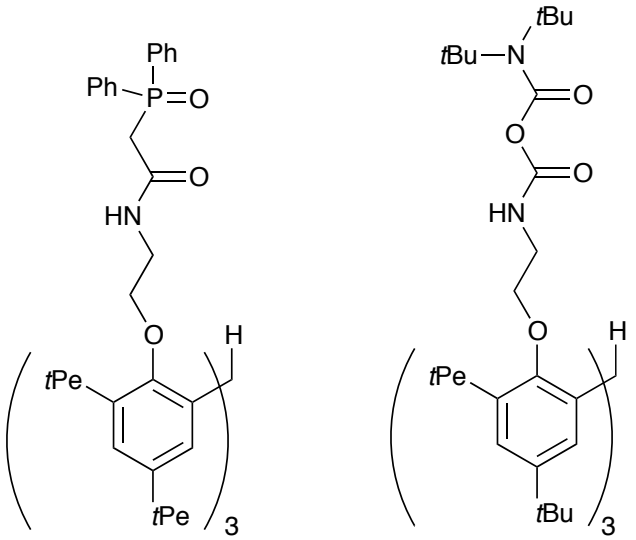

Figure 3.4. Ligands for the extraction and separation of actinide ions.[6]

3.2 Synthesis of [HC(3-*t*Bu-5-Me-C_6H_2OH))(3-*t*Bu-5-Me-C_6H_2O)μ-(3-*t*Bu-5-Me-C_6H_2O)Co(THF)]$_2$, 11

The dinuclear cobalt(II) aryloxide complex [HC(3-*t*Bu-5-Me-C_6H_2OH))(3-*t*Bu-5-Me-C_6H_2O)μ-(3-*t*Bu-5-Me-C_6H_2O)Co(THF)]$_2$ **11** was prepared in an 80% yield, after work up, by addition of one equivalent of [Co(N{$SiMe_3$}$_2$)$_2$(THF)] to HC(3-*t*Bu-5-Me-C_6H_2OH)$_3$ in toluene at room temperature, **equation 3.1**.

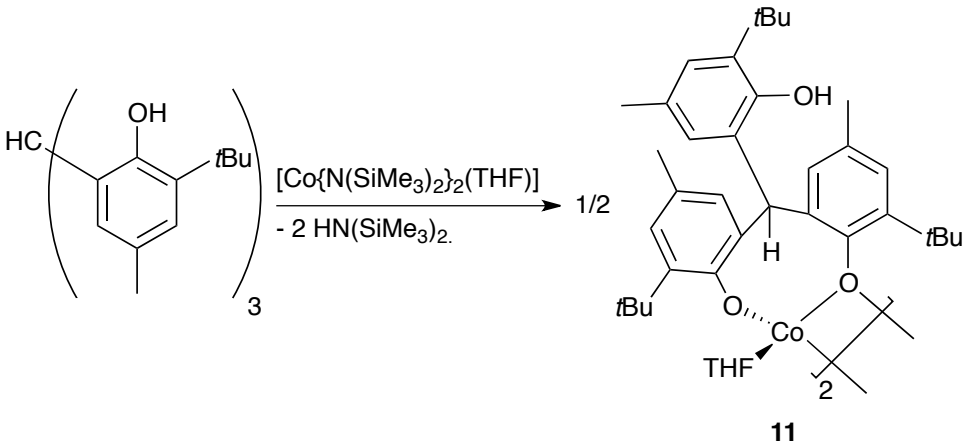

11 (3.1)

The ^{1}H NMR spectrum of **11** in d^8-THF shows broad, paramagnetically shifted ligand resonances from 70 to −70 ppm with the aryl groups being magnetically inequivalent. The three resonances due to the *t*Bu groups occur as singlets at −70.52, −7.62 and −0.88 ppm while the protons of the three Me groups resonate at 52.13, 46.36 and 39.92 ppm. There are also eight resonances integrating to a single proton corresponding to the inequivalent aromatic C-H's, alkyl C-H and OH protons, though they could not be assigned precisely due to the paramagnetism of the complex. The two resonances due the coordinated protio-THF can be seen at 3.61 and 1.76 ppm.

Crystals suitable for x-ray diffraction were grown by allowing a hot, concentrated toluene solution to cool to room temperature. In the solid state **11** is dimeric, **figure 3.5**.

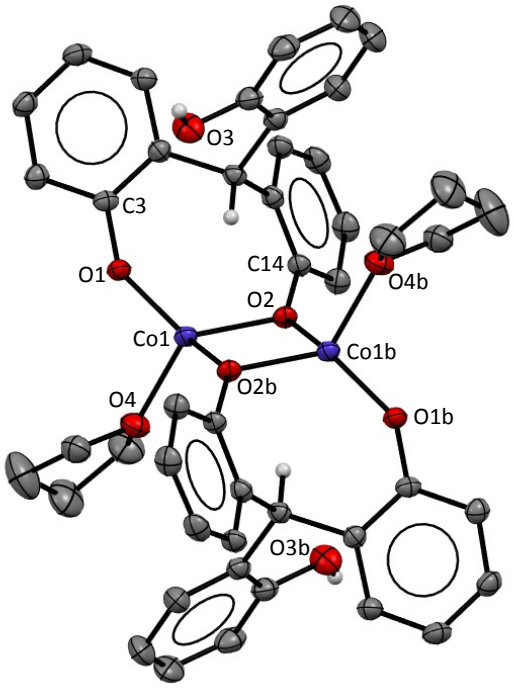

Figure 3.5. Solid state structure of **11**. Aromatic H atoms, Me and *t*Bu groups have been omitted for clarity. Displacement ellipsoids are drawn at 50% probability.

Table 3.1: Selected bond and contact distances (Å) and angles (°) for **11**.

Bond/Angle		Angle	
Co1-O1	1.8577(19)	O1-Co1-O4	99.23(9)
Co1-O2	1.9797(19)	O2-Co1-O2b	83.08(8)
Co1-O2b	1.9752(18)	O1-Co1-O2	117.08(8)
Co1-O4	2.029(2)	O4-Co1-O2b	99.95(5)
Co1$\cdots$Co1b	2.9603(7)	Co1-O1-C3	142.78(18)
Co1-O2-C14	119.3(2)	Co1-O2-Co1b	96.92(9)

The solid state structure shows that two phenol groups have been deprotonated, while the third remains protonated. At the core of the molecule is a planar {−Co−O−Co−O−} four membered ring with a Co1-O2-Co1b-O2b dihedral angle

of 0.00°, due an inversion centre, **table 3.1**. Each cobalt(II) centre is bound to three aryl oxides: one terminal aryloxide with a Co1-O1 bond length of 1.8577(19) Å, which is within the range of literature values of 1.826(2)[8] - 2.036(2) Å;[9] two bridging aryloxides with a Co1-O2 bond length of 1.9797(19) Å and a Co1-O2b bond length of 1.9852(18) Å which are within the range of previously published bridging Co-OAr bond lengths of 1.826[10] - 2.38(1) Å;[11] and a molecule of THF, from $[Co(N\{SiMe_3\}_2)_2(THF)]$, with a Co1-O4 bond length of 2.029(2) Å.

Co1 adopts a distorted tetrahedral geometry - a common geometry for cobalt(II) complexes[12] - with an O1-Co1-O4 angle of 99.23(9)°, an O2-Co1-O2b angle of 83.08(8)°, an O1-Co1-O2 angle of 117.08(8)° and an O4-Co1-O2b angle of 99.95(5)°. The Co···Co separation of 2.9603(7) Å is longer than the typical Co-Co single bond length of 2.46 Å.[13] The Co1-O2-Co1b angle is 96.92(9)° while the O2-Co1-O2b angle is 83.98(8)°. The terminal Co-aryloxide angle Co1-O1-C3, 142.78(18)°, is more obtuse than the monomeric two-coordinate cobalt(II) aryloxide $[Co(OC_6H_3\text{-}2,6(C_6H_2\text{-}2,4,6\text{-}Me_3)_2)_2]$ **CLVII**, **figure 3.6**, of 123.3(2)° reported by Power and coworkers.[14] Furthermore, the bridging Co1-O2-C14 angle of 119.3(2)° is smaller than the terminal Co1-O1-C3 angle of 142.78(18)°.

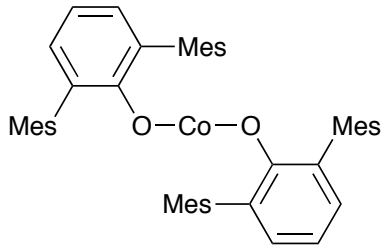

CLVII

Figure 3.6. Linear cobalt(II) aryloxide complex reported by Power and coworkers.[14]

The cobalt(II) complex $[Co(OAr^F)_2(DME)]_2$ ($Ar^F = C_6F_5$) **CLVIII**, **figure 3.7**, has been reported previously by Rheingold and coworkers.[15] Like **11**, it is

dimeric with two bridging and two terminal aryloxide groups bonding to each Co(II) centre with a solvent molecule, DME, completing the coordination sphere of the metal.

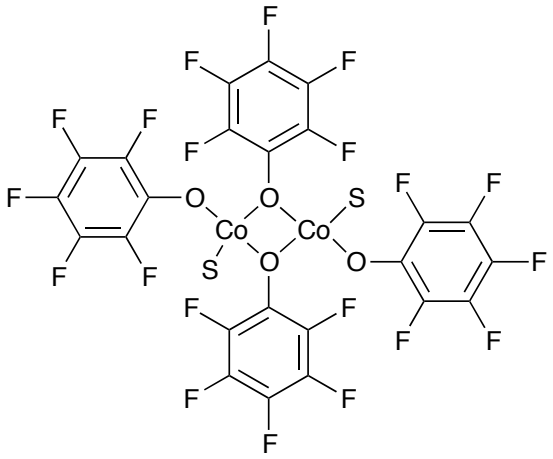

CLVIII
S = DME

Figure 3.7. Structure of $[Co(OAr^F)_2(DME)]_2$.[15]

With a bond length of 1.9267(12) Å, the terminal Co-aryloxide bond is longer than that of **11** of 1.8577(19) Å. Similarly, the bridging Co-O bond lengths of **CLVIII** are longer at 1.9857(10) and 2.0582(10) Å compared with 1.9797(19) Å in **11**. The bridging Co-O-Co angles of 104.46(7)° and 99.39(7)° are also larger than the bridging Co1-O2-Co1b angle of 96.92(9)° in **11**. However, the bridging O-Co-O angle of 78.08(5)° of **CLVIII** is smaller than the bridging O2-Co1-O2b angle of 83.08(8)° in **11**. Furthermore, the bridging Co-OAr angles of **CLVIII** of 127.77(4)° and 130.31(3)° are considerably more obtuse than the equivalent C1-O2-C14 angle of 119.3(2)° in **11**.

Previous work has shown that cobalt(II) aryloxide complexes can be used as polymerisation catalysts. The cobalt(II) *ate* complex $[Na(THF)_6Co(2,4,6\text{-}t\text{Bu-}OC_6H_2)_3]$ **CLIX**, **figure 3.8**, reported by Xu and coworkers has been shown to

ring-open polymerise *L*-lactide.[16]

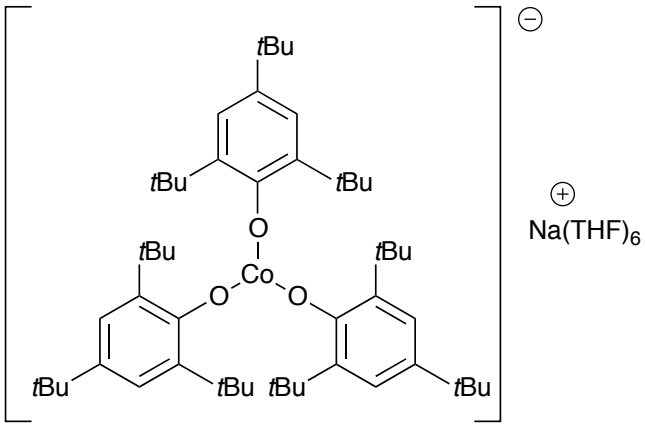

CLIX

Figure 3.8. [Na(THF)$_6$ Co(2,4,6-*t*Bu-OC$_6$H$_2$)$_3$], **CLIX**, which shows ring-opening polymerisation activity.[16]

Furthermore, Thomas and coworkers have prepared a series of cobalt complexes with tripodal ligands, **CLX** and **CLXI figure 3.9**, that contain one aryloxide group which polymerised lactide under solvent free conditions.[17]

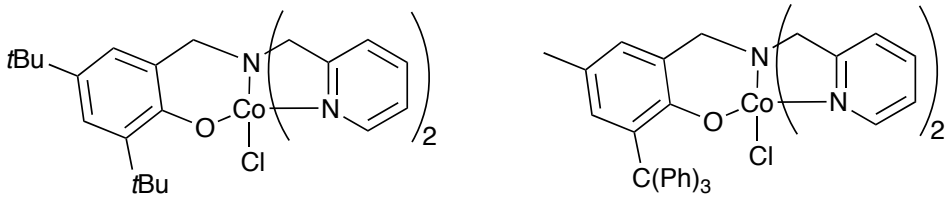

CLX **CLXI**

Figure 3.9. Cobalt complexes which display lactide polymerisation activity under solvent free conditions.[17]

3.3 Reactivity of 11 with pyridine *N*-oxide

The dioxygen chemistry of cobalt complexes has received much attention and Co(salen) complexes, in particular, are well known for their ability to bind dioxygen. For example, Avdeef and Schaefer have reported the structures of a [Co(salen)] **CLXII** complex in which dioxygen binds 'end-on' in a 1:1 ratio, **CLXIII equation 3.2**.[18] Here, the cobalt centre is oxidised from the + 2 to the + 3 oxidation state while the dioxygen forms a superoxo O_2^- ligand with the imidazole preventing dimerisation.

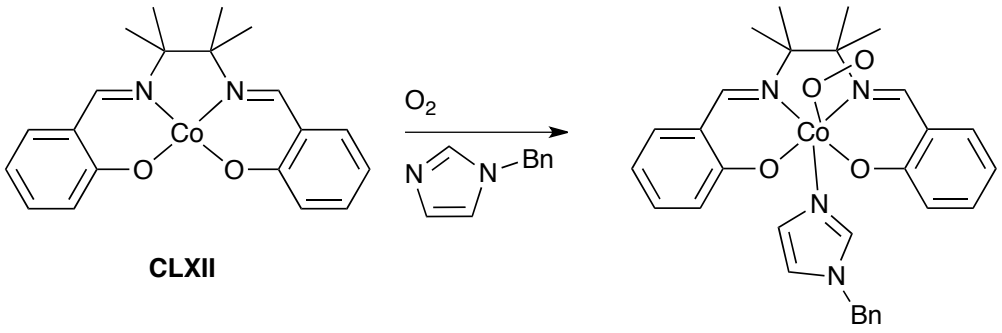

CLXII **CLXIII** (3.2)

Co(Salen)-O_2 complexes have also been used in the oxidation of organic substrates such as the oxidation of alkenes to alcohols and carbony compounds; the oxidation of phenols as well as the conversion of lignin to vanillin.[19] Additionally, Love and coworkers have shown that the dinuclear cobalt(II) complexes of the Schiff-base calixpyrrole 'pacman' macrocycle form bridging peroxo and superoxo complexes in a 9:1 ration when exposed to dioxygen.[20] Cobalt(II) catalysts have also been used in water splitting to produce oxygen.[21]

In order to probe the dioxygen chemistry of **11**, the complex was treated with two equivalents of pyridine *N*-oxide (py-*N*O). However, the reaction did not afford an oxidation product, instead the pyridine *N*-oxide adduct [HC(3-*t*Bu-5-Me-

$C_6H_2OH)(3\text{-}t\text{Bu-5-Me-}C_6H_2O)\mu\text{-}(3\text{-}t\text{Bu-5-Me-}C_6H_2O)Co(C_5H_5NO)]_2$ **12** was isolated, **equation 3.3**.

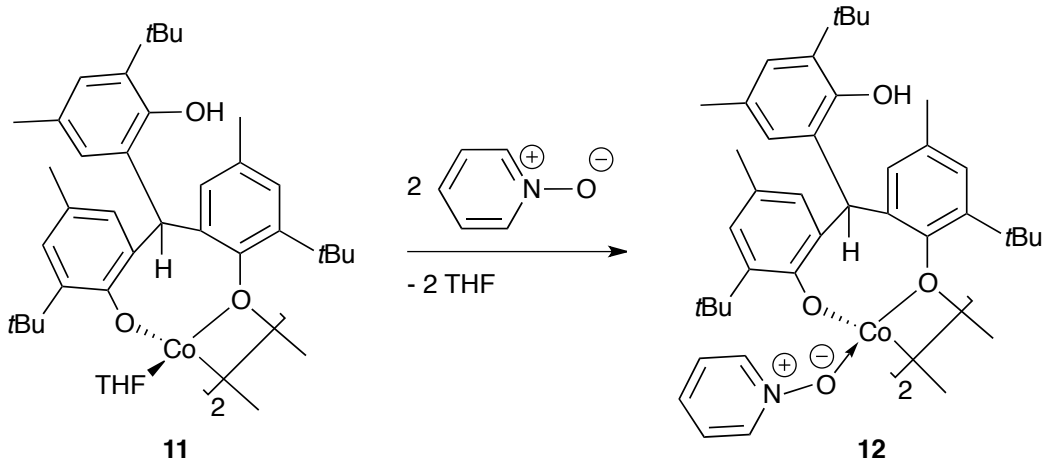

(3.3)

The ^{1}H NMR spectrum of **12** shows three magnetically inequivalent sets of aryloxide ligand resonances in the range of 60 to −60 ppm. The resonances due to the *t*Bu groups occur at 20.84, 0.41 and −4.57 ppm and are considerably shifted from the *t*Bu resonances of −70.52 −7.62 and −0.88 ppm in **11**. The three inequivalent methyl groups resonate at 38.91, 23.49 and −61.49 ppm and, similarly, there is a large shift from the Me resonances of **11** at 52.13, 46.36 and 39.92 ppm. The *o*- and *p*-CH's of the pyridine ring occur as broad singlets integrating to two protons each at 43.72 and 42.82 ppm.

X-ray diffraction quality crystals were grown by slowly cooling a hot THF solution to room temperature.

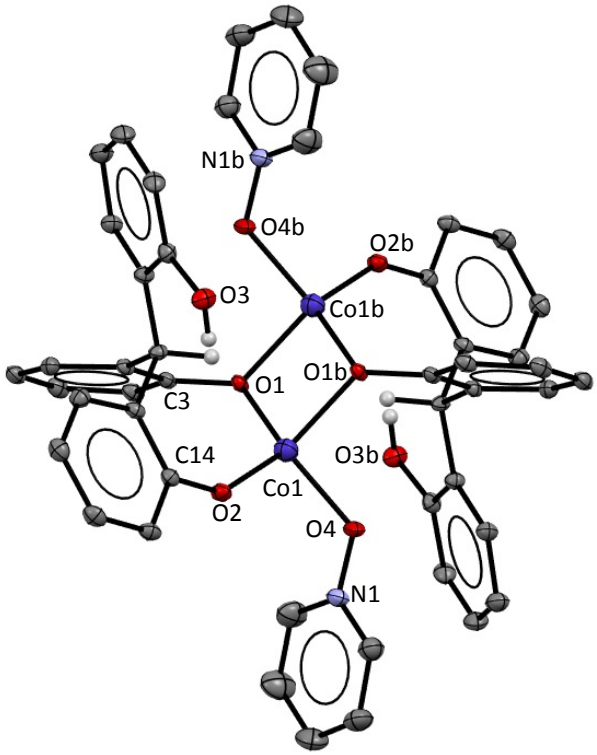

Figure 3.10. Solid state structure of **12**. For clarity aromatic H atoms, *t*Bu and Me groups have been omitted. Displacement ellipsoids are drawn at 50% probability.

Table 3.2: Selected bond and contact lengths (Å) and angles (°) of **12**.

Bond		Angle	
Co1-O1	1.9819(5)	O1-Co1-O1b	82.43(8)
Co1-O1b	1.9941(6)	O2-Co1-O4	99.95 (9)
Co1-O2	1.8717(4)	Co1-O2-C14	142.9(2)
Co1-O4	1.9542(3)	Co1-O4-N1	126.4(2)
Co1···Co1b	2.9910(7)	Co1-O1-Co1b	97.57(8)
N1-O4	1.3402(2)	Co1-O1-C3	121.1(2)

In the solid state **12** is dimeric, **figure 3.10**, with a {−Co−O−Co−O−} planar core with a dihedral angle of 0.00°, due to an inversion centre, **table 3.2**. The cobalt(II) centre lies in a distorted tetrahedral coordination environment with a O2-Co1-O4 angle of 99.95° and an O1-Co1-O1b angle of 82.43°. It is bound to one aryloxide with a Co1-O2 bond length of 1.8717(4) Å which is within the range of literature values of 1.826(2)[8] - 2.036(2) Å.[9] There are also two bridging aryloxides with a Co1-O1 length of 1.9941(6) Å which is within the range of previously published bridging Co-OAr bond lengths of 1.826[10] - 2.38(1) Å.[11]. The Co1-O2-C14 angle of 142.9(2)°, the Co1-O1-C3 angle of 121.1(2)° and the Co1-O1-Co1b angle of 97.57(8)° show no significant change from to the analogous angles of **11**.

Also coordinated to each cobalt centre is a molecule of pyridine *N*-oxide, with a Co1-O4 bond length of 1.9542(2) Å. This is shorter than the reported Co-$O_{\text{pyridine } N\text{-O}}$ bond length for $[Co^{II}(C_5H_5NO)_6](ClO_4)_2$ of 2.083(1) Å,[22] whilst the Co1-O2-N1 angle of 126.4(2)° is more obtuse when compared to the Co-O-N angle of 118.83(6)° in $[Co^{II}(C_5H_5NO)_6](ClO_4)_2$.[22] The N1-O4 bond length of 1.3402(2) Å is similar to that of free pyridine *N*-oxide of 1.33 Å and 1.37 Å,[23] showing that the pyridine *N*-oxide is only coordinated and has not reacted. The Co· · ·Co separation of 2.9910(7) Å is longer than the accepted Co-Co single bond length of 2.46 Å.[13]

Comparison with **11** shows an elongation of the terminal Co-O bond from 1.8577(19) Å in **11** to 1.8717(4) in **12**. Similarly, there is an elongation of the bridging aryoxide C-O bond lengths from 1.9752(18) Å in **11** to 1.9819(5) Å and 1.9941(6) Å in **12**. There is also an elongation of the Co-Co separation from 2.9603(7) Å in **11** to 2.9910(7) Å in **12**.

3.4 Synthesis of HC(3-*t*Bu 5-Me-C_6H_2OH)(3-*t*Bu-5-Me-C_6H_2O)μ-(3-*t*Bu-5-Me-C_6H_2O)Zn $(THF)_n$], 13

The analogous zinc(II) aryloxide complexes were also prepared, allowing definitive characterisation by ^{1}H NMR spectroscopy as the complex is diamagnetic. However, zinc aryloxide complexes are interesting in their own right. For example, Darensbourg and coworkers have prepared a series of zinc(II) aryloxide complexes which displayed catalytic activity for the copolymerisation of epoxides and CO_2,[24] while Dinjus and coworkers reported zinc(II) aryloxide complexes which could carboxylate acetophenone with CO_2.[25]

[HC(3-*t*Bu-5-Me-C_6H_2OH)(3-*t*Bu-5-Me-C_6H_2O)μ-(3-*t*Bu-5-Me-C_6H_2O)Zn $(THF)_n$] **13** was synthesised, in a 71% yield, by the reaction of [Zn(N{$SiMe_3$}$_2$)$_2$] with HC(3-*t*Bu-5-Me-C_6H_2OH)$_3$ in THF, **equation 3.4**.

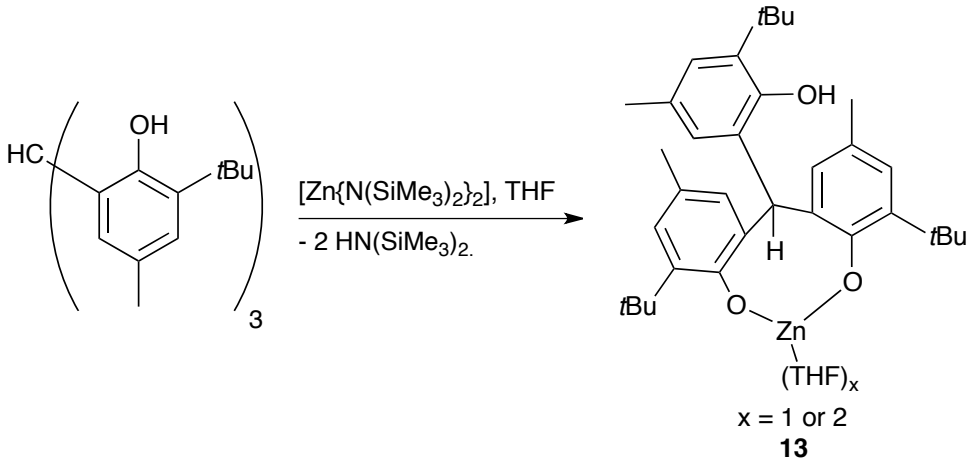

(3.4)

The ^{1}H NMR spectrum of **13** in d^8-THF, **figure 3.11**, shows that two of the phenol groups have been deprotonated. There are two resonances due to the *t*Bu groups in a 2:1 ratio: the two *t*Bu groups on the aryloxides resonate at 1.42

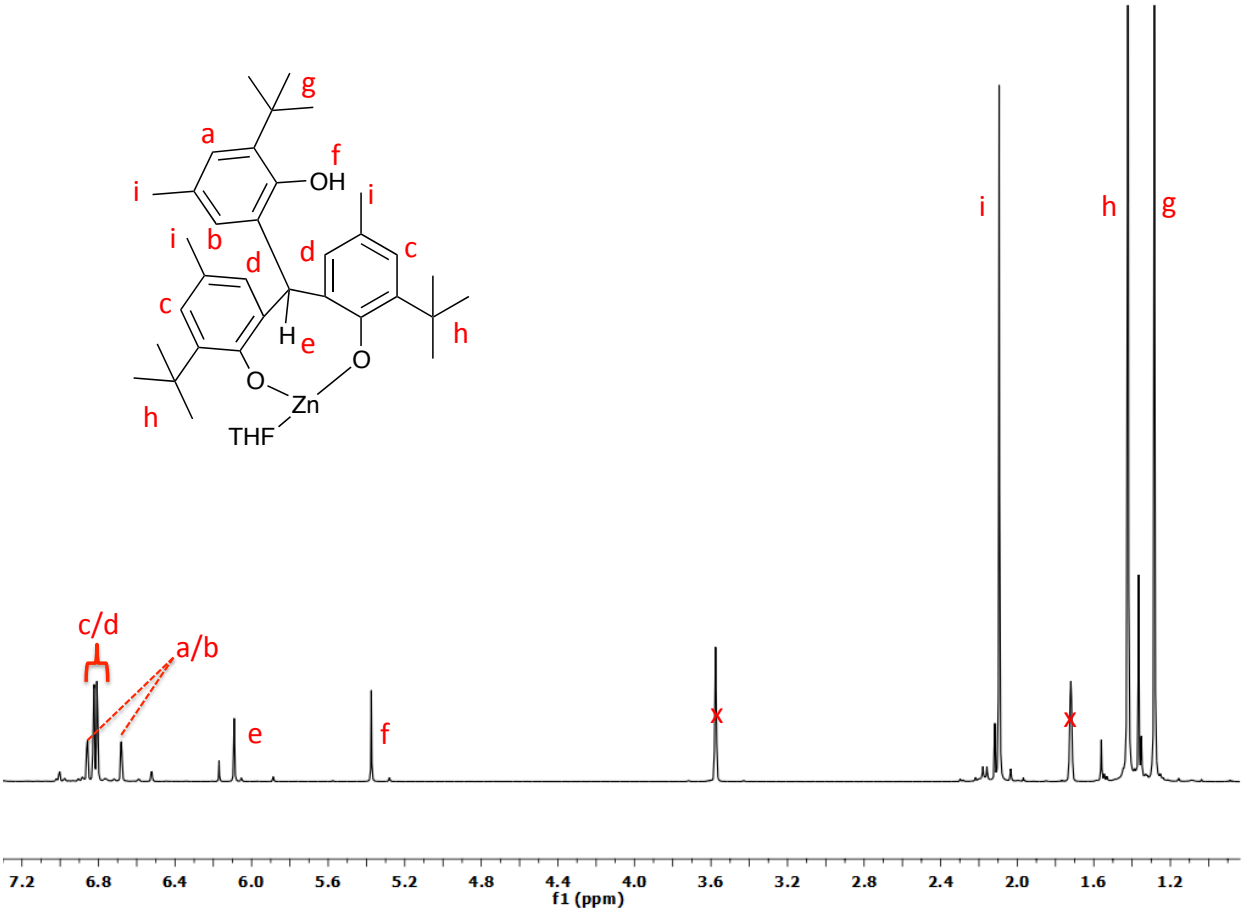

Figure 3.11. ^{1}H NMR spectrum of **13** in d^{8}-THF with interpretation. The red x's indicate residual protio-THF.

ppm while the *t*Bu group on the phenol resonates at 1.28 ppm. These resonances have shifted when compared to the *t*Bu resonances of HC(3-*t*Bu-5-Me-$C_6H_2OH)_3$ which are observed as a singlet at 1.37 ppm.[1] Unusually, the resonances due to the two different methyl environments are coincident at 2.09 ppm. This is similar to the Me signal of HC(3-*t*Bu-5-Me-$C_6H_2OH)_3$ which are equivalent and occur at 2.19 ppm. The remaining OH and central CH groups resonate at 5.37 and 6.03 ppm, respectively and are shifted when compared to the CH and OH signals of HC(3-*t*Bu-5-Me-$C_6H_2OH)_3$ which occur at 5.58 and 4.79 ppm, respectively. The

aromatic protons show a 2:2:1:1 pattern due to the 2:1 aryloxide to phenol ratio. Coordinated THF could not be seen in the ^{1}H NMR spectrum, possibley due to exchange. The two aryloxide groups are equivalent while the pendant phenol is inequivalent, a situation which is different to the ^{1}H NMR spectrum of **11**, where all three aryl groups are inequivalent and would be consistent with the complex being monomeric in solution.

Dried **13** was insoluble in arene solvents and heating the precipitate in arene or THF solvent produced a deep blue solution which, once analysed by ^{1}H NMR spectroscopy, proved to be decomposition products. This is possibly due to loss of the coordinated THF when the complex was dried under vacuum and decomposition occurring due to a reaction at the vacant coordination site. Crystals suitable for x-ray diffraction could not be obtained. A search of the literature provides examples of dinuclear structures with bridging and terminal aryloxides, such as those reported by Darensbourg and coworkers, **CLXIV figure 3.12**,[26] and by Dinjus and coworkers, **CLXV figure 3.12**.[25]

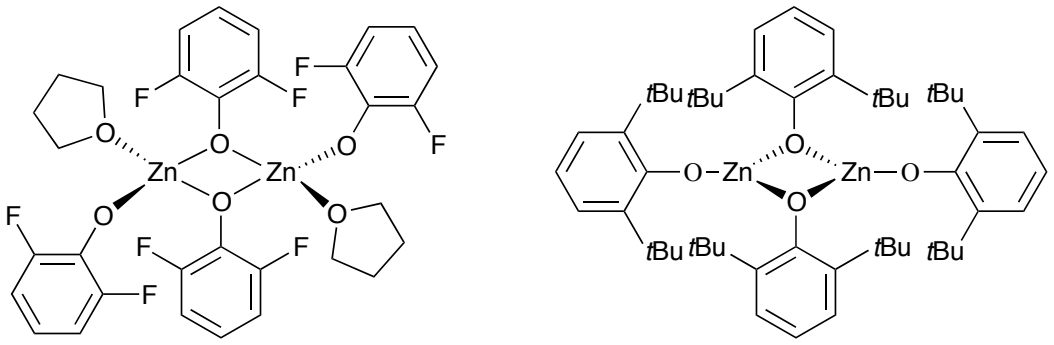

CLXIV **CLXV**

Figure 3.12. Dimeric zinc aryloxide complexes reported by Darensbourg and co-workers,[26] **CLXIV** and Dinjus and co-workers,[25] **CLXV**.

There are, however, also examples of monomeric zinc(II) aryloxide with two

aryloxides and two THF molecules coordinated to the zinc centre such as those reported by Caulton and coworkers, **CLXVI figure 3.13**,[27] and Darensbourg and coworkers, **CLXVII figure 3.13**.[24]

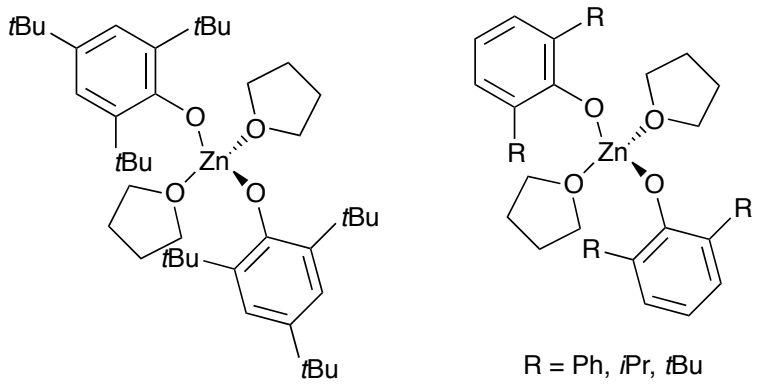

CLXVI **CLXVII**

Figure 3.13. Monomeric zinc aryloxide complexes reported by Caulton and co-workers,[27] **CLXVI** and Darensbourg and co-workers,[24] **CLXVII**.

Thus, it is equally possible that in the solid state **13** would be either monomeric **figure 3.14** left, or dimeric, **figure 3.14** left.

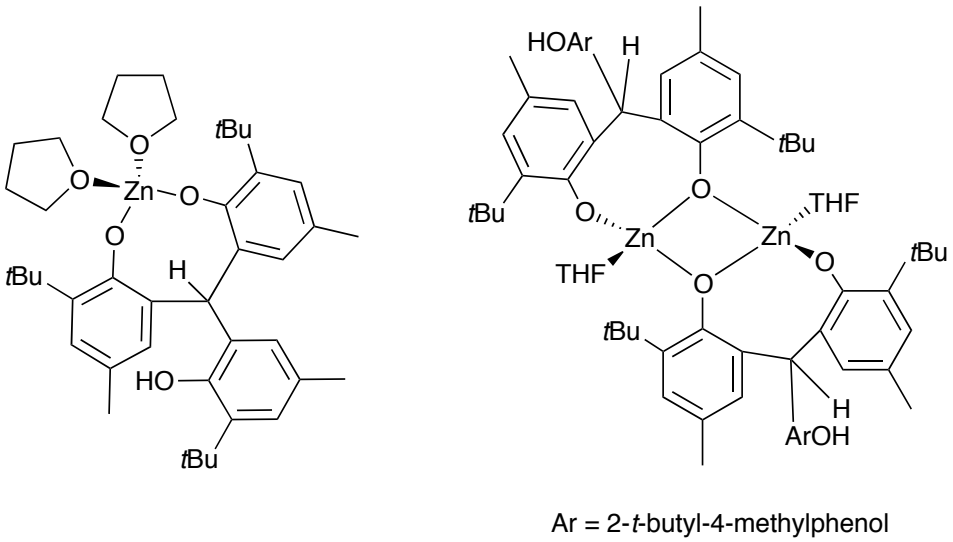

Figure 3.14. Two possible structures of **13**.

3.5 Synthesis of [HC(3-*t*Bu-5-Me-C_6H_2O)$_2$-μ-(3-*t*Bu-5-Me-C_6H_2O)KCo]$_2$, 14

In order to target d-/f-block heterobimetallic complexes via salt metathesis routes the potassium salt of **11** was synthesised. Carried out in toluene, the deprotonation of the remaining phenol of **11**with two equivalents of [KN($SiMe_3$)$_2$] yielded [HC(3-*t*Bu-5-Me-C_6H_2O)$_2$-μ-(3-*t*Bu-5-Me-C_6H_2O)KCo]$_2$ **14** as a deep blue precipitate, **equation 3.5**.

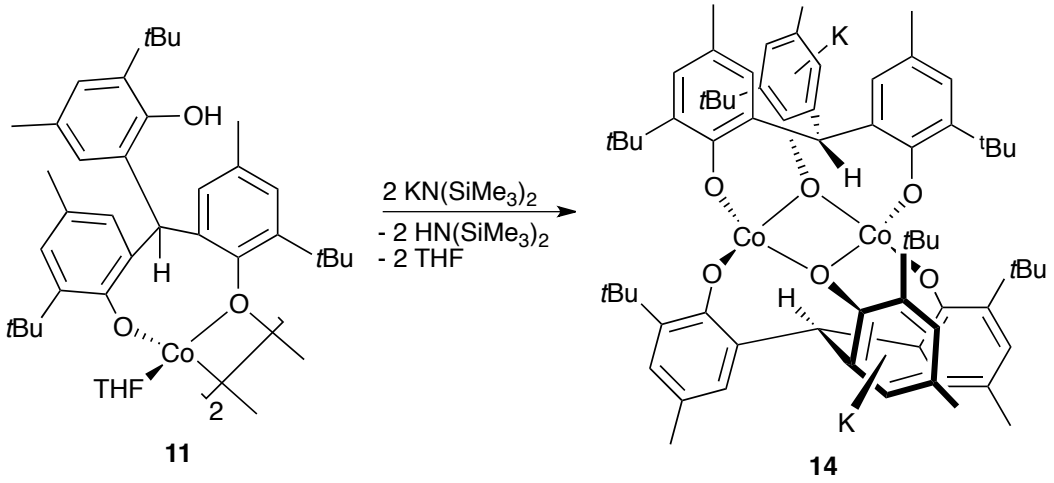

(3.5)

The ^{1}H NMR spectrum of **14** shows three magnetically inequivalent aryloxide groups paramgnetically shifted from 60 to −50 ppm with the protons of the *t*Bu groups resonating as broad singlets at −50.39, −14.58 and −1.81 ppm. These resonance are shifted when compared the *t*Bu resonances of **11** and **12**, **table 3.3**.

Table 3.3: Comparison of the ^{1}H NMR chemical shifts for the *t*Bu groups of **14**, **11** and **12**. Chemical shifts are given in ppm, ^{1}H NMR spectra recorded in d^8-THF.

14	**11**	**12**
−50.39	−70.52	20.84
−14.58	−7.62	0.41
−1.81	−0.88	−4.57

The three inequivalent Me groups resonate at −7.15, −4.09 and 46.09 ppm and are also shifted when compared to the Me resonances of **11** and **12**, **table 3.4**.

Table 3.4: The ^{1}H NMR chemical shifts for the Me groups of **14**, **11** and **12**. Chemical shifts are given in ppm, ^{1}H NMR spectra recorded in d^{8}-THF.

14	**11**	**12**
−7.15	52.13	38.91
−4.09	46.36	23.49
46.09	39.92	−61.49

Crystals suitable for x-ray diffraction were grown from a saturated benzene solution. The solid state structure, **figure 3.15**, shows that **14** is dunuclear.

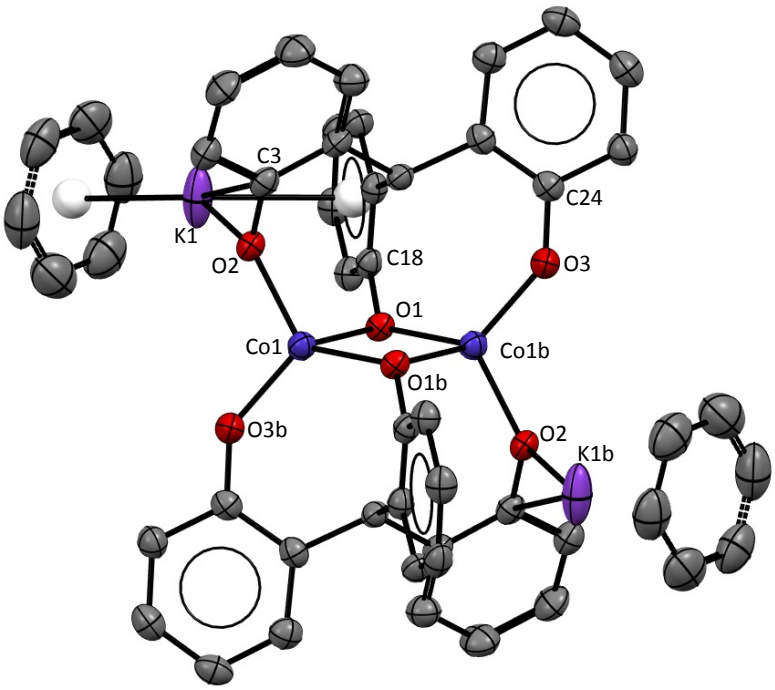

Figure 3.15. Solid state structure of **14**. For clarity selected H atoms, *t*Bu and Me groups have been omitted and displacement ellipsoids are drawn at 50% probability.

Table 3.5: Selelcted bond lengths (Å) for **14**.

Bond		Bond	
Co1-O2	1.928	K1-$OAr_{centroid}$	2.795
Co1-O1	2.034(2)	K1-$C_6H_{6centroid}$	3.000
Co1b-O1	1.993(2)	K1-O2	2.589(3)
Co1-O3b	1.880(2)	K1-C3	3.236(4)
Co1$\cdots$Co1b	2.9663(9)		

Table 3.6: Selected bond angles (°) for **14**.

Angle	
O1-Co1-O1b	85.13(9)
O2-Co1-O3b	111.86(10)
$OAr_{centroid}$-K1-$C_6H_{6centroid}$	118.88
Co1-O2-C3	130.8(2)
Co1-O1-Co1b	94.86(9)
Co1b-O3-C24	141.3(2)
Co1-O1-C18	125.0(2)

Each cobalt(II) centre has a distorted tetrahedral environment with an O1-Co1-O1b angle of 85.13(19)°, **table 3.6**, and an O2-Co1-O3b angle of 111.86(10)°. As with **11** and **12** there is a central, planar {−Co−O−Co−O−} core. Each ligand is bound to both cobalt centres via two terminal aryloxides with a Co1-O2 bond length of 1.928(2) Å, **table 3.5**, and a Co1-O3b bond length of 1.880(2) Å. The Co1-O3b bond length is of a similar length to the Co-O bond lengths of **11** and **12** of 1.8717(4) and 1.8577(19) Å, respectively, whilst the Co1-O2 is longer at 1.928(2) Å, **table 3.7**.

Table 3.7: Comparison of Co-$OAr_{terminal}$ bond lengths (Å).

14	**11**	**12**
1.880(2)	1.8577(19)	1.8717(4)
1.928(2)		

The third aryloxide bridges between the two cobalt centres with bond lengths of 2.034(2) Å and 1.993(2) Å between Co1-O1 and Co1b-O1, respectively. The Co1b-O3-C24 angle of 141.3(2)° is similar to the Co1-O2-C14 angle of 142.9(2)° in **11** and the Co1-O1-C3 angle of 142.78(18)° in **12**. However, the Co1-O2-C3 angle is significantly more acute at 130.86(9)°. The Co1-O1-C18 angle of 125.0(2)° is larger than the analogous angles in **11** and **12** of 119.3(2)° and 121.1(2)°, respectively. The Co1-O1-Co1b angle of 94.86(9)° slightly more acute than the Co1-O1-Co1b angle in **11** of 96.92° and 97.57(8)° in **12**.

The potassium centre is bound η^6 to the π-system of the bridging aryloxide unit and η^6 to the π-system of a molecule of benzene from the solvent with an a $OAr_{centroid}$-K1-$C_6H_{6centroid}$ angle of 118.88°. The potassium to aryloxide centroid, K1-$OAr_{centroid}$, bond length is 2.795 Å whilst the potassium to benzene centroid, K1-$C_6H_{6centroid}$, bond length is 3.000 Å. Additionally, the potassium is also interacting with the oxygen and *ortho*-carbon of one of the terminally bound aryloxides with a K1-O2 bond length of 2.589(3) Å and K1-C3 bond length of 3.236(4) Å. A similar coordination geometry is seen in the solid state structure of KCp in which each potassium adopts a distorted tetrahedral geometry being bound to four Cp rings.[28]

The Co···Co separation of 2.9663(9) Å is longer than the typical Co-Co single bond length of 2.46 Å[13] and shorter than the the Co···Co separation in **12** of 2.9910(7) Å. However, the Co···Co separation in **11** of 2.9603(7) Å is similar.

3.5.1 Salt-elimination reactivity of 14

Previous work by our group has shown that KCp elimination is an effective method of synthesising rare-earth NHC complexes.[29] To this end, two equivalents of $[CpY(L^{iPr})_2]$ were added to **14** in THF and heated to reflux for 16h in order to eliminate KCp, **equation 3.6**. However, ^{1}H NMR analysis showed that no reaction had occurred.

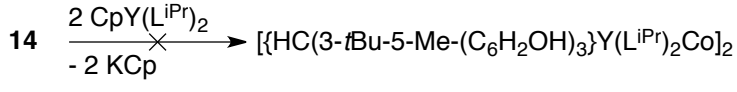

(3.6)

Alternatively, two equivalents of $[CpY(L^{iPr})_2]$ were added to **11** in THF and two equivalents of $[KN(SiMe_3)_2]$ added to form **14** *in situ*, **equation 3.7**. The reaction was carried out at both room temperature and reflux. Under both sets of conditions **14** was formed and did not react further.

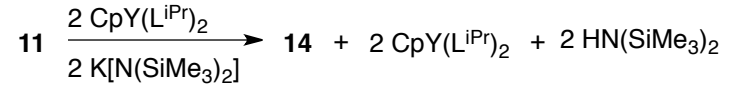

(3.7)

Similarly, no reaction occurred in the salt metathesis reaction between two equivalents of $[YCl_3(THF)_{3.5}]$ and **14** in THF at both room temperature or reflux, **equation 3.8**.

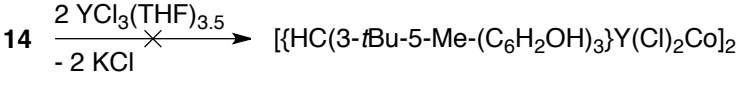

(3.8)

In order to increase the reactivity of **14**, two equivalents of 18-crown-6 were added in attempt to abstract the potassium ion and form an ion pair, **equation 3.9**. However, analysis of the ^{1}H NMR spectrum showed that no reaction occurred.

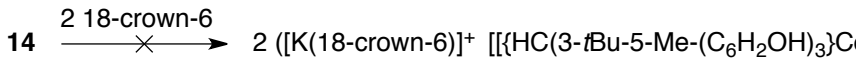

(3.9)

This is somewhat unusual as, in the zinc-potassium aryloxide complexes prepared by Doerrer and coworkers, **CLXVIII** and **CLXIX figure 3.16** the potassium ions coordinate to 18-crown-6 and not to the π-systems of the aryloxide ligands.[30]

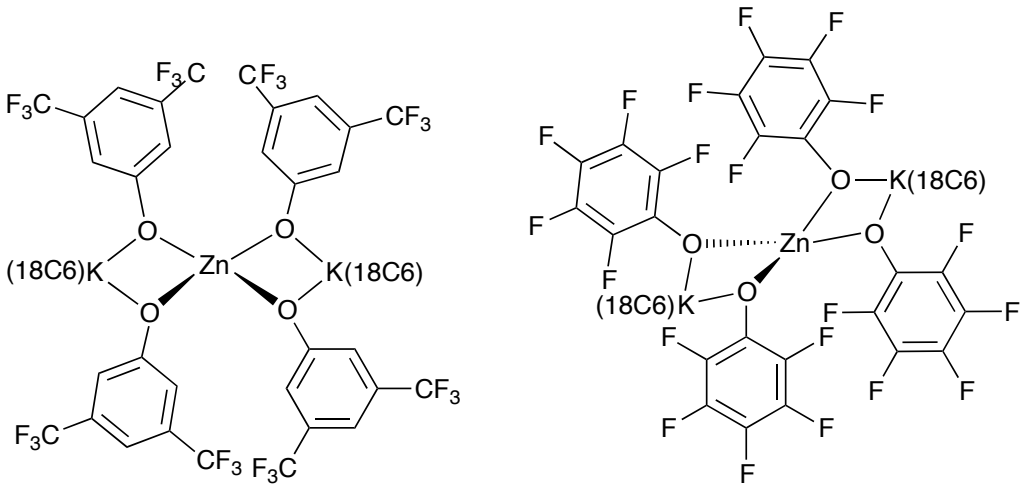

CLXVIII **CLXIX**

Figure 3.16. Heterobimetallic zinc/potassium complexes prepared by Doerrer and coworkers.[30]

3.6 Synthesis of [HC(3-*t*Bu-5-Me-$C_6H_2O)_2$-μ-(3-*t*Bu-5-Me-C_6H_2O)KZn]$_2$, 15

The heterobimetallic complex, [HC(3-*t*Bu-5-Me-$C_6H_2O)_2$-μ-(3-*t*Bu-5-Me-C_6H_2O)KZn]$_2$ **15** was synthesised in the reaction between **13** and two equivalents of [KN(Si$Me_3)_2$] whereby the product precipitated as a colourless solid, **equation 3.10**.

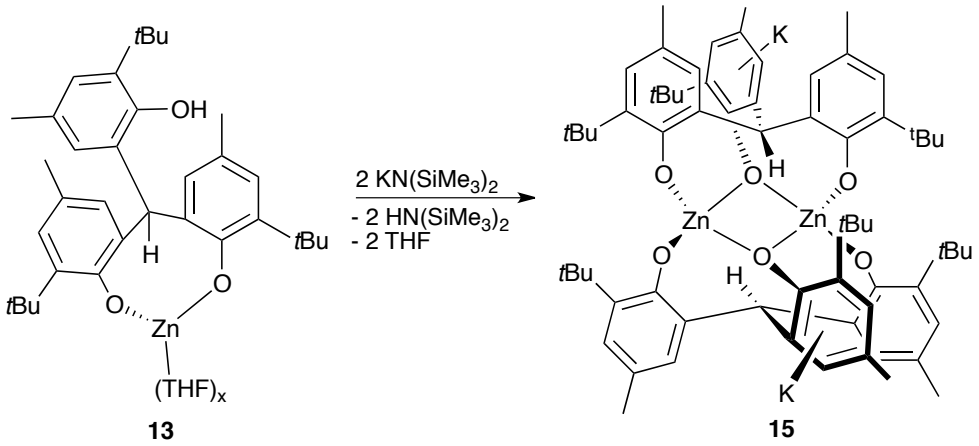

(3.10)

The ^{1}H NMR spectrum of **15** shows the *t*Bu groups resonate as overlapping singlets at 0.10-0.09 ppm, shifted upfield form the *t*Bu resonances of 1.42 ppm and 1.28 ppm in **13**. Similarly, the Me resonances have shifted from a single resonance at 2.09 ppm in **13** to three resonances at 1.34, 1.32 and 1.25 ppm in **15**. The central CH resonates at 6.56 ppm, shifted from 6.03 ppm in **13** while the aromatic protons resonate between 6.91 and 6.78 ppm. **15** is insoluble in arene solvents and only sparingly soluble in THF.

Single crystals suitable for x-ray crystallography were grown from a concentrated THF solution of **15**. In the solid state, **figure 3.17**, **15** adopts a dimeric structure similar to that of **14**. At the core of **13** is a planar {−Zn−O−Zn−O−} 4-membered ring with a Zn1-O3-Zn1b-O3b dihedral angle of 0.000(1)° and a Zn1···Zn1b separation of 2.9213(12) Å, **table 3.8**. This separation is significantly longer than the Zn-Zn single bonds reported by Carmona *et al.* of 2.305(3) Å[31] and by Yang *et al.* of 2.4208(6) to 2.4447(12) Å.[32] Each zinc(II) centre adopts a distorted tetrahedral geometry with an O1−Zn1−O2 angle of 109.99(9)° and an O3−Zn1−O3b angle of 87.56(8)°. The terminal Zn−O bond lengths of 1.902(2) Å for Zn−O1 and 1.878(2) Å for Zn−O2 are within the range of previously published terminal Zn-aryloxide bond lengths of 1.898(4)[33] to 2.412(1) Å.[34] The bridging

Zn−O bond lengths are longer at 2.0703(19) Å and 1.9748(18) Å for Zn1−O3 and Zn1−O3b, respectively and are within the range of previously published bridging Zn-aryloxide bond lengths of 1.896(8)[35] to 2.234(5) Å.[36] The Zn1-O1-C3 and Zn1b-O2-C30 bond angles are 132.9(2)° and 139.0(2)°, respectively.

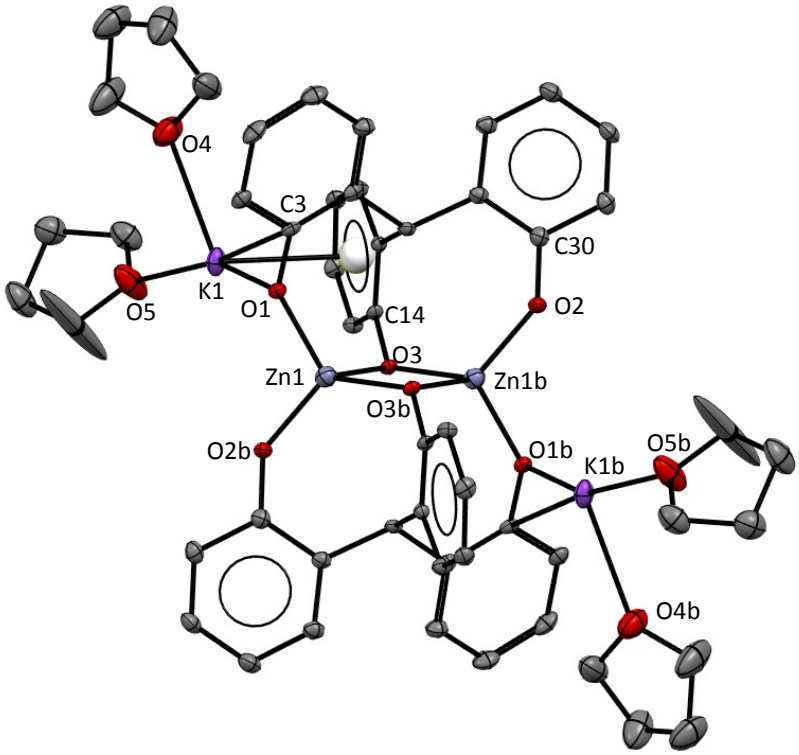

Figure 3.17. Crystal structure of **15**. For clarity, hydrogen atoms, Me and *t*Bu groups are omitted. Displacement ellipsoids are shown at 50% probability level.

The potassium ions are bound in an η^6 manner to the π-system of the bridging aryloxide with an $OAr_{centroid}$-K bond length of 2.883 Å, slightly longer than the $OAr_{centroid}$-K bond length of 2.795 Å in **14**. Completing the coordination sphere of the potassium ions are two molecules of THF with a K1-O4 bond length of 2.672(3) Å and a K1-O5 bond length of 2.635(3) Å.

Table 3.8: Selected bond lengths (Å) and angles (°) for **15**.

Bond		Bond\Angle	
Zn1-O1	1.902(2)	K1-O4	2.672(3)
Zn1-O2	1.878(2)	K1-O5	2.635(3)
Zn1-O3	2.0703(19)	O1-Zn1-O2	109.99(9)
Zn1-O3b	1.9748(18)	O3-Zn1-O3b	87.56(8)
$Ar_{centroid}$-K	2.883	Zn1-O3-Zn1b-O3b	0.000(1)
Zn1$\cdots$Zn1b	2.9213(12)	Zn1-O1-C3	132.9(2)
		Zn1-O3-Zn1b	92.44(7)
		Zn1b-O2-C30	139.0(2)

The zinc-potassium complex $[\{K(18C6)\}_2[Zn_2(OAr')_6]]$ ($Ar' = 3,5\text{-}CF_3\text{-}C_6H_3$), **CLXX figure 3.18**, has been reported previously by Doerrer and coworkers.[30] As with **15**, **CLXX** is dinuclear with two zinc centres and two potassium ions. Each zinc centre is bound to two terminal aryloxides and two bridging aryloxides. However, the potassium ions are coordinated to 18-crown-6 and to the oxygen of a bridging aryloxide in $[\{K(18C6)\}_2[Zn_2(OAr')_6]]$ whereas in **15**, it is bound to the π-system of the bridging aryloxide and THF.

Both **CLXX** and **15** have a similar Zn$\cdots$Zn separation (2.9971(6) Å and 2.9213(12) Å, respectively). The terminal Zn-ayloxide bonds in **CLXX** of 1.9016(16) and 1.9012(7) Å are similar to the analogous Zn1-O1 and Zn1-O2 bond lengths of 1.902(2) and 1.878(2) Å, respectively, in **15**. Moreover, the bridging Zn-aryloxide bond lengths are also similar at 2.0303(15) Å in **CLXX** and 1.9748(18) and 2.0703(19) Å in **15**. However, the O-Zn-O angle of 83.16(7)° is smaller than the equivalent O3-Zn1-O3b angle of 87.59(8)° in **15**. There is also a larger angle between the terminal aryloxides on each zinc, with an O-Zn-O angle of 118.42(7)° in **CLXX** compared with the smaller O1-Zn1-O2 angle of 109.99(9)° in **15**.

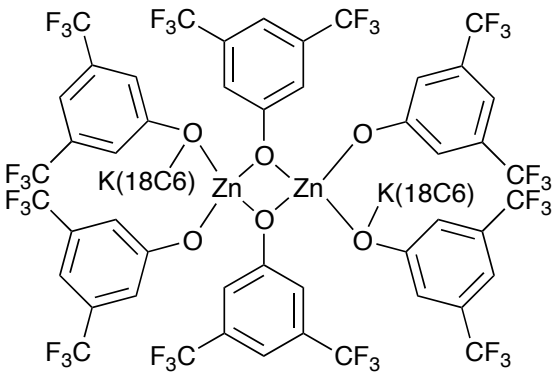

CLXX

Figure 3.18. $[\{K(18C6)\}_2[Zn_2(OAr')_6]]$.[30]

3.7 Reactivity of 11 with $[(L^{Mes})_2Ce(N\{SiMe_3\}_2)]$

As salt elimination methods of synthesising *d*-/*f*-block heterobimetallic complexes proved unsuccessful, attention turned to forming such complexes through protonolysis reaction. The pendant phenol group on **11** is ideally positioned to be deprotonated and thereby form a heterobimetallic complex.

Addition of two equivalents of the previously synthesised $[(L^{Mes})_2Ce(N\{SiMe_3\}_2)]$[37] to **11** in THF afforded, after work up, $[\{HC(3\text{-}t\text{Bu-}5\text{-Me-}C_6H_2OH)_3\}Ce(L^{Mes})_2]_2$ **16** as a yellow powder, **equation 3.11**.

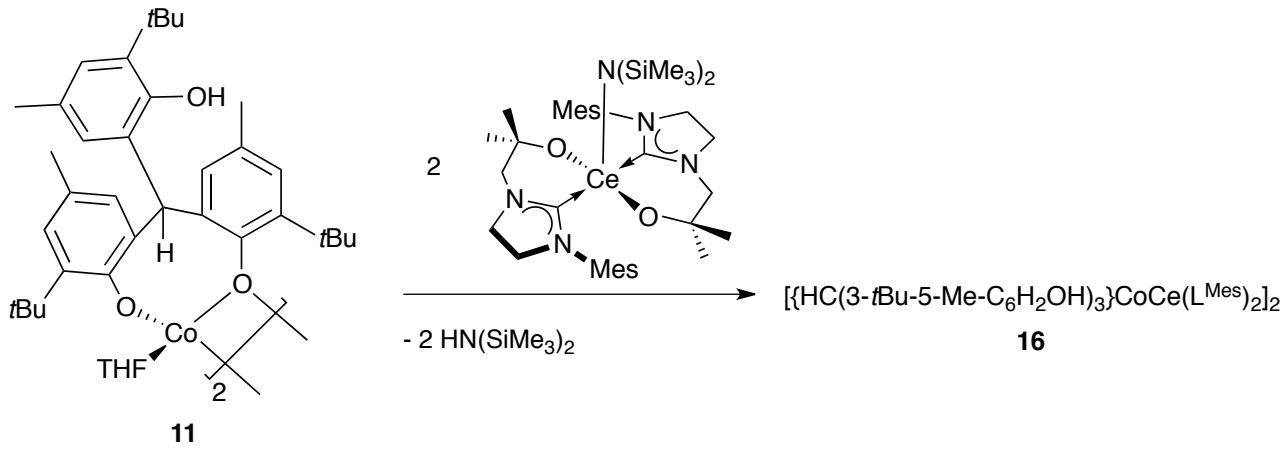

(3.11)

The ^{1}H NMR spectrum of **16** shows paramagnetically shifted ligand resonances between 80 to −60 ppm. Importantly, the $N(SiMe_3)_2$ resonance at −0.97 ppm in $[(L^{Mes})_2Ce(N\{SiMe_3\}_2)]$ is not present in the ^{1}H NMR spectrum whilst a resonance due to $HN(SiMe_3)_2$ is observed. There are three inequivalent *t*Bu groups resonating at 34.35, 0.31 and −8.66 ppm, a large change in chemical shift when compared to the *t*Bu resonances of **11** at −70.52, −7.62 and −0.88 ppm. The spectrum also shows ten resonances due to the protons of the methyl groups with three of these, at 4.31, −3.91 and −51.95 ppm integrating to six protons, corresponding to the *o*-Me of mesityl groups and one set of equivalent *gem*-dimethyl groups. Thus, the two L^{Mes} ligands are inequivalent, with the second set of *gem*-dimethyl protons being inequivalent, whereas the *gem*-dimethyl protons are all equivalent in $[(L^{Mes})_2Ce(N\{SiMe_3\}_2)]$, resonating as a broad singlet at at 0.81 ppm and integrating to 12 protons. The protons on the remaining methyl groups resonate at 46.26, 35.40, 20.53, −3.97, −9.48, −43.78 and −59.57 ppm. The resonances due to the CH_2 groups, consistant with two inequivalent L^{Mes} ligands, occurred at 52.13, 48.11, 30.62, 10.05 and 6.49 ppm. Additionally, the remaining very broad resonances of $[(L^{Mes})_2Ce(N\{SiMe_3\}_2)]$ at 22.4, 15.8, 9.6, 5.5 and −9.9 ppm are not

present in the ^{1}H NMR spectrum of **16**.

Crystals suitable for x-ray crystallography could not be obtained. However, the ^{1}H NMR spectrum shows that the two L^{Mes} ligands are inequivalent and that the three aryloxide groups are also inequivalent. As there is a mismatch between the hard cerium centre and the soft NHC donors and there are hard anionic oxygen donors bound to the cobalt centres it is likely that there has been some ligand redistribution, as was seen in **5** and **6**. At least one soft NHC donor is likely to be bound to a cobalt centre while a hard anionic oxygen donor is likely bound to the cerium centre and there is the possibility of the aryloxides bridging to the cobalt centre. **Figure 3.19** gives a possible structure for **16**.

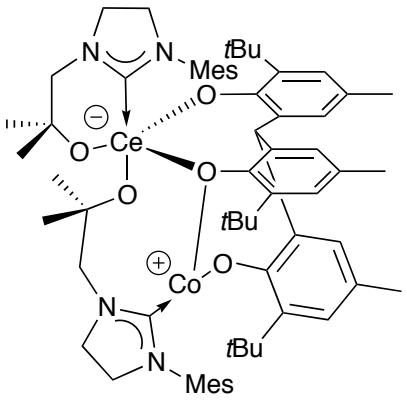

Figure 3.19. Possible structure of **16**.

3.8 Reactivity of 11 with $[(\{Me_3Si\}_2N)_2U\{N(SiMe_3)Si(Me_2)CH_2\}]$

Previous work by Sattelberger and coworkers has show that substituted phenols readily add across the An−CH_2 bond of $[(\{Me_3Si\}_2N)_2U\{N(SiMe_3)Si(Me_2)CH_2\}]$ (An = U, Th) to form heteroleptic uranium(IV) or thorium(IV) complexes with

both aryloxide and silylamide ligands.[38] Thus, in attempt to synthesis a cobalt-uranium heterobimetallic complex two equivalents of [($\{Me_3Si\}_2N)_2U\{N(SiMe_3)Si(Me_2)CH_2\}$] was added to **11** in benzene with the aim of deprotonating the pendant phenol, **scheme 3.1**.

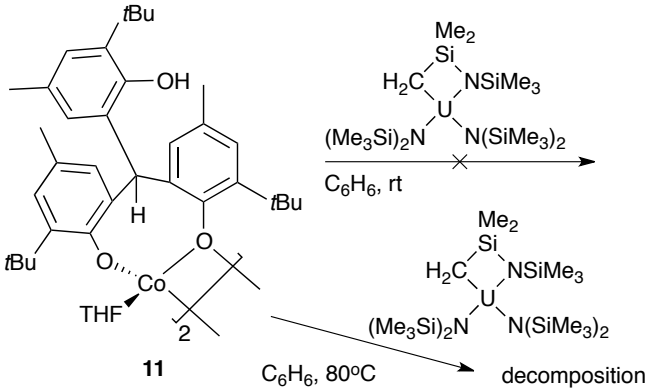

Scheme 3.1. Reactivity of **11** with [($\{Me_3Si\}_2N)_2U\{N(SiMe_3)Si(Me_2)CH_2\}$]

Analysis of the ^{1}H NMR when the reaction was carried out at room temperature spectrum showed no reaction had occurred. Heating the reaction mixture to 80°C for 1 h resulted in the decomposition of **11**.

3.9 Reaction of 11 with ceric ammonium nitrate, CAN

In attempt to synthesise the cerium(IV)-aryloxide complex, [[HC(3-*t*Bu-5-Me-$C_6H_2O)_2$(3-*t*Bu-5-Me-C_6H_2OH)]$Ce(NO_3)_2$] **17**, via the salt metathesis reaction two equivalents of [$(NH_4)_2Ce(NO_3)_6$] (ceric ammonium nitrate, CAN) were added to **11**. Analysis of the ^{1}H NMR spectrum of the resulting pink solution revealed protonated ligand HC(3-*t*Bu-5-Me-$C_6H_2OH)_3$, **scheme 3.2**.

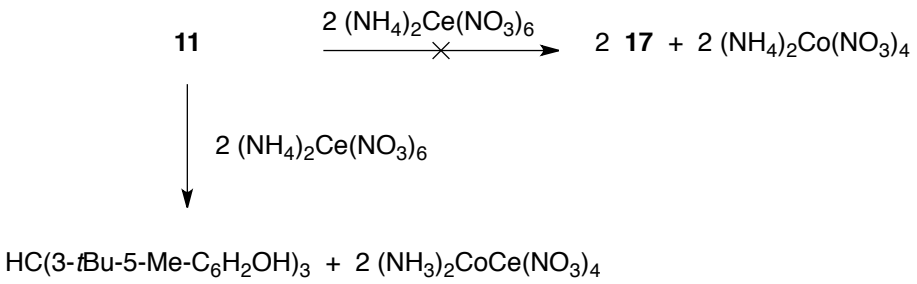

Scheme 3.2. Reactivity of **11** with CAN.

Instead of undergoing transmetallation, the aryloxide groups are reprotonated by two NH_4^+ molecules from CAN with $[(NH_3)_2CoCe(NO_3)_4]$ being a possible second product, though a search of the literature shows that such a compound has not been reported.

3.10 Summary

In summary, the cobalt- and zinc-aryloxide complexes **11** and **13** were prepared. The THF molecules of **11** could be displaced by the addition of pyridine-*N*-oxide to form the pyridine-*N*-oxide adduct **12**. The pendant phenol group of **11** could also deprotonated by $[(L^{Mes})_2Ce(N\{SiMe_3\}_2)]$ to form the heterobimetallic complex **16**.

The heterobimetallic complexes **14** and **15** were prepared from the addition of $[K(NSiMe_3)_2]$ to **11** or **13**, respectively. **14** proved highly stable and was inert to salt elimination reactions and showed no reactivity with 18-crown-6.

References

1. M. B. Dinger and M. J. Scott, *Eur. J. Org. Chem.*, 2000, 2467.

2. T. Yamato, M. Haraguchi, J. Nishikawa and S. Ide, *J. Chem. Soc., Perkin Trans. 1*, 1988, 609.

3. T. Yamato, L. K. Doamekpor and H. Tsuzuki, *Liebigs Ann./Recueil*, 1997, 1537.

4. M. B. Dinger and M. J. Scott, *Inorg. Chem.*, 2000, **39**, 1238.

5. M. B. Dinger and M. J. Scott, *Inorg. Chem.*, 2001, **40**, 1029.

6. K. Matloka, A. Gelis, M. Regalbuto, G. Vandegrift and M. J. Scott, *Sep. Sci. Technol.*, 2006, **41**, 2129.

7. K. Matloka, A. K. Sah, M. W. Peters, P. Srinivasan, A. V. Gelis, M. Regalbuto and M. J. Scott, *Inorg. Chem.*, 2007, **46**, 10549.

8. Q. Wang and X.-N. Fang, *Acta. Crystallogr., Sect. E*, 2006, **62**, m1946.

9. A. Pramanik, S. Abbina and G. Das, *Polyhedron*, 2007, **26**, 5225.

10. B. F. Hoskins and G. A. Williams, *Aust. J. Chem.*, 1975, **28**, 2593.

11. M. Hong, F. Jiang, X. Huang, W. Su, W. Li, R. Cao and H. Liu, *Inorg. Chim. Acta.*, 1997, **256**, 137.

12. F. A. Cotton, G. Wilkinson, C. A. Murillo and M. Bochman, *Advanced Inorganic Chemistry*, Wiley-Interscience, sixth edition, 1999.

13. L. Pauling, *Proc. Natl. Acad. Sci.*, 1976, **73**, 4290.

14. A. M. Bryan, G. J. Long, F. Grandjean and P. P. Power, *Inorg. Chem.*, 2014, **53**, 2692.

15. M. V. Petersen, A. H. Iqbal, L. V. Zakharov, A. L. Rheingold and L. H. Doerrer, *Polyhedron*, 2013, **52**, 276.

16. C. Yuan, X. Xu, Y. Zhang and S. Ji, *Chin. J. Chem.*, 2012, **30**, 1474.

17. M. J.-L. Tschan, J. Gao, S. K. Raman, E. Brulé, T. Roisnel, M.-N. Rager, R. Legay, G. Durieux, B. Rigaud and C. M. Thomas, *Dalton Trans.*, 2014, **43**, 4550.

18. A. Avdeef and W. P. Schaefer, *J. Am. Chem. Soc.*, 1976, **98**, 5153.

19. C. L. Bailey and R. S. Drago, *Coord. Chem. Rev.*, 1987, **79**, 321.

20. M. Volpe, H. Hartnett, J. W. Leeland, K. Wills, M. Ogunshun, B. J. Duncombe, C. Wilson, A. J. Blake, J. McMaster and J. B. Love, *Inorg. Chem.*, 2009, **48**, 5195.

21. M. W. Kanan and D. G. Nocera, *Science*, 2008, **321**, 1072.

22. J. S. Wood, R. K. Brown and M. S. Lehmann, *Acta. Crystallogr., Sect. C*, 1986, **42**, 410.

23. D. Ulku, B. P. Huddle and J. C. Morrow, *Acta. Crystallogr., Sect. B*, 1971, **27**, 432.

24. D. J. Darensbourg, M. W. Holtcamp, G. E. Struck, M. S. Zimmer, S. A. Niezgoda, P. Rainey, J. B. Robertson, J. D. Draper and J. H. Reibenspies, *J. Am. Chem. Soc.*, 1999, **121**, 107.

25. M. Kunert, M. Bräuer, O. Klobes, H. Görls, E. Dinjus and E. Anders, *Eur. J. Inorg. Chem.*, 2000, 1803.

26. D. J. Darensbourg, J. R. Wildeson, J. C. Yarbrough and J. H. Reibenspies, *J. Am. Chem. Soc.*, 2000, **122**, 12487.

27. R. L. Geerts, J. C. Huffman and K. G. Caulton, *Inorg. Chem.*, 1986, **25**, 1803.

28. R. E. Dinnebier, U. Behrens and F. Olbrich, *Organometallics*, 1997, **16**, 3855.

29. P. L. Arnold, T. Cadenbach, I. H. Marr, A. A. Fyfe, N. L. Bell, R. Bellabarba, R. P. Tooze and J. B. Love, *Dalton Trans.*, 2014, **43**, 14346.

30. J. S. Lum, P. E. Chen, A. L. Rheingold and L. H. Doerrer, *Polyhedron*, 2013, **58**, 218.

31. I. Resa, E. Carmona, E. Gutierrez-Puebla and A. Monge, *Science*, 2004, **305**, 1136.

32. J. Gao, S. Li, Y. Zhao, B. Wu and X.-J. Yang, *Organometallics*, 2012, **31**, 2978.

33. L. Mąkloski, K. Zelga, R. Petrus, D. Kubicki, P. Zarzycki, P. Sobota and J. Lewiński, *Chem. Eur. J.*, 2014, **20**, 14790.

34. J. Wang, W. Chen, X. Liu, C. Wesdemiotis and Y. Pang, *J. Mater. Chem. B*, 2014, **2**, 3349.

35. J. Gao, R. A. Zingaro, J. H. Reibenspies and A. E. Martell, *Org. Lett.*, 2004, **6**, 2453.

36. M. Fondo, N. Ocampo, A. M. García-Deibe and J. Sanmartín, *Inorg. Chem.*, 2009, **48**, 4971.

37. P. L. Arnold, Z. R. Turner, A. I. Germeroth, I. J. Casely, R. Bellabarba and R. P. Tooze, *Dalton Trans.*, 2010, **39**, 6808.

38. J. M. Berg, D. L. Clark, J. C. Huffman, D. E. Morris, A. P. Sattelberger, W. E. Streib, W. G. V. D. Sluys and J. G. Watkin, *J. Am. Chem. Soc.*, 1992, **114**, 10811.

Chapter 4

Reactivity of NHC Complexes with Acidic C-H and N-H bonds and their use as Catalysts for Organic Reactions

4.1 Introduction

NHCs have also been employed as organocatalysts, as well as being important ligands for metal complexes. They have proved useful organocatalysts for the benzoin condensation,[1][2] **scheme 4.1** and the Stetter reaction,[3][4] **scheme 4.1**, as they react umpolug with electrophilic carbonyl groups to form nucleophilic acyl anion equivalents. Furthermore, their Brønsted basicity has been exploited in transesterification,[5][6][7] **scheme 4.1**, and acylation reactions.[8][9][10]

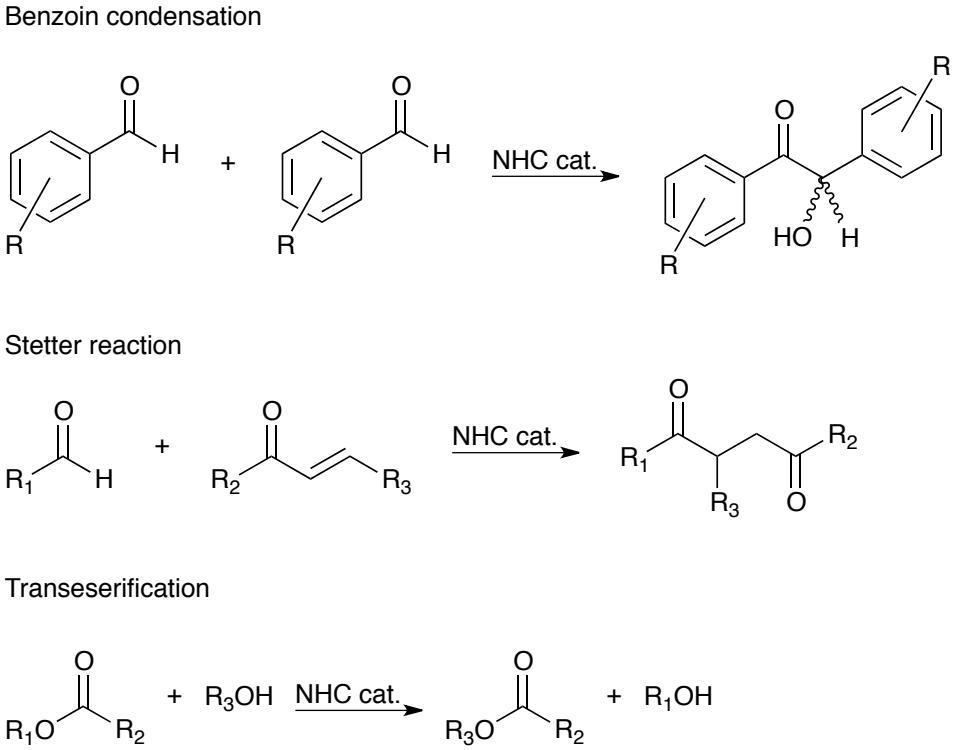

Scheme 4.1

Previous work carried out within the Arnold group has shown that polar substrates E-X (E = $SiMe_3$, PPh_2, BBN, $SnBu_3$; X = Cl, I, N_3) can be cleaved heterolytically across the yttrium- or cerium-NHC bond of alkoxy tethered NHC ligand rare earth complexes **CLXXI**^{Y} and **CLXXI**^{Ce}, **scheme 4.2**, to form the zwitterionic complexes **CLXXII**^{Y} and **CLXXII**^{Ce}, respectively. Subsequent heating of these complexes resulted in the elimination of the functionalised substrate E−N$(SiMe_3)_2$ and the complexes **CLXXIII**^{Y} and **CLXXIII**^{Ce}. Addition of [KN$(SiMe_3)_2$] resulted in the reformation of **CLXXI**^{Y} and **CLXXI**^{Ce}. This resulted in the formation of new N-E bonds at a redox innocent metal centre.[11][12]

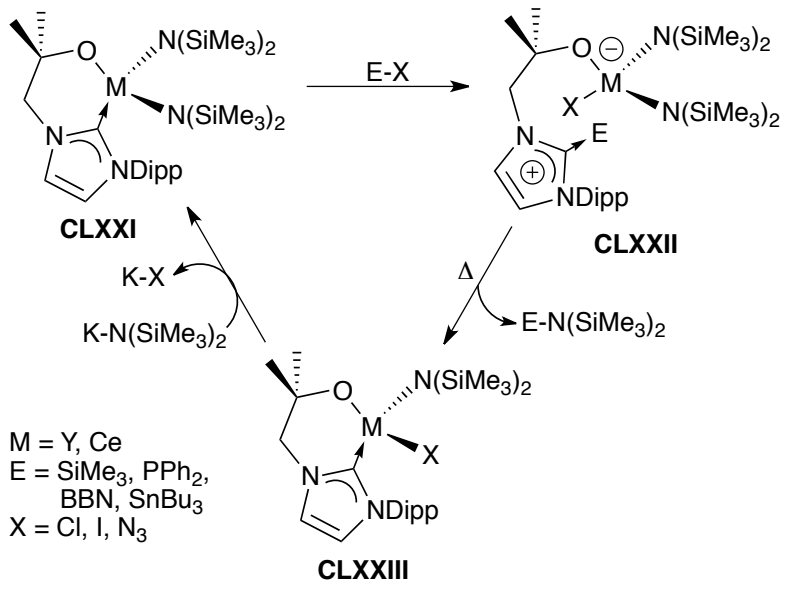

Scheme 4.2. Heterolytic cleavage of polar organic substrates by rare-earth NHC complexes $\mathbf{CLXXI}^{\mathrm{Y}}$ and $\mathbf{CLXXI}^{\mathrm{Ce}}$.[11][12]

Furthermore, the heteroleptic yttrium complex $[(\mathrm{Cp})_2\mathrm{Y}(\mathrm{L}^{i\mathrm{Pr}})]$, **CLXXIV scheme 4.3**, has been shown to activate the N-H bond of pyrrole and indole to form $[(\mathrm{Cp})_2\mathrm{Y}(\mathrm{HL}^{i\mathrm{Pr}})(\mathrm{C_4H_4N})]$ **CLXXV** and $[(\mathrm{Cp})_2\mathrm{Y}(\mathrm{HL}^{i\mathrm{Pr}})(\mathrm{C_8H_6N})]$ **CLXXVI**, respectively. In both cases the N-H bond is heterolytically cleaved across the labile yttrium-carbene bond to form a zwitterionic complex.[13]

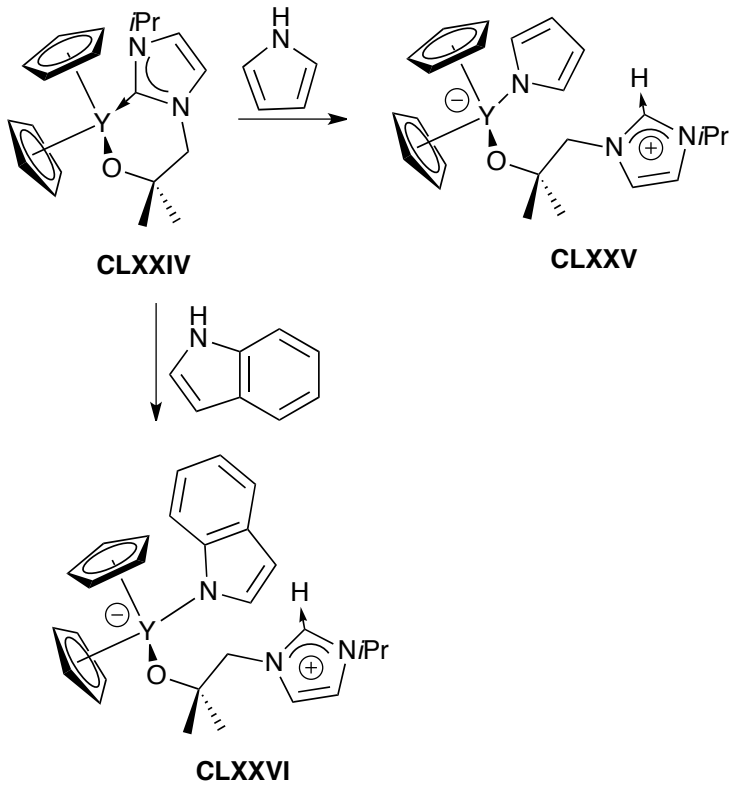

Scheme 4.3. Reactivity of $[(Cp)_2Y(L^{iPr})]$ **CLXXIV** with pyrrole and indole.[13]

The heteroleptic cerium(III) complex $[(Cp)_2Ce(L^{iPr})]$, **CLXXVIII scheme 4.4**, has been shown to react with the acidic C-H bond of alkynes resulting in the formation of $[(Cp)_2Ce(HL^{iPr})(CCR)]$ **CLXXVIII** (R = Me_3Si or Ph). This then underwent ligand redistribution to form $[(Cp)_3Ce(HL^{iPr})]$ **CLXXIX**, which could be isolated by crystallisation, and $[(Cp)Ce(CCR)_2(HL^{iPr})]$ **CLXXX** which then decomposed further. **CLXXIX** could also be prepared by the reaction of $[(Cp)_2Ce(L^{iPr})]$ with CpH.[13]

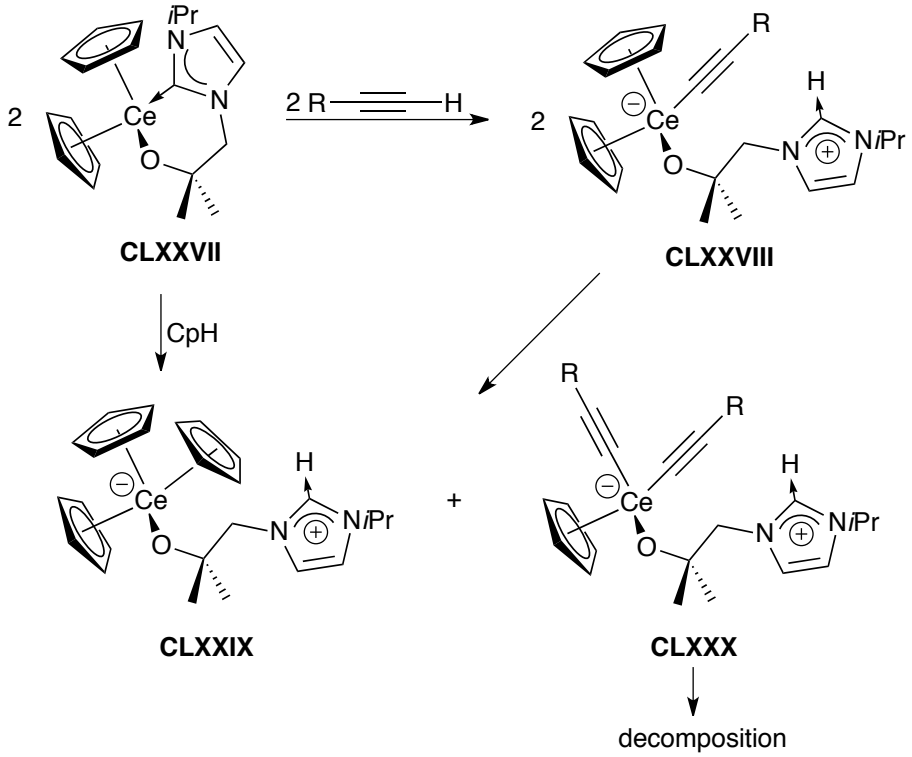

Scheme 4.4. Reactivity of $[(Cp)_2Ce(L^{iPr})]$, **CLXXVII** with CpH and RC≡CH (R = Me_3Si, Ph).[13]

Furthermore, unpublished previous work done within the group has shown that the heteroleptic cerium(III) complex $[(L^{Mes})_2Ce(N\{SiMe_3\}_2)]$ reacts with benzoyl chloride and pyridine to form $[(C_6H_5C(O)C_5H_5N)]_3^+[Ce^{III}Cl_6]^{3-}$ **CLXXXI** as a crystalline solid, **scheme 4.5**.[14]

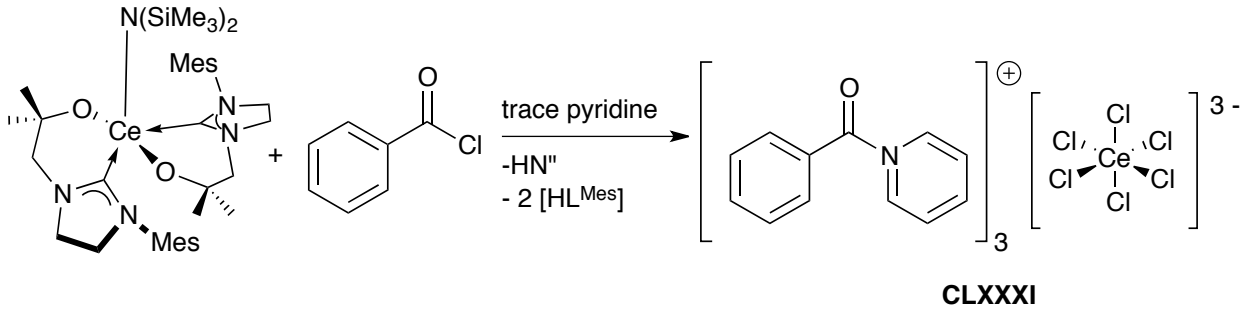

CLXXXI

Scheme 4.5. Reactivity of $[(L^{Mes})_2Ce(N\{SiMe_3\}_2)]$ with benzoyl chloride.[14]

Stack and coworkers have reported the $C_{carbene}$-halogen reductive elimination from the copper(I)-NHC complex $[XCu(1\text{-}C\{NDippCH\}_2)]$ (X = Cl, Br, I) **CLXX XII**, **scheme 4.6**.[15] Treatment of **CLXXXII** with two equivalents of the oxidant $[Cu(CF_3SO_3)_2]$ resulted in the formation of $[X(1\text{-}C\{NDippCH\}_2)]^+$ **CLXXXIII** with the loss of Cu, **scheme 4.6**.

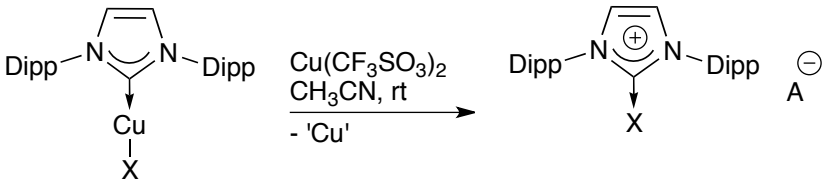

CLXXXII

X = Cl, Br, I

CLXXXIII

X = Cl, A = SbF_6
X = Cl, A = CF_3SO_3
X = I, A = I_3

Scheme 4.6. Reductive halogenation reaction of **CLXXXII** to form **CLXXXIII**.[15]

It was noted that this $C_{carbene}$-X reductive elimination should be considered as a potential decomposition pathway for high-valent metal complexes supported by NHCs, especially under oxidative conditions.

This chapter looks at the reactivity of the previously synthesised cerium(III)- and cerium(IV)-NHC complexes $[Ce(L^{iPr})_3]$ and $[Ce(L^{iPr})_4]$,[16] **figure 4.1**, with acidic C-H and N-H bonds and their use as catalysts for organic transformations.

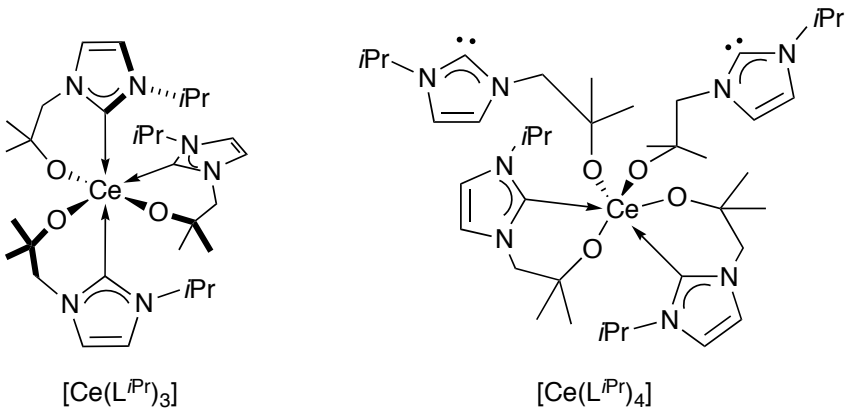

Figure 4.1. Structure of $[Ce(L^{iPr})_3]$ and $[Ce(L^{iPr})_4]$.[16]

Based on ^{1}H NMR spectroscopic evidence, $[Ce(L^{iPr})_3]$ is predicted to have C_{3v} symmetry in solution at room temperature on the NMR timescale with the three ligands bound bidentate. X-ray diffraction data shows that $[Ce(L^{iPr})_4]$ has two ligands bound bidentate through both anionic oxygen and carbene donors and two pendant ligand bound through the anionic oxygen donors only. There is a fluxional process between the free and bound carbenes which can be inhibited by the addition of two equivalents of 9-BBN, **equation 4.1**.[16]

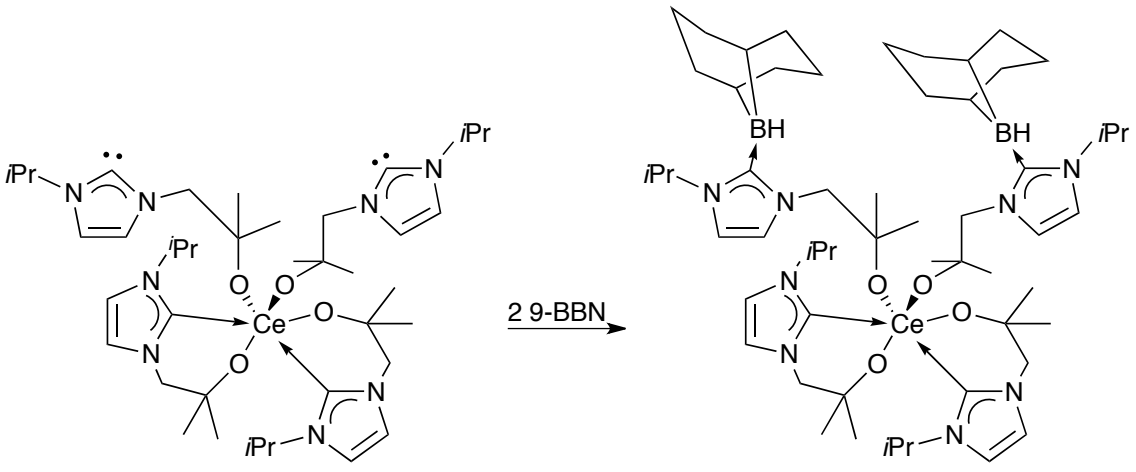

(4.1)

The reactivity of $[Fe(L^{Mes})_2]$, **3**, as a hydrogenation and hydroboration catalyst was also investigated. This work was carried out in collaboration with Alistair MacNair of Dr Stephen P. Thomas' group. These contributions are numbered separately.

4.2 Reactivity of $[Ce(L^{iPr})_3]$ with acidic C-H bonds

4.2.1 Alkynes

A series of reactions between $[Ce(L^{iPr})_3]$ and a number of terminal alkynes RC≡CH (R = Me_3Si, Ph, *t*Bu) was carried out with a 1:1 and 1:3 $[Ce(L^{iPr})_3]$:alkyne ratio, **scheme 4.7**. The alkynes have pK_as in the range of 25-29, with the exact value for R = Ph of 28.8 in DMSO.[17]

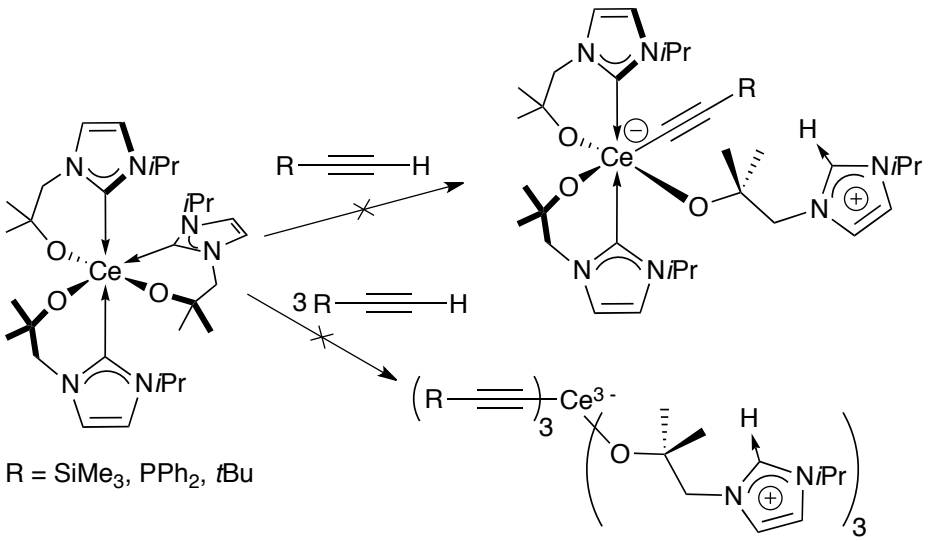

Scheme 4.7. Reactivity of $[Ce(L^{iPr})_3]$ with RC≡CH, R = $SiMe_3$, Ph, *t*Bu.

Each of the reactions was carried out in THF and in benzene and at both room temperature and reflux. However, under all conditions no reaction occurred with each ^{1}H NMR spectrum showing only unreacted $[Ce(L^{iPr})_3]$ and alkyne.

4.2.2 Diphenylacetone

The ketone 1,1-diphenylacetone has been previously shown to undergo C-H bond activation by **CLXXIV** to give $[(Cp)_2Y(HL^{iPr})(OC(Me)CC(Ph)_2)]$ **CLXXXIV** when heated to 60°C for 1 h, **scheme 4.8**.[13] 1,1-Diphenylacetone has a pK_a of 19.4 and is able to bind to the yttrium centre in the enolate form once deprotonated.

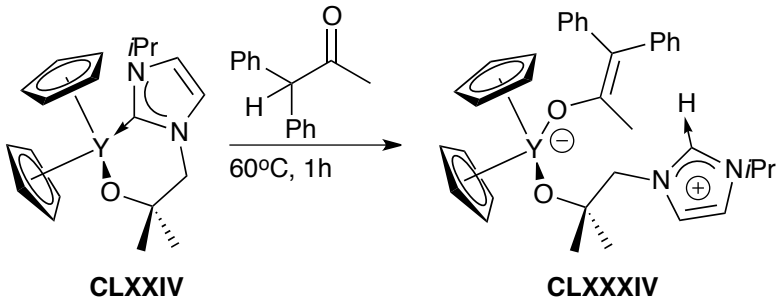

CLXXIV **CLXXXIV**

Scheme 4.8. Reaction of $[(Cp)_2Y(L^{iPr})]$ with 1,1-diphenylacetone.[13]

A single equivalent of 1,1-diphenylacetone was added to $[Ce(L^{iPr})_3]$; the reaction was carried out in THF and in benzene and at room temperature and reflux, **scheme 4.9**. However, analysis of the ^1H NMR spectrum showed only unreacted 1,1-diphenylacetone and $[Ce(L^{iPr})_3]$ irrespective of the reaction conditions. There was also no evidence of hydrogen bonding between an oxygen atom of a ligand and the substrate.

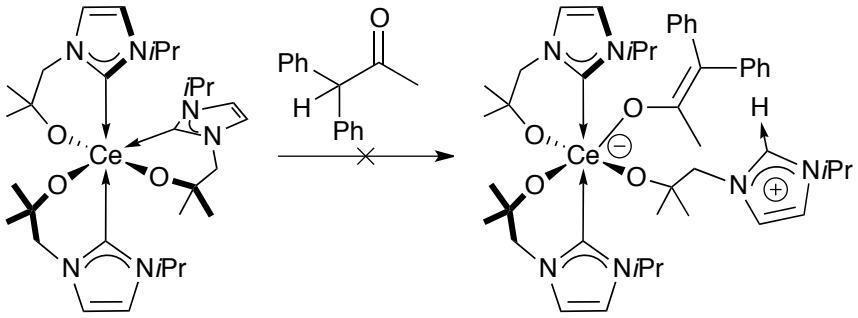

Scheme 4.9. Reaction of $[Ce(L^{iPr})_3]$ with 1,1-diphenylacetone.

4.2.3 Indene and Fluorene

The reactivity of $[Ce(L^{iPr})_3]$ with indene and fluorene was also investigated. Indene has a pK_a of 20.1 in DMSO[18] while fluorene has a pK_a of 22.6 in DMSO.[19]

Thus, a single equivalent of indene or fluorene was added to $[Ce(L^{iPr})_3]$ and the reaction carried out in both toluene and THF, **scheme 4.10**. However, analysis of the ^1H NMR spectrum showed only unreacted starting material. Heating the reaction at reflux for 16 h gave no reaction.

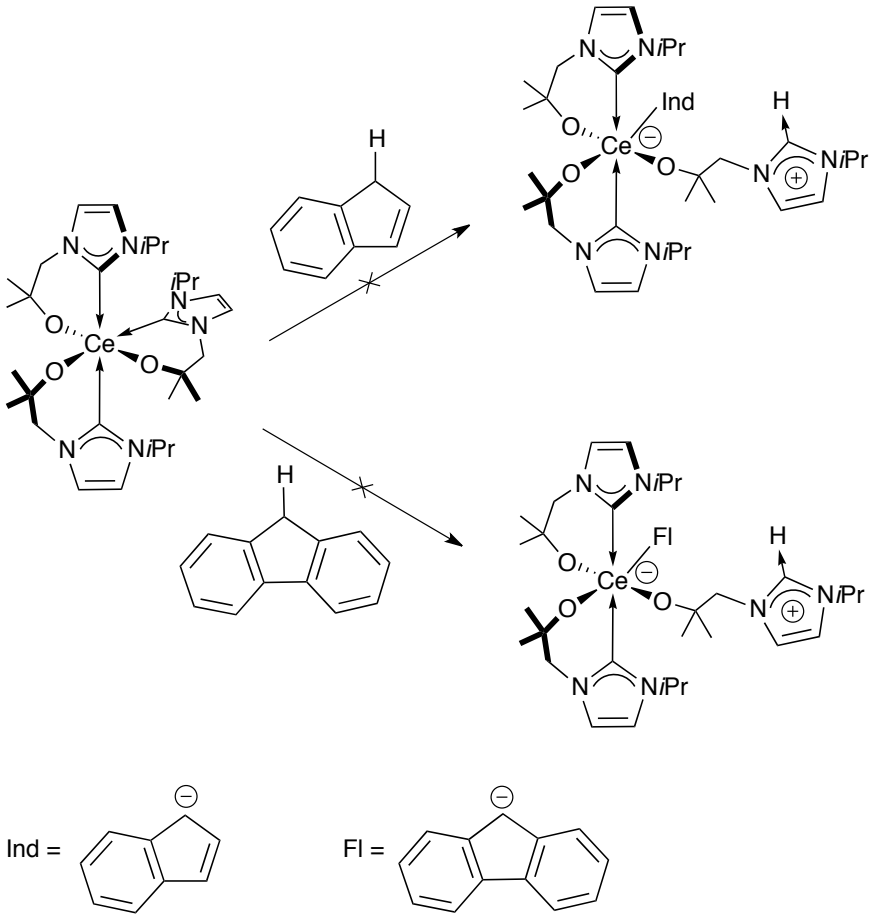

Scheme 4.10. Reactivity of $[Ce(L^{iPr})_3]$ with indene and fluorene.

The cerium(III)-NHC complex [Ce(L^{iPr})$_3$] displayed no C-H activation reactivity with terminal alkynes, 1,1-diphenylacetone or carbocycles. However, work carried out within the group has shown that heteroleptic complexes **CLXXIV** and **CLXXVII** do show C-H bond activation chemistry with these organic substrates.[13] It is proposed that the strongly electron donating O^- and NHC ligand set renders the cerium centre insufficiently Lewis acidic to activate the substrate for C-H cleavage.

4.3 Reactivity of [Ce(L^{iPr})$_3$] with acidic N-H bonds

4.3.1 Pyrrole

Pyrrole has an acidic N-H bond with a pK_a of 23.0[20] and the resulting anionic nitrogen is a good ligand for hard rare-earth metals. For exmple, Okuda and coworkers have shown that this N-H bond can be deprotonated by [Y(η^5:η^1-$C_5Me_4SiMe_2NCMe_3$)(CH_2SiMe_3)(THF)] **CLXXXV** to form [Y(η^5:η^1-$C_5Me_4SiMe_2NCMe_3$)(NC_4H_4)(DME)] **CLXXXVI** with the loss of $SiMe_4$, **scheme 4.11**.[21]

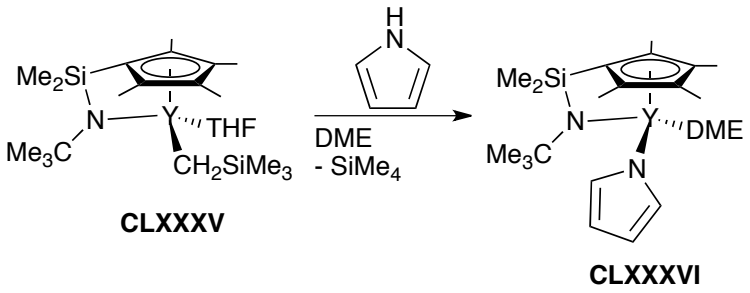

CLXXXV CLXXXVI

Scheme 4.11. Deprotonation of pyrrole by [Y(η^5:η^1-$C_5Me_4SiMe_2NCMe_3$)(CH_2SiMe_3)(THF)], **CLXXXV**.[21]

Thus, one equivalent of pyrrole was added to [Ce(L^{iPr})$_3$] in THF, **scheme 4.12**.

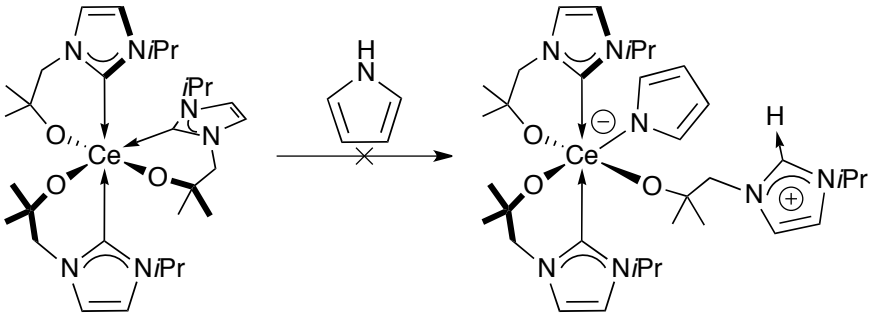

Scheme 4.12. Reactivity of $[Ce(L^{iPr})_3]$ with pyrrole.

The ^{1}H NMR spectrum showed $[Ce(L^{iPr})_3]$ and unreacted pyrrole. There was no evidence of a hydrogen bond between the pyrrole N-H and the oxygen tether of a ligand as seen for the analogous reaction between $[Sc(L^{iPr})_3]$ and pyrrole, **scheme 4.13**.[13]

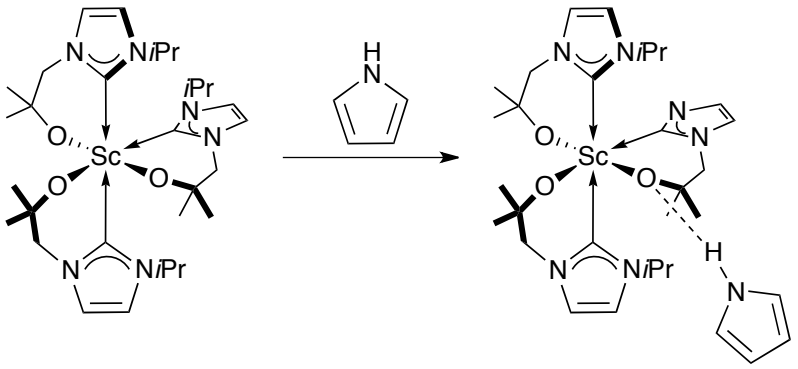

Scheme 4.13. Reactivity of $[Sc(L^{iPr})_3]$ with pyrrole.[13]

The reaction was repeated in toluene but no reaction occurred. Heating the reaction mixture to reflux (in THF or toluene) or using three equivalents of pyrrole had no effect on the reaction.

4.3.2 Indole

Indole has an acidic N-H bond with a pK_a value of 21.0[20] and like pyrrole the anionic nitrogen resulting from the removal of this proton is an excellent ligand for hard rare-earth centres. Wang and coworkers have shown that treatment of $[M(CH_2SiMe_3)_3(THF)_2]$ (M = Y, Dy, Yb) with one equivalent of the substituted indole 3-(tBuN=CH)C_8H_5NH gives the dimeric product *trans*-[(μ-η^2:η^1:η^1-3-{tBuCH(CH_2SiMe_3)}Ind)M(THF)(CH_2SiMe_3)]$_2$ (Ind = indolyl) **CLXXXVII**, **scheme 4.14**. Here, the amine has been deprotonated and an alkyl CH_2SiMe_3 group inserts into the imido functionality to give an amido functional group which bridges to a second metal centre.[22]

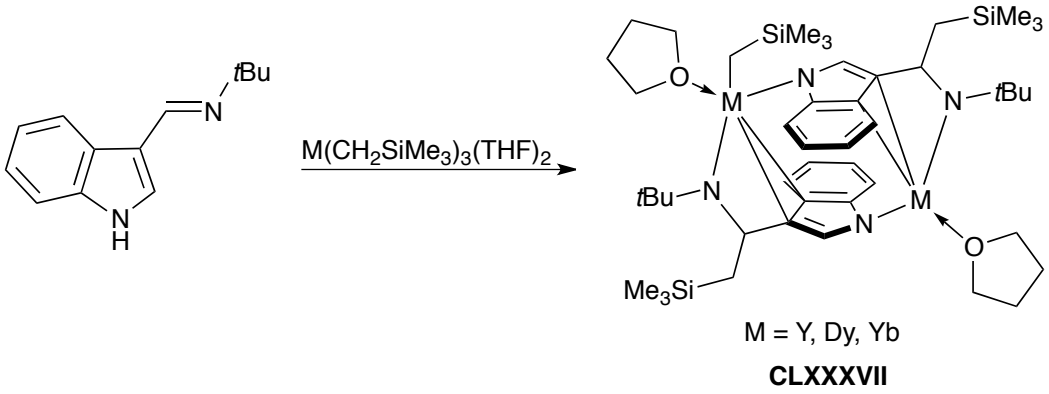

Scheme 4.14. Reactivity of $[M(CH_2SiMe_3)_3(THF)_2]$ (M = Y, Dy, Yb) with 3-(tBu N=CH)C_8H_5NH.[22]

The yttrium and dysprosium complexes showed high catalytic activity and high regio- and stereoselectivity for isoprene 1,4-*cis*-polymerisation.[22]

Addition of one equivalent of indole to $[Ce(L^{iPr})_3]$ showed no reactivity across the metal-NHC bond, **scheme 4.15**.

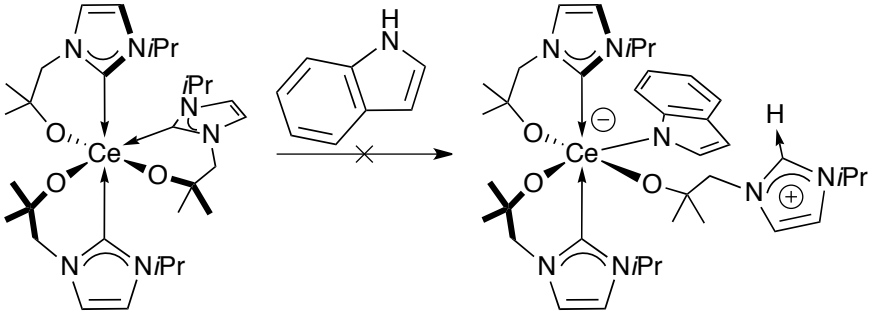

Scheme 4.15. Reactivity of $[Ce(L^{iPr})_3]$ with indole.

Attempts to drive the reaction to completion by changing the solvent from THF to toluene, heating the reaction to reflux or extending the reaction time lead to the same result *i.e.* no reaction was observed.

Overall, $[Ce(L^{iPr})_3]$ showed no reactivity with the acidic N-H bond of pyrrole or indole. Previous work done within the group has shown that the heteroleptic cerium complex **CLXXVII** displayed no reactivity with pyrrole or indole while the yttrium analogue **CLXXIV** heterolytically cleaved the N-H bond, **scheme 4.3**.[13] It is proposed that the cerium centre is not Lewis acidic enough to heterolytically cleave the N-H bond across the Ce-$C_{carbene}$ bond.

4.4 Reactivity of $[Ce(L^{iPr})_3]$ with benzyl phenyl ether - a lignin model

Lignin is a complex, three dimensional amorphous polymer present in wood which is thought to derive from the polymerisation of three monomers: *p*-coumaryl, coniferyl and sinapyl alcohols, **figure 4.2**, which are bound together through ether linkages and carbon-carbon bonds.[23][24]

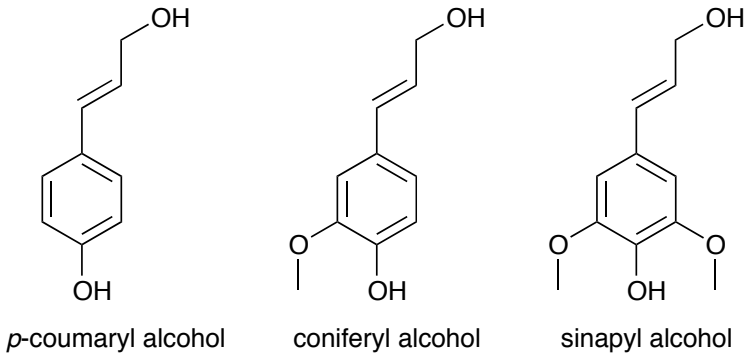

Figure 4.2. Monomeric units of lignin.

Noble metals have been shown to breakup the polymer into alkanes and alcohols.[25][26][27] In order to simplify the polymer's complexity, model compounds are often used one of which is benzyl phenyl ether which models the ether linkage on the polymer.[23] Thus, in an attempt to heterolytically cleave the ether linkage of benzyl phenyl ether, one equivalent was added to $[Ce(L^{iPr})_3]$ in THF, **scheme 4.16**.

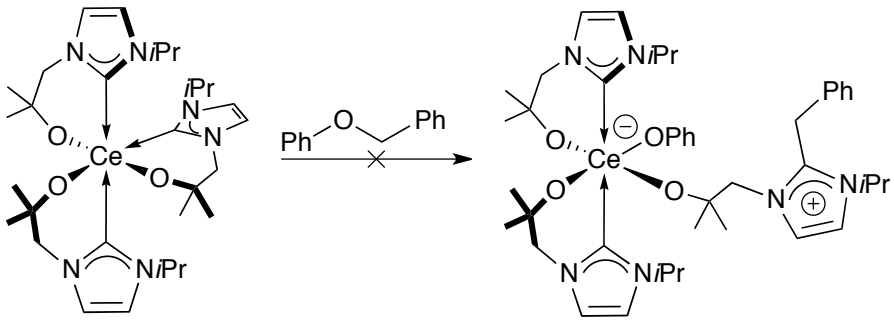

Scheme 4.16. Reactivity of $[Ce(L^{iPr})_3]$ with benzyl phenyl ether.

Analysis of the ^{1}H NMR spectrum showed no reaction had occurred. Heating the reaction to reflux for 16 h or carrying out the reaction on benzene (at room temperature or reflux) did not have any effect upon the reaction.

4.5 Reactivity of $[Ce(L^{iPr})_3]$ with benzoyl chloride

Reactions such as the benzoin condensation and Stetter reaction have aldehydes as substrates. In order to probe the reactivity of $[Ce(L^{iPr})_3]$, the more reactive benzoyl chloride was initially used and in excess to see if $[Ce(L^{iPr})_3]$ would catalyse the coupling of benzoylchloride with benzene which was also the solvent. 1,4-Diazabicyclo[2.2.2]octane (DABCO) was added in order to capture any HCl produced. However, when the reaction was carried out the acylazolium decomposition product $[BzOC(Me)_2CH_2(1\text{-}C(Bz)\{NCHCHN\}iPr)]Cl$ **18** ($Bz = C(=O)C_6H_5$) was isolated with $CeCl_3$ being formed as an insoluble precipitate, **scheme 4.17**

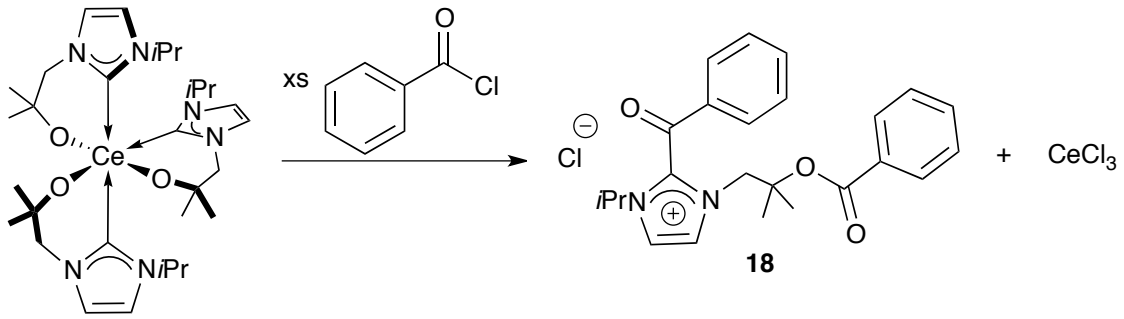

Scheme 4.17. Decomposition of $[Ce(L^{iPr})_3]$ to form $[(Bz)OC(Me)_2CH_2(Bz)\{CNCHCHN\}iPr]Cl$ **18** and $CeCl_3$.

In a possible mechanism, **scheme 4.18**, a molecule of benzoyl chloride coordinates to $[Ce(L^{iPr})_3]$ and then undergoes rearrangement to form $[Ce(L^{iPr})_2Cl]$ and the carbene $[(Bz)OC(Me)_2CH_2(1\text{-}C\{NCHCHN\}iPr)]$ **19**. This process repeats a further two times to form $CeCl_3$ and, overall, three equivalents of **19**. Each molecule of **19** reacts with benzoyl chloride to give **18**.

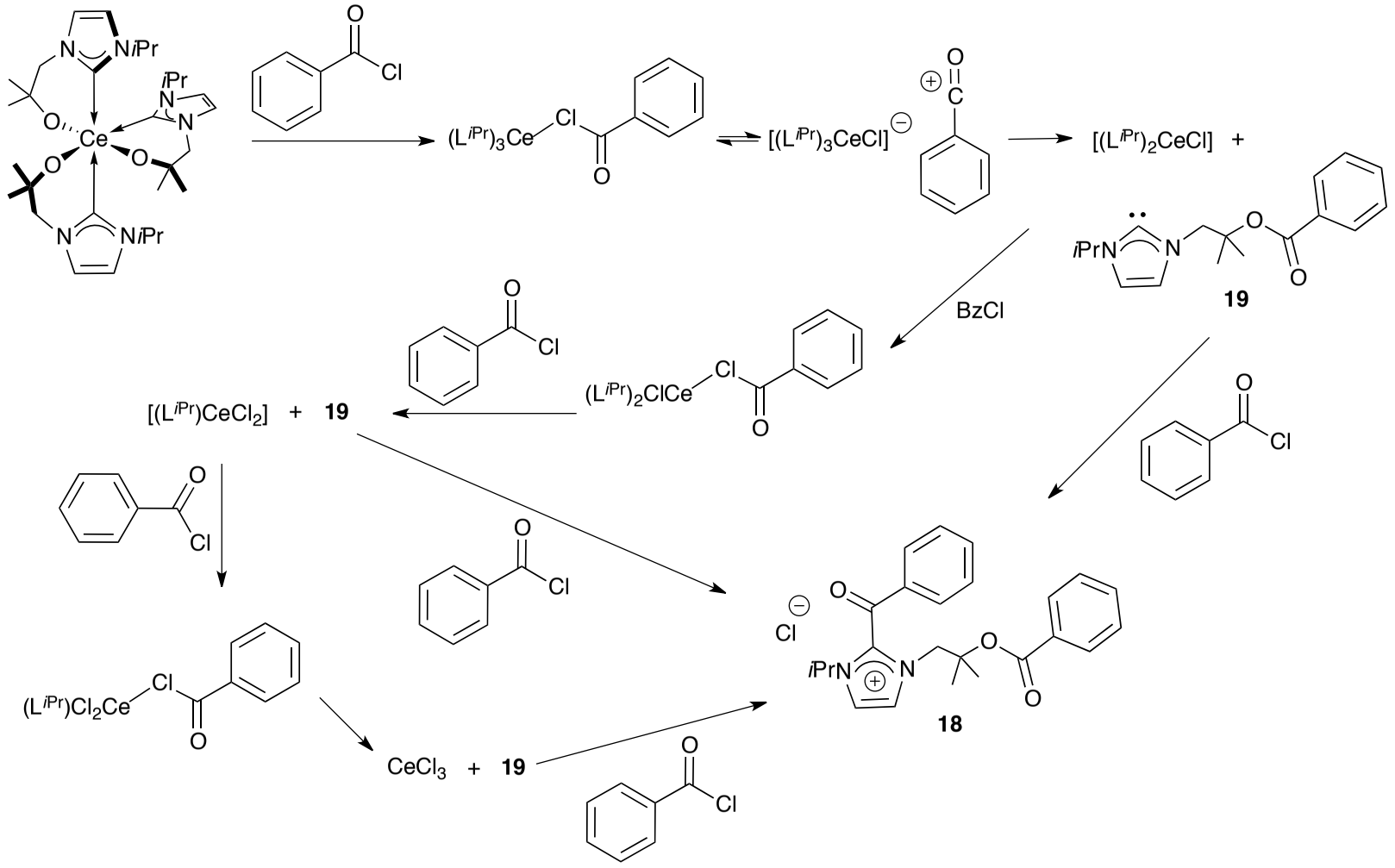

Scheme 4.18. Possible mechanism for the formation of **18**.

18 was isolated as a crystalline solid after it was isolated from the $CeCl_3$ by filtration, **figure 4.3**.

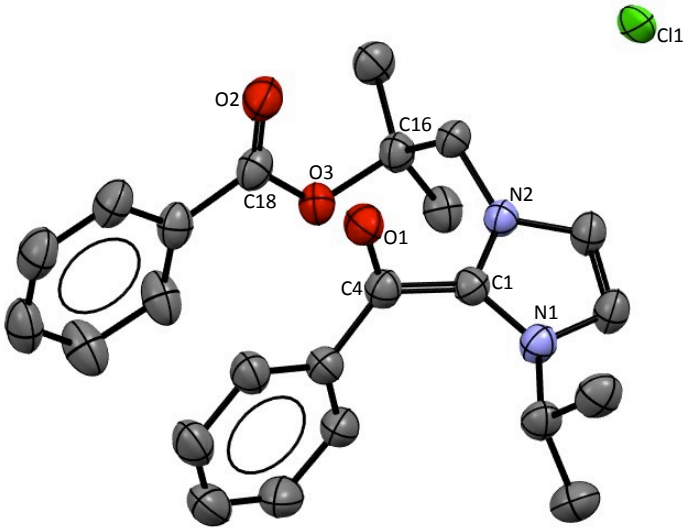

Figure 4.3. Solid state structure of **18**. For clarity, the hydrogen atoms are omitted. Displacement ellipsoids are shown at 50% probability.

Table 4.1: Selected bond lengths (Å) of **18**.

Bond		Bond	
C1-C4	1.499(4)	C1-N2	1.344(4)
C18-O3	1.348(3)	O1-C4	1.223(3)
C1-N1	1.341(3)	O2-C18	1.212(4)

The C1-C4 bond length, **table 4.1**, of 1.499(4) Å and the C18-O3 bond length is 1.348(3) Å. The ketone group has a C4-O1 bond length of 1.223(4) Å and the ester group has a C18-O2 bond length of 1.2121(4) Å and a C18-O3 bond length of 1.348(3) Å. The C1-N1 and C1-N2 bond lengths are similar at 1.341(2) and

1.344(4) Å, respectively.

The similar acylazoliums {N(Me)C(H)C(H)N(Me)C(C(O)R)}OTf (R = Ph **CLXXXVIII**,[28] $(CH_2)_2$Ph **CLXXXIX**,[28] C=CPh **CXC**,[29] OTf = $CF_3SO_3^-$) have been previously prepared by the reaction of the lithium salt of *N*-methylimidazole, prepared *in situ*, and an ester. *N*-methylation using MeOTf allowed crystallisation to occur, **scheme 4.19**.

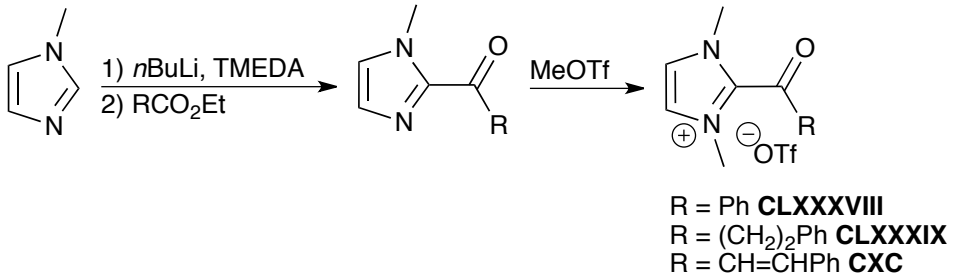

Scheme 4.19. Acylazolium molecules prepared by Studer and coworkers.[28][29]

In each structure the two N-$C_{carbene}$ bonds were of a similar length: 1.345(3) and 1.343(3) Å for **CLXXXVIII**; 1.349(3) and 1.346(3) Å for **CLXXXIX**; and 1.347 and 1.335 Å for **CXC**. These bond lengths are similar to the N1-C1 and N2-C2 bond lengths of 1.341(3) and 1.344(4) Å, respectively, of **18**. Furthermore, the $C_{carbene}$-$C_{carbonyl}$ bond lengths of 1.497(3), 1.496(3) and 1.485 Å for **CLXXXVIII**, **CLXXXIX** and **CXC**, respectively, are similar to the C1-C4 bond length of 1.499(4) Å for **18**.

However, the proligand salt [$HOCMe_2CH_2$(1-CH{NCHCHN*i*Pr})]I, [H_2L^{iPr}]I[30] **figure 4.4**, has two different N-$C_{carbene}$ distances of 1.352(6) and 1.402(6) Å both of which are longer than the N1-C1 and N2-C2 bond lengths of 1.341(3) and 1.344(4) Å, respectively, for **18**.

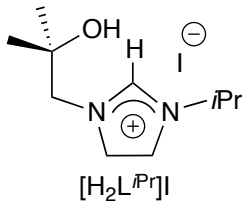

Figure 4.4. Structure of $[H_2L^{iPr}]I$.[30]

As a result of this complex decomposition, acyl chlorides were deemed too reactive and the reactivity with aldehydes was investigated instead.

More generally, Studer and coworkers[31] have shown that the Breslow intermediate resulting from the addition of an NHC to acetylenic[32][33][34][35] or olefinic[31][35][36] conjugated aldehydes are readily transformed into acylzolium cations thereby allowing solid state characterisation. The acylazolium cations can then undergo O-acylations with oxygen nucleophiles such as alcohols to give esters or conjugate addition with soft carbon nucleophiles, **scheme 4.20**.[37]

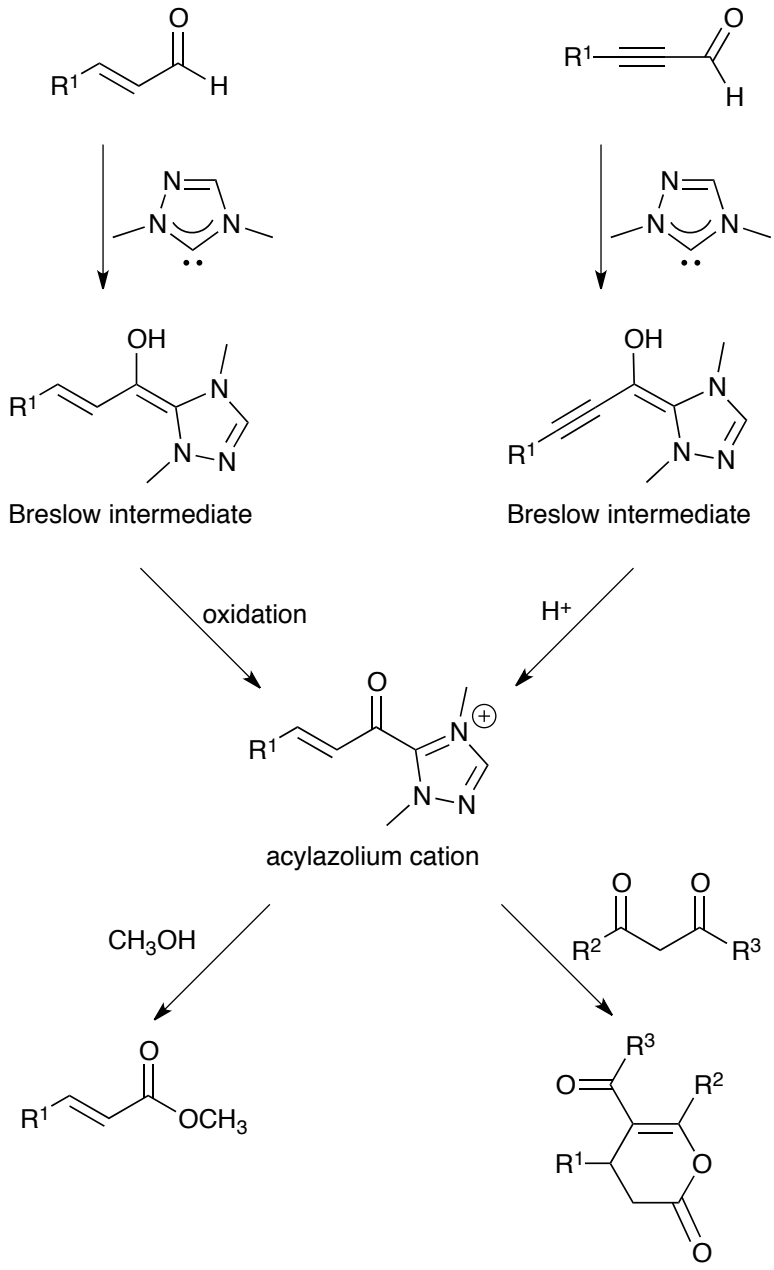

Scheme 4.20. Synthesis and reactivity of acylazolium cations.

4.6 $[Ce(L^{iPr})_4]$ as a catalyst for the benzoin condensation

In order to test the reactivity of $[Ce(L^{iPr})_4]$ to catalyse the benzoin condensation, an acetonitrile solution containing two equivalents of benzaldehyde was added to a solution of $[Ce(L^{iPr})_4]$ whereupon a precipitate immediately formed, **scheme 4.21**.

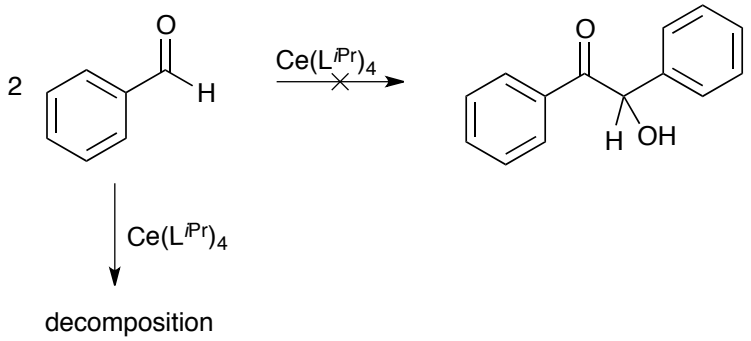

Scheme 4.21. Reactivity of $[Ce(L^{iPr})_4]$ with bezaldehyde.

The supernatant was isolated by filtration and analysed by ^{1}H NMR spectroscopy. This showed decomposition species were present and that the benzoin condensation had not occurred as there was no resonance due to the OH proton. Multiple septets were observed from 3 to 5 ppm, none of which corresponded to the ligands of $[Ce(L^{iPr})_4]$ or HL^{iPr}, indicating decomposition of the cerium complex into multiple products. The precipitate was insoluble even in hot pyridine and could not be analysed by ^{1}H NMR spectroscopy and is likely to be cerium-containing decomposition products.

4.7 Coupling benzyl chloride and benzaldehyde

Work carried out by Deng and coworkers has shown that NHCs and thiazoles can be used to mediate the coupling between aromatic benzyl halides and aldehydes to give three possible products: $Ar^1C(O)CH_2Ar^2$ **CXCI** (the main product), $Ar^1C(O)OCH_2Ar^2$ **CXCII** (resulting from exposure to air during the reaction) and $Ar^1C(O)CH(Ar^2)CH_2(Ar^2)$ **CXCIII** (a side product), **scheme 4.22**.[38]

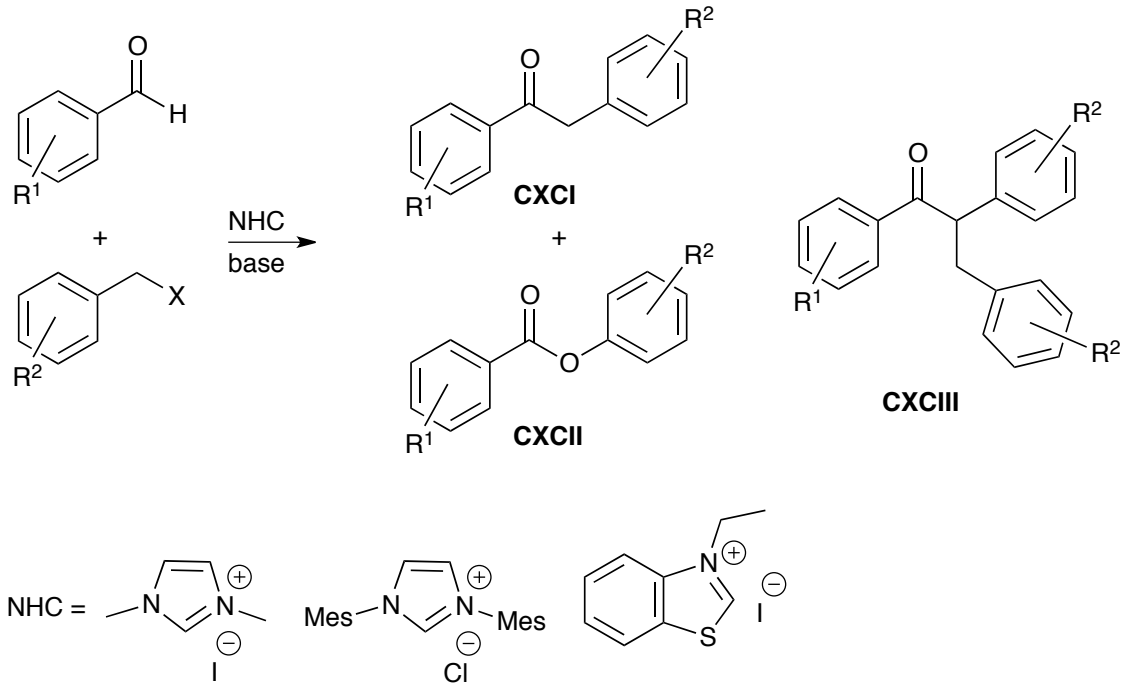

Scheme 4.22. NHC mediated coupling between benzyl chloride and benzaldehyde.

Here, the NHC was generated *in situ* by deprotonating the imidazoline with an appropriate base (triethylamine (TEA); 1,8-diazabicyclo[4.5.0]undec-7-ene (DBU); DABCO or 1,5-diazabicyclo[4.3.0]non-5-ene) (DBN).

4.7.1 Using $[Ce(L^{iPr})_3]$

To this end, one equivalent of $[Ce(L^{iPr})_3]$ was added to a solution of benzyl chloride and benzaldehyde in pyridine, which acted as both a solvent and base, **scheme 4.23**. A base was required as the HCl produced from the coupling reaction would react with $[Ce(L^{iPr})_3]$ causing decomposition. Upon addition of $[Ce(L^{iPr})_3]$ a colourless precipitate formed and was isolated by filtration. The precipitate was insoluble even in hot pyridine and consequently no ^1H NMR spectrum could be recorded. It is likely that this precipitate is a result of the the cerium-containing decomposition products. The ^1H NMR spectrum of the supernatant was diamagnetic and no sensible interpretation could be made: there were several multiplets in the aromatic region but no integrals corresponding to the diastereotopic CH_2 protons of the product. Additionally, the ^1H NMR spectrum of the supernatant showed only a small quantity of the organic starting materials indicting that they reacted with $[Ce(L^{iPr})_3]$ decomposing the complex instead of being activated for coupling.

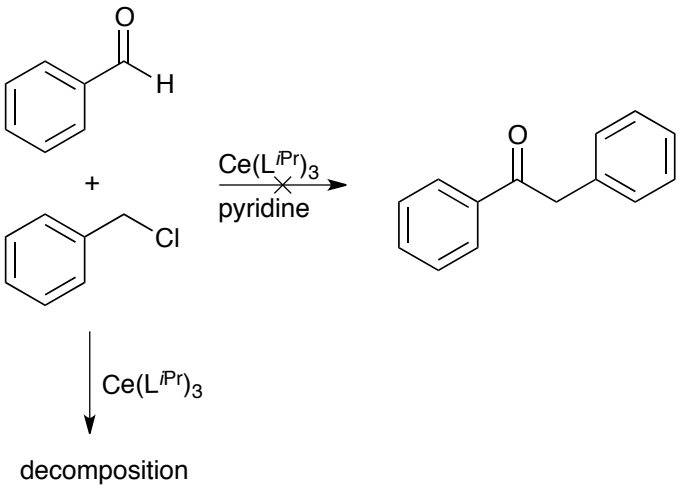

Scheme 4.23. Reactivity of $[Ce(L^{iPr})_3]$ in the coupling of benzaldehyde and benzyl chloride.

The use of DABCO or TEA in place of pyridine had no effect on the reactivity. Here, benzaldehyde, benzyl chloride and an equivalent of base were mixed in THF and one equivalent of $[Ce(L^{iPr})_3]$ added. Again, a precipitate of decomposed cerium material formed.

4.7.2 Using $[Ce(L^{iPr})_4]$

Similar reactivity was observed when $[Ce(L^{iPr})_4]$ was used to mediate the coupling reaction, **scheme 4.24**. Upon addition of $[Ce(L^{iPr})_4]$ to a pyridine solution of benzyl chloride and benzaldehyde a colourless precipitate formed which was insoluble even in refluxing pyridine. It is likely this precipitate is cerium decomposition products. The ^{1}H NMR spectrum of the supernatant showed multiple decomposition products which did not correspond to $[Ce(L^{iPr})_4]$ or HL^{iPr}.

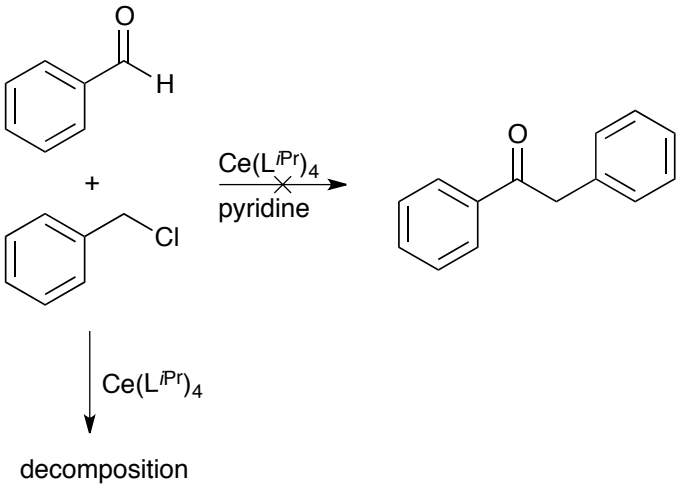

Scheme 4.24. Reactivity of $[Ce(L^{iPr})_4]$ in the coupling of benzaldehyde and benzyl chloride.

4.8 Catalytic hydrogenation and hydroboration of alkenes and carbonyls with $[Fe(L^{Mes})_2]$ 3

This work carried out in this section was done in collaboration with Dr Stephen P. Thomas and the practical work was carried out by Alistair MacNair.

Iron, being the fourth most abundant element in the earth's crust as well as its low cost, long-term availability,[39] low toxicity to humans and the environment, make it a viable alternative to high cost and often significantly toxic precious metal catalysts.[40]

4.8.1 Hydrogenation

Iron complexes have been shown to catalyse the hydrogenation of unsaturated organic molecules. For example, Milstein and coworkers have reported the iron(II) complex **CXCIV** which catalyses the reduction of ketones to alcohols. The reaction is carried out a room temperature with 0.05 mol% **CXCIV**, 0.1 mol% KO*t*Bu under 4.1 atm H_2 and accommodated a range of substrates with varying yields, **scheme 4.25**.[41]

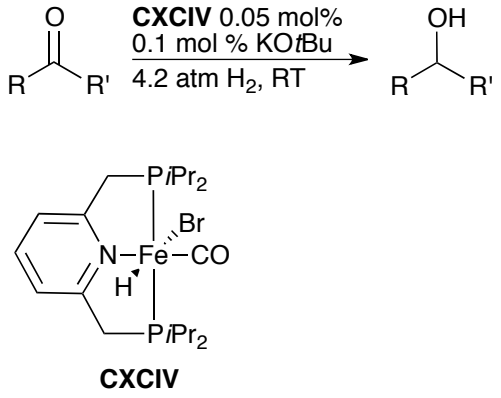

Scheme 4.25. Hydrogenation of ketones to alcohols using **CXCIV** as a catalyst as reported by Milstein and coworkers.[41]

Furthermore, Chirik and coworkers have reported a range of iron complexes which catalyse the hydrogenation of unfunctionalised and sterically hindered alkenes to the corresponding alkane under 4 atm H_2 and 5 mol% catalyst.[42]

Complex **3** shows no catalytic hydrogenation reactivity toward alkenes, aldehydes or ketones. Pressurising a mixture of $Ph(CH_2)_2CH{=}CH$ and 5 mol% **3** in THF with 50 bar H_2 for 18 h at room temperature did not result in the reduction of the alkene to the coresponding alkane, **scheme 4.26**.

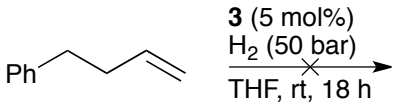

Scheme 4.26. Hydrogenation of alkenes with **3** as a catalyst.

Additionally, when benzaldehyde or PhC(=O)Me and 5 mol% **3** in THF were pressurised with 50 bar of H_2 and stirred for 18 h at room temperature no hydrogenation occurred, **scheme 4.27**.

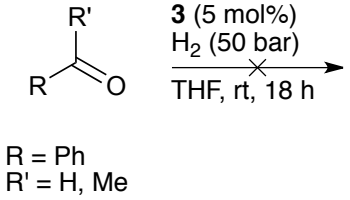

Scheme 4.27. Hydrogenation of a mixture of aldehydes or ketones with **3** as a catalyst.

4.8.2 Hydroboration

Hydroboration involves the addition of HBR_2 across unsaturated carbon-carbon double or triple bonds, carbon-oxygen or carbon-nitrogen double bonds. Hydroboration of C=C double or C≡C triple bonds gives two possible products: linear or branched, **scheme 4.28**.

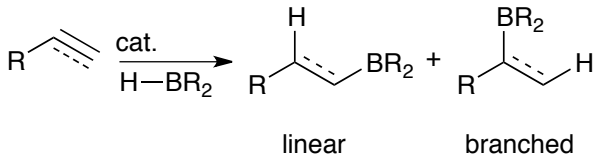

Scheme 4.28. General scheme for hydroboration of alkenes and alkynes.

The products of the hydroboration of alkenes and alkynes - alkyl boranes and allyl boranes, respectively - are important starting materials for the Suzuki cross-coupling reaction.[43][44][45]

While B_2H_6 readily adds to CC multiple bonds, the addition of more complicated boranes is often slow. For example, the addition of catecholborane to alkynes and alkenes requires 70 and 100°C, respectively, for 2-4 h,[46] and Männig and Nöth showed that addition of a rhodium catalyst ([RhCl(CO)(PPh_3)$_2$], [RhCl(CO)(AsPh_3)$_2$] or [RhCl(COD)$_2$]) allowed the reaction to proceed at room temperature.[47]

Männig and Nöth also showed that the regiochemistry of the hydroboration reaction may be controlled by the use of a catalyst.[47] When catecholborane was added to the unsaturated ketone **CXCV** in the absence of any catalyst, reduction of the carbonyl group occurred to give the boric ester **CXCVI**, **scheme 4.29**, while the presence of a rhodium catalyst resulted in the reduction of the alkene functionality to give the boronic ester **CXCVII**, **scheme 4.29**.

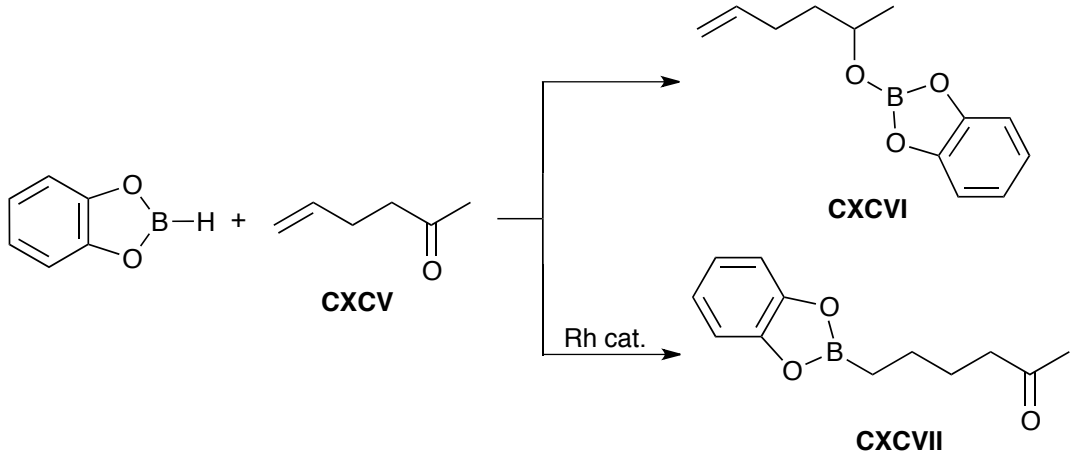

Scheme 4.29. Hydroboration of **CXCV** with catecholborane with and without Rh catalyst.[47]

Treatment of benzaldehyde or PhC(=O)Me with with one equivalent of pinacolborane (HBpin, HB{$(OCMe_2)_2$}) and 5 mol% **3** formed the corresponding linear product **A** in a quantitative yield when stirred in THF for 2 h, **scheme 4.30**.

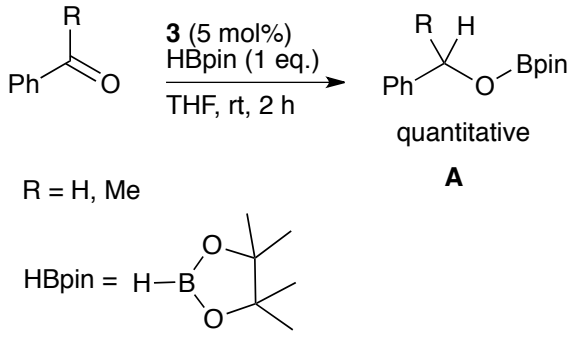

Scheme 4.30. Hydroboration of aldehydes and ketones using **3** as a catalyst.

Furthermore, the terminal alkenes 4-R-$C_6H_4(CH_2)_2CH{=}CH$ (R = *t*Bu **B**, H **C**) were treated with 1.5 equivalents of catecholborane and 5 mol% **3** and stirred for 2 h in THF at room temperature. Upon work-up with H_2O_2 and NaOH, the linear alcohol was isolated in a 60 % yield when R = *t*Bu **D** and a 75 - 80 % yield

when R = H **E**, **scheme 4.31**.

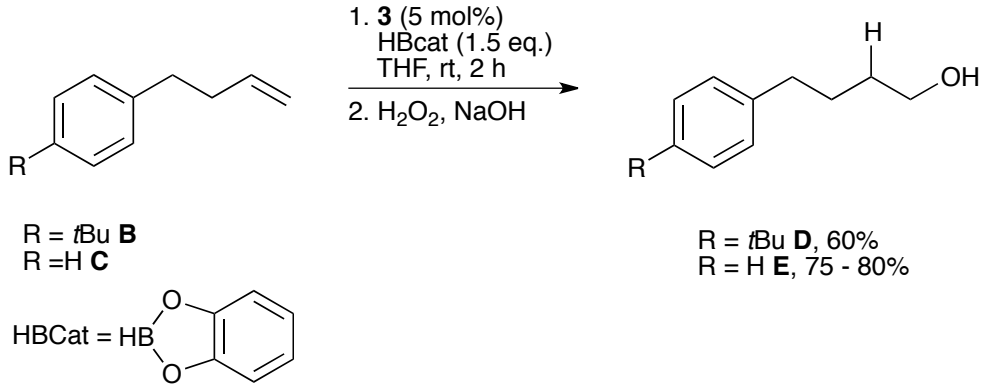

Scheme 4.31. Hydroboration of terminal alkenes using **3** as a catalyst.

4.9 Summary

In summary, $[Ce(L^{iPr})_3]$ showed no activation chemistry when exposed to acidic C-H or N-H bonds with pK_a's in the range of 19.4 to 28.8. Additionally, there was no evidence of hydrogen bonding between $[Ce(L^{iPr})_3]$ and the acidic C-H or N-H bonds. $[Ce(L^{iPr})_3]$ also showed no C-O activation chemistry when treated with benzyl phenol ether. This could be due to strong coordination of the NHC to the cerium centre or the cerium cation being insufficiently Lewis acidic. This is possibly due to the ligand set rendering the metal insufficiently Lewis acidic for C-H, N-H or C-O activation.

When an excess of benzoyl chloride was added to $[Ce(L^{iPr})_3]$ the acylazolium salt **18** forms from compound decomposition. When $[Ce(L^{iPr})_3]$ was used as a catalyst for the benzoin condensation or the coupling of benzyl chloride and benzaldehyde, the complex decomposed with no formation of the coupling products. $[Ce(L^{iPr})_4]$ also did not act as a catalyst for the benzoin condensation, instead it underwent decomposition.

While **3** showed no catalytic activity for the hydrogenation of alkenes, aldehydes and ketones it did display catalytic activity for the hydroboration of alkenes, aldehydes or ketones. In these cases the linear product was formed in yields of $>$ 60 %.

References

1. D. Enders, A. Grossmann, J. Fonert and G. Raabe, *Chem. Commun.*, 2010, **46**, 6282.

2. Y. Shimakawa, T. Morikawa and S. Sakaguchi, *Tetrahedron Lett.*, 2010, **51**, 1786.

3. Q. Liu, S. Perreault and T. Rovis, *J. Am. Chem. Soc.*, 2008, **130**, 14066.

4. D. A. DiRocco, K. M. Oberg, D. M. Dalton and T. Rovis, *J. Am. Chem. Soc.*, 2009, **131**, 10872.

5. G. A. Grasa, T. Güveli, R. Singh and S. P. Nolan, *J. Org. Chem.*, 2003, **68**, 2812.

6. R. Singh and S. P. Nolan, *Chem. Commun.*, 2005, 5456.

7. V. Nair, S. Bindu and V. Sreekumar, *Angew. Chem., Int. Ed.*, 2004, **43**, 5130.

8. T. Kano, K. Sasaki and K. Maruoka, *Org. Lett.*, 2005, **7**, 1347.

9. L. Candish and D. W. Lupton, *Chem. Sci.*, 2012, **3**, 380.

10. A. Grossmann and D. Enders, *Angew. Chem., Int. Ed.*, 2012, **51**, 314.

11. Z. R. Turner, R. Bellabarba, R. P. Tooze and P. L. Arnold, *J. Am. Chem. Soc.*, 2010, **132**, 4050.

12. P. L. Arnold, Z. R. Turner, R. Bellabarba and R. P. Tooze, *J. Am. Chem. Soc.*, 2011, **133**, 11744.

13. P. L. Arnold, T. Cadenbach, I. H. Marr, A. A. Fyfe, N. L. Bell, R. Bellabarba, R. P. Tooze and J. B. Love, *Dalton Trans.*, 2014, **43**, 14346.

14. A. I. Germeroth, Ph.D. thesis, University of Edinburgh, 2012.

15. B.-L. Lin, P. Kang and T. D. P. Stack, *Organometallics*, 2010, **29**, 3683.

16. I. J. Casely, S. T. Liddle, A. J. Blake, C. Wilson and P. L. Arnold, *Chem. Commun.*, 2007, 5037.

17. F. G. Bordwell, G. E. Drucker, N. H. Andersen and A. D. Denniston, *J. Am. Chem. Soc.*, 1986, **108**, 7310.

18. F. G. Bordwell and G. E. Drucker, *J. Org. Chem.*, 1980, **45**, 3325.

19. W. S. Matthews, J. E. Bares, J. E. Bartmess, F. G. Bordwell, F. J. Cornforth, G. E. Drucker, Z. Margolin, R. J. McCallum, G. J. McCollum and N. R. Vanier, *J. Am. Chem. Soc.*, 1975, **97**, 7006.

20. F. G. Bordwell, G. E. Drucker and H. E. Fried, *J. Org. Chem.*, 1981, **46**, 632.

21. S. Arndt, A. Trifonov, T. P. Spaniol, J. Okuda, M. Kitamura and T. Takahashi, *J. Organomet. Chem.*, 2002, **647**, 158.

22. G. Zhang, Y. Wei, L. Guo, X. Zhu, S. Wang, S. Zhou and X. Mu, *Chem. Eur. J.*, 2015, **21**, 2519.

23. J. Zakzeski, P. C. Bruijnincx, A. L. Jongerius and B. M. Weckhuysen, *Chem. Rev.*, 2010, **110**, 3552.

24. M. Stöcker, *Angew. Chem., Int. Ed.*, 2008, **47**, 9200.

25. N. Yan, C. Zhao, P. J. Dyson, C. Wang, L. Liu and Y. Kou, *ChemSusChem*, 2008, **1**, 626.

26. H. W. Park, J. K. Kim, U. G. Hong, Y. J. Lee, J. H. Song and I. K. Song, *Catal. Surv. Asia*, 2013, **17**, 119.

27. M. Kleinert and T. Barth, *Energy Fuels*, 2008, **22**, 1371.

28. R. C. Samanta, S. D. Sarker, R. Fröhlich, S. Grimme and A. Studer, *Chem. Sci.*, 2013, **4**, 2177.

29. R. C. Samanta, B. Maji, S. D. Sarker, K. Bergander, R. Fröhlich, C. Mück-Lichtenfeld, H. Mayr and A. Studer, *Angew. Chem., Int. Ed.*, 2012, **51**, 5234.

30. P. L. Arnold, I. J. Casely, Z. R. Turner and C. D. Carmichael, *Chem. Eur. J*, 2008, **14**, 10415

31. S. D. Sarker and A. Studer, *Angew. Chem., Int. Ed.*, 2010, **49**, 9266.

32. J. Kaeobamrung, J. Mahatthananchai, P. Zheng and J. W. Bode, *J. Am. Chem. Soc.*, 2010, **132**, 8810.

33. Z.-Q. Zhu, X.-L. Zheng, N.-F. Jiang, X. Wan and J.-C. Xiao, *Chem. Commun.*, 2011, **47**, 8670.

34. D. Du, Z. Hu, J. Jin, Y. Lu, W. Tang, B. Wang and T. Lu, *Org. Lett.*, 2012, **14**, 1274.

35. J. Mahatthananchai and J. W. Bode, *Chem. Sci.*, 2012, **3**, 192.

36. Z.-Q. Rong, M.-Q. Jia and S.-L. You, *Org. Lett.*, 2011, **13**, 4080.

37. L. R. Domingo, J. A. Sáez and M. Arnó, *Org. Biomol. Chem.*, 2014, **12**, 895.

38. L. Lin, Y. Li and W.-P. Deng, *Tetrahedron Lett.*, 2010, **51**, 3571.

39. S. Enther, K. Junge and M. Beller, *Angew. Chem., Int. Ed.*, 2008, **47**, 3317.

40. M. D. Greenhalgh, A. S. Jones and S. P. Thomas, *ChemCatChem*, 2015, **7**, 190.

41. R. Langer, G. Leitus, Y. Ben-David and D. Milstein, *Angew. Chem., Int. Ed.*, 2011, **50**, 2120.

42. R. P. Yu, J. M. Darmon, J. M. Hoyt, G. W. Margulieux, Z. R. Turner and P. J. Chirik, *ACS Catal.*, 2012, **2**, 1760.

43. N. Miyaura, K. Yamada and A. Suzuki, *Tetrahedron Lett.*, 1979, **20**, 3437.

44. N. Miyaura and A. Suzuki, *J. Chem. Soc., Chem. Commun.*, 1979, 866.

45. N. Miyaura and A. Suzuki, *Chem. Rev.*, 1995, **95**, 2457.

46. H. C. Brown and S. K. Gupta, *J. Am. Chem. Soc.*, 1971, **93**, 1816.

47. D. Männig and H. Nöth, *Angew. Chem., Int. Ed.*, 1985, **24**, 878.

Chapter 5

Conclusions

The heterobimetallic complexes **5** and **6** were prepared using the bidentate L^{Mes} ligand to bridge between the two metal centres. However, these complexes did not display cooperative reactivity. Instead, the reactivity of **5** with isocyanides or CO and **6** with phenols was identical to the reactivity of $[(\{Me_3Si\}_2N)_2U\{N(SiMe_3)Si(Me_2)CH_2\}]$ with isocyanides, CO and phenols. This highlights one of the significant problems with uranium chemistry, namely that uranium ions form strong bonds with hard, anionic ligands such as those formed in the activation of small and organic molecules.[1]

Further work to circumvent this reactivity should include replacing the ancillary $[N(SiMe_3)_2]$ ligands on the uranium ion to disfavour the formation of the monometallic complexes. This could also make **5** and **6** more thermally stable an therefore allowing a greater scope for reaction conditions as well as enable reaction with CO_2 - where the $[N(SiMe_3)_2]$ ligands react with CO_2[2] - to proceed without decomposition occurring.

In addition, the tris(3,5-dialkyl-2-phenoxy)-methane molecule HC(3-*t*Bu-5-Me-$C_6H_2O^-)_3$ was shown to be a useful ligand for supporting both *s*-/*d*-block and *d*-/*f*-block heterobimetallic complexes. However, preparation of *d*-/*f*-block heter-

obimetallic complexes from the *s*-/*d*-block heterobimetallic complex **14** was not possible, likely due to the highly stable structure of **14**. Instead, the *d*-/*f*-block heterobimetallic complex **16** was prepared by a deprotonation reaction between the monometallic complex **14** and $[(L^{Mes})_2Ce(N\{SiMe_3\}_2)]$. Further work should include structural characterisation of **16** and exploration of its reactivity towards C-H and small molecule activation.

The monometallic complex $[Ce(L^{iPr})_3]$ displayed no C-H or N-H activation reactivity. This could be due to the cerium centre being insufficiently Lewis acidic due to the coordinated alkoxide groups to cause C-H or N-H cleavage across the Ce-$C_{carbene}$ bond. Other work carried out within the Arnold group has shown that replacing one or two of the L^{iPr} ligands with a Cp ligand can induce C-H or N-H bond cleavage across the the Ce-$C_{carbene}$ bond.[3]

In addition, neither $[Ce(L^{iPr})_3]$ or $[Ce(L^{iPr})_4]$ displayed any reactivity for the catalysis of Stetter reaction, benzoin condensation or the coupling of benzyl chloride with benzaldehyde, instead decomposition resulted. This is likely a result of the formation of anionic intermediates which bind strongly to the cerium centre and the irreversible formation of new C-C and C-O bonds between the ligand and substrate. Such reactivity was demonstrated by the isolation of **18** from the reaction of $[Ce(L^{iPr})_3]$ with excess benzoyl chloride.

However, $[Fe(L^{Mes})_2]$ did catalyse the hydroboration of alkenes, aldehydes and ketones. Further work should look at isolating intermediates to determine if the H-B bond cleaves across the Fe-$C_{carbene}$ bond or if the H-B bond oxidatively adds across the iron centre.

References

1. A. R. Fox, S. C. Bart, K. Meyer and C. C. Cummins, *Nature*, 2008, **455**, 341.

2. P. L. Arnold, Z. R. Turner, A. I. Germeroth, I. J. Casely, G. S. Nichol, R. Bellabarba and R. P. Tooze, *Dalton Trans.*, 2013, **42**, 1333.

3. P. L. Arnold, T. Cadenbach, I. H. Marr, A. A. Fyfe, N. L. Bell, R. Bellabarba, R. P. Tooze and J. B. Love, *Dalton Trans.*, 2014, **43**, 14346.

Chapter 6

Experimental

6.1 General Methods and Instrumentation

All manipulations were carried out using standard Schlenk line or glovebox techniques under an atmosphere of dinitrogen. Pyridine, benzene and 1,4-dioxane were distilled from potassium under dinitrogen in a solvent still prior to use. Hexane, diethyl ether, CH_2Cl_2, toluene and THF were degassed by sparging with dinitrogen and dried by passing though a column of activated sieves in Vacuum Atmospheres solvent towers. Solvents were stored over activated 4 Å molecular sieves. Deuterated solvents (d^5-pyridine, d^8-THF, d^8-toluene and C_6D_6) were boiled over potassium, vacuum transferred and freeze-pump-thaw degassed three times prior to use.

HL^{Mes},[1] $[Fe(N\{SiMe_3\}_2)_2]$,[2] $[Co(N\{SiMe_3\}_2)_2(THF)]$,[3] $[(\{Me_3Si\}_2N)_2An\{N(SiMe_3)Si(Me_2)CH_2\}]$ (An = Th, U)[4] and $[Zn(L^{Mes})_2]$[5] were synthesised according to literature methods.

^1H NMR, $^{13}C\{^1H\}$ NMR and ^{29}Si NMR spectra were recorded on a Bruker AVA

400, AVA 500 or PRO 500 operating at 400 MHz, 400 MHz and 500 MHz, respectively. ^{1}H NMR and ^{13}C{^{1}H} NMR spectra were referenced internally to residual protio-solvent (^{1}H) or solvent (^{13}C) resonances and are reported to tetramethylsilane ($\delta = 0$ ppm). Chemical shifts are quoted in δ (ppm) and coupling constants in Hertz.

Elemental analyses were carried out by Mr. Stephen Boyer at the London Metropolitan University.

X-ray crystallographic data were collected at 170 K on an Oxford Diffraction Excalibur diffractometer using graphite monocromated Mo-Kα ($\lambda = 0.71073$ Å) radiation equipped with an Eos CCD detector or at 120 K on an Oxford Diffraction Supernova diffractometer using mirror chromated Cu-Kα radiation ($\lambda = 1.5418$ Å) and an Atlas CCD detector. Structures were solved using either SHEL-XS-97 direct methods, SHEL-XS-97 Patterson[6] methods or SIR-92 and refined using a full-matrix least square refinement on $|F|^2$ using SHEL-XS-97.[6] All programs were used within the WinGx suite.[7] All non-hydrogen atoms refined with anisotropic displacement parameters and parameters were constrained to parent atoms and refined using a riding model.

6.2 Experimental procedures described in chapter two

Attempted synthesis of $[(\{Me_3Si\}_2N)Ce(L^{Mes})_2{\cdot}CoI_2]$ 1

A solution of $[(\{Me_3Si\}_2N)Ce(L^{Mes})_2]$ (0.200 g, 2.44×10^{-4} mol) in THF (5 mL) was added to a suspension of CoI_2 (0.760 g, 2.44×10^{-4} mol) in THF (15 mL). The suspension was stirred at room temperature for 16 h after which time the

solution was decanted away from the precipitate into a Schlenk tube and the volatiles removed under reduced pressure. The resulting yellow solid was analysed by ^{1}H NMR spectroscopy and the spectrum showed resonances corresponding to [({Me_3Si}$_2$N)Ce(L^{Mes})$_2$].

Attempted synthesis of [(Cp)Y(L^{iPr})$_2$·Fe{N($SiMe_3$)}$_2$] 2

A solution of [Fe(N{$SiMe_3$}$_2$)$_2$] (0.190 g 5.03×10^{-4} mol) in toluene (5 mL) was added to a solution of [(Cp)Y(L^{iPr})$_2$] (0.260 g, 5.03×10^{-4} mol) in toluene (5 mL) and the brown solution stirred at room temperature for 16 h. The volatiles were removed under reduced pressure and the resulting solid analysed by ^{1}H NMR spectroscopy. The resonances were assigned to starting the materials.

Synthesis of [Fe(L^{Mes})$_2$] 3

A solution of HL^{Mes} (1.83 g, 7.04 mmol) in benzene (5 mL) was added to a solution of [Fe(N{$SiMe_3$}$_2$)$_2$] (1.32 g, 3.52 mmol) in benzene (5 mL). The resulting solution was stirred at room temperature for 16 h during which time a green precipitate formed. The precipitate was collected by filtration, washed with hexane (3×10 mL) and dried under reduced pressure to afford **3** as a green solid. Yield: 1.38 g (68%). Diffraction quality crystals were grown from a concentrated benzene solution at room temperature.

^{1}H NMR (C_6D_6, MHz): 26.80 ppm (br s, 6H, OC(CH_3)), 3.63 ppm (br s, 9H, *o*-CH_3 and *p*-CH_3), −24.08, −52.55, −75.13 (br s, 2H each, CH_2). Anal. Found (Calcd for $C_{32}H_{46}FeN_4O_2$): C, 66.81 (66.89), H, 7.96 (8.07), N, 9.88 (9.75).

Synthesis of $[Co(L^{Mes})_2]$ 4

A solution of HL^{Mes} (0.644 g, 2.55 mmol) in hexanes (5 mL) was added to a solution of $[Co(N\{SiMe_3\}_2)_2(THF)]$ (0.576 g, 1.28 mmol) in hexanes (10 mL). The resulting solution was stirred at room temperature for 16 h during which time a yellow precipitate formed. The precipitate was collected by filtration, washed with hexane (3 × 10 mL) and dried under reduced pressure to afford **4** as yellow solid. Yield: 0.632 g (85%).

Anal. Found (Calcd for $C_{32}H_{46}CoN_4O_2$): C, 66.36 (66.53), H, 8.03 (8.16), N, 9.70 (9.62).

Synthesis of $[(L^{Mes})Fe(\mu\text{-}L^{Mes})U(\mu\text{-}\{N(SiMe_3)Si(Me)_2CH_2\})(N\{SiMe_3\}_2)_2]$ 5

A solution of **3** (0.500 g, 8.67×10^{-4} mol) in benzene (5 mL) was added a solution of $[(\{Me_3Si\}N_2)_2U\{N(SiMe_3)Si(Me_2)CH_2\}]$ (0.662 g, 8.67×10^{-4} mol) in benzene (5 mL). The resulting solution was stirred at room temperature for 16 h during which time the solution became a brown\yellow colour. The volatiles were removed under reduced pressure to afford **5** as a brown solid. Yield: 0.891 g (76 %). Diffraction quality crystals were grown from a concentrated benzene solution at room temperature.

^{1}H NMR (C_6D_6): 91.57 (br s, 3H, CH_3), 78.73 (br s, 3H, CH_3), 52.08 (br s, 9H, SiCH_3), −18.34 (br s, 18H,N(Si{CH_3}$_3$)$_2$), −26.51 (br s, 18H, N(Si{CH_3}$_3$)$_2$), −62.55 (br s, 2H, CH_2), −75.28 (br s, 2H, CH_2), −87.57 (br s, 2H, CH_2).

^{29}Si NMR (C_6D_6): 1.96 (SiMe$_2$), −21.84 (N{SiMe$_3$}$_2$), −74.60 (SiMe$_3$), −81.96 (N{SiMe$_3$}$_2$). Anal. Found (Calcd for $C_{50}H_{99}UFeN_7O_2Si_6$): C, 46.68 (46.45), H, 7.65 (7.72), N, 7.81 (7.58).

Alternative synthesis of 5

A solution of **3** (0.240 g, 4.17×10^{-4} mol) in toluene (5 mL) was added to a solution of $[U(N\{SiMe_3\}_2)_3]$ (0.300 g, 4.17×10^{-4} mol) in toluene (5 mL). The solution stirred at room temperature for 16 h, during which time the solution became a yellow\brown colour. The volatiles were removed under reduced pressure to afford **5** as a brown solid. Yield: 0.261 g (51 %). Diffraction quality crystals were grown form a concentrated benzene solution at room temperature.

Synthesis of $[(\mathbf{L^{Mes}})Co(\mu\text{-}\mathbf{L^{Mes}})U(\mu\text{-}\{N(SiMe_3)Si(Me)_2CH_2\})(N\{SiMe_3\}_2)_2]$ 6

A solution of **4** (0.287 g, 4.97×10^{-4} mol) in THF (5 mL) was added to a solution of $[(\{Me_3Si\}N_2)_2U\{N(SiMe_3)Si(Me_2)CH_2\}]$ (0.357 g, 4.97×10^{-4} mol) in THF (5 mL). The solution was stirred at room temperature for 16 h during which time the solution turned a red\brown colour. The volatiles were removed under reduced pressure to afford **6** as a brown solid. Yield: 0.519 g (81%). Diffraction quality crystals were grown form a concentrated benzene solution at room temperature.

^{1}H NMR (C_6D_6): 96.41 (s, 2H, CH_2), 54.67 (s, 3H, CH_3), 50.58 (s 9H, Si(CH_3)$_3$), −0.27 (s, 18H, N(Si{CH_3}$_3$)$_2$), −4.39 (s, 3H, CH_3), −20.82 (s, 3H, CH_3), −29.35 (br s, 2H, CH_2), −39.70 (s, 18H, N(Si{CH_3}$_3$)$_2$).

^{29}Si NMR (C_6D_6): −21.86.

Anal. Found (Calcd for $C_{50}H_{99}UCoN_7O_2Si_6$): C, 46.23 (46.34), H, 7.61 (7.70), N, 7.39 (7.57).

Synthesis of $[(\{Me_3Si\}_2N)_2U\{N(SiMe_3)Si(Me_2)C(CH_2)N(2,6-Me-C_6H_3)\}]$ 8

A solution of **5** (52 mg, 4.19×10^{-5} mol) in benzene (5 mL) was added to a solution of 2,6-dimethyl isonitrile (5 mg, 4.19×10^{-5} mol) in benzene (3 mL) and the solution was stirred for 2 h during which time the solution turned dark green. The volatiles were removed under reduced pressure to afford a green solid. Diffraction quality crystals of **8** were grown from a concentrated THF solution at −30°C. Yield: 8 mg (36%).

^{1}H NMR (C_6D_6): 3.87 (s, 6H, $(CH_3)_2$), $-3,81$ (s, 9H, $Si(CH_3)_3$), −6.29 (br s, 36H, $2 \times N(Si\{CH_3\}_2)_2$).

General method for 5 + azides

A solution of RN_3 (R = Ph_3Si, Ad, TMS) (7.74×10^{-5} mol) in toluene (5 mL) was added to a solution of **5** (100 mg, 7.74×10^{-5} mol) in toluene (5 mL). The solution was stirred at room temperature for 16 h then the volatiles removed under reduced pressure. The resulting solid was analysed by ^{1}H NMR spectroscopy and, under each set of conditions, the resonances assigned to the starting materials.

A solution of azide RN_3 (R = Ph_3Si, Na) (7.74×10^{-5} mol) in toluene (5 mL) was added to a solution of **5** (100 mg, 7.74×10^{-5} mol) in toluene (5 mL) and irradiated by UV radiation for 4 h. The volatiles was removed under reduced pressure and the resulting solid was analysed by ^{1}H NMR spectroscopy and, under each set of conditions, the resonances assigned to the starting materials

General method for 5 + boranes

A solution of BR_3 (R = Ph, C_6H_5) or IBBN (7.74×10^{-5} mol) in toluene (5 mL) was added to a solution of **5** (100 mg, 7.74×10^{-5} mol) in toluene (5 mL). The solution was stirred for 16 h then the volatiles removed under reduced pressure. The resulting solid was analysed by ^{1}H NMR spectroscopy and, in each case, the resonances assigned to the starting materials.

5 + *m*CPBA

A solution of *m*CPBA (7 mg, 4.03×10^{-5} mol) in toluene (3 mL) was added to a solution of **5** (50 mg, 4.03×10^{-5} mol) in toluene (5 mL) and stirred at room temperatrue for 16 h. The volatiles were removed under reduced pressure and the resulting solid analysed by ^{1}H NMR spectroscopy - the resonances corresponded to the starting materials. The reaction mixture was heated to 40°C and subsequent analysis by ^{1}H NMR spectroscopy showed decomposition of **5** occurred.

5 + KC_8

A solution of **5** (50 mg, 4.03×10^{-5} mol) in THF (5 mL) was added to a suspension of KC_8 (5 mg, 4.03×10^{-5} mol) in THF (3 mL) and the reaction mixture was stirred at room temperature for 16 h during which time a grey precipitate of graphite formed. The solution was decanted away from the graphite precipitate into a Schlenk tube and the volatiles were removed under reduced pressure. Analysis by ^{1}H NMR spectroscopy showed decomposition of **5**.

5 + CO_2

In a Youngs tap NMR tube, a C_6D_6 solution of **5** (23 mg, 1.78 × 10^{-5} mol) was degassed then pressurised with a 1 bar atmosphere of CO_2. The resulting dark brown solution was analysed by ^{1}H NMR spectroscopy and the resonances deemed to be decomposition.

5 + H_2

In a Youngs tap NMR tube, a C_6D_6 solution of **5** (18 mg, 1.40 × 10^{-5} mol) was degassed before being pressurised with a 1 bar atmosphere of H_2. The resulting dark brown solution was analysed by ^{1}H NMR spectroscopy and the resonances deemed to be decomposition.

Synthesis of CXLVI

In a Youngs tap NMR tube, C_6D_6 solutions of **6** (18 mg, 1.39 × 10^{-5} mol) and 2,6-di-*tert*-butylphenol (6 mg, 2.78 × 10^{-5} mol) were combined and mixed well. The solution turned pale yellow and was heated to 85 °C for $\frac{1}{2}$ h. The volatiles were removed under reduced pressure and slow cool recrystallisation from toluene (3 mL) at −30 °C afforded crystals of **CXLVI**. Yield: 11mg (43 %)

^{29}Si NMR (C_6D_6): 20.23, −132.16.

Synthesis of [(L^{Mes})Zn(μ-L^{Mes})Th(μ-{N(SiMe$_3$)Si(Me)$_2$CH$_2$})(N{SiMe$_3$}$_2$)$_2$] 9

In a Youngs tap NMR tube, C_6D_6 solutions of [Zn(L^{Mes})$_2$] (16 mg, 2.81 × 10^{-5} mol) and [({Me_3Si}N_2)$_2$Th{N(SiMe$_3$)Si(Me$_2$)CH$_2$}] (20 mg, 2.81 × 10^{-5} mol) were

combined and mixed well. Quantitative yield by ^{1}H NMR spectroscopy.

^{1}H NMR (C_6D_6): 6.94 (s, 2H, Ar *H*), 6.82 (s, 2H, Ar *H*), 4.31 (t, 1H, HC*H*, J = 5.1 Hz), 3.37 (t, 1H, HC*H*, J = 5.1 Hz), 3.12 (d, 1H, *gem* C*H*), 2.84 (m, 8H, backbone CH_2), 2.59 (d, 1H, *gem* C*H*), 2.13 (d, 2H, tether CH_2), 3.12 (d, 1H, *gem* C*H*), 2.03 (d, 2H, tether CH_2), 0.92 (s, 3H, *p*-CH_3), 0.80 (s, 6H, *o*-CH_3), 0.59 (s, 9H, Si(CH_3)$_3$), 0.54 (s, 6H, Si(CH_3)$_2$), 0.45 (s, 3H, *p*-CH_3), 0.39 (s, 36 H, N(Si{CH_3}$_3$)$_2$), 0.34 (s, 6H, *o*-CH_3).

3 + [({Me_3Si}$_2$N)$_2$U{N($SiMe_3$)$SiMe_2CH_2$BBN-H}]

In a Youngs tap NMR tube, C_6D_6 solutions of **3** (12 mg, 2.02×10^{-5} mol) and [({Me_3Si}$_2$N)$_2$U{N($SiMe_3$)$SiMe_2CH_2$BBN-H}] (17 mg, 2.02×10^{-5} mol) were combined and mixed well. The resulting dark green solution analysed by ^{1}H NMR spectroscopy and the resonances were assigned to starting materials.

Synthesis of 10

In a Youngs tap NMR tube, C_6D_6 solutions of **5** (containing a Na^+ impurity) (24 mg, 1.77×10^{-5} mol) and 2,6-di-*tert*-butylphenol (11 mg, 5.30×10^{-5} mol) were combined and mixed well. Diffraction quality crystals were grown from this concentrated C_6D_6 solution at room temperature.

6.3 Experimental procedures described in chapter three

Synthesis of [HC(3-*t*Bu-5-Me-C_6H_2OH)(3-*t*Bu-5-Me-C_6H_2O)μ-(3-*t*Bu-5-Me-C_6H_2O)Co(THF)]$_2$ 11

A solution of HC(3-*t*Bu-5-Me-$C_6H_2OH)_3$ (0.208g, 4.14×10^{-4} mol) in toluene (5 mL) was added to a solution of [Co(N{$SiMe_3$}$_2$)$_2$(THF)] (0.187 g, 4.14×10^{-4} mol) in toluene (5 mL). The solution was stirred at room temperature for 2 h during which time a brown precipitate formed. The precipitate was isolated by filtration, washed with hexane (3×10 mL) and dried under reduced pressure to afford **11** as a pink\brown solid. Yield: 0.209 g (80 %). Diffraction quality crystals were grown from a toluene solution via slow cooling of a hot solution to room temperature overnight.

^{1}H NMR (d^8-THF): 52.13 (s, 3H, CH_3), 46.36 (s, 3H, CH_3), 39.92 (s, 3H, CH_3), 3.61 (coord. THF), 1.76 (ccord. THF), −0.88 (s, 9H C(CH_3)), −7.62 (s, 9H C(CH_3)), −70.52 (s, 9H C(CH_3)), 69.25, 52.13, 45.14, 39.30, 23.08, 14.88, 14.14, −5.53 (br s, 1H each, ArCH and ArOH). Anal. Found (Calcd for $C_{76}H_{88}Co_2O_6$): C, 72.86 (72.97), H, 7.86 (7.92), N, 0.00 (0.00)

Synthesis of [HC(3-*t*Bu-5-Me-C_6H_2OH)(3-*t*Bu-5-Me-C_6H_2O)μ-(3-*t*Bu-5-Me-C_6H_2O)Co(py-*N*O)]$_2$ 12

A solution pyridine *N*-oxide (18 mg, 1.91×10^{-4} mol) in THF (5 mL) was added to a solution of **11** (121 mg, 9.58×10^{-5} mol) in THF (3 mL). The solution was stirred at room temperature for 2 h during which time a green precipitate formed. The precipitate was isolated by filtration, washed with hexane (3×10 mL) and

dried under reduced pressure to afford **12** as a green solid. Yield: 104 mg (83%). Diffraction quality crystals were grown from THF solution via slow cooling of a hot solution to room temperature overnight.

^{1}H NMR (d^8-THF): 43.72, 42.82 (s, 2H each, pyridinium *alpha*- and *beta*-C*H*'s), 38.81 (s, 3H, CH_3), 20.84 (br s, 9H, C(CH_3)), 0.41 (s, 9H, CH_3), −4.57 (s, 9H, CH_3), −61.49 (s, 9H, CH_3), 59.24, 45.16, 37.22, 26.11, 17.44, 15.63, 12.55, −16.22 (s, 1H each, ArC*H*, pyC*H* and O*H*). Anal. Found (Calcd for $C_{78}H_{98}Co_2N_2O_8$): C, 71.54 (71.38), H, 7.54 (7.62), N, 2.14 (2.24)

Synthesis of [HC(3-*t*Bu-5-Me-C_6H_2OH)(3-*t*Bu-5-Me-C_6H_2O)μ-(3-*t*Bu-5-Me-C_6H_2O)Zn(THF)$_n$]$_2$ 13

A solution of [Zn(N{SiMe$_3$}$_2$)$_2$] (0.990 g, 2.56 mmol) in toluene (5 mL) was added to a solution of HC(3-*t*Bu-5-Me-C_6H_2OH)$_3$ (1.289 g, 2.56 mmol) in toluene (5 mL). The solution was stirred at room temperatrue for 4 h during which time a colourless precipitate formed. The precipitate was isolated by filtration, washed with hexane (3 × 10 mL) and dried under reduced pressure to afford **13** as a colourless solid. Yield: 2.08 g (71%).

^{1}H NMR (d^8-THF): 6.91 (s, 1H, phenol C*H*), 6.82 (s, 2H, aryloxide C*H*), 6.78 (s, 2H, aryloxide C*H*), 6.67 (s, 1H, phenol C*H*), 6.03 (s, 1H, C*H*), 5.37 (s, 1H, O*H*), 2.09 (s, 9H, *p*-CH_3), 1.42 (s, 18H, aryloxide *t*Bu), 1.28 (s, 9H, phenol *t*Bu),

Synthesis of [HC(3-*t*Bu-5-Me-C_6H_2O)$_2$-μ-(3-*t*Bu-5-Me-C_6H_2O)KCo]$_2$ 14

A solution of [KN(SiMe$_3$)$_2$] (33 mg, 1.66 × 10^{-4} mol) in toluene (5 mL) was added to a suspension of **11** (105 mg, 8.31 × 10^{-5} mol) in toluene (10 mL). The reaction mixture was stirred at room temperature for 16 h during which time a blue

precipitate formed. The precipitate was isolated by filtration, washed with hexane (3 × 10 mL) and dried under reduced pressure to afford **14** as a purple solid. Yield: 95 mg (92 %). Diffraction quality crystals were grown from a concentrated benzene solution at room temperature.

^{1}H NMR (C_6D_6): 58.40 (two overlapping resonances, 2H, 2 × C*H*), 50.56 (br s, 1H, C*H*), 48.28 (s, 1H, C*H*), 46.09 (s, 3H, CH_3), 25.04 (br s, 1H, C*H*), 23.03 (s, 1H, C*H*), −1.81 (br s, 9H, *t*Bu), −4.09 (s, 3H, CH_3), −7.16 (s, 3H, CH_3), −14.49 (br s, 9H, *t*Bu), −50.31 (br s, 9H, *t*Bu). Anal. Found (Calcd for $C_{68}H_{86}Co_2O_6K_2$): C, 68.18 (68.32), H, 7.18 (7.25), N, 0.00 (0.00)

Synthesis of [HC(3-*t*Bu-5-Me-C_6H_2O)$_2$-μ-(3-*t*Bu-5-Me-C_6H_2O)KZn]$_2$ 15

A solution of [KN($SiMe_3$)$_2$] (38 mg, 1.93 × 10^{-4} mol) in toluene (5 mL) was added to a suspension of **13** (109 g, 9.63 × 10^{-5} mol) in toluene (10 mL). The reaction mixture was stirred at room temperature for 16 h during which time a colourless precipitate formed. The precipitate was isolated by filtration, washed with hexane (3 × 10 mL) and dried under reduced pressure to afford **15** as a colourless solid. Yield: 59 mg (54 %). Diffraction quality crystals were grown from a concentrated THF solution at room temperature.

^{1}H NMR (d^8-THF): aromatic protons 6.56 (s, 1H, C*H*), 1.34 (s, 2H, CH_3), 1.32 (s, 2H, CH_3), 1.25 (s, 2H, CH_3), 0.10 (overlapping s, 27H, *t*Bu).

Anal. Found (Calcd for $C_{68}H_{86}Zn_2O_6K_2$): C, 66.19 (66.03), H, 7.17 (7.20), N, 0.00 (0.00)

Synthesis of [{HC(3-*t*Bu-5-Me-$C_6H_2O)_3$}CoCe(L^{Mes})$_2$]$_2$ 16

A solution of [($\{Me_3Si\}_2N)_2Ce(L^{Mes})_2$] (2.02 g, 2.50 × 10^{-4} mol) in THF (10 mL) was added to a solution of **11** (0.158 g, 1.25 × 10^{-4} mol) in THF (5 mL). The reaction mixture was stirred at room temperature for 8 h to afford a yellow solution. The volatiles were removed under reduced pressure, the resulting solid was washed with hexane (3 × 10 mL) and dried under reduced pressure to afford **16** as a yellow\brown solid. Yield: 94 mg (62 %).

^{1}H NMR (d^8-THF): 52.13 (s, 2H, CH_2), 48.11 (s, 2H, CH_2), 46.26 (s, 3H, CH_3), 35.40 (s, 3H, CH_3), 34.35 (s, 9H, *t*Bu), 30.62 (s, 2H, CH_2), 20.53 (s, 3H, CH_3), 10.05 (s, 2H, CH_2), 6.49 (s, 2H, CH_2), 4.31 (s, 6H, *o*-CH_3), 0.31 (s, 9H, *t*Bu), −3.97 (s, 3H, CH_3), −3.91 (s, 6H, *o*-CH_3), −8.66 (s, 9H, *t*Bu), −9.48 (s, 3H, CH_3), −43.78 (s, 3H, CH_3), −51.95 (s, 6H, *gem* CH_3), −59.57 (s, 3H, CH_3).

11 + [($\{Me_3Si\}_2N)_2U\{N(SiMe_3)Si(Me_2)CH_2\}$]

In a Youngs tap NMR tube, d^8-THF solutions of **11** (16 mg, 1.27 × 10^{-5} mol) and [($\{Me_3Si\}_2N)_2U\{N(SiMe_3)Si(Me_2)CH_2\}$] (18 mg, 1.56 × 10^{-5} mol) were combined and mixed well. ^{1}H NMR spectroscopic analysis showed resonances corresponding to starting materials. Heating the reaction mixture to 40°C resulted in decomposition.

11 + ceric ammonium nitrate

In a Youngs tab NMR tube, d^8-THF solutions of **11** (17 mg, 1.35 × 10^{-5} mol) and ceric ammonium nitrate (15 mg, 2.69 × 10^{-5} mol) were combined and mixed well. The solution turned purple immediately and analyses by ^{1}H NMR spectroscopy displayed resonances corresponded to HC(2,4-*t*Bu-$C_6H_2OH)_3$.

6.4 Experimental procedures described in chapter four

General procedure for the addition of alkynes (1 equivalent) to $[Ce(L^{Mes})_3]$

In a Youngs tap NMR tube, d^8-THF or C_6D_6 solutions of $[Ce(L^{Mes})_3]$ (20 mg, 2.92×10^{-5} mol) and (R = $SiMe_3$, Ph, *t*Bu) (2.92×10^{-5} mol) were combined and mixed well. The resulting yellow solution was heated to reflux for 16 h. The reaction was analysed by ^{1}H NMR spectroscopy and the resonances assigned to the starting materials.

General procedure for the addition of alkynes (3 equivalents) to $[Ce(L^{Mes})_3]$

In a Youngs tap NMR tube, d^8-THF or C_6D_6 solutions of $[Ce(L^{Mes})_3]$ (20 mg, 2.92×10^{-5} mol) and (R = $SiMe_3$, Ph, *t*Bu) (8.77×10^{-5} mol) were combined and mixed well. The resulting yellow solution was heated to reflux for 16 h. The reaction was analysed by ^{1}H NMR spectroscopy and the resonances assigned to the starting materials.

$[Ce(L^{Mes})_3]$ + diphenyl acetone

In a Youngs tap NMR tube, d^8-THF solutions of $[Ce(L^{Mes})_3]$ (18 mg, 2.63×10^{-5} mol) and diphenyl acetone (6 mg, 2.63×10^{-5} mol) were combined and mixed well. The reaction mixture was heated to reflux for 16 h and then analysed by ^{1}H NMR spectroscopy. The resonances of the ^{1}H NMR spectrum were assigned to starting material.

$[Ce(L^{Mes})_3]$ + benzyl phenol ether

In a Youngs tap NMR tube, d^8-THF solutions of $[Ce(L^{Mes})_3]$ (37 mg, 5.43×10^{-5} mol) and benzyl phenol ether (10 mg, 5.43×10^{-5} mol) were combined and mixed well. The yellow solution was heated to reflux for 16 h. The resonances of the ^{1}H NMR spectrum were assigned to starting material.

$[Ce(L^{Mes})_3]$ + indene

In a Youngs tap NMR tube, d^8-THF solutions of $[Ce(L^{Mes})_3]$ (17 mg, 2.49×10^{-5} mol) and indene (3 mg, 2.49×10^{-5} mol) were combined and mixed well. The reaction mixture was heated to reflux for 16 h and then analysed by ^{1}H NMR spectroscopy. The resonances of the ^{1}H NMR spectrum were assigned to starting material.

$[Ce(L^{Mes})_3]$ + fluorene

In a Youngs tap NMR tube, d^8-THF solution of $[Ce(L^{Mes})_3]$ (22 mg, 3.22×10^{-5} mol) and fluorene (5 mg, 3.22×10^{-5} mol) were combined and mixed well. The reaction mixture was heated to reflux for 16 h and then analysed by ^{1}H NMR spectroscopy. The resonances of the ^{1}H NMR spectrum were assigned to starting material.

$[Ce(L^{Mes})_3]$ + pyrrole

In a Youngs tap NMR tube, d^8-THF solutions of $[Ce(L^{Mes})_3]$ (50 mg, 1.46×10^{-5} mol) and pyrrole (5 mL, 1.46×10^{-5} mol) were combined and mixed well. The reaction mixture was heated to reflux for 16 h and then analysed by ^{1}H NMR

spectroscopy. The resonances of the ^{1}H NMR spectrum were assigned to starting material.

$[Ce(L^{Mes})_3]$ + indole

A solution of indole (17 mg, 1.46 $\times$ 10^{-4} mol) in THF (3 mL) was added to a solution of $[Ce(L^{Mes})_3]$ (100 mg, 1.46 $\times$ 10^{-4} mol) in THF (5 mL). The resulting solution was heated to 90°C for 8 h to afford an orange solution. The volatiles were removed under reduced pressure to afford a yellow solid which ^{1}H NMR spectroscopic analysis showed to be starting materials.

Synthesis of $[BzOC(Me)_2CH_2(1\text{-}C(Bz)\{NCHCHN\}iPr)]Cl$ 18

Solutions of benzoyl chloride (140 mg, 1.01 mmol) in benzene (5 mL) and DABCO (112 mg, 1.01 mmol) in benzene (5 mL) were added to a solution of $[Ce(L^{Mes})_3]$ (0.250 g, 3.66 $\times$ 10^{-4} mol) in benzene (5 mL). The resulting mixture was stirred at room temperature for 16 h during which time a colourless precipitate formed. The solution was decanted away from the precipitate and diffraction quality crystals of **18** were grown from a concentrated benzene solution at room temperature.

$[Ce(L^{Mes})_4]$ as a catalyst for the benzoin condensation

In a Youngs tap NMR tube, d^3-acetonitrile solutions of $[Ce(L^{Mes})_4]$ (14 mg, 1.44 $\times$ 10^{-5} mol) and benzaldehyde (6 μL, 2.89 $\times$ 10^{-5} mol) were combined and mixed well. After 4 h a colourless precipitate formed. The solution was decanted away from the precipitate and the supernatant analysed by ^{1}H NMR spectroscopy. The ^{1}H NMR spectrum showed decomposition had occurred.

[Ce(L^{Mes})$_3$] as a catalyst for coupling benzyl chloride and benzaldehyde

In a Youngs tap NMR tube, d^3-acetonitrile solutions of [Ce(L^{Mes})$_3$] (30 mg, 4.39 $\times$ 10^{-5} mol) and benzaldehyde (9 μL, 8.78 $\times$ 10^{-5} mol) were combined and mixed well. After 4 h a colourless precipitate formed. The solution was decanted away from the precipitate and the supernatant analysed by ^{1}H NMR spectroscopy. The ^{1}H NMR spectrum showed decomposition had occurred.

[Ce(L^{Mes})$_4$] as a catalyst for coupling benzyl chloride and benzaldehyde

In Youngs tap NMR tube, d^5-pyridine solutions of [Ce(L^{Mes})$_4$] (10 mg, 1.16 $\times$ 10^{-5} mol), benzaldehyde (1.18 μL, 1.16 $\times$ 10^{-5} mol) and benzyl chloride (1.3 μL, 1.16 $\times$ 10^{-5} mol) were combined and mixed well. After 4 h a colourless precipitate formed. The solution was decanted away from the precipitate and the supernatant analysed by ^{1}H NMR spectroscopy. The ^{1}H NMR spectrum showed decomposition had occurred.

6.4.1 Catalytic activity of 3 as a hydrogenation or hydroboration catalyst

The following experimental work was carried out by Alistair MacNair.

Catalytic reaction were carried out in a Radley's Carousel 12 position reactor or in glass inserts in an autoclave. The reactions were analysed by ^{1}H NMR spectroscopy and\or gas chromatography mass spectrometry (GCMS) by comparison with authentic samples. GCMS conditions: Injector temp.: 50°C for 2 min; ramps

20°C/min to 300°C; hold for 2 min.

General procedure for the catalytic hydrogenation of alkenes, aldehydes or ketones using 3

An alkene, aldehyde or ketone (1.00 mmol) was added to a solution of **3** (29 mg, 0.05 mmol) in THF. The reaction vessel was sealed, charged to 50 bar H_2 and stirred at 25°C. After 18 h the reaction mixture was allowed to cool to room temperature and the pressure released. The crude reaction mixture was filtered through celite and the solvent removed under reduced pressure. 1,3,5-Timethoxybenzene (17 mg, 0.10 mmol) was added as an internal standard, and the crude mixture was analysed by ^{1}H NMR spectroscopy and/or GCMS.

General procedure for the catalytic hydroboration of alkenes using 3

A solution of alkene (1.00 mmol) in THF was added to as solution of **3** (29 mg, 0.05 mmol). Catecholborane (0.180 g, 1.50 mmol) was added in one portion to the resulting mixture, THF (1 mL) was added ensuring that the sides of the reaction vessel were washed. After stirring at 25°C for 2 h the reaction mixture was cooled to 0°C and an aqueous solution of NaOH (1 M, 3 mL/H_2O_2 (30% wt in water, 2 mL)[8] was added and the resulting mixture stirred for 0.5 h, the organic layer was then extracted with diethyl ether (2 × 10 mL), washed with a saturated solution of NaCl (10 mL), dried over $MgSO_4$, and the solvent removed under reduced pressure. 1,3,5-Trimethoxybenzene (17 mg, 0.10 mmol) was added as an internal standard and the the crude product was analysed by ^{1}H NMR spectroscopy and\or GCMS.

General procedure for the catalytic hydroboration of aldehydes or ketones using 3

The aldehyde or ketone (1.00 mmol) was added to a solution of **3** (29 mg, 0.05 mmol) and 1,3,5-trimethoxybenzene (17 mg, 0.10 mmol, internal standard) in THF (1mL). Pinacolborane (0.192 g, 1.50 mmol) was added in one portion to the resulting mixture and THF (1 mL) was added ensuring that the sides of the reaction vessel were washed. After stirring at 25°C for 2 h and an aliquot (approx. 0.2 mL) was taken from the reaction vessel. The aliquot was filtered through celite, eluted with *d*-chloroform and analysed by ^{1}H NMR spectroscopy.

References

1. P. L. Arnold, I. J. Casely, Z. R. Turner and C. D. Carmichael, *Chem. Eur. J*, 2008, **14**, 10415.

2. R. A. Andersen, K. Faegri, J. C. Green, A. Haaland, M. F. Lappert, W.-P. Leung and K. Rypdal, *Inorg. Chem.*, 1988, **27**, 1782.

3. B. Cormary, F. Dumestre, N. Liakakos, K. Soulantica and B. Chaudret, *Dalton Trans.*, 2013, **42**, 12546.

4. A. Dormund, A. E. Bouadili, A. Aaliti and C. Moise, *J. Organomet. Chem.*, 1985, **288**, C1.

5. P. L. Arnold, I. J. Casely, Z. R. Turner, R. Bellabarba and R. P. Tooze, *Dalton Trans.*, 2009, 7236.

6. G. Sheldrick, *Acta. Crystallogr., Sect. A*, 2008, **64**, 112.

7. L. Farrugia, *J. Appl. Crystallogr.*, 1999, **32**, 837.

8. C. E. Grant and G. C. Fu, *J. Org. Chem.*, 1996, **61**, 3224.

Appendix 1

Table 1 CIF data for compounds **3 - 8**

Compound Reference	**3**	**5**[a]	**5**[b]	**6**	**8**
Chemical Formula	$C_{32}H_{46}FeN_4O_2$	$C_{50}H_{99}FeN_7O_2Si_6U$	$C_{50}H_{99}FeN_7O_2Si_6U$	$C_{50}H_{99}CoN_7O_2Si_6U$	$C_{27}H_{62}N_4Si_6U$
Formula Mass	574.58	1292.78	1292.78	1334.92	921.48
Crystal System	Monoclinic	Monoclinic		Monoclinic	Triclinic
a/Å	43.655(5)	22.6103(4)	22.6247(6)	16.1388(2)	11.62523(15)
b/Å	11.246(5)	16.2317(2)	16.2440(10)	19.9389(2)	11.98479(15)
c/Å	12.798(5)	20.7926(4)	20.7956(10)	21.3989(4)	16.8404(3)
a/°	90.000(5)	90	90	90	110.1899(13)
β/°	91.563(5)	106.682(2)	106.666(4)	106.294(2)	94.1775(12)
γ/°	90.000(5)	90	90	90	100.7396(10)
Unit cell volume/ Å^3	6281(4)	7309.8(2)	7321.7(6)	6609.37(16)	2139.49(5)
Temperature/ K	170	170	170	170	170
Space group	P 1 21/c 1	P 1 21/c 1		P 1 21/n 1	P -1
Z	8	4		4	2
Radiation Type	MoK\α	MoK\α	MoK\α	MoK\α	MoK\α
Absorbtion coefficient, μ/mm^{-1}	0.513	2.544		2.847	3.989
No. of reflections measured	147809	52221		78542	138792
No. independent reflections	17276	16722		15121	13247
R_{int}	0.085	0.0504		0.0357	0.0459
$R[F^2 > 2\sigma(F^2)]$	0.127	0.0406		0.0358	0.0236
$wR(F^2)$	0.2255	0.102		0.0919	0.0536
Goodness of fit on F^2	1.253	1.038		1.033	1.063

[a]Disordered solvent removed using SQUEEZE

[b]Alternative synthesis, unit cell only

Appendix 1

Table 1 CIF data for compounds **10 - 18**

Compound Reference	**10**	**11**	**12**	**14**	**15**	**18**
Chemical Formula	$C_{106}H_{155}O_7N_8Fe_3Na$	$C_{98}H_{130}Co_2O_8$	$C_{94}H_{130}CO_2N_2O_{12}$	$C_{116}H_{134}Co_2K_2O_6$	$C_{84}H_{118}O_{10}Zn_2K_2$	$C_{24}H_{27}ClN_2O_3$
Formula Mass	2156.36	1553.88	1597.86	1820.4	1640.97	426.93
Crystal System	Monolinic	triclinic	Monolinic	Triclinic	Monoclinic	Monoclinic
a/Å	24.1768(6)	11.5545(6)	11.617(5)	11.7463(3)	14.563(5)	11.6030(4)
b/Å	20.7097(4)	14.2568(5)	19.588(5)	14.9341(5)	15.261(5)	10.8447(3)
c/Å	27.6012(7)	14.6264(6)	19.188(5)	15.0751(5)	19.714(5)	18.6864(5)
a/°	90	101.700(3)	90.000(5)	83.295(3)	90.000(5)	90
β/°	114.793(3)	111.421(4)	93.253(5)	79.882(2)	95.757(5)	101.101(3)
γ/°	90	93.566(4)	90.000(5)	88.831(2)	90.000(5)	90
Unit cell volume/ Å^3	12545.9(5)	2171.69(16)	4359(2)	2582.55(14)	4359(2)	2307.33(12)
Temperature/ K	120	170	120	170	120	120
Space group	P 1 21/n 1	P-1	P 1 21/c 1	P -1	P 1 21/n 1	P 1 21/a 1
Z	4	1	4	1	2	4
Radiation Type	MoK\α	MoK\α	CuK\α	MoK\α	CuK\α	CuK\α
Absorbtion coefficient, μ/mm^{-1}	0.392	0.825	0.441	0.661	0.705	1.677
No. of reflections measured	190318	40641	53144	46804	132958	23351
No. independent reflections	22925	10327	9082	11860	9105	4752
R_{int}	0.0608	0.0438	0.0417	0.055	0.0897	0.061
$R[F^2 > 2\sigma(F^2)]$	0.0616	0.0555	0.0613	0.0629	0.0514	0.0634
$wR(F^2)$	0.1551	0.1552	0.1562	0.1828	0.129	0.189
Goodness of fit on F^2	1.072	1.052	1.199	1.035	1.100	1.082